CRANFIELD INSTITUTE OF TECHNOLOGY

SCHOOL OF MECHANICAL ENGINEERING

Ph.D. Thesis

Academic Year 1984-5

C. MELO

Improved Convective Heat Transfer and Air Infiltration Models for Building Thermal Simulation

Supervisor: G.P. Hammond

June 1985

This thesis is dedicated to my

wife and daughter, Leila and Anna Paula

and to my parents,

Marçal and Margarida

SUMMARY

'Intermediate-level' computer codes are advocated as being the most appropriate for meeting the requirements of dynamic building thermal models. Such codes may be developed via the 'computer-generalization' of analytical solutions and data correlations, which are then verified using higher-level computational procedures and/or experimental measurements. Two intermediate-level computer codes are described: one to model the convective heat exchange at the external facades of a building (WIND-CHT program), and the other to calculate the hourly mean rates of air infiltration into buildings (FLOW program). These codes take into account most of the key parameters such as wind speed and direction, the change in shape and height of the atmospheric boundary-layer over different terrains, the relative dimensions of the building, the indoor-outdoor temperature difference and the leakage characteristics of the building. Both the WIND-CHT and FLOW programs are compared with field experimental data, and good agreement is shown.

The sensitivity of two dynamic building thermal models to the external convection and air infiltration input data are then assessed. The NBSLD (National Bureau of Standards Load Determination) 'response factor' program (1981) and the BRE (British Research Establishment) 'admittance procedure' program (1984) were chosen for this purpose. The sensitivity of these models to the internal convection input data was also assessed. In this case the ROOM-CHT program,developed by Alamdari and Hammond (1982) was employed. Both models displayed a considerable variation in their results when the 'traditional' input data were replaced by the 'improved' values, although the extend of the impact of the convection and infiltration models is likely to depend on the conditions prevailing in and around the particular building being simulated.

ACKNOWLEDGMENTS

I would like to thank my supervisior, Mr. G. P. Hammond, for his invaluable guidance during this work and also for his advice and constructive criticism during the writing of this thesis.

I am also grateful to Dr. F. Alamdari for his help regarding the use of the ROOM-CHT program and for all the help he and his family provided to make my stay in this country pleasant.

The financial support provided by the Conselho Nacional de Desenvolvimento Cientifico e Tecnologico-Brazil is also acnowledged. My thanks are also due to all members of the Department of Mechanical Engineering of the Federal University of Santa Catarina-Brazil, particularly Dr. R. T. S. Ferreira and my colleagues of the Thermal Sciences group.

The ROOM-CHT program and the general concept of 'intermediate-level' calculation methods were developed at Cranfield with the financial support of UK Science and Engineering Research Council (SERC) Grants GR/B/5010.2 and GR/C/2419.0. Access to the UK Meteorological Data Base was also provided under these grants, which form part of the SERC's specially promoted programme on 'Energy in Buildings'.

Finally, I would like to thank all the members of my family, mainly my father, for their support during this last three years.

CONTENTS

FIGURES

NOTATION

A	Area, m^2
a	Fourier series coefficients [equation (3.14)]
Al	Leakage area, m^2
b	Logarithmic series coefficients [equation (3.15)]
C	Flow coefficient, $m^3 s^{-1} Pa^{-m}$ [equation (3.1)]
Ceq	Rate of heat convected from equipment into the room at time t, W
Cli	Rate of heat convected from lights into the room at time t, W
Coc	Rate of heat convected from occupants into the room at time t, W
Cp	Wind pressure coefficient
Cpr	Specific heat of air, J $Kg^{-1} °C^{-1}$
CR	Common ratio of response factors [equation (4.7)]
D	Side ratio [equation (3.15)]
d	Displacement height, m [equation (2.45)]
E	Emissivity factor
F	Grey body shape factor
Fc	Wind pressure coefficient shielding correction factor
Fs^*	Building stack effect parameter [equation (3.8)]
Fw^*	Building wind parameter [equation (3.7)]
g	Acceleration due to gravity, m s^{-2}
Gr	Grashof number
h	Heat transfer coefficient, W $m^{-2} °K^{-1}$
Ha	Average height of the adjacent structures, m
Hb	Height of the building, m
I	Air Infiltration rate, ACH

Iw	Hourly air change rate during the winter months, ACH
K	Von Karman's constant [equation (2.45)]
k	Thermal conductivity, W m^{-1} °K^{-1}
K1,K2,K3	Constants [equation (3.3)]
L	Effective length, m [equation (2.56)]
Mi	Mass flow rate of outdoor air infiltrating into the room, Kg h^{-1}
Ms	Mass flow rate of the supply air from the central mechanical ventilation system, Kg h^{-1}
N	Ratio of height of level above ground to building height [equation (3.19)]
n	Flow exponent [equation (3.1)]
NR	Number of response factors
NS	Number of enclosure surfaces
Nu	Nusselt number
P	Perimeter, m [equation (2.56)]
Pb	Atmospheric pressure, Pa
Pd	Pressure difference due to stack pressure, Pa
Pr	Prandtl number
Ps	Velocity pressure at reference height in the free air-stream, Pa [equation (3.11)]
Pw	Surface wind pressure, Pa
Q	Air infiltration rate, $m^3 s^{-1}$
q	Heat flux, W m^{-2}
QLS	Sensible cooling load, W
Qsun	Global solar radiation on a horizontal surface, W m^{-2}
Qstack	Stack dominated infiltration, $m^3 s^{-1}$
Qvent	Mechanical ventilation, $m^3 s^{-1}$
Qwind	Wind dominated infiltration, $m^3 s^{-1}$
R	Thermal resistance, m^2 °K W^{-1}

Ra	Rayleigh number
Rda	Gas constant of dry air, J $Kg^{-1}°K^{-1}$
Re	Reynolds number
Req	Rate of heat radiated from equipment and absorbed by surface i at time t, W
Rl	Fraction of the effective leakage that is horizontal [equation (3.7)]
Rli	Rate of heat radiated from lights and absorbed by surface i at time t, W
Roc	Rate of heat radiated from occupants and absorbed by surface i at time t, W
Rs	Rate of solar energy coming through the windows and absorbed by surface i at time t, W m^{-2}
S	Turbulence scale [equation (2.53)]
St	Stanton number
Ta	Internal air temperature, °C
Tav	Time-averaged value of all the (absolute) internal surface temperatures, °K
Te	External air temperature, °C
Ti	Inside surface temperature, °C
To	Outside surface temperature, °C
Tu	Turbulence intensity [equation (2.53)]
Ts	Supply air temperature from the central mechanical ventilation system, °C
V	Wind velocity, m s^{-1}
Vav	Average wind velocity over the building facade, m s^{-1}
Vf	Wall shear of 'friction' velocity, m s^{-1}
Vg	Gradient velocity, m s^{-1}
Vs	Wall-jet peak velocity at any downstream location, m s^{-1}
Wb	Outside wet-bulb temperature, °C
X	Response factor related to the inside wall temperature, W $m^{-2}°C^{-1}$ [equation (4.7)]

x	Distance to neutral pressure level, m
Y	Response factor related to the outside wall temperature, W $m^{-2}°C^{-1}$[equation (4.7)]
Z	Height above ground level, m
Zg	Height at which the gradient velocity is attained, m
Zo	Average height of roughness elements, m
Z1	Distance between the ground and the room ceiling level,m
Z2	Distance between the ground and the room floor level, m

Subscripsts

a	Ambient air
b	Buoyancy-driven flow
c	Convection
cb	Convection and radiation
cd	Conduction
ce	Ceiling
cr	Critical condition
e	External air
es	Internal energy sources
f	Forced convection flow
fl	Floor
i	Inside surface
L	Effective lenght
le	Leeward wall
m	Maximum value
o	Outside surface
p	Parallel flow

r	Radiation
ro	Roof level
s	Separated flow
st	Stagnation flow
t	Time
to	Total
wi	Windward wall
z	Height above ground level
10	10 metres above ground level
28	28 metres above ground level

Superscripts

'	Wind measurement site

Greek Symbols

α	Power index in mean velocity profile power law [equation (2.46)]
β	Constant that depends on type of terrain [equation (3.7)]
γ	Constant that depends on type of terrain [equation (3.7)]
ΔP	Pressure difference, Pa
ΔT	Temperature difference, °C
δ	Air infiltration rate correction factor [equation (4.23)]
η	Surface orientation w.r.t. the wind direction
θ	Angle of attack, degrees
λ	Ratio of neutral pressure level to building height
ν	Kinematic viscosity, $m^2 s^{-1}$

ξ	Wall azimuth, degrees
ρ	Air density, Kg m^{-3}
σ	Stefan-Boltzman constant, W $m^{-2}K^{-4}$
τ	Ground level surface shear stress, N m^{-2}
ϕ	Weighting function [equation (2.66)]
ψ	Wind direction, degrees
Λ	Thermal draft coefficient [equation (3.19)]

Special symbol

ACH	Air changes per hour

CHAPTER 1

CHAPTER 1 - INTRODUCTION

1.1 - ENERGY CONSERVATION AND THE BUILT ENVIRONMENT

In the aftermath of the energy crisis of the early 1970's limiting energy comsumption has become one of the most important priorities in an industrialised society. Consideration of energy in relation to the building sector reveals that more than 50 percent of all delivered energy is associated with buildings (Fig.1.1) and of this,more than 60 percent ,in the United Kingdom, is used for the provision of spatial confort (Fig.1.2) (Ref.1). Prediction of energy requirements for buildings is therefore a problem of ever increasing importance to designers and owners of buildings. High fuel costs and short fuel supplies demand that heat gains and losses be more carefully accounted for, since these factors determine the energy required to maintain a particular building environment. The need therefore exists for research into energy use in buildings aimed at conservation of energy through improved design. In the last decade a large amount of the effort in this area has been concerned with the development of building thermal simulation computer programs which permit a rapid appraisal of alternative design strategies.

1.2 - THERMAL RESPONSE OF A BUILDING

A building may been considered, from a thermal viewpoint,as a complex network of thermal resistances and capacitances linked by conductive, convective and radiative processes. The way this complex circuit is treated, determines the solution technique which is employed. Currently, the most widely used calculation methods for the thermal design of buildings are based on steady state procedures, in which the heat supplied to the structure is balanced by the heat lost from it, while storage of heat in the building fabric is ignored. These traditional methods display many inadequacies including the omission of any consideration of the dynamic response of buildings, an inability to realistically deal with many of the energy flows occurring within a building, and an inability to effect the correct relationship between the building fabric and the proposed plant operational strategy.

In consequence, such steady state concepts are unable to answer a number of questions that are now being asked in the search for energy-conscious designs. There is clearly a need to improve the knowledge and understanding of the way in which buildings respond to fluctuating external temperatures and to intermittent heat supply. Dynamic thermal models have recently been developed that are able to meet these needs. They employ a variety of approaches including harmonic, response factors and finite difference techniques. Day (Ref.2) presents a review of the efforts of the UK Science and Engineering Research Council to stimulate research in this area.

1.3 - MAIN UNCERTAINTIES OF BUILDING THERMAL MODELS

A comprehensive study of the new generation of building thermal models by the International Energy Agency (Ref.3) concluded that their accuracy is presently limited by uncertainties in the input data, particularly for air infiltration and convective heat transfer rates. The emphasis in these modern models is placed on simulating the thermal performance of the building fabric, whereas convective heat exchange and air infiltration rates are modelled using rather crude approximations.

Building thermal modellers have typically utilised the empirical data correlation for buoyancy-driven convection recommended in the ASHRAE (Ref.4) and CIBSE (Ref.5) design guides when specifying convection coefficients within dwellings and offices. Such correlations are applied irrespective of whether the air circulation is induced by buoyancy-driven or forced convection. Recent field and laboratory 'environmental chamber' measurements (Ref.6-8) have, not suprisingly, shown that forced convective heating and/or mechanical ventilation of enclosures gives rise to internal convective transfer rates that are much higher than the guide values. Waters (Ref.9) has demonstrated that the accuracy of his implicit finite difference building thermal model is strongly dependent on the correct choice of internal exchange coefficients when simulating mechanically ventilated structures.

In an attempt to identify the nature and variability of convective heat exchange at the internal surfaces of the building envelope, Hammond and his co-workers have evolved a 'hierarchy' of interacting and interdependent approaches to calculating surface coefficients, initially for warm-air heated and/or mechanically ventilated rooms. These range from 'lower -level' approaches, such as wall jet profile analysis (Ref.10-11) and improved data correlations for buoyancy-driven convection (Ref.12), to the development of a 'high-level' flow model based on the finite difference analogues to the governing 'elliptic' equations for the complex, jet-induced room airflow (Ref.13). Both the higher and lower-level models have been used to develop an verify an 'intermediate-level' computer code (Ref.14), called ROOM-CHT (ROOM Convective Heat Transfer) program,which formed the basis for generating input convective heat transfer data for dynamic building thermal models. Details of this code are presented by Alamdari (Ref.13).

Most of the dynamic computer codes still evaluate wind related heat losses by employing average heat transfer coefficients based either on the work of Jurges (Ref.15) or Rowley et al (Ref.16). Among the limitations in the equations proposed by these workers, are two especially relevant to building applications. The first limitation is that they are based on parallel flow experiments, whereas the wind direction is, in general, not parallel to the walls. The second is the absence of any dependence on surface length which is contrary to the well established fact that boundary layer heat transfer coefficients are length dependent. In laminar boundary layer flow on

a flat surface, for instances, the average heat transfer coefficient decrease with the square root of the surface length. In view of these inadequacies, it is difficult to justify employing either Jurges' or Rowley's results for wind related heat loss calculations. This realization served as the initial motivation for the development of an intermediate-level program for calculating the external convection coefficients from buildings (Ref.17). Details of this code, which is called the WIND-CHT (Wind-induced Convective Heat Transfer) program, are given in the next chapter.

The lack of an adequate method for estimating the infiltration heat loss from a building constitutes another major deficiency in the present generation of building thermal models. Two methods are commonly adopted by modellers for estimating air infiltration rates into buildings. The first, and most widely used, is the air change method, which is an entirely empirical technique. It is based on assuming an air change rate for each assumed room and then averaging them over the whole house volume. The ratios for each room are dependent upon the relative location of the room inside the structure, as well as the number of walls with exterior windows and doors.Typical air changes rates for various types of rooms are provided by ASHRAE (Ref.4) which were presumably based on past experience. The second popular method for estimating infiltration rates employs empirical correlations between infiltration rates and weather data, usually based on long-term field measurements. This technique uses measured hourly data to generate various regression equations relating the two sets of variables. Such methods were developed at a time when fuel was cheap and only gross approximations were of interest. In these days the need is for a model which can accurately predict the air infiltration rates and internal air flow as functions of the wind parameters, indoor-outdoor temperature differences and operating cycles of air handling systems. In order to overcome this problem a computer program, called FLOW, has been developed (Ref.18). The program estimates the hourly mean rate of air infiltration into buildings with sufficient accuracy to meet the needs of building dynamic thermal models. Details of this code are given in chapter 3.

1.4 - THE DEVELOPMENT OF INTERMEDIATE-LEVEL METHODS

The way in which the intermediate-level calculation methods have been developed is illustrated by the schematic diagram shown in Fig.1.3 (Ref.19). The blocks within the dashed line represent the iterative process of developing and verifying such methods.

1.4.1 - The development process

The classification scheme adopted for the various calculation method 'levels' is intended to reflect the potential generality, rather than their scientific sophistication. The term 'higher-level'

method is reserved for computational procedures that attempt to solve approximations to the governing elliptic, partial-differential equations for a complex flow field. In the development of intermediate-level models the computer has been employed as a tool for 'generalising', the results of lower-level calculations methods. However, although the resulting computer codes are capable of handling much more complex geometries than traditional methods, the range of application of the intermediate-level procedures is still limited, and they need to be used in conjuction with a broad flow classification scheme.

1.4.2 - The verification process

The intermediate-level calculation methods have been verified using experimental data, obtained from full and scale tests and, in the case of the model for internal convection , the computed results of a higher-level code. This procedure was conceived as an iterative (or feedback) process, as implied by the block diagram in Fig.1.3, from which ad hoc corrections to the intermediate-level codes would be made where necessary. In reality, only the model for external convection was modified in this way, when it was found that laboratory-scale data correlations did not correspond to full-scale building heat transfer measurements on windward facades.

1.5 - THE AIM OF THE PRESENT WORK

The aim of the present work was to develop intermediate-level, sub-system models for calculating the external convective heat transfer coefficients around buildings and the hourly mean rates of air infiltration into them. The second purpose of this work was to assess the sensitivity of modern building thermal models of varying levels of complexity to input values for the external and internal convection coefficients, and air infiltration rates. The dynamic models that have been chosen are those developed by the US National Bureau of Standards (Ref.20), the NBSLD 'response factor' program, and by the Building Research Establishment (Ref.21), the Admittance Procedure (a 'harmonic' program). Accuracy constraints imposed on these building thermal models by input heat transfer and infiltration data will equally limit more complex models.

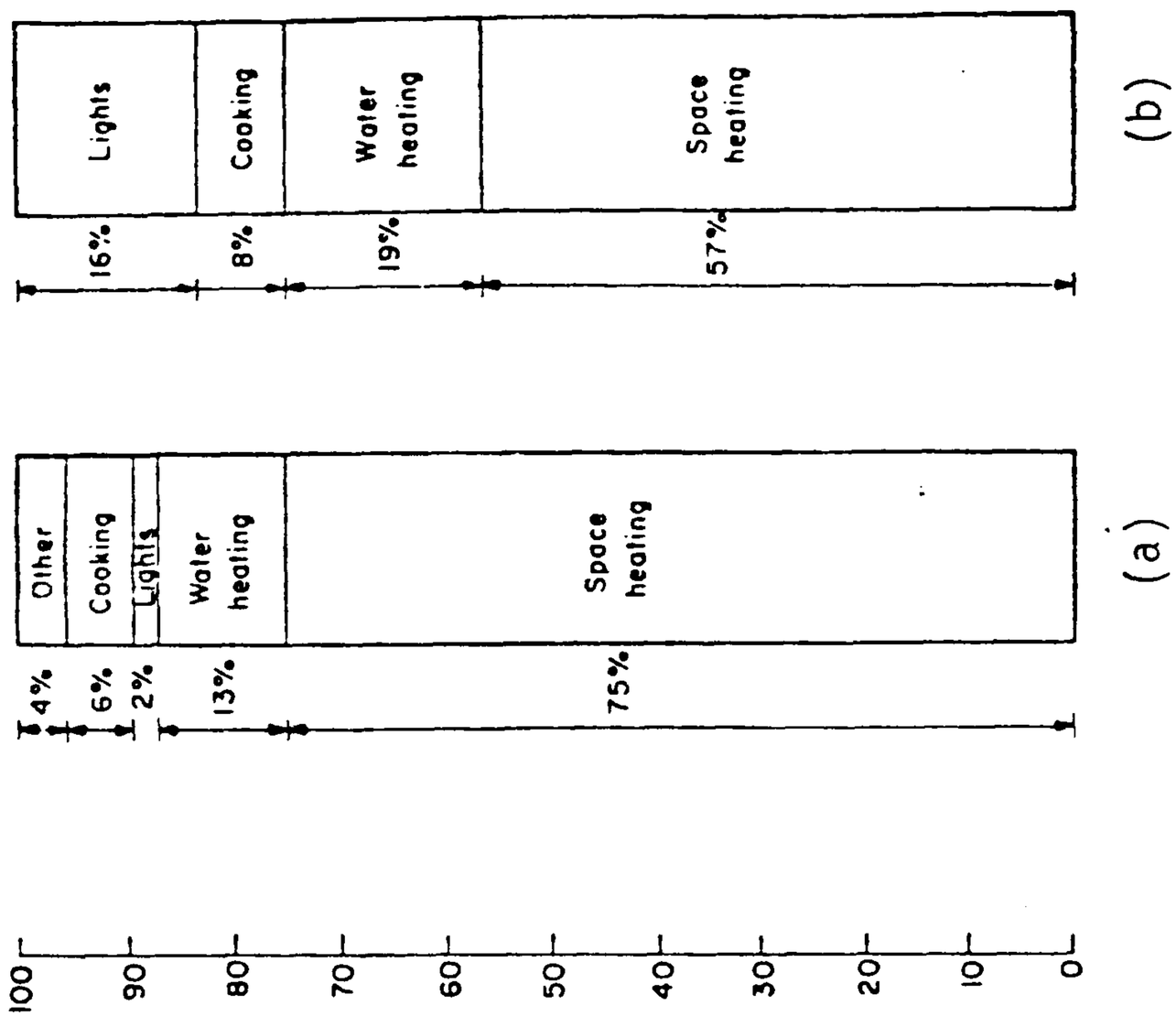

Fig. 1.2 Structure of energy use: a) domestic and b) commercial {After Clarke (Ref. 1)}

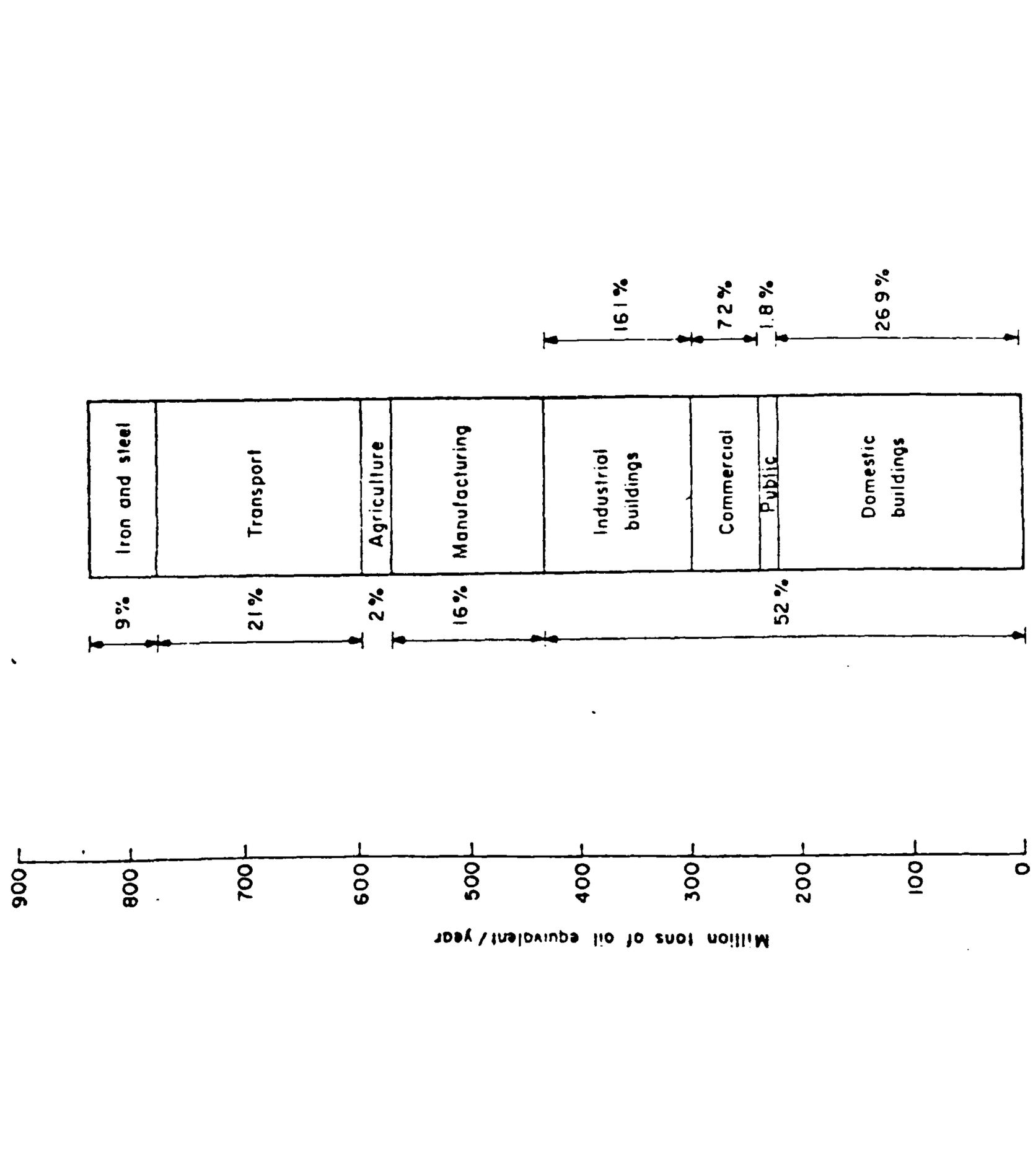

Fig. 1.1 Delivered energy demand: Europe 1977 {After Clarke (Ref. 1)}

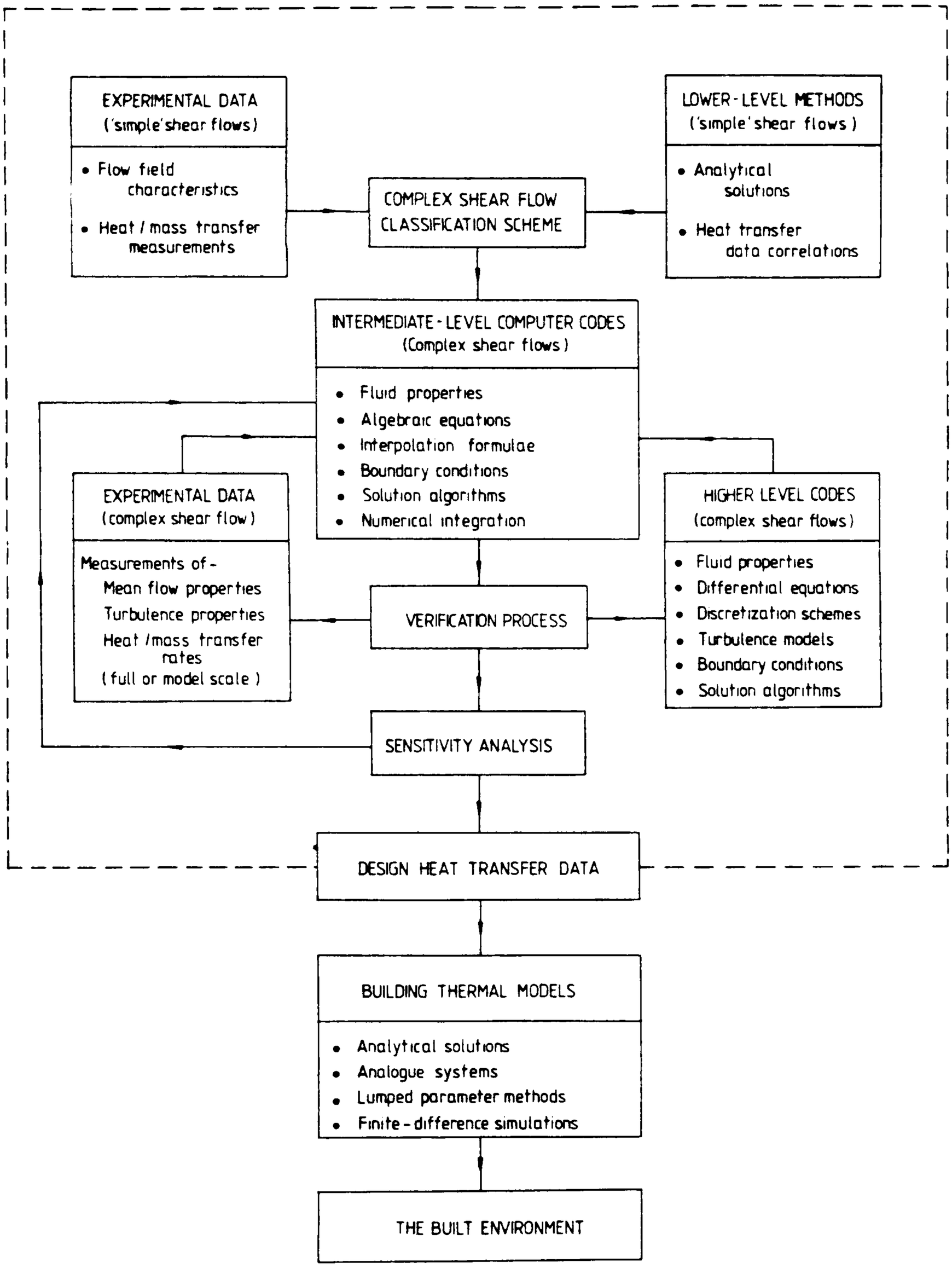

Fig. 1.3 Development sequence of intermediate-level computer programs

CHAPTER 2

CHAPTER 2 - AN INTERMEDIATE-LEVEL MODEL FOR EXTERNAL CONVECTION FROM BUILDINGS

2.1 - INTRODUCTION

Design guides in Britain (Ref.23) and America (Ref.4) provide simple methods of estimating convective heat losses from buildings, although these cannot accurately reflect the complex mechanism of heat transfer over the whole of a buildings' surface. They recommend data correlations for the exterior convective heat transfer coefficient over buildings which are simple algebraic functions of wind speed, albeit with widely differing empirical coefficients. Such correlating equations take no account of the predominant wind direction, the change in shape and height of the atmospheric boundary layer over different terrain, or the relative dimensions of the building. Nevertheless, they are commonly adopted for use in building thermal models.

In an effort to obtain improved predictions an intermediate-level model for external convection has recently been developed and incorporated into a computer program called the WIND-CHT code, which is fully described in the next sections.

2.2 - THE NATURE OF CONVECTIVE HEAT TRANSFER

The process involving the transfer of heat between a solid surface and a fluid, either a liquid or gas, is called convection. Since a fluid is able to move, the process of heat transfer involves a transport of energy associated with this fluid motion, in addition to the mechanism of conduction(molecular interaction). Heat is initially transferred from the building surface to the adjacent 'stagnant' air layer by conduction. The presence of this stagnant layer results from the fact that the velocity of the flow falls to zero at the surface, due to the socalled 'no slip' condition. Energy is subsequently transported from high temperature regions to lower ones by motion within the air itself. The nature of this fluid movement therefore has a significant effect on the magnitude of the heat transferred to or from the surface.

It is customary to divide convection problems into two classes, depending on how the fluid motion arises. The two categories are forced and buoyancy-driven convection. In forced convection the fluid motion is caused by some external means, such as by a fan, pump, or by atmospheric winds. In contrast, buoyancy-driven, alternatively called free or natural, convection is induced by buoyancy forces within the fluid. These forces arise from density differences that always accompany temperature variations in the fluid.

Another essential step in the treatment of any convection problem is to determine whether the flow is laminar or turbulent, since the convection transfer rates depend strongly on which of these conditions exists. When a fluid moves in such a manner that a particle with the same density as the fluid describes a smooth line that is essentially parallel to the boundary, the flow phenomenon is called laminar. In the turbulent flow the influence of the fluctuating momentum flux dominates, and the fluid motion departs from a smooth layerlike flow to a situation where there is significant motion in the direction transverse to that of the main mass flux. Such action is very effective in transferring heat from the surface into the mainstream of the fluid and consequently heat transfer coefficients for turbulent flow are much higher than those for laminar flow for a given fluid. The subdivision of the laminar and turbulent flow regimes depend on the velocity of the air, the roughness of the surface over which it is passing and, to a lesser extend, upon the viscosity of the air.

2.2.1 - The convection coefficient

Regardless of the particular nature of the convection heat transfer mode, the appropriate rate equation is of the form

$$q = h_c \Delta T \qquad (2.1)$$

where q, the convective heat flux, is proportional to the difference between the surface and fluid temperatures, ΔT. This fact was discovered by Sir Isaac Newton, who experimented with small objects heated in a forge and then cooled outside in the wind. Expression (2.1) is therefore known as Newton´s law of cooling, and the proportionality constant h_c, is reffered to as the heat transfer coefficient, which depends on the surface geometry, the nature of the fluid motion and a number of the fluid thermodynamic and transport properties.

2.2.2 - Dimensional analysis

It can be shown through dimensional analysis that a functional relationship exists such that

$$Nu = f(Re, Pr, Gr) \qquad (2.2)$$

It is important to note that such correlation is only pertinent when forced and buoyancy-driven convection effects are of comparative importance. Generally, the combined effects of buoyancy-driven and forced convection must be considered whenever $(Gr/Re^2) \approx 1$. If the inequality $(Gr/Re^2) << 1$ is satisfied, buoyancy- driven effects may be neglected and

$$Nu = f(Re,Pr) \tag{2.3}$$

Conversely, if $(Gr/Re^2)>>1$, forced convection effects may be negleted and

$$Nu = f(Gr,Pr) \tag{2.4}$$

In the strict sense, a buoyancy-driven convection flow is one that is induced solely by buoyancy forces, in which case there is no well-defined forced convection velocity and $(Gr/Re^2)=\infty$.

2.3 - PREVIOUS RESEARCH INTO CONVECTIVE HEAT TRANSFER FROM BUILDINGS

2.3.1 - Theoretical forced convective heat transfer from a flat plate in parallel flow

Despite its simplicity, parallel 'boundary-layer' flow over a flat plate occurs in numerous engineering applications. Moreover, this geometry is often a reasonable approximation for flow over slightly contoured surfaces.

In this type of flow two different correlations are established according whether the flow is laminar or turbulent (Ref.22). Solution of the boundary-layer equations for laminar flow over a flat plate of length L yields the following relation for the average Nusselt number.

$$Nu_L = 0.664\ Re_L^{1/2}\ Pr^{1/3} \tag{2.5}$$

For turbulent flow over the entire plate, the following semi-empirical relation may be used to compute the average coefficient

$$Nu_L = 0.036\ Re_L^{4/5}\ Pr^{1/3} \tag{2.6}$$

Since the turbulent boundary layer is generally preceeded by a laminar boundary layer, it is convenient to consider mixed boundary layer conditions. If transition occurs sufficciently far upstream of the leading edge, the surface average coefficient will be influenced by conditions in both the laminar and turbulent boundary layers. In this case, the average convection heat transfer coefficient for the entire plate may be obtained using:

$$Nu_L = (0.036\ Re_L^{4/5} - A)Pr^{1/3} \tag{2.7}$$

where the constant A is determined by the value of the critical Reynolds number, Re_{cr}. That is,

$$A = 0.036\ Re_{cr}^{4/5} - 0.664\ Re_{cr}^{1/2} \qquad (2.8)$$

If typical transition Reynolds number of, say, $Re_{cr} = 5x10^5$ is assumed, equation (2.7) reduces to

$$Nu_L = (0.036\ Re_L^{4/5} - 835)Pr^{1/3} \qquad (2.9)$$

which is valid for $5x10^5 < Re \leq 10^8$.

2.3.2 - Experimental studies of forced convective heat transfer from flat plates

One of the first investigations in this field was made by Jurges in 1924, as quoted by Mc Adams (Ref.15). Jurges used a heated copper plate, approximately 0.5 m square, mounted vertically flush with the walls of a wind tunnel. The plate was maintained at 51°C while air, initially at 20°C, was blown over the plate,parallel to the surface. Two surface textures roughnesses were examined, and expressions developed for two different wind speed ranges. The first range includes free stream wind speeds from 0 to 5 m s^{-1}, and in the second, wind speeds greater than 5 m s^{-1}. For the first range, the convection coefficient h_c, was found to be a linear function of the wind speed ,V, and could be represented by the following relations:

$$h_c(smooth) = 4.0\ V + 5.6 \qquad (2.10)$$

$$h_c(rough) = 4.2\ V + 6.2 \qquad (2.11)$$

For the second range, Jurges´ data was better represented by power-law expressions:

$$h_c(smooth) = 7.1\ V^{0.78} \qquad (2.12)$$

$$h_c(rough) = 7.5\ V^{0.78} \qquad (2.13)$$

These formulae have been adopted by Duffie and Beckman (Ref.24), for calculating the forced convective heat loss from the front cover of a solar collector, and also in the CIBSE guide (Ref.23).

The data presented by ASHRAE (Ref.4) for external surface heat transfer coefficients uses measurements made during the 1930´s by Rowley and his associates (Ref.16). They conducted a comprehensive

set of wind tunnel tests in order to investigate the effect of surface texture, air velocity and temperature range on the variability of the surface coefficient. Their experimental apparatus included a 0.30 m multi-blade fan, driven by a variable speed motor, blowing air from a refrigerated room along rectangular ducting measuring 0.15x0.30 m in section. At approximately 5.18 m from the fan, the air passed over and parallel to a 0.30x0.30 m square heated test plate. This plate was inserted in the side of the duct flush with its inside surface. The air was then passed through a return bend and brought back to the cold room. The air velocity was measured at the centre of the duct with a pitot-static tube, while the air temperature was measured by placing a thermocouple 25 mm from the test surface.

It was possible to change the test plates, and thereby examine the effect of surface finish. Surfaces which were considered to be most typical of building construction were used for these tests. In making tests on each surface, several different air velocities were selected and runs were made at different mean temperatures for each velocity. Surfaces included in the testing were glass, brick, smooth plaster, clear white pine, rough plaster, concrete and stucco.

The results showed that for a constant air velocity a higher mean temperature of the plate and air brought about a slightly higher surface coefficient. The effect of surface roughness on the coefficient was much greater, with the surface coefficient for stucco being almost twice that for glass. It was also found that the relationship between surface heat transfer and wind velocity was almost linear. Fig.2.1 shows the heat transfer coefficient for each of the materials tested as a function of the wind velocity at a mean temperature of -6.6°C.

The experiments described above apply to parallel flow past a surface. Realising that in practice the wind could blow at any angle to the building's surface, Rowley and Eckley (Ref.25) examined flat plate directional effects by varying the angle of incidence between a test surface and the wind. The apparatus consisted essentially of a heated vertical surface on a rotatable support placed with the centre line 0.30 m in front of the outlet end of a duct 7.62 m long and 0.76 m in diameter. The heated plate was 0.38 m square, with a 0.30 m wing or extension wall on the leading side in order to direct the wind over the surface and to minimize the disturbance by eddy current at the leading edge of the test plate. In making the tests, plate glass and smooth pine surfaces were used, and tests were made at angles varying from 0 to 90 degrees through 15 degrees increments. For each angle, the velocity in the air duct was varied from 0 to 13 m s^{-1}. The mean plate-air temperature was held constant at 28°C.

It was found that for wind velocities up to 7 m s^{-1} the coefficients were substantially the same for angles of incidence between 15 to 90 degrees, all being less than for parallel flow. Above 7 m s^{-1}, the coefficients were reduced as the angle between the surface and air stream was increased. It was concluded therefore, that the heat transfer coefficients obtained from the parallel flow experiments (Ref.16) would be sufficiently accurate for most practical cases.

The measurements of Jurges (Ref.15) and Rowley et al (Ref.16) were also restricted to surfaces with heated lengths of 0.50 and 0.30 m respectively. In an attempt to quantify the effects of varying the heated surface length, Parmellee and Huebscher (Ref.26) conducted an experiment using a vertical heated smooth flat plate, placed in a wind tunnel, swept by a horizontal parallel air stream. Data are presented for turbulent, laminar and transitional boundary-layer flow. Here the convection coefficient is significantly affected by the surface length, the average value decreasing for increasing surface length. This effect, which is now a well established fact, arises because the air flowing across the heated surface has its greatest cooling influence near the leading edge and has progressively less effect along the surface.

Sogin (Ref.27,28) carried out a series of experiments with the objective of measuring the heat transfer by forced convection from immersed surfaces to totally separated regions of flow. The essential feature of the experiment was a bluff flat-plate strip (171 mm longx25.4 mm thick) in two-dimensional flow. The downstream face was intrumented for measuring distributions of temperature and heat flux in the horizontal plane of symmety of the wind tunnel. There were nine contiguous measuring stations, 17 mm centre to centre, and the Reynolds number, based on the chord length, ranged from 10^5 to $4.4x10^5$.

The data were satisfactorily correlated by an equation of the type

$$Nu_L = B\ Re^{2/3} \tag{2.14}$$

when the fluid properties were evaluated at the mean film temperature. The coefficent B depended upon the configuration and the location on the rear surface. Thus, B had practically the uniform value of 0.20 with a standard dispersion(ratio of standard deviation to mean value) of 2.5 percent for a flat-plate strip at 90 degrees angle of attack. In this case, therefore, equation (2.14) reduces to

$$Nu_L = 0.20\ Re^{2/3} \tag{2.15}$$

Richardson (Ref.29) examined several experimental studies of heat and mass transfer in fully-separated, turbulent flows, and also concluded that the Nusselt number at the rear of a bluff body normal to an air stream was proportional to the 2/3 power of Reynolds number. He found that at the rear stagnation point on a circular cylinder, the value of the coefficient B ranged between about 0.13 and 0.25 for all available measurements (in 1963), with a mean value of about 0.175.

2.3.3 - Experimental studies of forced convective heat transfer from three dimensional bluff bodies

Rowley and Eckley (Ref.25) concluded that for all practical purposes the surface coefficients obtained for air flow parallel to the surface could be used without any correction for wind direction. Nevertheless, their graph of surface coefficients for glass showed a significant variation with angle of incidence, e.g. at $V = 4.5$ m s^{-1} there is a 20 percent difference between the surface coefficient for angles of incidence of 0 and 60 degrees. Subsequently, Oliphant (Ref.30) performed experiments in order to determine the air velocity across the front cover of a solar collector and to observe any dependence on wind direction. The solar collector test rig consisted of two flat plate collectors each with outside dimensions 1.32x0.60 m and separated by a gap of 0.37 m. The collectors faced North and were inclined at an angle of 31 degrees. Although no correlation was presented by Oliphant, his data showed that the meteorological wind speed was between 1.3 and 3 times greater than air velocity parallel to the collector, depending on wind direction.

Sparrow and Tien (Ref.31) conducted experiments to determine the average heat transfer coefficients for forced convection airflow over a square plate of finite thickness that was inclined and yawed relative to the oncoming flow. The experiments involved mass transfer measurements and were carried out via the naphathalene sublimation technique. The naphthalene square test plate (76.2 mm sidex2.38 mm thick) was mounted in the test section of a low speed, low turbulence wind tunnel. The turbulence level measured in the test section was approximately 0.2 percent. The parameters that were varied during the course of the experiments included the Reynolds number, the angle of attack and the angle of yaw. The Reynolds number, based on the free-stream velocity and the side of the square plate, ranged between about $2x10^4$ and 10^5 . Values for the angle of attack of 90,65,45 and 25 degrees were chosen, while yaw angles of only 0,22.5 and 45 degrees were chosen due to the symmetry of the square plate. It was found that owing to the strongly three-dimensional nature of the flow, the heat transfer coefficients decreased by only 5 percent as the angle of attack varied from 90 to 25 degrees and increased by about 1 percent over the entire range of yaw angles. In view of this insensitivity Sparrow and Tien recommended a single expression to represent all the data within an accuracy of 2.5 percent:

$$Nu_L = 0.931\, Re_L^{1/2}\, Pr^{1/3} \qquad (2.16)$$

They compared this relation with those arising from Jurges work (Ref.15), using a solar collector as an example. For a wind velocity of 3.05 m s^{-1}, equation (2.10) gave a heat transfer coefficient of about 17.8 W $m^{-2}\,°K^{-1}$, independent of the size of the collector plate. With this same wind velocity as input, equation (2.16), yielded a heat transfer coefficient of 8.7 W $m^{-2}\,°K^{-1}$ and 6.15 W $m^{-2}\,°K^{-1}$ for a 1.22 m and

2.44 m square collector plate, respectively. Consequently, Sparrow and Tien (ref.31) concluded that Jurges' equation leads to a substantial overestimation of the wind-related heat losses from the collector plate.

Sparrow, Ramsey and Mass (Ref.32) extended the range of study beyond that of Sparrow and Tien (Ref.31) by considering a finite-width rectangular plate. The experimental apparatus and procedure were basically the same as used previously (Ref.31). Wind tunnel measurements were made using a naphthalene plate (50.8x127x1.9 mm thick) inclined at angles of attack from 25 to 90 degrees to an oncoming flow. The Reynolds number range extended from about $2x10^4$ to $9x10^4$. Two basic plate configurations were analysed. One of these, referred to as the narrow plate, had its longer side oriented vertically whereas the second, or wider,plate had it on a horizontal plane. The heat transfer coefficients for the wider plate were found to be independent of the angle of attack in the range investigated. The results, in this particular case, were well correlated by the expression:

$$Nu_L = 0.939\ Re_L^{1/2}\ Pr^{1/3} \qquad (2.17)$$

In the case of the narrow plate, the heat transfer coefficient tended to lie below those for the wider plate, and in this case an overall spread of about 20 percent in the data was observed. A least-squares fit of the narrow plate data yielded:

$$Nu_L = 0.870\ Re_L^{1/2}\ Pr^{1/3} \qquad (2.18)$$

with deviations of +8 and -12 percent. Finally, an equation which represented all the data from the wider-plate, narrow-plate and the square plate (Ref.31) tests for angles of attack between 90 and 25 degrees, was presented:

$$Nu_L = 0.86\ Re_L^{1/2}\ Pr^{1/3} \qquad (2.19)$$

This expression yields a maximum error of about $\pm$10 percent. The characteristic dimension L, used in equations (2.17), (2.18), and (2.19) is an effective length defined as 4 times the surface area divided by the perimeter of the plate. It is analogous to the hydraulic diameter used in fluid mechanics.

Tien and Sparrow (Ref.33) performed wind tunnel experiments to study the flow patterns and the distribution of local forced convective heat transfer coefficient produced by tilting a square plate with respect to the wind direction. Sparrow et al (Ref.32) extended this study to rectangular plates. To determine the patterns of fluid flow adjacent to the plate surface, the oil/lampblack flow visualization technique was employed. The flow visualization

photographs taken by Sparrow and his associates showed that when the plate was situated normal to the flow, there was a stagnation zone in the central region of the plate with a surrounding region of radial outflow. As the plate was inclined, the stagnation zone progressively moved forward and ultimately disappeared. Inspection of the local heat transfer coefficient distribution plotted by Tien and Sparrow (Ref.33) showed that the lowest heat transfer coefficient occurred in the stagnation zone. The coefficients increased in the radial direction from the centre to the edges.

Sparrow, Nelson and Tao (Ref.34) carried out wind tunnel experiments to determine the magnitude of the forced convective heat transfer coefficient on the leeward face of a pitched roof. The model was a roof-like structure which included two sloping square faces (76.2 mm side), serving as the windward and leeward surfaces. Each of the sloping surfaces of the model made an angle of 45 degrees with the horizontal, so the angle between then was 90 degrees. The model was then placed in a wind tunnel and the heat transfer coefficients determined by again employing the naphathalene sublimation technique together with the analogy between mass and heat transfer. The Reynolds number range extended from about 2.5×10^4 to 10^5. The heat transfer coefficients on both the leeward and windward faces were displayed graphically as a function of the Reynolds number. It was found that for the windward face the results were well correlated by the expression:

$$Nu_L = 0.97\ Re_L^{1/2}\ Pr^{1/3} \qquad (2.20)$$

The authors did not correlate the data for the leeward side. However their experimental data are well correlated by the expression:

$$Nu_L = 0.16\ Re_L^{2/3}\ Pr^{1/3} \qquad (2.21)$$

The relationships derived by Sparrow and his co-workers (Ref.31-34) have the attraction of great simplicity. They are also related to a three-dimensional bluff body, and therefore might be considered appropriate for application to building surfaces. However since Sparrow's experiments were made in a wind tunnel with a uniform air stream there is a need to determine whether or not his results can be used to predict convective heat exchange in the natural environment. Test, Lessmann and Johary (Ref.35) performed experiments with this purpose in mind.

In earlier wind tunnel studies Test and Lessmann (Ref.36) observed that free stream disturbances dramatically increased heat transfer. A turbulence level of 2.5 percent compared to average speed resulted in a general elevation in heat transfer coefficients of 50 to 60 percent. These results were in line with those reported from previous wind tunnel studies, such as those of Junkhan and Serovy (Ref.37). The free-stream turbulence level in the atmosphere can be

quite high, and it might therefore be expected that heat transfer coefficients in the natural environment would be higher than in a low turbulence wind tunnel. Consequently, Test et al (Ref.35) carried out experiments in the natural environment and compared them to the previous wind tunnel results (Ref.36).

The prototype plate for outdoors experiments was 1.22 m long, 0.81 m wide and 0.20 m high. Special side attachments of width 0.4 m at an angle of 45 degrees were placed on the prototype in order to mantain approximately two-dimensional flow over the finite width body when exposed to varying wind directions. The top surface of the prototype contained three rows of heating units and there were eight units in each row. The heating units consisted of two (15.2x14.8x0.635 cm thick) copper pieces, with the spaces between them filled with 0.635 cm of a low viscosity electrical grade epoxy. All data were taken at night in order to avoid any solar radiation inputs. The heat transfer coefficients were calculated from the temperature difference between the two copper plates, the thermal resistance of the epoxy , and the difference between the upper plate temperature and the ambient air. The turbulence intensity of the wind flow was in the range of 20 to 50 percent. The accuracy of the experimental results was estimated to be $\pm$6%, due to uncertainty in the temperature measurement, epoxy resistance and estimation of radiation and conduction losses.

The experimental data was obtained at an angle of attack of 40 degrees and again showed a dramatic increase in heat transfer coefficient to about 200 percent above that in the wind tunnel. Thus, Test et al concluded that data correlations based on low turbulence intensity wind tunnel tests, such as those obtained by Sparrow's group (Ref.31-34), significantly underestimate the heat transfer due to wind flow in the natural environment.

Sturrock (Ref.38) undertook wind tunnel experiments to measure velocity profiles and convective heat transfer distributions around three-dimensional bluff bodies. The models consisted of 0.23 m and 0.30 m cubes mounted in a laminar flow wind tunnel. The heat meter system was provided by a strip of nichrome wire wrapped around the cube. The convection coefficient was determined from the power input to the nichrome. The heat transfer distribution was then measured by moving the strip along the face in 25 mm steps. The influence of the wind direction on the results was investigated by rotating the models through 180 degrees in 15 degrees increments.

Some of the conclusions arising from Sturrock's work (Ref.38) are summarized by Cole and Sturrock (Ref.39) in their comprehensive review paper. The local convective heat transfer coefficients measured on a particular face of the cube were different from those measured on flat plates and also were significantly dependent upon the orientation of that face relative to the wind direction. The highest convection coefficients were found to occur on the surfaces whose normal made an angle of 30 degrees to the wind direction. Higher values were observed near the edges of the surfaces. The convection coefficients on leeward surfaces were found to be about half those on windward surfaces. Finally, it was concluded that the average convection

coefficient on a exposed face of a 0.23 m cube was a linear function of the wind speed over the range 3-10 m s^{-1}, according to the following relationship

$$h_c = 5.7\ V + 23 \qquad (2.22)$$

Sturrock (Ref.38) also made nocturnal field measurements of the convective heat transfer at a limited number of points on the external surface of a 26 m high tower block under natural conditions. The field values were different from those obtained in his previous wind tunnel investigation. Two new relationships were then suggested

$$h_c = 5.7\ V + 11.4 \qquad (2.23)$$

for windward surfaces, and

$$h_c = 5.7\ V \qquad (2.24)$$

for leeward surfaces.Where V is the wind speed measured above the roof surface by a mast-mounted anemometer.

A series of tests to determine the convective heat transfer coefficients on a full-scale building was undertaken by Ito, Kimura and Oka (Ref.40). It is worth describing this work in some detail since it appears to be one of the most comprehensive study availabe at present. The building under test was a 6 storey office block having an open L-shaped plan, located in Tokyo. The measurement technique used was based on two identical heat flow meter panels mounted side by side on the outside surface of the building.They were maintained at slightly different temperatures, so that the convective heat transfer coefficient could be obtained from the difference in heat flow measured at the two flow meter panels. The speed and direction of incident wind was measured at a point 8 m above roof level, and the air flow velocity was taken 0.30 m from the panel surface. These values were read by sampling at 1 minute intervals. A total of four pairs of readings were taken; at the centre and edge of the third, fourth, fifth and sixth floors of the building, respectively. The measurements were made during winter nights in order to avoid the effect of solar radiation. Under this condition the outdoor air temperature above the roof and near the wall were similar. It was also attempted to obtain values of convective heat transfer coefficients for summer conditions, when the effect of buoyancy-driven convection is important especially on calm but sunny days. Unfortunately satisfactory results were not obtained because of the frequent and sudden changes in solar radiation.

Although the results presented by Ito et al contain a fairly high degree of scatter, they show that the convective heat transfer coefficient tends to vary linearly with air flow velocity near the wall and that this variation is independent of wind direction. It was also observed that the air flow velocity near the wall was approximately 1/3 to 1/5 of the wind speed above building for windward surfaces, when the wind speed was greater than 2 m s^{-1}. On leeward surfaces, or for windward surfaces with wind speed less than 2 m s^{-1}, the local flow velocity was found to be about 0.5 m s^{-1}. Consequently, Ito et al recommended that the estimation of the convective heat transfer should be broken down into two different steps. In the first step, the velocity near the surface of interest should be calculated taking into account the relative wind direction to the surface and the surface location on the building. In the second step an appropriate relationship between convective heat transfer and the air flow velocity near the surface should be used.

Ito et al proposed the following relation for this purpose:

$$h_c = 18.6\ V_o^{0.605} \qquad (2.25)$$

However, their data also suggests that the heat transfer coefficient increases with height and towards the edge of the building, for a given value of wind speed.

Burns (Ref.41) has summarized results of the wind tunnel and field measurements reported in his thesis (Ref.42). These experiments were made on flat plates, cubes and on a small building. Details of the experimental apparatus and procedure are given by Burns (Ref.42).

The experimental data from the cubes tests are presented for three turbulence levels (0, 4 and 10%), and for wind directions ranging from -90 to 90 degrees (zero degree corresponds to a face being parallel to the direction of the mean flow).The highest convective heat transfer coefficient was found to occur at an incident angle of 20 degrees for all turbulence levels involved. For windward surfaces (incidence angle in between 90 and -10 degrees) the convection coefficients tended to increase significantly with increasing turbulence level and also to vary with changing wind direction. For leeward surfaces (incidence angle in between -10 and -90 degrees) the measured convection coefficients showed little variation with either incidence angle or turbulence intensity.

The full scale test was undertaken on a small glass-clad building (4.1x3.6x2 m high) situated on the flat roof of a 4 storey building and exposed to the prevailing winds. The heat transfer coefficients measured for three different sets of wind velocity, turbulence intensity and wind direction [(5.01m s^{-1},16.5%,185°), (7.98m s^{-1},17.9%,275°),(6.62m s^{-1},15.7%,252°)] were graphically presented. The average convective heat transfer coefficients for all three wind conditions were about 30 W m^{-2} °K^{-1} and 10 W m^{-2} °K^{-1} on windward and leeward surfaces, respectively.

Kelnhofer and Thomas (Ref.43) conducted experiments to determine local and average forced convective heat transfer coefficients on the exterior surface of a sharp-edged cube (127 mm side) mounted on the floor of a wind tunnel. Tests were undertaken in a low turbulence uniform flow and a high turbulence shear flow for a range of Reynolds number and flow directions. The effects of a single neighbouring model were also investigated.

The wind tunnel provided uniform flow with a turbulence intensity of 0.1%. The shear flow employed represented a theoretical 1/3-power velocity profile. This profile is similar to the profile associated with the atmospheric boundary layer flow over an urban area. The turbulence levels recorded during the shear flow tests varied from 0 to 10%.

For both uniform and shear flow condition the highest convective heat transfer coefficients occurred near the upper and side edges. The lowest values occurred near the flow stagnation region. The ratios of maximum to minimum heat transfer coefficients on the windward face for both uniform and shear flow condition were 1.88 and 1.73, respectively. On the leeward face the rate of heat transfer was nearly uniform and approximately 30% lower than on the other faces. Although local values of heat transfer coefficient varied with wind direction, the average value for the cube was practically independent of wind direction. It was also found that the cube average heat transfer coefficient was reduced by 20% in uniform flow compared to shear flow.

Sharples (Ref.44,45) undertook the most recent experimental work on convective heat transfer on a full-scale buiding. He made nocturnal field measurements on the 18 storey (20x36x78 m high) Arts Tower at Sheffield University,UK. The method used for measuring the convective heat transfer coefficients was similar to that employed by Ito et al (Ref.40). Heat transfer data were taken at central sites, on the 6th, 14th and 18th floors and at an edge site on the 18th floor. All data (except the weather station wind speed) were recorded simultaneously by sampling at 1 minute intervals for a 12 hour period.

The heat transfer coefficients were correlated with wind speeds recorded 1 m from the building's surface, 6 m above the roof and at a local weather station. The relationship between the convective heat transfer coefficient and all three wind speeds considered were analysed using least-squares regression analysis techniques. For both windward and leeward surfaces data were found to be satisfactorily represented by a linear function.

Sharples found that the heat transfer coefficients on windward surfaces for a given wind speed increases with height and towards the edge of the building, whereas only small variations were observed on leeward facades. He found that the relationship between the convective heat transfer coefficient and the near-surface air flow velocity was dependent on the relative wind direction, contrary to the findings of Ito et al (Ref.40). Sharples therefore proposed a simple algorithm for calculating the convection coefficient for the worst case(18th floor edge site) in which the local air flow velocity is

first determined for either the windward or leeward surfaces, and then the transfer coefficient is evaluated from this velocity. The local, near-surface air velocity was given by:

$$V_o = 1.8\ V_{10} + 0.2 \qquad (2.26)$$

for windward surfaces, and

$$V_o = 0.2\ V_{10} + 1.7 \qquad (2.27)$$

for leeward surfaces. The convective heat transfer coefficient on either surface is then determined from the simple relation:

$$h_c = 1.7\ V_o + 5.1 \qquad (2.28)$$

2.3.4 - Assessment of the previous forced convective heat transfer relationships

The purpose of the above review was to evaluate existing relationships for the convective heat exchange at the external surfaces of the building envelope. The research work that has previously been carried out in this field may be divided into two main types:

a) the earlier wind tunnel experiments dealing with parallel flow past a flat plate; and

b) wind tunnel experiments and field measurements dealing with bluff objects.

The results from the first group do not appear to be satisfactory for quantifying the energy flows arising at the external surfaces of three-dimensional bluff bodies submerged in the atmospheric boundary layer, despite the fact that they have persisted in design manuals for many years. The fundamental flat plate relationships used by British (Ref.23) and American (Ref.4) design guides contain no allowance for surface length, wind direction, turbulence intensity of flow, separation of flow or surface element location on a facade.

Convective heat transfer depends on the characteristic Reynolds number, the free-stream turbulence intensity, and ground interaction effects, induced when a a building is within the atmospheric boundary-layer. Wind tunnel measurements can account for Reynolds number scaling, but do not appear to simulate the other two factors adequately. The achievement of complete dynamic similarity between model and full-scale is therefore very difficult to accomplish.

The relationships for predicting the convection coefficient derived from field measurement studies display large disparities. It is difficult to ascertain whether these disagreements are the result of differences instrumentation and calculation methods, or simply reflect a variability due to the very small number of systematic studies that have been made.

All field measurements studies identified the dependence of the convection coefficient upon the wind velocity profile around the building, drawing a distincton between windward and leeward facing surfaces. They also indicate that the largest heat transfer coefficients are likely to be found on corner sites at the highest level of windward building facades. On the other hand, the convective heat transfer coefficients on leeward surfaces were found to be fairly constant over the entire facade.

In the final analysis none of the previous experimental studies provide, by themselves a reliable base for estimating convective heat transfer rates from buildings.

A satisfactory mathematical solution to the problem is also not feasible due to the complicate wind patterns around buildings. Cermack (Ref.46) classifies the flow problem as one that involves the non-linear action of nonhomogeneous, nonuniforn, turbulent approach flow with three-dimensional turbulent boundary layers and separated flows over the body. The approach flow profile varies with location, i.e., whether the terrain is open country, on the edge of a city or in the heart of the city. Furthermore, local velocity patterns may be strongly influenced by other bluff bodies nearby, such as buildings, trees or hills. In order to take account of these factors an intermediate-level model computer code (called the WIND-CHT program) was developed, and is described in section 2.6 below.

2.4 - CURRENT DESIGN STANDARDS

Having reviewed the previous studies concerned with wind-induced convective heat transfer from buildings, it is now possible to summarize the origins and recommendations found in the current design guides.

2.4.1 - CIBSE Guide

This guide (Ref.23) provides British archictects and engineers with a design procedure for handling external convection which can be briefly described. It recommends that the thermal resistance of the wall's exterior surface, R_o, be calculated from the following expression:

$$R_o = 1/(E\ h_r + h_c) \qquad (2.29)$$

It is assumed that the surface emissivity E, is about 0.9 for normal building materials and 0.05 for low emissivity surfaces. The radiative heat transfer coefficient h_r, is approximately equal to 5.7 and 4.6 W $m^{-2}\,°K^{-1}$ at mean temperatures of 20°C and 0°C, respectively. It is recommended that the convection coefficient h_c, is determined from Jurges' relationship (Ref.15).

$$h_c = 4.1\ V_{ro} + 5.8 \qquad (2.30)$$

where V_{ro} is the wind speed at roof level. The values for the contants in this expression are a compromise between those for rough and smooth surfaces originally suggested by Jurges (see section 2.3.2 above).

Three wind speeds are suggested in the guide that correspond with 'sheltered', 'normal' and 'severe' conditions. These velocities are 1, 3, and 9 m s^{-1} respectively, and the wind speed over walls is taken to be 2/3 of the roof value. The guide also gives typical locations where these three conditions might be found:

Sheltered:	Up to 3rd floor level in city centres
Normal:	Most suburban and country situations: 4th-8th floor levels in city centres
Severe:	Coastal situations:exposed or hilly sites: above 5th floor level for suburban and country sites:above 9th floor level for city centres.

2.4.2 - ASHRAE Guide

This guide presents Rowley's results (Ref.16) for a variety of building textures in a graphical form, without correlating his experimental data. However, the ASHRAE task group (Ref.47) suggested the following curve fits to Rowleys' data:

$$h_{cb} = 5.89\ V + 11.58 \text{ (stucco)} \qquad (2.31)$$

$$h_{cb} = 0.0284\ V^2 + 4.07\ V + 12.49 \text{ (brick and rough plaster)} \qquad (2.32)$$

$$h_{cb} = 4.19\ V + 10.78 \text{ (concrete)} \qquad (2.33)$$

$$h_{cb} = -0.0568\ V^2 + 4.0\ V + 8.23 \text{ (clear pine)} \qquad (2.34)$$

$$h_{cb} = 3.10\ V + 10.26 \quad \text{(smooth plaster)} \tag{2.35}$$

$$h_{cb} = -0.0355\ V^2 + 3.33\ V + 8.23 \quad \text{(glass)} \tag{2.36}$$

where h_{cb} represents the combined convective and radiative heat transfer coefficient. The ASHRAE handbook (Ref.4) states that under these measurement conditions the radiative component was approximately 4.0 W $m^{-2}\,°K^{-1}$. Rowley's data is displayed graphically in Fig.2.1.

2.4.3 - ASHRAE task group

The ASHRAE task group (Ref.47), developed a simple algorithm for calculating the convective heat transfer coefficient which is based on the field measurements of Ito et al (Ref.40). Firstly the angle of attack relative to the building facade, θ, is calculated by the following expression:

$$\Theta = \xi + 180 - \Psi \tag{2.37}$$

where ξ is the wall azimuth angle (positive degrees westwards from South and negative eastward) and Ψ is the wind direction (angle measured clockwise from North). When the absolute value of Θ, from equation (2.37), is greater than 180 degrees, the following correction is applied:

$$\Theta = 360 - |\Theta| \tag{2.38}$$

Secondly, the near-surface air velocity is determined for either the windward or leeward surfaces. For windward surfaces ($\theta < 90°$) it is given by:

$$V_o = 0.25\ V_{10} \tag{2.39}$$

for wind speeds greater than 2 m s^{-1}, and

$$V_o = 0.5 \tag{2.40}$$

for wind speeds less than 2 m s^{-1}. For leeward surfaces ($\theta \geq 90°$) the near-surface air velocity is computed by:

$$V_o = 0.3 + 0.05\ V_{10} \tag{2.41}$$

Finally, the convective heat transfer coefficient on either surface is computed from the simple equation:

$$h_c = 18.6\ V_o^{0.605} \qquad (2.42)$$

A comparison between the algorithms presented in this section is illustrated in Fig.2.2.

2.5 - THE WIND AND ITS SIMULATION

2.5.1 - Air flow around buildings

The pattern of air flow around a building depends on the characteristics of the approaching wind, on the immediate surroundings, and on the size and shape of the building itself. Buildings of even moderately complex shape may generate flow patterns too complicate to generalize, thus only flow patterns around buildings of simple rectangular cross-section will be considered.

Fig.2.3, which is an illustration based on wind tunnel results obtained by Penwarden and Wise (Ref.48), shows how a low building upwind of a tall building influences the pattern of fluid flow. When the angle of attack relative to the windward surface is equal to zero a stagnation zone exists on this face at (C). Flow accelerates outwards from this region in all directions. The downward flow experiences an adverse pressure gradient and flow separation occurs at the front base. Some of the air deflected downwards forms a vortex (B), which then stretches out sideways and wraps around the building in a characteristic horseshoe shape. The flow separates at the sharp edges so that the back face, roof and sides are inside the recirculating flow region. If the building has sufficient depth in the direction of the flow, the wind flow will reattach to the building and generate two distinct regions of separated flow; on the building and in its wake.

2.5.2 - The structure and behaviour of the natural wind

The atmospheric boundary layer is the lower region of the atmosphere from which momentum is extracted in order to compensate for the shear stress at the earth's surface. The wind developed in this region varies widely in structure because of strong dependence upon topography, surface roughness features and the possible occurence of thermal stratification. Above the layer of influence by surface shear

stress, the air moves purely under the influence of pressure gradients, which are caused by the differential heating of the earth´s surface by the Sun, and attains what is known as the gradient velocity, Vg. The height at which the gradient velocity is attained will be denoted by Zg and is generally of the order of 300-600 m.

The atmospheric boundary layer can be broken down into at least two regions of different properties. Close to the surface the variation of shear stress with height is approximately constant. This defines the ´surface layer´ which extends from the ground up to roughly 30-100 metres depending upon the terrain. Bounded at the bottom by the surface layer and extending to the top of the atmospheric boundary layer is the ´Eckman layer´. In this layer the shear stress falls off from the constant value of the surface layer to the practically zero value in the free atmosphere.

Several formulae have been suggested to describe the variation of the wind velocity with height. One of them is the logarithmic profile obtained by utilizing the flat-plate boundary layer ´mixing length´ hypothesis of Prandtl and von Karman,

$$V_z/Vf = [\ln(Z/Zo)]/K \qquad (2.43)$$

where V_z is the mean velocity at height Z, Vf is the socalled friction velocity, Zo the roughness length and K is the von Karman´s constant (≈ 0.4). The friction velocity is defined by:

$$Vf = (\tau/\rho)^{1/2} \qquad (2.44)$$

where τ is the shear stress at the surface and ρ the air density.

In the case of flow over urban areas (large roughness elements) the velocity profile undergoes a ground level displacement d, therefore equation (2.43) should be modified as follows

$$V_z/Vf = \{\ln[(Z-d)/Zo]\}/K \qquad (2.45)$$

Unfortunatelly it was observed by Counihan (Ref.50), in his comprehensive review paper, that the ´logarithmic law´ is only applicable to the surface layer. This fact was also observed by Davenport (Ref.51) who commented that although the logarithmic profile agrees well with measurements in the surface layer over natural surfaces of roughness varying between smooth mud flats, water and thick grass, it has not yet been demonstrated experimentally to be representative of urban areas. Therefore the reliability of the log-law in providing numerical prediction of the wind speed profile does not appear to be greater than the simple power-law profile given by:

$$V_z / Vg = (Z/Zg)^{\alpha} \qquad (2.46)$$

where α is a constant which depends on the roughness of the ground.

To determine values of α and Zg for different surfaces, Davenport (Ref.51) collected together mean wind profile data for a wide range of countries and terrains and suggested the representative values given in Table 2.1 and displayed graphically in Fig.2.4. The profiles for three types of terrain: open country, a suburban area and an urban centre are shown in Fig.2.5.

Tab.2.1 - Wind profile parameters for three types of Terrain.
[After Davenport (Ref.51)]

TERRAIN	Zg (m)	α
Flat open country	275	0.16
Suburban area	400	0.28
City centre	500	0.40

The main objection to the power-law approach for defining the mean wind profile is its dependence on the non-fundamental parameters α and Zg both of which have a somewhat nebulous physical meaning. The justification for adopting this approach are firstly its simplicity and secondly the fact that both α and Zg can be systematically related to the fundamental parameters defining the roughness of a surface and its effects, principally Zo and Vf.

It should be pointed out that in this section it was assumed that the surface of the ground was uniform for a sufficient distance upwind for steady state conditions to be established. This is obviously not always the case. This problem has however been treated by Taylor (Ref.52) who determined approximately the fetch distance necessary for the new wind profile to be established up to a given height after a change in roughness. He concluded that the ratio between the fetch distance and the height is not constant, but varies with the height and amount of change in roughness. He also suggested, as a rough rule, that a fetch distance of about 100-150 times the height should be adequate for most practical situations.

2.6 - THE WIND-CHT PROGRAM

In the development of this intermediate-level code, the computer has been employed to generalise available data correlations for the individual flow regimes that prevail around buildings, such as the stagnation, boundary layer and separated flow regimes. The way in which the program has been developed is outlined below.

2.6.1 - The velocity scale

Meteorological measurements are usually made in open terrain (e.g. airports) while residential buildings are more commonly located in sheltered areas. The wind speed must therefore be adjusted to take into account the fact that the wind profile changes in accordance with the type of terrain. To calculate the wind speed at one site from measured data at another site, it is first necessary to adopt a relationship that adequately represents the velocity profile. The power-law due to Davenport (Ref.51) has been chosen for this purpose. Assuming that the gradient velocity,Vg, is independent of the terrain type, the wind speed at the desired site can be calculated from the relationship below:

$$V_z = (Z/Z')\,(Zg'/Zg)\,V_z' \qquad (2.47)$$

where the unprimed quantities refer to the desired site and the primed quantities refer to the wind measurement site.

The velocity scale used in the WIND-CHT program to determine the appropriate Reynolds number, is the integral value obtained from the wind profile over the area of the building surface of interest. This is more logical than the common, but arbitrary, practice of adopting the wind speed at 10 metres above ground as the velocity scale. Thus,

$$Vav = \int_{z_1}^{z_2} V\,dZ \;/\; \int_{z_1}^{z_2} dZ \qquad (2.48)$$

where Z1(Z2) is the distance between the ground and room ceiling (floor) levels. Substituting equation (2.47) into equation (2.48) and integrating, yields:

$$Vav = Vg\{(Z2^{\alpha+1} - Z1^{\alpha+1})/[Zg^{\alpha}\,(Z2-Z1)\,(\alpha+1)]\} \qquad (2.49)$$

2.6.2 - The indexation of the surface elements

Each surface element is characterized by an index, η, according to its orientation with respect to the wind direction. A surface is identified as windward (η=3), leeward (η=2) or parallel (η=1) when the absolute value of θ, obtained from equations (2.37) and (2.38) is respectively less than, greater than or equal to 90 degrees. For leeward surfaces the following correction for the angle of attack is employed:

$$|\theta| = |\theta| - 180 \qquad (2.50)$$

2.6.3 - The convective heat transfer relationships

The idea of the WIND-CHT program is to split out the different surfaces of the building and to treat them separately from a heat transfer point of view. Five different types of flow are considered; (i)typical boundary layer flow, (ii)completely separated flow, (iii)stagnation flow, (iv)buoyancy-driven convection flow, and (v)combined flow.

(i) Typical boundary layer flow (η=1)

In this type of flow an interpolation formula similar to that employed by Alamdari and Hammond (Ref.12) was used to generate from the standard correlations [eq.(2.5),(2.9)], an expression for the side-wall boundary layer which is valid for laminar, transitional and turbulent flow. This formula has the following form,

$$Nu_\rho = \{(0.664\ Re^{1/2}\ Pr^{1/3})^6 + [(0.036\ Re^{4/5} - 835)Pr^{1/3}]^6\}^{1/6} \qquad (2.51)$$

This equation above is valid for $5x10^5 < Re \leq 10^8$. For lower Reynolds number only the first part of the equation, corresponding to the laminar flow, is employed.

ii) Completely separated flow (η=2)

The free stream turbulence intensity has little effect upon heat transfer at the rear stagnation point of a bluff body (Ref.29,41,42), and consequently the convective heat transfer is practically constant in the lee of the building (Ref.40,43-45). The Nusselt number dependence is therefore satisfactorily correlated by Sogin's relationship

$$Nu_s = 0.20\ Re^{2/3} \qquad (2.52)$$

iii) Stagnation flow (η=3)

Unfortunately, laboratory-scale correlations for the stagnation flow, such as that proposed by Sparrow et al (Ref.32), were found to be unrepresentative of the, albeit very limited, field measurements (see Figure 2.6). This is probably due to the combined influence of high wind turbulence intensity, and building ground interaction effects (Ref.35-37,41-43). Thus, a more general functional

relationship might be expected to take the form

$$Nu_{st} = f(Re,Pr,Tu,S) \qquad (2.53)$$

where Tu is the turbulence intensity and S the turbulence scale. No such relationship has so far been obtained from the earlier experimental studies and therefore, a new power-law correlation was developed by Grandrille, Hammond and Melo (Ref.17) from the field measurements on office buildings by Ito et al (Ref.40) and by Sharples (Ref.44). These data sets display a wider variation between themselves than would have been desired, but they are the only suitable available. Sturrock's field measurements (Ref.38) were disregarded since his results are unrealistically large due to the very small size and high working temperatures of his heating elements (Ref.45).

The present correlation was obtained using the least squares regression analysis for all the available data of Ito and Sharples. Sharples experiment (Ref.44) provided several pairs of data (h_c, V_{10}) for different sites on the building facade. An urban terrain (α=0.4, Zg=500m) was assumed for the purposes of developing the correlation. The meteorological wind velocity recorded at 10 m above ground was then related to the average wind velocity over the facade, according to Davenport's power-law profile,

$$Vav = 0.2844\ V_{10}\ (Z2^{1.4} - Z1^{1.4})/(Z2-Z1) \qquad (2.54)$$

Using this average velocity the corresponding Reynolds number was calculated

$$Re = Vav\ L/\nu \qquad (2.55)$$

where L is a length scale that corresponds to the socalled hydraulics diameter used in fluid dynamic, and defined by:

$$L = 4\ A/P \qquad (2.56)$$

The corresponding Nusselt number was then defined by:

$$Nu = h_c L/k \qquad (2.57)$$

In this way from each pair (h_c, V_{10}) it was possible to calculate a pair (Nu,Re). Equation (2.58) was then obtained by applying the least squares fit method .

$$\log Nu = -1.6927 + 0.7929 \log Re \qquad (2.58)$$

An urban terrain was also assumed for Ito's experiment (Ref.40). As in this case the meteorological wind velocity has been recorded at approximately 28 metres above ground, the average wind velocity may be expressed by

$$Vav = 0.1844\ V_{28}\ (Z2^{4.4} - Z1^{1.4})/(Z2-Z1) \qquad (2.59)$$

Following the same procedure used for Sharples' experimental data, the following relationship was then obtained

$$\log Nu = 0.0144 + 0.5851 \log Re \qquad (2.60)$$

An average between equation (2.58) and (2.60) yielded

$$\log Nu = -0.8393 + 0.6890 \log Re \qquad (2.61)$$

or

$$Nu_{st} = 0.14\ Re^{0.69} \qquad (2.62)$$

where all the thermal properties are evaluated at a film temperature of 15°C, typical of the built environment.

Figure 2.6 shows a comparison between the present correlating equation (2.62) and the field measurements made by Ito et al (Ref.40), Sharples (Ref.44) and Burns (Ref.42). Burns' data were not employed when developing equation (2.62) due to their small number. However, they seen to be adequately distributed along the straight line, shown in Figure 2.6, corresponding to the present correlating equation.

iv) Buoyancy-driven convection flow

In the case of buoyancy-driven convection, the heat transfer coefficient is itself a function of the temperature difference, as well as the length of the surface and the physical properties of the convected fluid. Dimensional analysis may be employed to correlate experimental data reflecting this dependence in terms of dimensionless parameters

$$Nu = B\ Ra^{n} \qquad (2.63)$$

The exponent n is found to be about 1/4 for low Rayleigh numbers typically in the range $10^4<Ra<10^6$, which correspond to laminar flow induced by short surface lenghts and/or small temperature differences. Conversely for $Ra>10^{10}$ transition to turbulent flow occurs, and n asymptotes to a value of 1/3. Thus, conventional practice is to calculate the heat transfer coefficient via data correlations of the form of equation (2.63), using an exponent of 1/4 for Rayleigh numbers less than about 10^8 and 1/3 otherwise. This two-part correlation, implying an abrupt transition, has been adopted in the CIBSE guide (Ref.5). However, the sudden change in the exponent,n, may induce numerical instability when used in conjunction with some of the new generation of dynamic building thermal models (Ref.12).

Improved data correlations for buoyancy-driven convection from buildings surfaces have been derived by Alamdari and Hammond (Ref.12). These correlating equations provide a smooth fit to data across the full range of laminar, transitional and turbulent airflows, in contrast to the 'standard' two-part model. These improved data correlations for vertical and horizontal surfaces respectively are:

$$Nu_b = [(0.58\ Ra^{1/4})^6 + (0.11\ Ra^{1/3})^6]^{1/6} \qquad (2.64)$$

and

$$Nu_b = [(0.54\ Ra^{1/4})^6 + (0.14\ Ra^{1/3})^6]^{1/6} \qquad (2.65)$$

v) Combined flow

The final component of the WIND-CHT program is the weighting function used to interpolate convection coefficients when the wind direction is non-orthogonal to the building surfaces.

The approach adopted for inclusion of the wind direction was to combine the relevant correlation in such a way that, the limiting conditions are satisfied. Thus when the angle of attack relative to the oncoming flow (θ) is equal to zero, only stagnation or separated flow's correlation was considered. Conversely when θ is equal to 90 ,only the parallel flow was considered. When θ lay between 0 and 90 degrees , an interpolation between the two limiting conditions is employed. The form of the Nusselt number relation for the combined flow suggested by Grandrille, Hammond and Melo (Ref.17) is:

$$Nu_f = \phi\ Nu_{s/st} + (1-\phi)Nu_p \qquad (2.66)$$

where ϕ is a weighting function with the following boundary conditions,

$$\emptyset = 1 \; ; \quad \text{when } \theta = 0^{\circ}$$

$$\emptyset = 0 \; ; \quad \text{when } \theta = 90^{\circ}$$

A simple cosine square relation was adopted for the weighting function (Ref.17), as this gave a plausible variation between the various combinations of the pure flows, in the absence of reliable field measurements. Thus equation (2.66) was reduced to

$$Nu_f = \cos^2\theta \; Nu_{s/st} + (1-\cos^2\theta) Nu_p \qquad (2.67)$$

Finally, in accordance to Siebers et al (Ref.53), a geometric mean of the buoyancy-driven and forced convective heat transfer coefficient was employed when mixed convection prevailed, i.e.,

$$Nu = (Nu_f^3 + Nu_b^3)^{1/3} \qquad (2.68)$$

Figure 2.7 shows a isometric view of the convective heat transfer coefficient as a function of the wind velocity and angle of attack for a vertical windward surface (5.0x3.0 m high) at ground level an located in an urban area, calculated using the WIND-CHT program.

The wind velocity for this and for all subsequent figures, in this chapter, is the local velocity recorded at the standard height of 10 metres above the ground.

2.6.4 - Comparisons with field measurement data

The capabilities of the WIND-CHT program are illustrated by Figures 2.8 to 2.11, where its computations for the city centre multi storey Arts Building at Sheffield University are compared with Sharples' data (Ref.44). The WIND-CHT program yields only the average heat transfer coefficient on the facade, which in this particular case is 36 metres long. The computations are therefore considerably higher than the experimental results taken at the mid-position and conversely lower than those taken at the edge of the facade.

Figure 2.12 shows a comparison between the WIND-CHT program computations and the data correlations recommended in the CIBSE guide (Ref.23) and by the ASHRAE task group (Ref.47). The experimental data set is a combination of measurements obtained by Sharples (Ref.44) at the edge and in the middle of each test facade. These comparisons demonstrate the ability of the WIND-CHT code to account for the

influence of building height relative to that of the atmospheric boundary layer. Unfortunately, the field measurements necessary to illustrate its capabilities for simulating the effect of wind direction upon the heat transfer from individual surfaces of a building are currently not available.

2.7 - CONCLUSIONS

The computations of the WIND-CHT program correspond well with experimental data obtained from real buildings. It appears to offer the best prospect for meeting the requirements of the new generation of dynamic building thermal models in terms of accuracy, economy and use friendliness. However, it should be pointed out that such a program in not able to model, in all details, fluid flow conditions in the outdoor environment such as unsteadiness, turbulence level and scale, and directionality due to special features in the surrounding.

Consequently, the program can only approximate any particular building application. Despite these reservations the information provided by the program serves as a valuable guide to design.

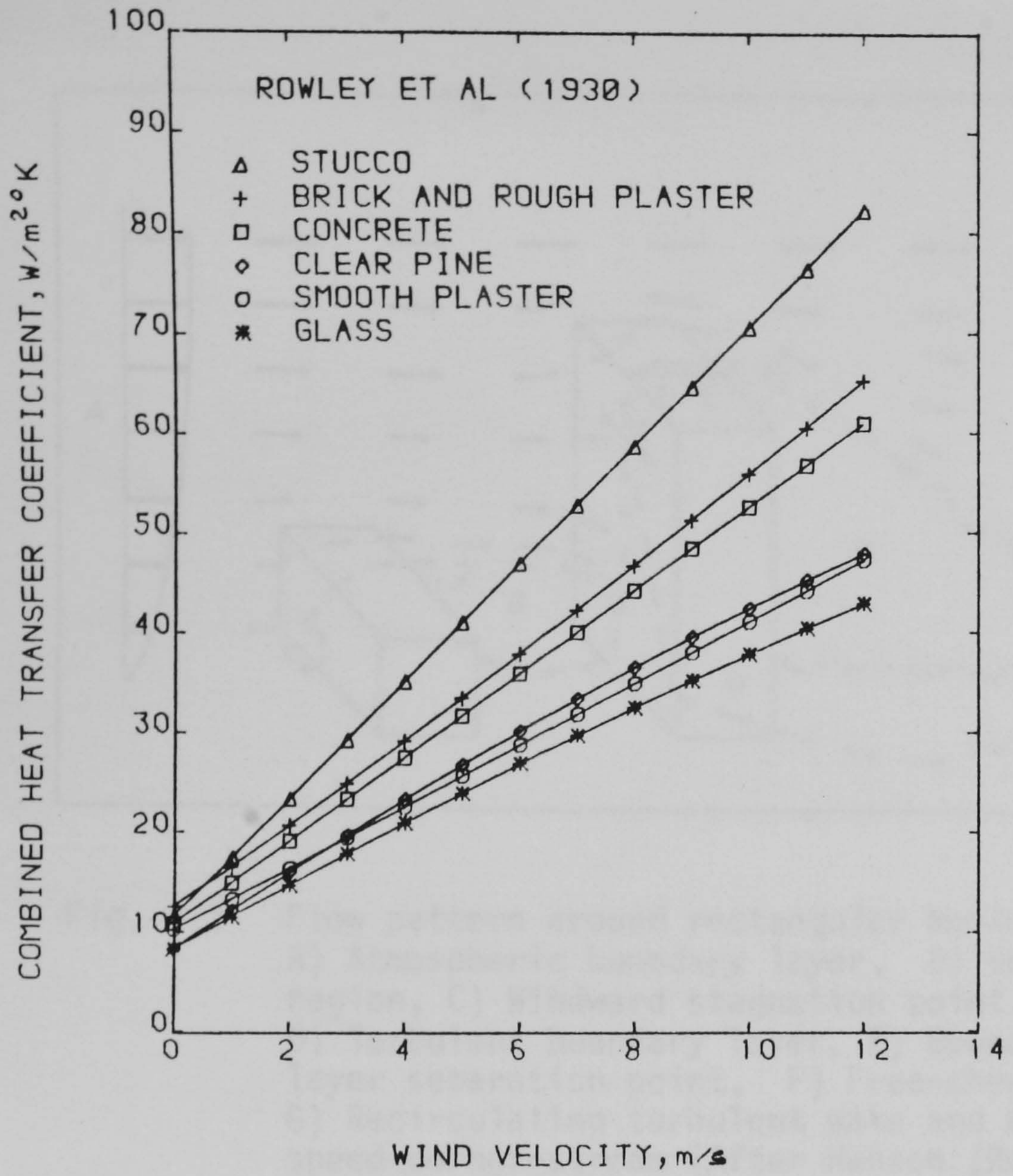

Fig. 2.1 Surface heat transfer as a function of wind speed

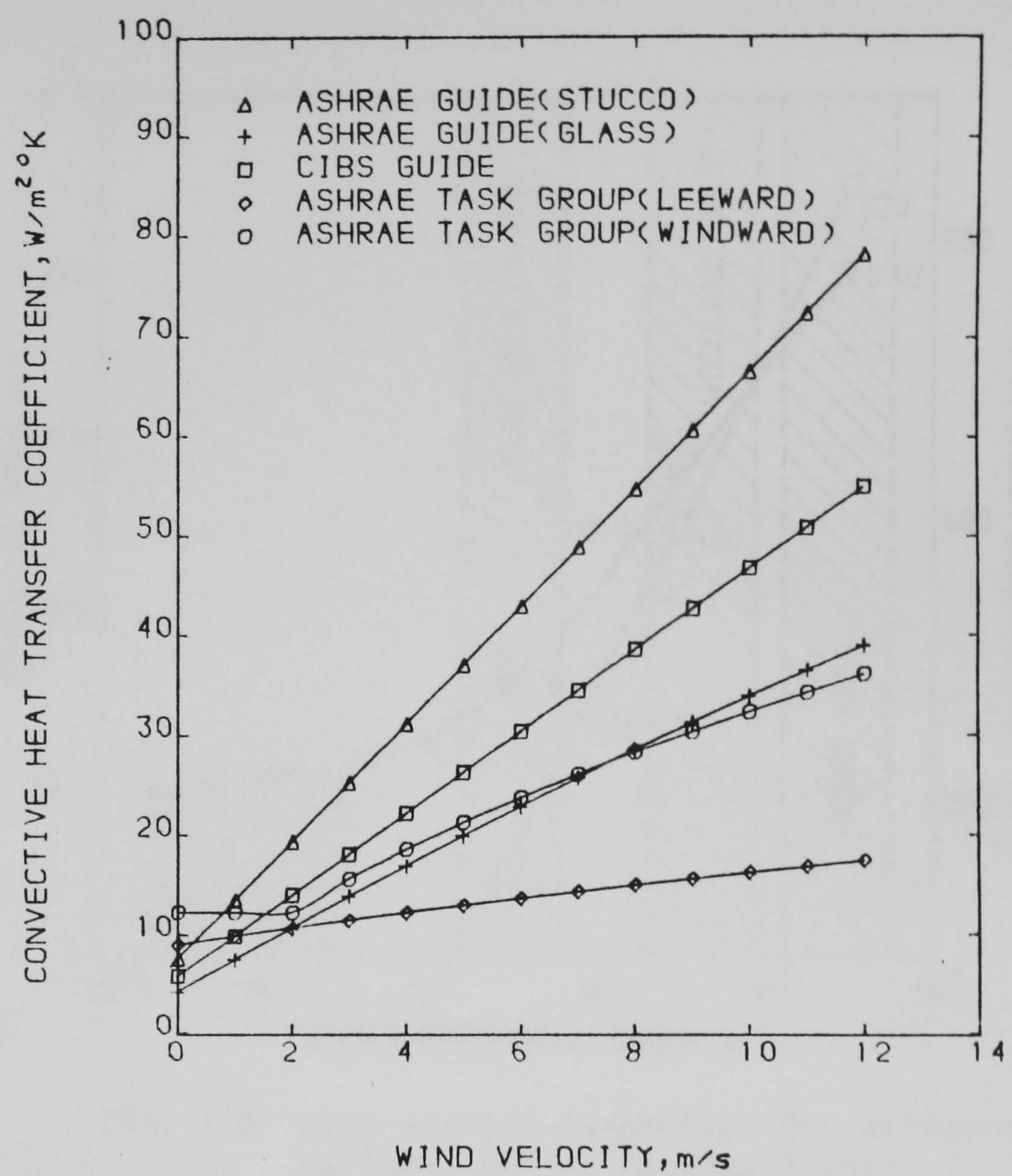

Fig. 2.2 Comparison between guide recommendations for the convective heat transfer coefficient on buildings' facades

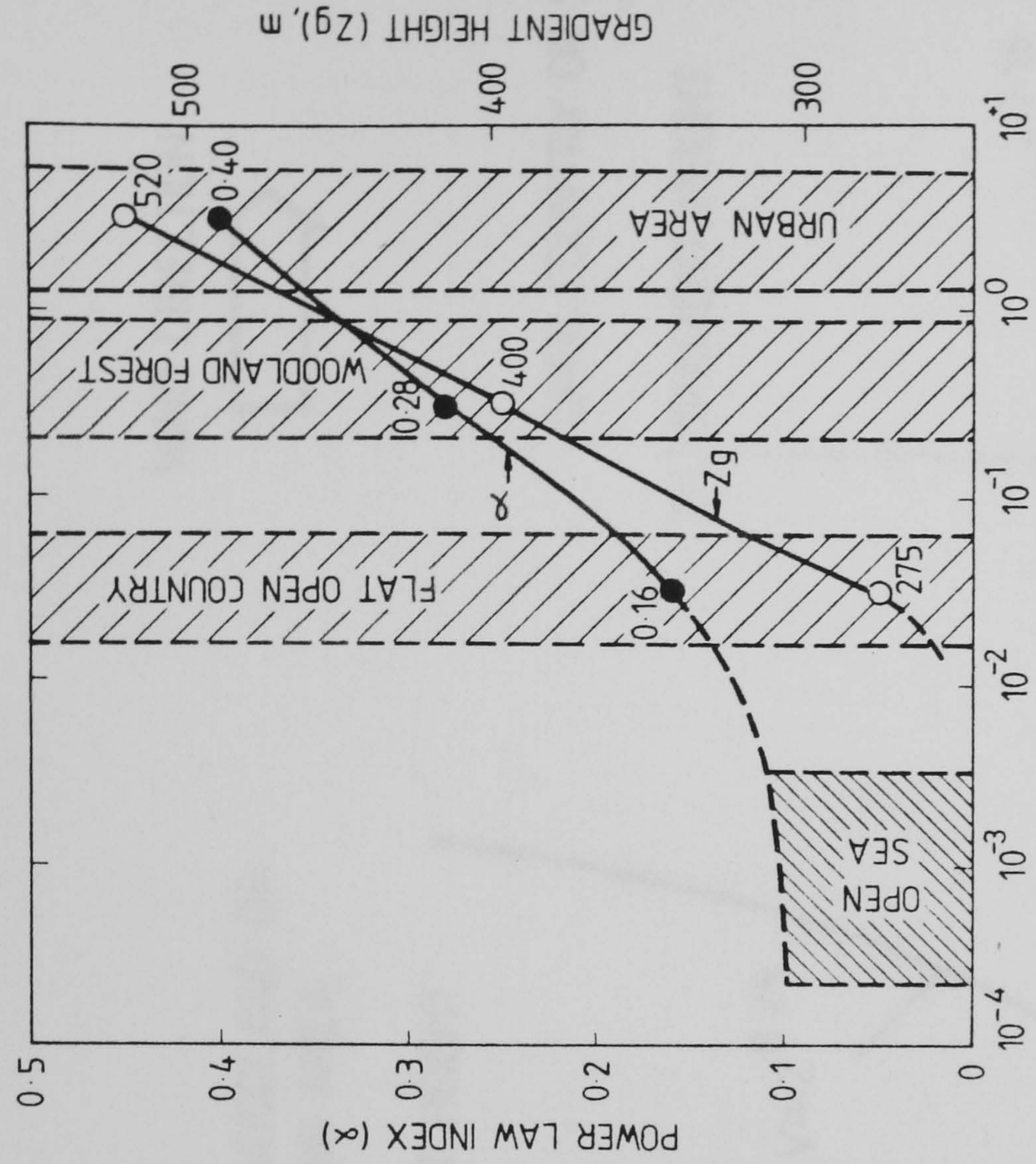

Fig. 2.4 Wind profile parameters for different surfaces {After Davenport (Ref. 51)}

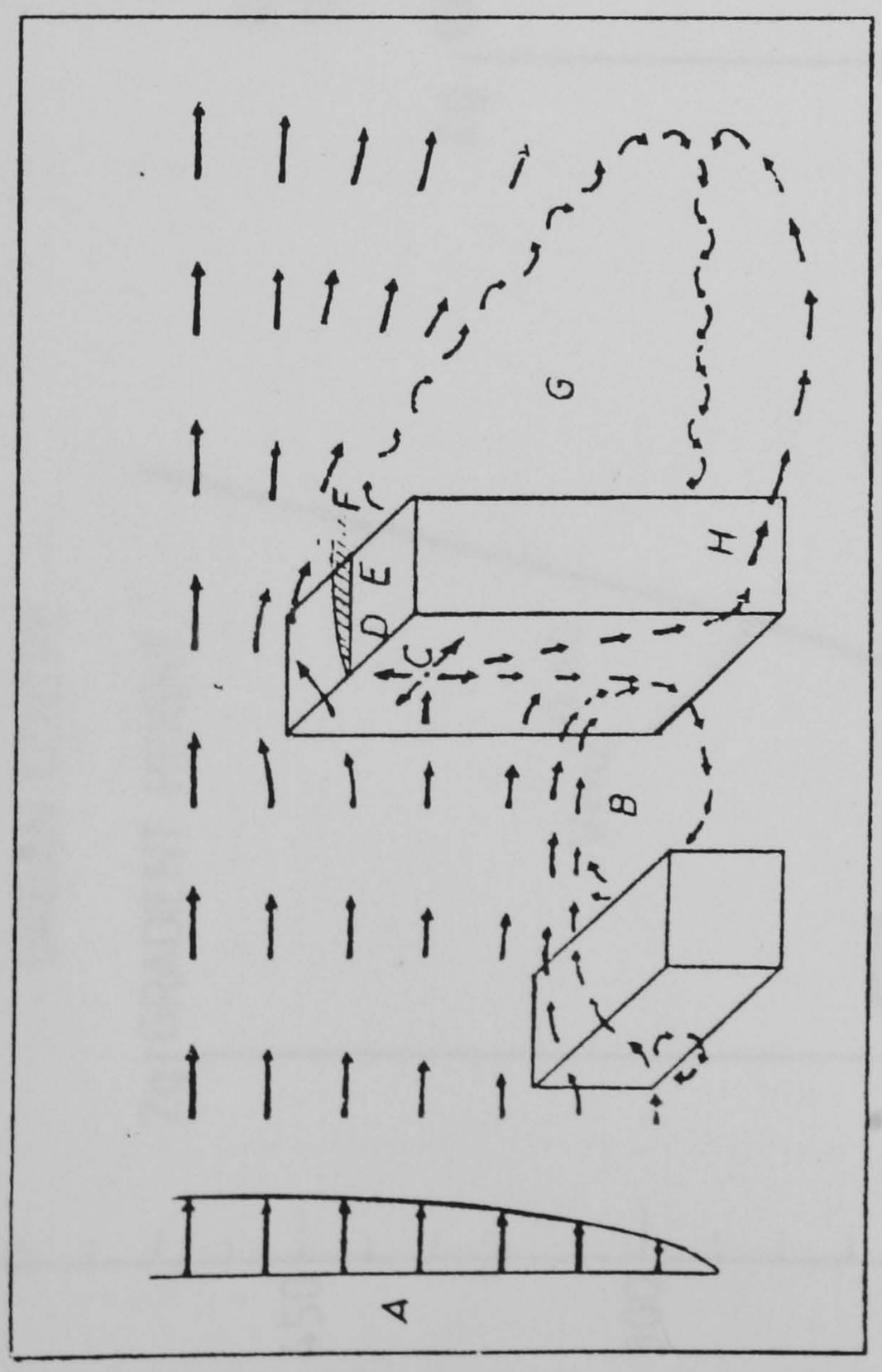

Fig. 2.3 Flow pattern around rectangular buildings: A) Atmospheric boundary layer, B) Vortex region, C) Windward stagnation point, D) Turbulent boundary layer, E) Boundary-layer separation point, F) Free-shear layer, G) Recirculating turbulent wake and H) High speed corner-stream {After Hanson (Ref. 49)}

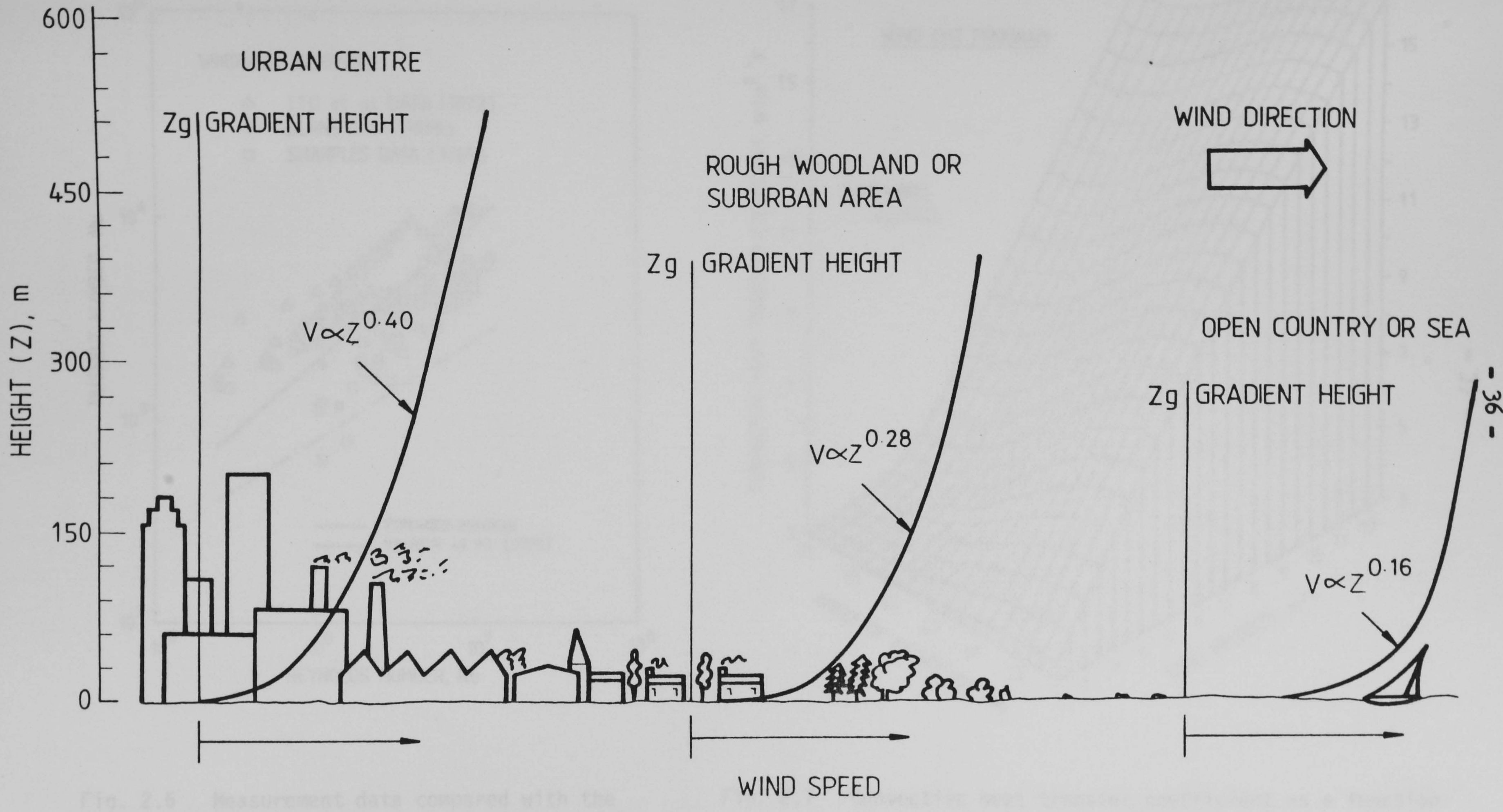

Fig. 2.5 Mean wind velocity profiles over terrains of differing roughness {After Davenport (Ref. 51)}

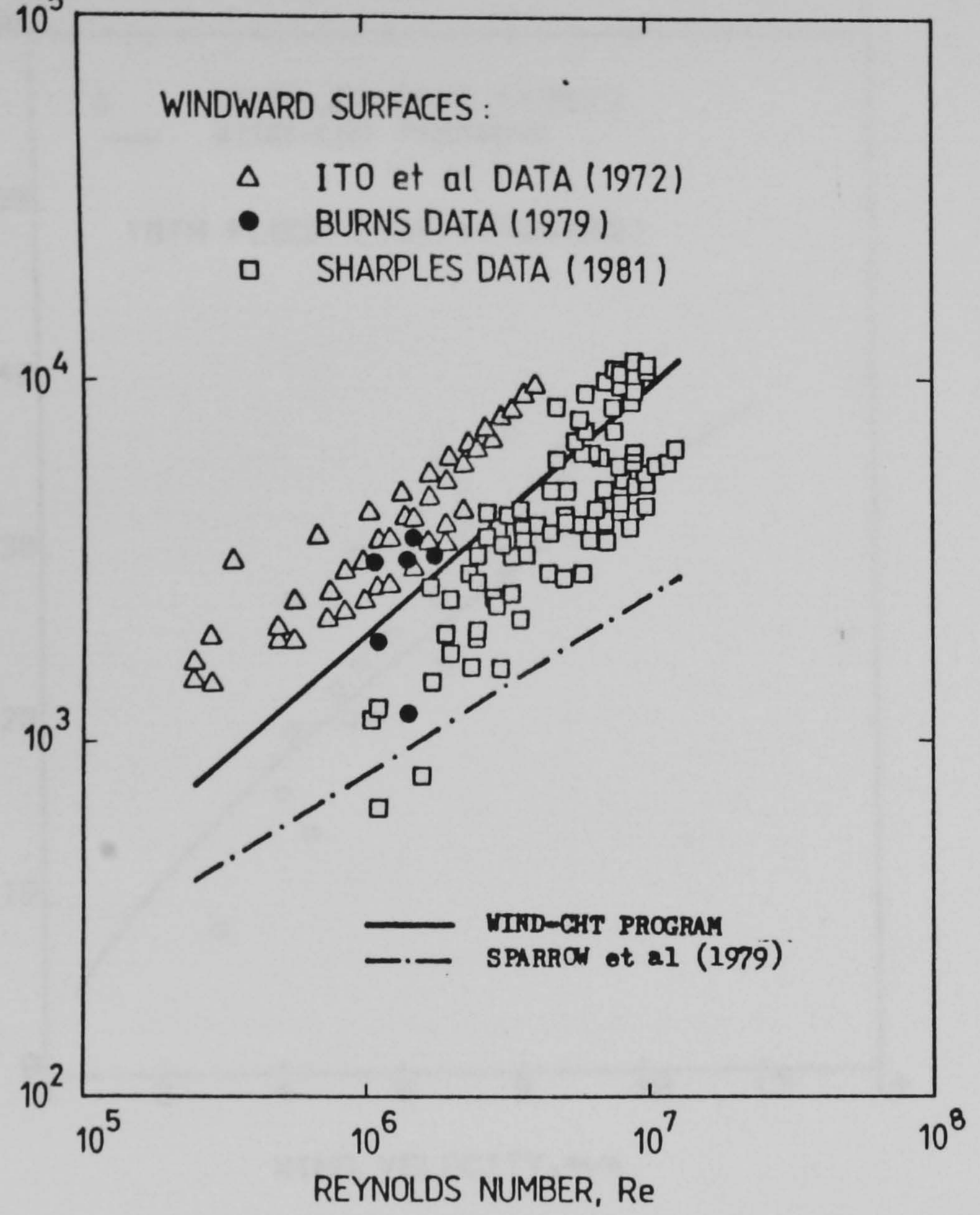

Fig. 2.6 Measurement data compared with the stagnation flow correlations used in the WIND-CHT program and that proposed by Sparrow et al (Ref. 32)

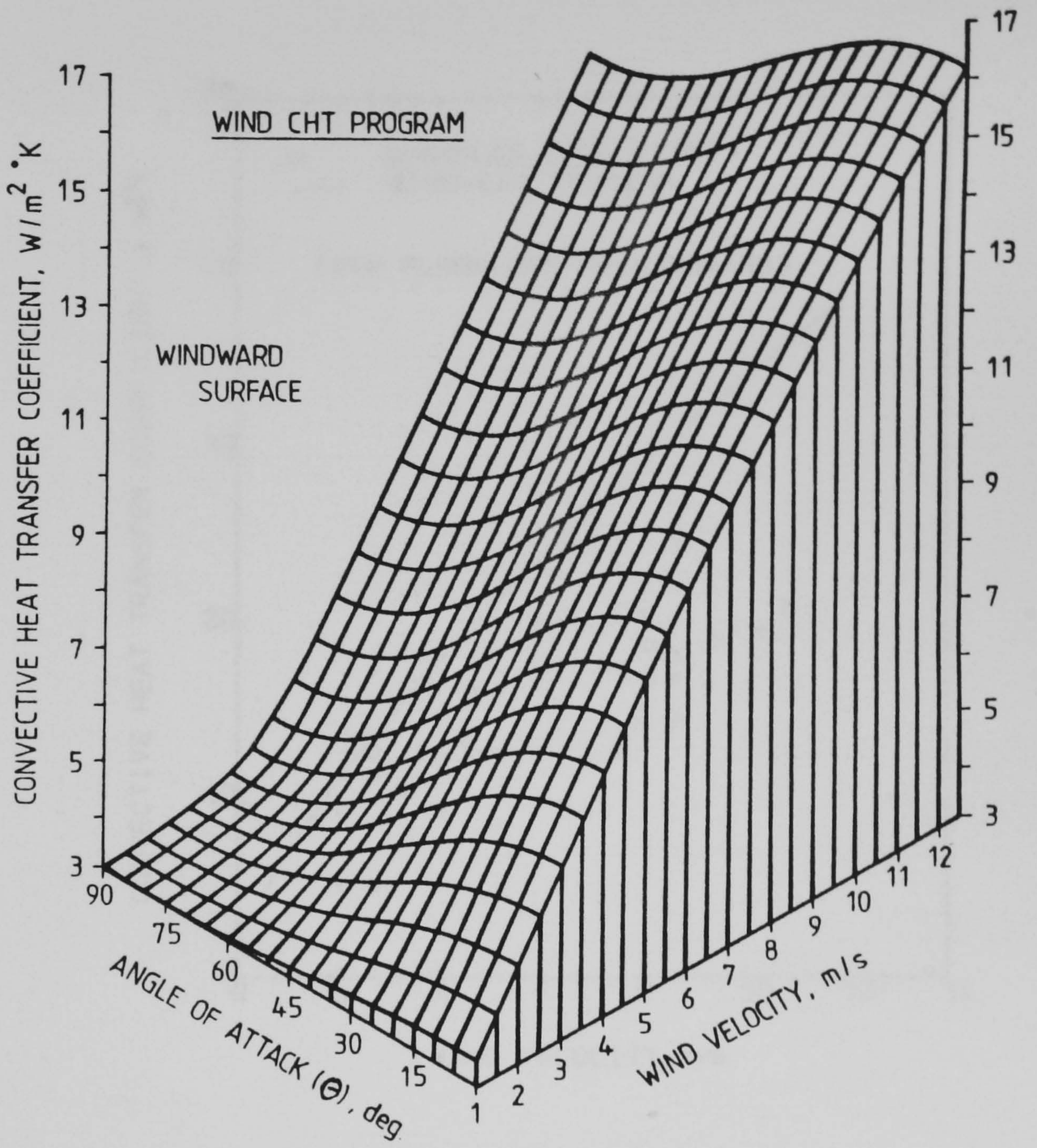

Fig. 2.7 Convective heat transfer coefficient as a function of wind velocity and angle of attack

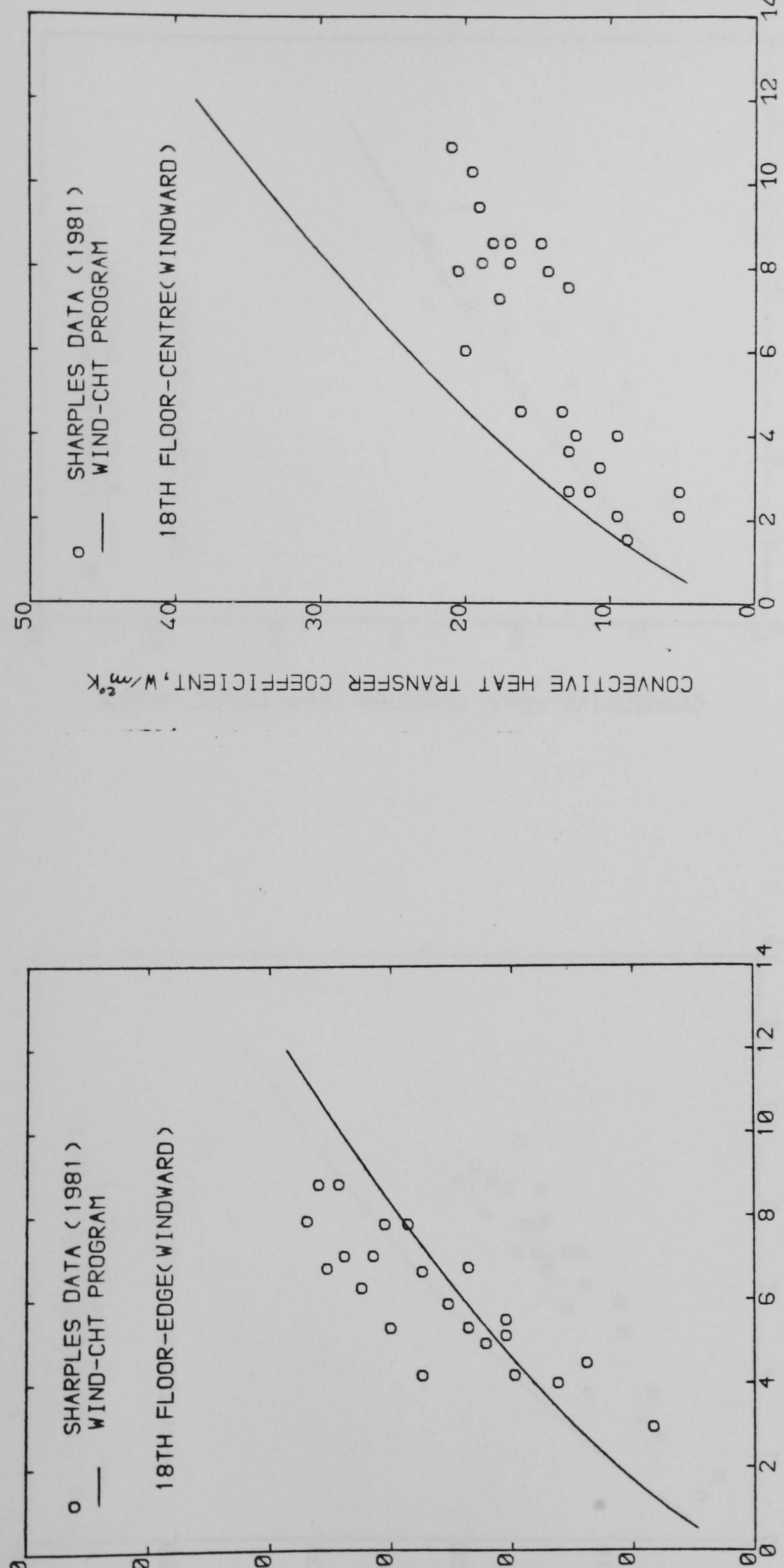

Fig. 2.8 Comparison between the WIND-CHT program computations and Sharples' field measurements on windward facades: a) 18th floor (edge), and b) 18th floor (centre).

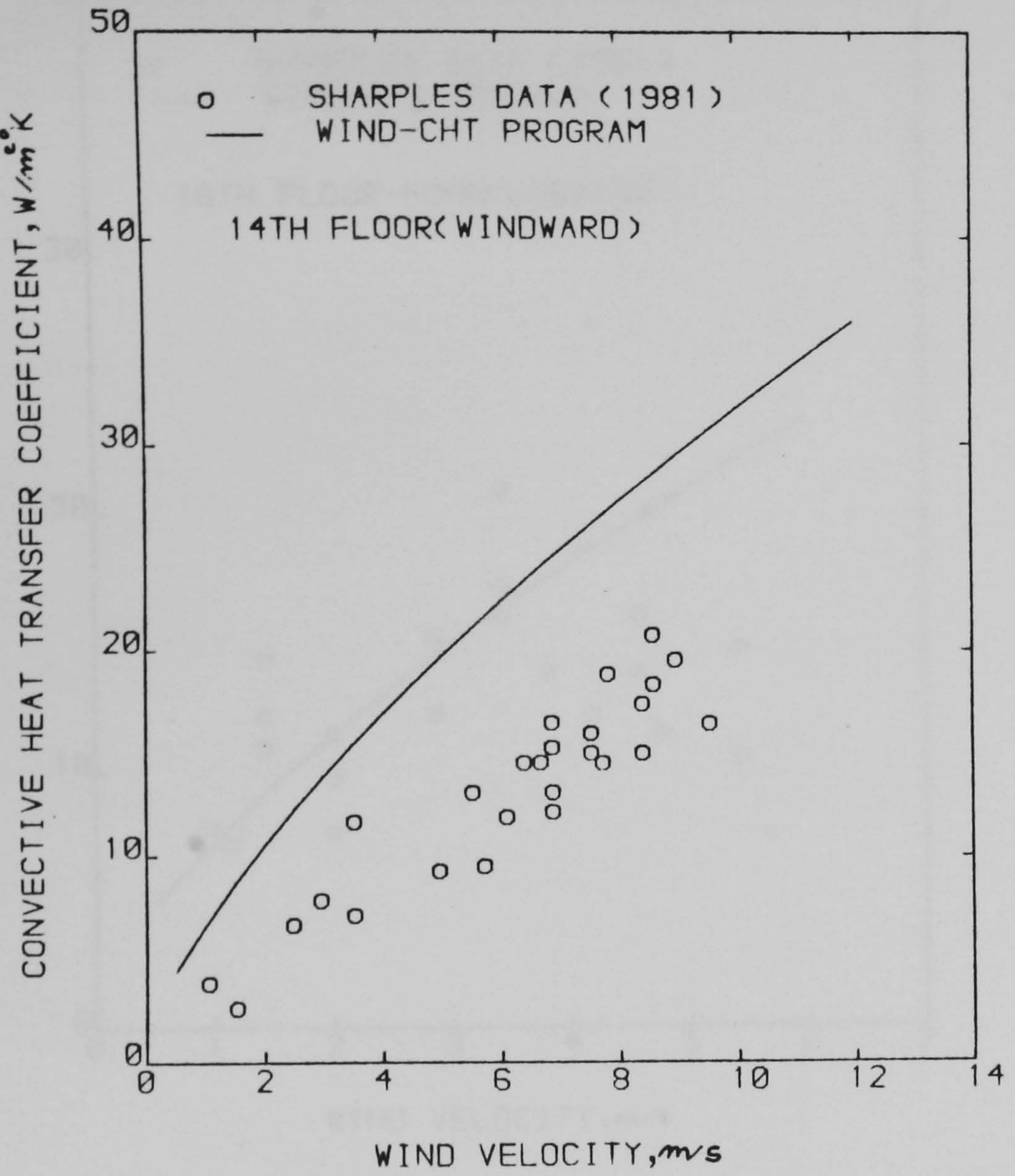

(a)

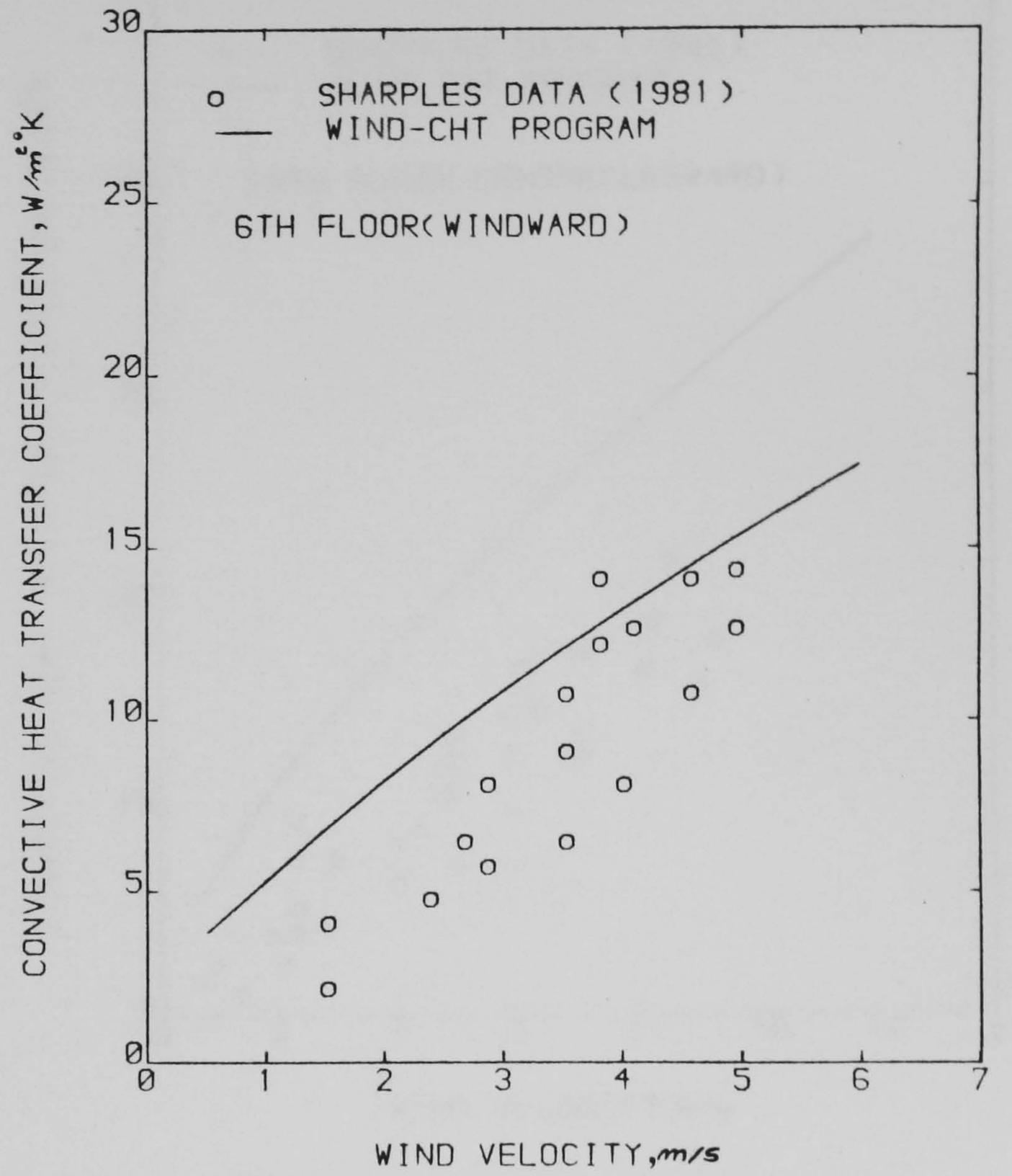

(b)

Fig. 2.9 Comparison between the WIND-CHT program computations and Sharples' field measurements on windward facades: a) 14th floor, and b) 6th floor

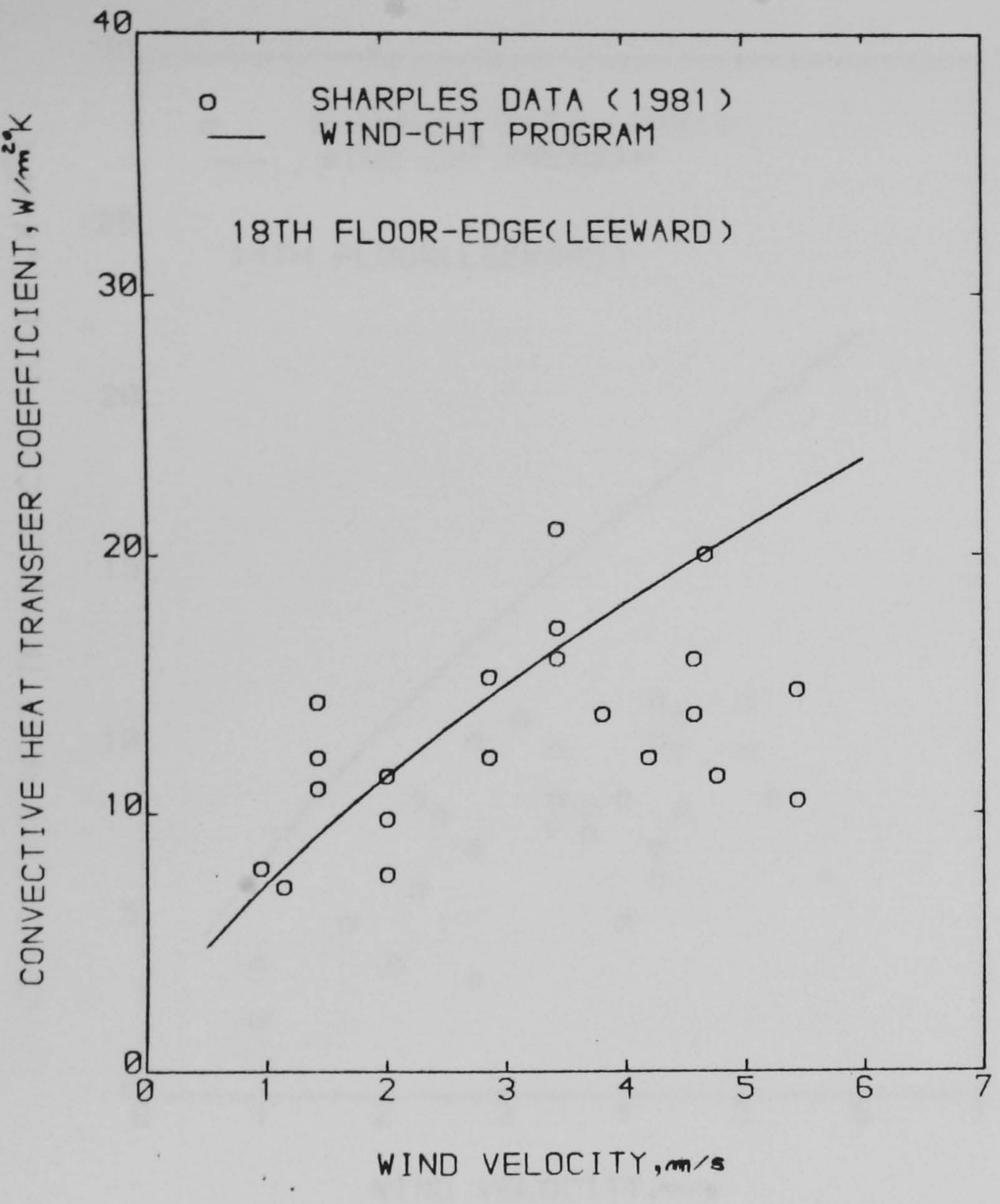

(a)

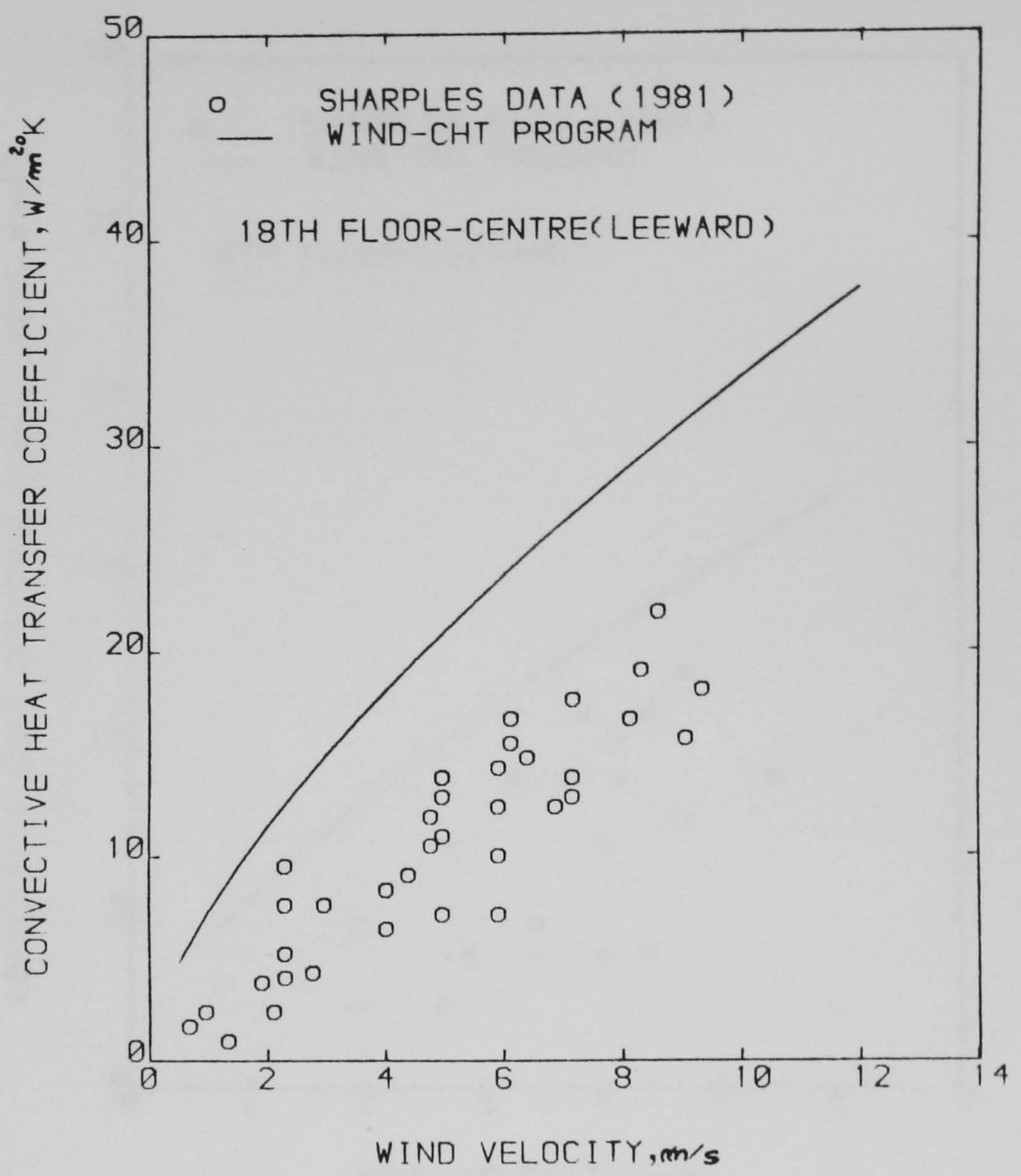

(b)

Fig. 2.10 Comparison between the WIND-CHT program computations and Sharples' measurements on leeward facades: a) 18th floor (edge), and b) 18th floor (centre)

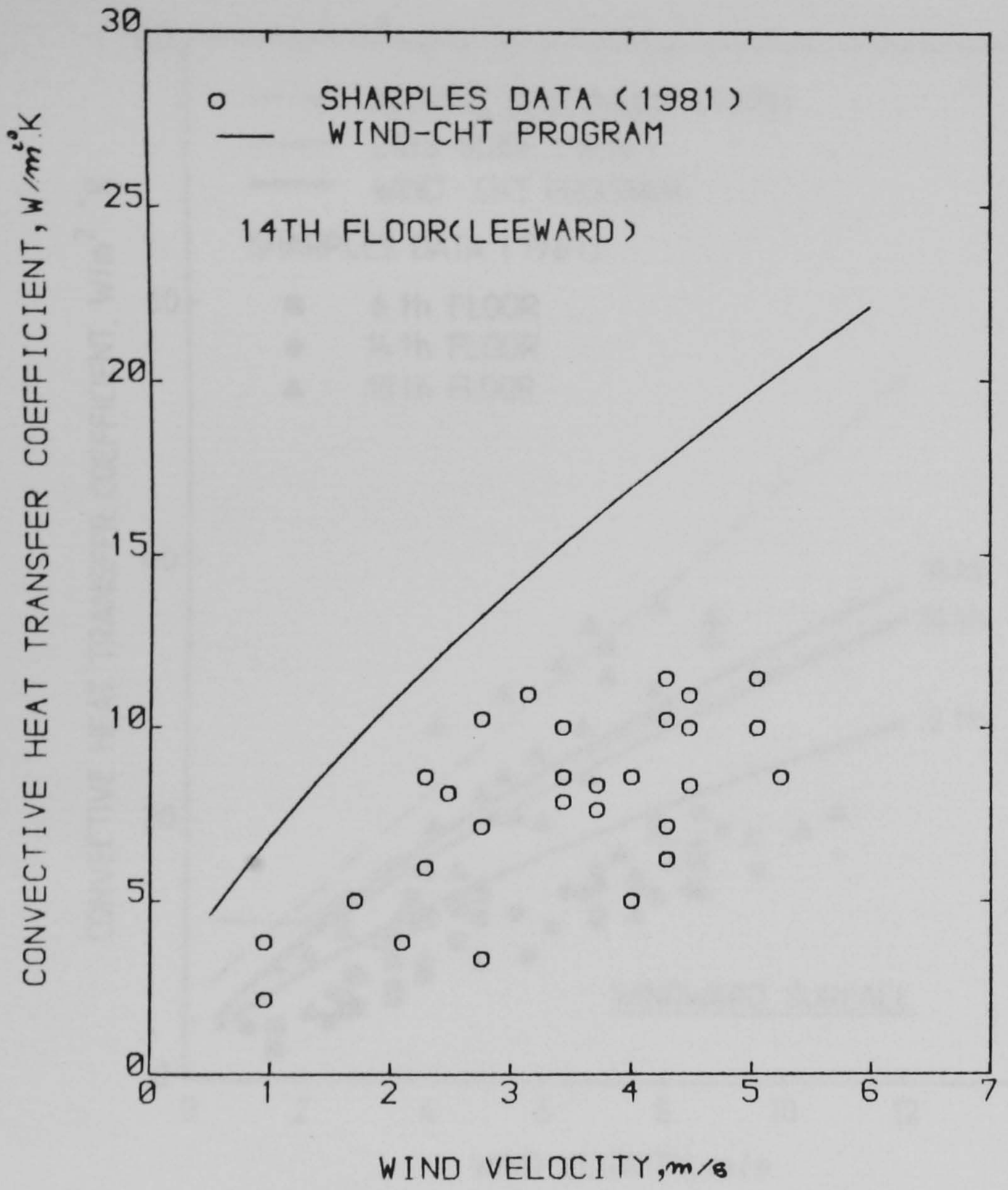

(a)

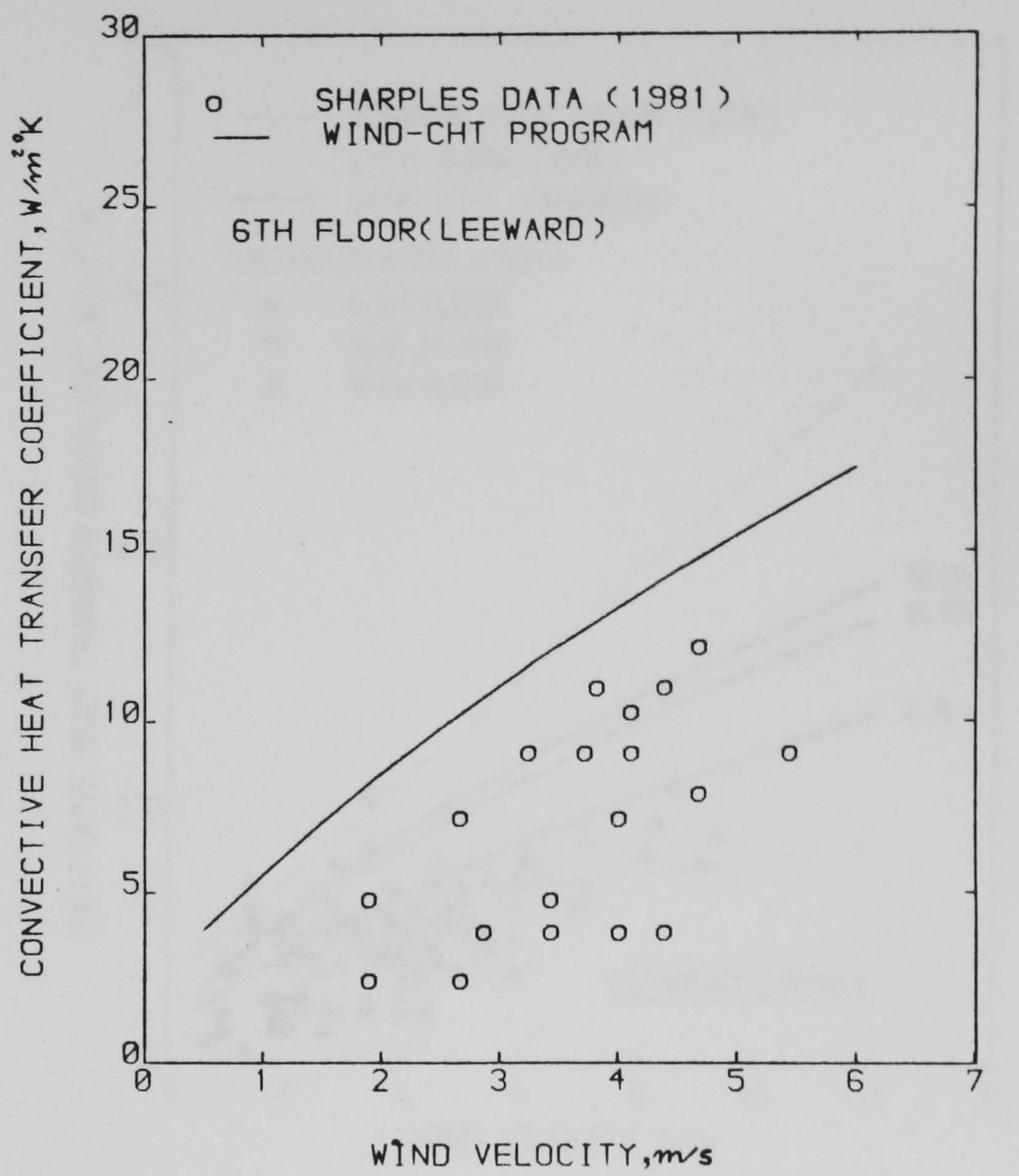

(b)

Fig. 2.11 Comparison between the WIND-CHT program computations and Sharples' measurements on leeward facades: a) 14th floor and b) 6th floor

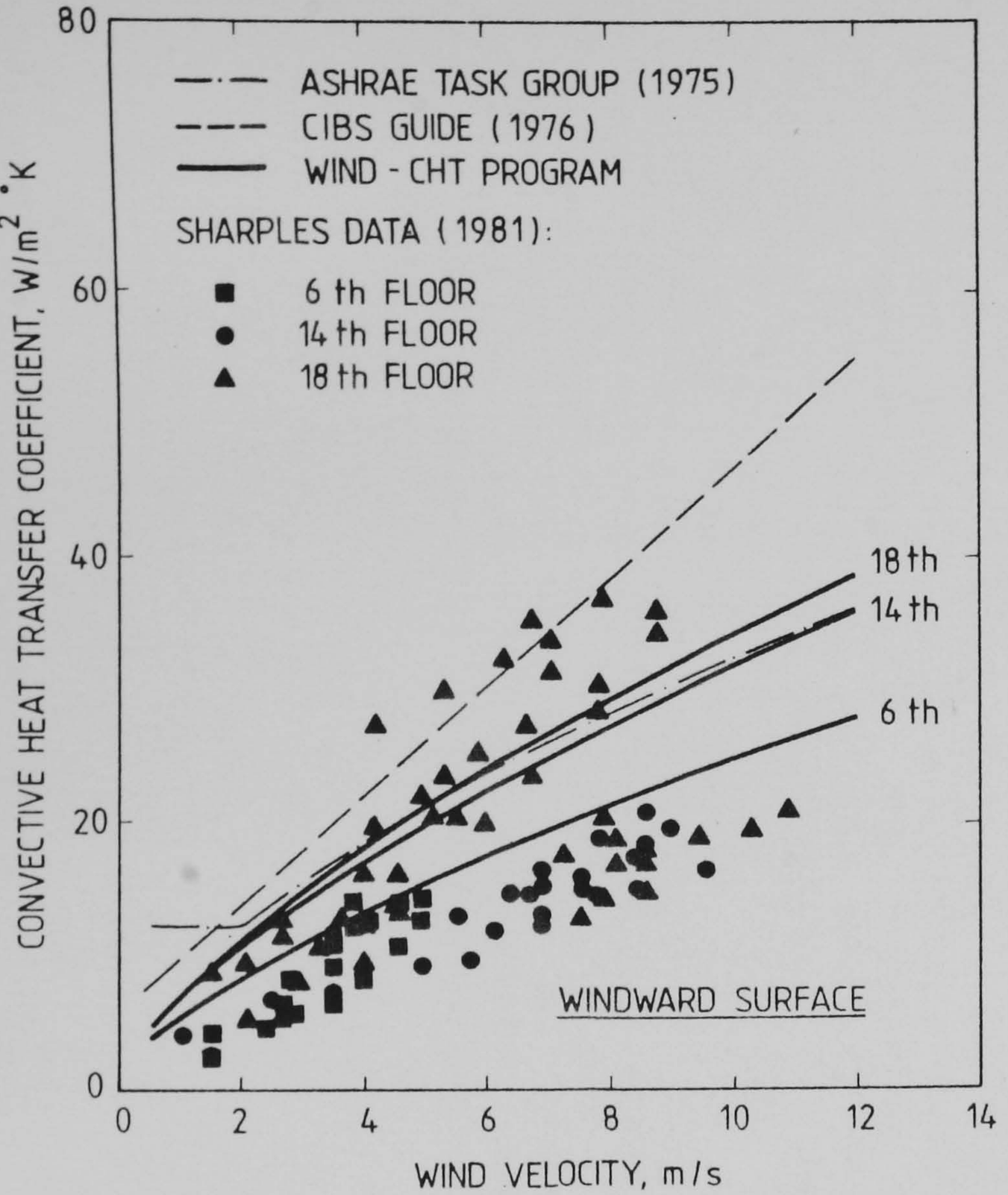

(a)

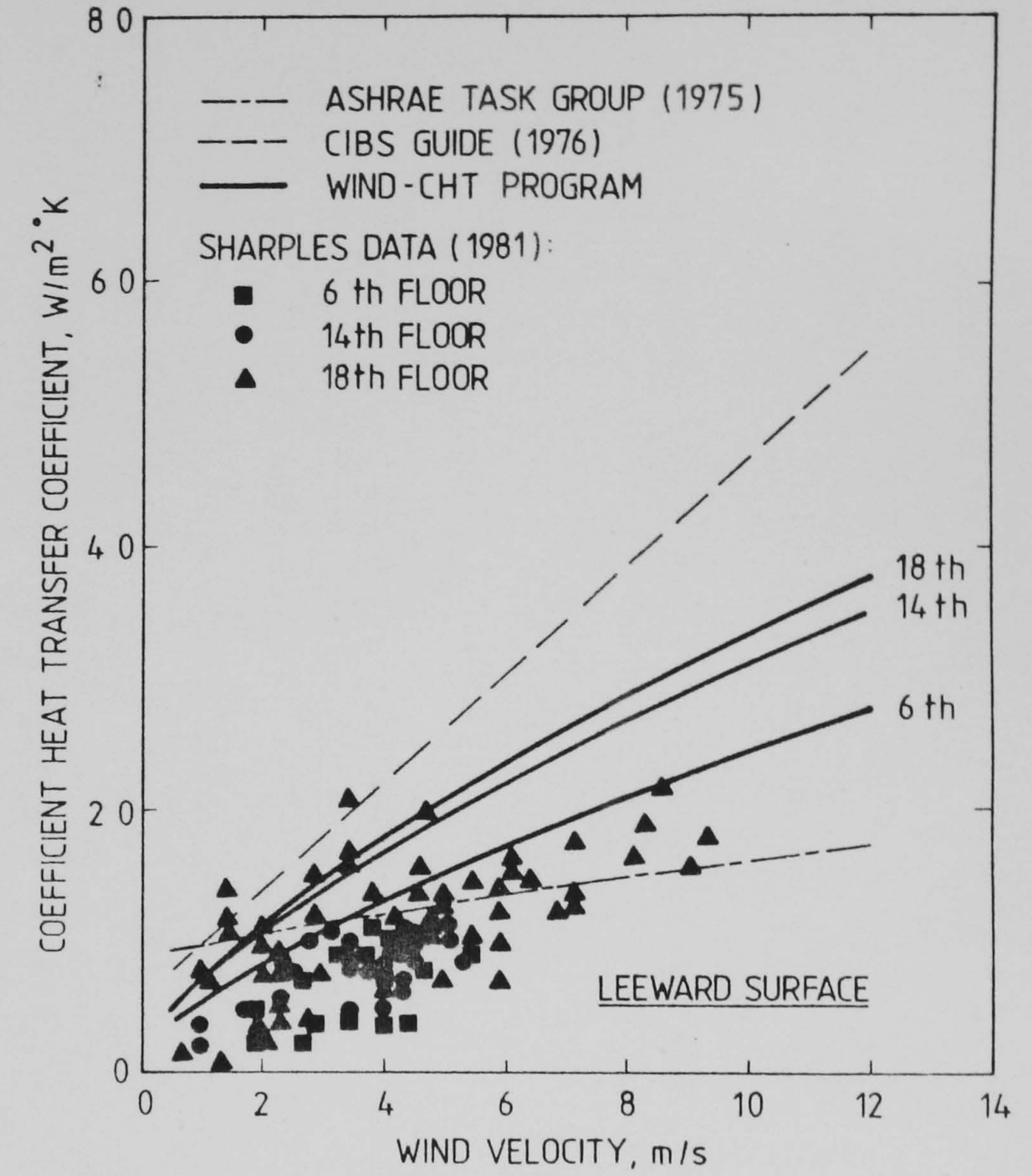

(b)

Fig. 2.12 Comparison between the WIND-CHT program computations and the standard guide data correlations: a) Windward surface and b) Leeward surface

CHAPTER 3

CHAPTER 3 - AN INTERMEDIATE-LEVEL MODEL FOR AIR INFILTRATION RATES INTO BUILDINGS

3.1 - INTRODUCTION

The development of computer programs for the modelling of energy flows in buildings is inhibited by a lack of information on the heat loss due to air infiltration according to Irving (Ref.3). This is rather suprising in view of the fact that infiltration accounts for a major fraction (25% to 50%) of the total heating and cooling loads in buildings. The traditional methods for calculating infiltration employ large safety margins, and this usually results in over-estimating the heating plant capacity. It is therefore necessary to improve on these methods, as an over-estimation of plant capacity would lead to unnecessarily high investments and reduced efficiency.

In order to compute the air infiltration into a structure, a knowledge of the air leakage characteristics of the cracks is required, together with a means for determining the pressure differences across them induced by wind action, stack effect and mechanical ventilation. The leakage characteristics of cracks may arguably be estimated with sufficient accuracy on the basis of published values such as those given by ASHRAE (Ref.4). However ,an analysis of the resulting pressure differentials usually requires sophisticated and time-consuming calculations.

Many computer programs have been developed in order to calculate infiltration. However most models presently in use are either not within the public domain or are written as research tools, rather than for meeting the needs of dynamic building thermal models. In order to overcome this problem a computer program, called FLOW, has been developed. This code differs from previous calculation methods in that the wind pressure coefficients, and consequently the pressure distribution around the building, are determined internally. In doing so, it accounts for the nature and roughness of the surrounding terrain and the consequent atmospheric boundary layer, the wind speed and direction, the building proportions and for any external shielding. The FLOW program can be run using either a single cell approach, in which the interior of the building is assumed to be at a single uniform pressure, or as a multi-cell model. In the latter case, the interior is subdivided into zones of differing pressure interconnected by leakage paths. The change from single- to multi-cell model, or vice-versa, is controlled by simple alteration to the input data.

3.2 - CURRENT GUIDE TECHNIQUES FOR THE PREDICTION OF AIR INFILTRATION RATES

3.2.1 - ASHRAE guide

This guide (Ref.4,chapter 22) describes four methods for estimating air infiltration rates into buildings, and these are outlined below:

i) Air change method

This method is based on the assumption that similar types of buildings with normal construction and under some 'average' weather conditions, would have similar infiltration rates. Thus, tabulated values of leakage rates are given for residential buildings which are classified according to the distribution of openings in the external walls. An allowance for weather stripping is also applied, and this typically accounts to a reduction of up to 33%.

The procedure for calculating the air infiltration rates involves multiplying the volume of each room by the appropriate air change rate. The sum of all of the leakage rates is then divided by the total building volume to get the building leakage rate in terms of air changes per hour. The effective infiltration rate may then be taken as one-half of this total because air flows into the building through the 'windward' openings are balanced by an equal amount of air flowing out of the other, 'leeward' openings.

ii) Crack method

In this case, the air infiltration estimates are based on measured leakage characteristics of the building components (window, window frames, doors, door frames and diffusion through walls) at selected pressure differentials from 25 to 75 Pa. The following equation then relates the infiltration rate, Q, to the pressure difference, ΔP, acting across any crack:

$$Q = C \Delta P^{n} \qquad (3.1)$$

The flow coefficient, C, and the flow exponent, n, depend on the nature of the crack. The ASHRAE handbook goes on to show that the pressure difference across the windward wall is given by:

$$\Delta P_{wi} = (Pw_{wi} - Pw_{le})/[1 + (Al_{wi}/Al_{le})^{1/n}] \quad (3.2)$$

where Pw is the wind pressure and Al the leakage area.

For a square building with leakage openings uniformly distributed and with the wind blowing at 45 degrees to a wall, two sides of the structure will face the wind, while the other two will face away from the wind. Then $Al_{wi}/Al_{le} = 1$ and $\Delta P_{wi} = 0.5(Pw_{wi} - Pw_{le})$. The same building with wind normal to one face will have one windward side and effectively three leeward sides. Consequently $Al_{wi}/Al_{le} = 1/3$ and $\Delta P_{wi} = 0.85(Pw_{wi} - Pw_{le})$, with the exponent n equal to a value of 0.65. Thus, both the effective wind pressure and the effective crack length are influenced by the wind direction and distribution of cracks.

The pressure due to the chimney (or 'stack') effect, although small in one- or two-storey buildings, must be added to the wind generated pressure in order to find the total pressure across windward surfaces. This effect results from the temperature difference between the internal and external air, and is outlined in section 3.3.

The leakage characteristics of many of a building's components , such as windows and doors, are reasonably well documented. However large variations can occur, depending on design, on quality control in manufacture, and, particularly, on the quality of installation. In the case of some other building components such as sill plates and ceilings, the leakage characteristics have not been well characterized, giving rise to consequent uncertainty in estimating infiltration rates.

The main limitation of the crack method is the difficulty in estimating the pressure differential to which the various components are actually exposed, under appropriate design conditions of temperature and wind.

iii) Regression analysis

Another approach to the prediction of infiltration rates is based on empirical correlations derived using regression analysis of data from field measurements. The correlation usually takes the following form

$$I = K1 + K2\ \Delta T + K3\ V \quad (3.3)$$

where I is the infiltration rate in air changes per hour, ΔT is the indoor-outdoor temperature difference, V is the wind speed and K1,K2,K3 are empirical constants derived from field measurements. Typical values of the constants suitable for different classes of houses are presented in the ASHRAE handbook (Ref.4).

iv) The LBL model

This model, developed at the Lawrence Berkley Laboratory-USA (Ref.54), was one of the first single-cell models to be developed specifically to use the results of building pressurization tests. In this case the infiltration rate, Q, is the larger of two values Qstack and Qwind, in which;

$$Qstack = Fs^{*} Al\ \Delta T^{1/2} \tag{3.4}$$

$$Qwind = Fw^{*} Al\ V^{2} \tag{3.5}$$

where Qstack is the stack dominated infiltration, Qwind is the wind dominated infiltration, and Fs* and Fw* are dimensionless building parameters. The effective leakage area, Al, is computed by assuming the flow to be proportional to the square-root of the applied pressure,

$$Al = Q/(2\ \Delta P/\rho)^{1/2} \tag{3.6}$$

where Q is the leakage air flow at 4 Pa determined by means of a building pressurization test.

The wind parameter, Fw^{*}, is defined by the following equation,

$$Fw^{*} = [\beta (Z_{\alpha}/10)^{\gamma} / \beta' (Z'/10)^{\gamma'}]\ (3-Rl)/9 \tag{3.7}$$

where Rl is the ratio of the leakage area of the horizontal surfaces of the building to the total leakage area of the building $\{=[(Al_{\alpha} + Al_{fl})/Al_{to}]\}$, Z_{α} is the height of the floor of the attic of the building, Z' is the height of wind speed measurement, and $\beta, \gamma, \beta', \gamma'$ are empirical constants defined for different classes of terrain.

The stack parameter, Fs^{*}, is given by

$$Fs^{*} = [(2 + Rl)/9]\ [2\ g\ Z_{\alpha}/Ta]^{1/2} \tag{3.8}$$

where g is the acceleration of gravity and Ta is the absolute temperature of the interior of the building. The many assumptions made in the derivation of the above equations are detailed by Sherman and Grimsrud (Ref.54,55).

The leakage area of floor and ceiling can be determined by measurement, by inspection, or by making some appropriate assumption. Direct measurement of the leakage curve for the floor and ceiling is the most accurate method. However, this is difficult and time-consuming, since it requires isolating the floor and ceiling from the rest of the structure and conducting a separate fan pressurization test.

The crudest assumption employed in this model, as it is presented in the ASHRAE handbook (Ref.4), is that the shielding coefficients are always assumed to be those of an exposed structure. In reality most of the buildings are, of course, sheltered by neighbouring obstructions. In a subsequent work, Sherman and Grimsrud (Ref.55) have improved the performance of their model by using shielding coefficients for five different shielding classes, and by employing the following equation to calculate the air infiltration rates:

$$Q = (Qstack^2 + Qwind^2 + Qvent^2)^{1/2} \qquad (3.9)$$

where Qvent represents any mechanical ventilation. Despite these improvements,the accuracy of their model is still limited by the assumption that the leakage of the walls does not change from wall to wall, and also that the shielding coefficients are the same for all faces for a given wind direction. The model also assumes, when calculating the wind building parameter (Fw^*), that the wind speed at 10 metres level has the same value near the building as at the wind measurement site. This assumption is valid only when both terrains are of the same class, which is rarely the case.

3.2.2 - CIBSE guide

This guide (Ref.56) describes two methods for estimating air infiltration rates into buildings,which are outlined below:

i) Air change method

The recommended values of design infiltration rates in the CIBSE guide are classified with respect to building types assuming normal exposure and an average ratio (25%) of openable areas (windows and doors) to external wall area. For higher ratios of openable areas in the external walls, these values are increased by 25-50%. The infiltration rates are also increased by 50 % for severely exposed sites, and decreased by 33% for sheltered sites.

ii) Crack method

The nomogram (Fig. 3.1) which forms the basis of this method has been taken from Jackman's work on ventilation of tall office buildings (Ref.57). He performed a study using an electrical network analysis method. The problem was then reduced to an electrical circuit of resistances in which currents corresponded to air flows and the potential differences represented pressure differentials. In using the nomogram [which is reproduced in the CIBSE guide (Ref.56)], the wind speed at 10 metres level is firstly corrected for building height and type of terrain. Secondly, the basic infiltration rate, given per metre of window crack, is found by extending a horizontal line from the previous nomogram point until it intersects an appropriate window wall leakage coefficient line. Corrections can be made for the internal resistance, to air flow in the building; the correction factor being 1.0 where there is little or no internal resistance and dropping as the internal airtightness increases. The total infiltration rate is computed by determining a representative total leakage area which depends upon the window distribution. This is one half of the total glazed area for a building glazed on two faces or the area of the vertical diagonal plane through the building for one uniformly glazed on four sides.

3.3 - THE FLOW PROGRAM

3.3.1 - Assumptions

The program uses similar basic assumptions to those employed in other infiltration programs. These are:

1. that the building is considered as a series of compartments, each of which has a specified number of air flow paths into and out of it through which infiltration may occur;

2. that each flow path has a characteristic flow resistance, which may be expressed by an equation relating airflow through it to pressure difference acting across it;

3. that wind forces and stack effect produce external pressures outside each opening in the building which are time-invariant over the period of time considered in the calculation;

4. that the internal air temperature in the building is uniform throughout the building.

The assumption that the wind velocity is constant within an one-hour interval, and the consequent effect on the calculated air infiltration rates is discussed in section 3.3.2 below. The variation of the internal air temperature affects the pressure due to the 'stack' effect. This pressure is combined with the wind pressure, which has usually a much higher absolute value, in order to calculate the total pressure. The total pressure is then raised to a power of 0.5-0.7 to calculate the air infiltration rate. Consequently, the assumption that the internal air temperature is uniform throughout the building will have only a minor effect on the calculated air infiltration rates.

3.3.2 - Description of the mathematical model

i) Air leakage characteristics of orificies and cracks

The basic driving forces for air infiltration are the pressure differentials across the various components of the building envelope generated by wind pressure, stack effect (caused by a temperature difference between the indoor and outdoor air) and by any mechanical ventilation. These pressure differentials act upon the various orificies and cracks in the building envelope to produce flow according to the classical orifice theory:

$$Q = C \Delta P^{n} \qquad (3.10)$$

The value of the exponent n depends on the pressure difference across the crack. At very low pressures the flow is dominated by viscous forces and at high pressures, by inertial forces. Therefore, at low pressures n will be close to 1.0 rather than 0.5 which is approached at high pressures. At intermediate pressures the behaviour will be a mixture of these effects. The ASHRAE handbook (Ref.4) indicates that the values of n in the types of orificies usually found in residential structures will be of the order of 0.5 to 0.65.

The values of C greatly vary depending upon the type of crack and may be determined directly from leakage tests made on each leakage path or from published values such as those given in chapter 22 of the ASHRAE Handbook (Ref.4).

ii) Infiltration by wind

A wind blowing on a building exerts a pressure which is highest at the centre of the windward wall (which is taken to be the stagnation point of the flow), and is given by:

$$Ps = \rho V^2/2 \qquad (3.11)$$

where Ps is the velocity pressure in the free air stream, and V is the wind speed at a given elevation. This wind speed can be deduced from that measured at the nearest weather station, following the procedure described in the sub-section 2.6.1.

The surface pressure generated by the wind action varies in a complex way over building facades, due partly to the wind speed gradient, partly to the presence of neighbouring buildings, and partly due to the aerodynamic characteristics of flow round a bluff body. However, it can be adequately calculated for the present purposes from a pressure coefficient, Cp, defined as:

$$Cp = Pw/Ps \qquad (3.12)$$

Positive values of Cp are associated with stagnation regions, where the total surface pressure is higher than the reference static pressure, while negatives values are associated with separated flow regions, where the total surface pressure is always less than the reference static pressure.

Most of the infiltration models presently in use require the specification of the pressure coefficients for different wind directions as a set of input data. The common procedure is to select these coefficients from existing codes of practice, in spite of the fact that these pressure coefficients are primarily intended for wind load applications and therefore represent the maximum values for each particular building facade. In practice, the pressure distribution is usually non-uniform, and difference between the average and extreme values can be quite large. This can be as much as 50% in the case of windward faces (Ref.58).

The inadequacy of the wind pressure coefficients arising from the existing codes of practice for simulating the effects of shelter (Ref.59), led to the use of two different techniques based on wind tunnel results. The first technique was developed from Bowen's experimental results (Ref.61). It can be used for calculating the wind pressure coefficients when the average height of the adjacent structures, Ha, is in between 16% and 100% of the height of the building itself, Hb. Bowen measured the wind pressure coefficients on the walls and roof of a rectangular building model which was set in a simulated high density urban area. The 1/400 scale model building had plan dimensions of 7.6 cm by 11.4 cm, and heights varied from 3.8, to 22.9 cm. It was mounted at the centre of a turntable surrounded by a number of 3.8 cm high blocks of the same plan dimensions as the model building, thereby simulating the high density urban area. Tests were carried out at twelve wind angles, from 0 to 90 degrees in 5 degrees increments, using a power law velocity profile with an exponent of 0.43. The mean pressure coefficients at various heights on a particular wall, related to the wind dynamic pressure at roof level, were then plotted against the fraction of the building height at which they were measured for each wind angle and building that was tested.

The graphical presentation originally used by Bowen was not, of course, suitable for computer application, and a computer routine was therefore developed in order to use Bowen's results to predict the wind pressure coefficients. This was performed by feeding the routine with the values of the wind pressure coefficients, for 6 different heights on each of the four sides and for 12 wind angles. By using the Lagrange interpolation technique the wind pressure coefficients for any height across any wall and for any wind angle are then calculated. The results thus obtained are related to a minimum degree of shielding of Ha/Hb=1/6, and a correction factor for shielding has then to be applied. If a flow exponent, n, of 0.65 (generally accepted for cracks) is assumed, the air flow correction factor of shielding presented by Shaw (Ref.63) reduces to:

$$Fc = (Cp)_{Ha/Hb} / (Cp)_{1/6} = 1.24\, e^{-1.31\, Ha/Hb} \qquad (3.13)$$

where Fc is the wind pressure coefficient correction factor of shielding.

The second technique considered was the 'harmonic analysis' method (Ref.58,60). Shaw (Ref.60) used this approach to present the wind pressure coefficients measured across the external walls of two schools in analytical form. Allen (Ref.58) using data extracted from Bowen (Ref.61) and Akins, Peterka and Cermak (Ref.62), showed that the mean wind pressure coefficients for any symmetrical building can be represented by a Fourier series. The series coefficients are dependent on the aspect ratio and on the degree of shielding. It was decided to use this technique only for exposed structures (Ha/Hb<1/6), since very good estimates of the wind pressure coefficients for sheltered buildings (1/6<Ha/Hb≤1) were obtained by using the first technique (Ref.18). The Fourier series takes the following harmonic form:

$$Cp(\theta) = a_0 + \sum_{m=1}^{7} a_m \cos(m\theta) \qquad (3.14)$$

where θ is the wind angle of attack. The coefficients, a_m, in equation (3.14) are represented by a logarithmic series dependent only on the aspect ratio, D, of the form:

$$a_m = b_0 + b_1 \ln D + b_2 \ln D^2 + \ldots + b_n \ln D^n \qquad (3.15)$$

where D is the ratio of the perpendicular length to the width of wall being considered. The values of the coefficients b_n for pressure coefficients referenced to the local wind profile are given in Table 3.1. This is the reference wind, which is the value of the wind speed used for estimating the velocity pressure, given by equation (2.54).

Finally, using the ideal gas law, the surface wind pressure can be obtained by the following equation

$$Pw = Pb\ V^2\ Cp/(Rda\ Te\ 2) \qquad (3.16)$$

where Pb is the atmospheric pressure, Rda is the gas constant of dry air and Te is absolute temperature of the outside air.

The FLOW program like most of the current generation infiltration modelling programs, assumes a steady flow situation with a constant pressure drop across the crack, thereby implying a constant wind velocity on the outside of the building. This rarely, if ever, happens. In reality the wind pressures on a building fluctuate continously with time. These fluctuations are caused by approach wind gusts and high turbulence levels generated by flow separations. However, the way in which these complex pressure variations will influence the infiltration process is difficult to predict.

Much research has been undertaken in order to identify the contribution arising from fluctuating flow. Among some of the recent contributions are papers by Hill and Kusuda (Ref.64), Potter (Ref.65), Grimsrud et al (Ref.66) and Etheridge and Nolan (Ref.67). Etheridge and Alexander (Ref.68), included an expression in their infiltration model for estimating the contribution due to turbulence. It is based on the experimental data obtained by Etheridge and Nolan (Ref.67), and pressumes that the pressure field has a Gaussian distribution, and requires the knowledge of the root-mean-square value of the pressure difference across the building facade for each leakage path. Unfortunatelly, no conclusive evidence regarding the overall benefit of this term was found during the validation study undertaken by Liddament and Allen (Ref.59). A more elaborate method relating flow through a crack to a fluctuating pressure is therefore required before incorporating such effect into a infiltration model. This can be attained, for instance, by recording the pressure coefficients under various degrees of free-stream turbulence in a wind tunnel. In this case the resulting pressure coefficients can also be related to the time variation of the wind speed. However, the wind turbulence level is not usually recorded at weather stations, and therefore such an 'improved' model would not be able to calculate accurately the air infiltration rates due to the absence of input meteorological data.

The FLOW program was developed with the aim of being incorporated as a subroutine into different building thermal simulation programs. In this way sensitivity of building thermal models to input infiltration data could be assessed. Most of these models use meteorological input data averaged over a period of one-hour; and therefore an one-hour averaged value of the wind speed was used for estimating the air infiltration rates, disregarding, in this way, any influence of time variation of the wind pressure within one-hour averaging time.

iii) Infiltration by stack effect

Air at a given temperature has a manometric pressure that varies approximately linearly with height, with a slope proportional to the air density. Since the density is inversely proportional to the temperature, it follows that the temperature differences between air inside and outside the building causes pressure differences that drive infiltration. This phenomenom is called the 'stack' or 'chimney' effect. In cold weather, this pressure difference causes air to enter the lower floors of the building and leave through the upper floors. In hot weather the flow directions are reversed and generally less significant. At some intermediate height a neutral pressure level exists where the internal and external pressures are equal. The stack effect pressure when measured at a height x above or below the neutral level is then given by:

$$Pd = \rho_e \, g \, x - \rho_a \, g \, x \qquad (3.17)$$

where Pd is the pressure difference due to stack effect, and x is the distance to neutral pressure level (positive if above neutral level and negative below). Assuming that the air behaves in a similar manner to the ideal gas, then equation (3.17) can be reduced to

$$Pd = 0.0342 \, Pb \, x \, (1/Te - 1/Ta) \qquad (3.18)$$

This equation implies that there is no resistance to air movement inside the building. It is, therefore, necessary to multiply the values arising from equation (3.18) by the thermal draft coefficient, μ, which depends on the air tightness of the exterior walls relative to that of the interior construction (Ref.69). With the interior completely open, the value of μ will approach unity, whereas with each storey completely sealed from others it will approach zero. The values of μ, as determined experimentally by Tamura and Wilson (Ref.70), for a few multi-storey office buildings ranged from 0.63 to 0.88.

Replacing x by $(N-\lambda)H_b$, as indicated by Shaw and Tamura (Ref.71), the following equation is then obtained

$$Pd = 0.0342 \, Pb \, (N-\lambda) \, Hb \, \mu \, (1/Te - 1/Ta) \qquad (3.19)$$

where N is the ratio of height of level above ground to building height, and λ is the ratio of neutral pressure level to building height (usually equal to 0.5).

iv) Combined action of wind and stack effect

Buildings, in general, are subject to both wind and stack effects simultaneously. The external pressures acting on the exterior walls of a building are considered qualitatively in Figure 3.2 for a building with uniform openings above and below midheight and without significant internal resistance to flow. Figure 3.2(a) shows the vertical distribution of pressure difference between outside and inside pressure caused by stack effect only, when the inside pressure is taken as the zero reference. When there are both wind and stack effects, the distribution of pressure difference will be dependent on whether the opening is situated on the windward or leeward side, as shown in Figures 3.2(b) and 3.2(c). In the windward side, the outside pressure is increased by the positive wind pressure, causing the neutral zone level to rise upwards, and thereby increasing the infiltration. In contrast the exfiltration from the leeward side increases because the neutral zone is pulled down by the negative wind pressure. Thus, the resultant pressure difference on the exterior walls of buildings at any level can be approximated by the algebraic sum of the pressure difference due to wind and the pressure difference due to stack effect.

v) Calculation of the internal pressures

The building under consideration is divided, within the FLOW program, into a set of nodes inter-connected by flow paths. Each node represents a space inside or outside the structure, in which the pressure may be assumed to be uniform. The internal pressures are calculated assuming that the amount of air entering each limited space, or zone, of a building through cracks is equal to the amount of air escaping from the zone. Thus, the basic mathematical procedure is to obtain a solution to a set of pressure difference equations of the following type:

$$\sum_{i=1}^{m} C_{i,j} (P_i - P_j)^{n_{i,j}} = 0 \qquad (3.20)$$

where $C_{i,j}$ and $n_{i,j}$ are the flow coefficient and flow exponent applicables to the air flow between the spaces i and j respectively, and m represents the total number of air flow paths of node j.

The effects of air-handling systems are taken into account by specifying either the excess amount of supply over exhaust air in each space via equation (3.20).The solution, in effect, determines the degree of pressurization caused by the mechanical ventilation system, in conjunction with the natural pressures.

Typically building networks will have a large number of nodes, consequently matrix methods for solving the non-linear set of equations would currently be cumbersome and expensive in terms of computing requirements. The Newton-Raphson iterative technique for multiple equations and unknowns has, therefore, been adopted for the FLOW program. This enables the internal node pressures to be

progressively adjusted until the total flow into each node is less than a specified residual value. When the solution to the set of equations is obtained the air flow rate for each path is calculated according to equation (3.1).

A computational program was then written in Fortran IV language based on the equations described in this section. Figure 3.3 illustrates a flow chart of the FLOW program. The subroutines WIND and GEOM used by this infiltration model are described in the sub-sections 2.6.1 and 2.6.2.

3.3.3 - Comparisons with field measurement data

An important part in the development of any air infiltration model is to determine the limits of its accuracy by comparison with field measurements. Unfortunatelly, very few of the research papers giving full scale data give sufficient information for reliable comparative calculations to be carried out. In particular, data concerning the external climate of the building is often lacking. To assist in this task Liddament and Allen (Ref.59) prepared three key data sets so that the full range of applicability of any model being tested can then be assessed. The first data set is based on measurements made in an isolated, detached dwelling in Switzerland, the second in a detached dwelling in Ottawa, Canada and the third in a mid-terrace , three storey dwelling in Runcorn, UK. Liddament and Allen (Ref.59) suggested that the model performance should be considered satisfactory if the computational results fall within $\pm$ 25% of the measured infiltration rate. This 'error criterion' was derived on the basis of possible errors resulting from measurements inaccuracies in both the input data and the air infiltration rate measurements.

The FLOW program was run using all three of the key data sets, and the results for each are discussed below in turn.

i) Swiss test data (Maugwill house)

The air leakage distribution was estimated in a similar way to that employed by Liddament and Allen (Ref.59), during the tests with the BSRIA model. The component leakage was used directly, while the deficit between total and component leakage was evenly distributed along the roof/wall and the gable/roof junctions. The assumed flow network is illustrated in Figure 3.4 and the corresponding leakage characteristics of each flow path are given in Table 3.2. The wind pressure coefficients were calculated using the 'harmonic analysis method', since this house lies on an exposed position. The atmospheric pressure was taken as 0.94×10^5 Pa, since the house is situated at 600 metres above sea level. Nodes 14-16 were assumed to be influenced by stack pressure only, since the slope prevents the direct action of the wind on these nodes. The effective building volume for calculating the infiltration in terms of air changes per

hour was taken as the volume of the six rooms where the tracer gas was injected (children's room-west, children's room-east, master room, studio, staircase and living room). Figure 3.5(a) and Table 3.3 show the computations of the single-cell version of the FLOW program against the experimental data. Good agreement between the calculation and measurement was achieved, with all but three (actually 83%) of the calculations being within 25% of measurement.

ii) Canadian test data (HUDAC 'upgraded' house)

The leakage distribution for the HUDAC house was based on the assumption of uniform distribution of cracks around the building. In this way, the flow coefficient for each facade is a direct function of the facade area. The assumed flow network is illustrated in Figure 3.6 and the corresponding leakage characteristics of each flow path are given in Table 3.4. Node 2, as indicated by Liddament and Allen (Ref.59), can be assumed to be influenced only by the stack pressure, since the garage prevents the direct action of the wind on this node. The wind pressure coefficients were calculated using the regression analysis based on Bowen's data, since this house is partially sheltered. For the moderately exposed N,NW,W and NE wind directions, a degree of shielding (Ha/Hb) of 1/6 was assumed. For the sheltered S and E wind directions a degree of shielding of 1/2 and 1 was assumed. Figure 3.5(b) and Table 3.5 show the computations of the single-cell version of the FLOW program against the experimental data. Consistent agreement was also obtained for this test house, with 37 of the 49 values (75%) falling inside the 25% band. The very low summer measurements tended to be under-estimated by the model. The measurement of very low infiltration rates are very difficult to make, and this is likely to be the main reason for this disparity.

iii) United Kingdom test data (Runcorn house)

The leakage distribution for the Runcorn house was considered in a similar way as the Maugwill house. The given leakage characteristics of windows and doors were used directly, while the deficit between component and total building leakage was evenly distributed along the rear and front roof/wall junctions. The assumed flow network is illustrated in Figure 3.7 and the corresponding leakage characteristics of each flow path are given in Table 3.6. The wind pressure coefficients were calculated using the 'regression analysis method' with a degree of sheltering (Ha/Hb) of 1, since this house is subjected to a heavy local shielding. Figure 3.8 and Table 3.7 show the calculations of the single-cell version of the FLOW program against the experimental data. Consistent results were also achieved for this test house, with 11 of the 15 (73%) calculated values being within the specified tolerance bands.

In all three previous validation studies the interior of the building was treated as a single zone. This assumption was made for the Maugwill and HUDAC houses because the leakage characteristics of

the internal doors were not given, infering that they were kept open during the measurements. For the Runcorn house, although the leakage characteristics of the internal doors are presented, the experimental results were also obtained keeping all the internal doors open.

No field experimental data set appears to be available in the open literature against which a multi-cell infiltration technique can be adequately tested. Although the Runcorn test house experimental results are not strictly appropriate for comparison with the multi-cell calculations (as discussed above), it was decided to use this data set in order to demonstrate the potential of the multi-cell version of the FLOW program. In doing so, the given total leakage was distributed in accordance with the distribution of component leakage. Consequently 44.7% of the total leakage was considered to be distributed along the rear wall, 33.6% along the front wall and 21.7% along the roof. The leakage coefficient of a particular part of the walls/roof was estimated as being proportional to the exposed area (uniform distribution of cracks). The assumed flow network is shown in Figure 3.9 and the corresponding leakage characteristics of each flow path are given in Table 3.8. Figure 3.10 and Table 3.9 show the prediction of the multi-cell version of the FLOW program against the experimental data. The calculated air infiltration rates, plotted in Figure 3.10 represent a volume-weighted average of the individual room infiltration rates. The calculated multi-cell results were obtained by assuming that all internal doors were kept closed, while the experimental results were taken with all internal doors open. This is, obviously, the major reason for the apparent poor agreement (55%) shown in Figure 3.10 and Table 3.9. Nevertheless, these results indicate the potential at least of the multi-cell version of the FLOW program.

3.4 - CONCLUSIONS

A method has been presented for computing the air infiltration rates into buildings, taking into account most of the key dependent variables, such as wind speed and direction, the variation in shape and height of the atmospheric boundary layer over different terrains, the building proportions, the indoor-outdoor temperature difference, and the leakage characteristics of the building. A simple procedure for calculating the wind pressure coefficients for a building surrounded by lower structures of uniform height was developed by using the pressure data obtained from a wind tunnel model study. For exposed buildings the representation of the wind pressure coefficients by a Fourier series, as suggested by Allen (Ref.58), was found to be quite adequate.

Table 3.10 shows a comparison between various infiltration models based on the work of Liddament and Allen (Ref.59). The only two models that achieve a similar accuracy to that of the FLOW model are the LBL and BRE models. However, they can only be applied to single zone systems. It should also be noted that the LBL model requires whole-house pressurisation test data for the building considered

before it can be employed. Consequently, it cannot be used to evaluate infiltration rates at the design stage of a building. The FLOW program is able to utilise component leakage data, such as that given in the ASHRAE handbook (Ref.4).

The proposed method does not take into account the infiltration rate caused by fluctuating pressures arising from turbulence. More information is required in this area to assess its contribution to the pressures generated on the external surfaces of a building. Despite this reservation, the agreement between calculation and measurement for all the data sets was felt to be good especially considering the uncertainties in interpreting the data.

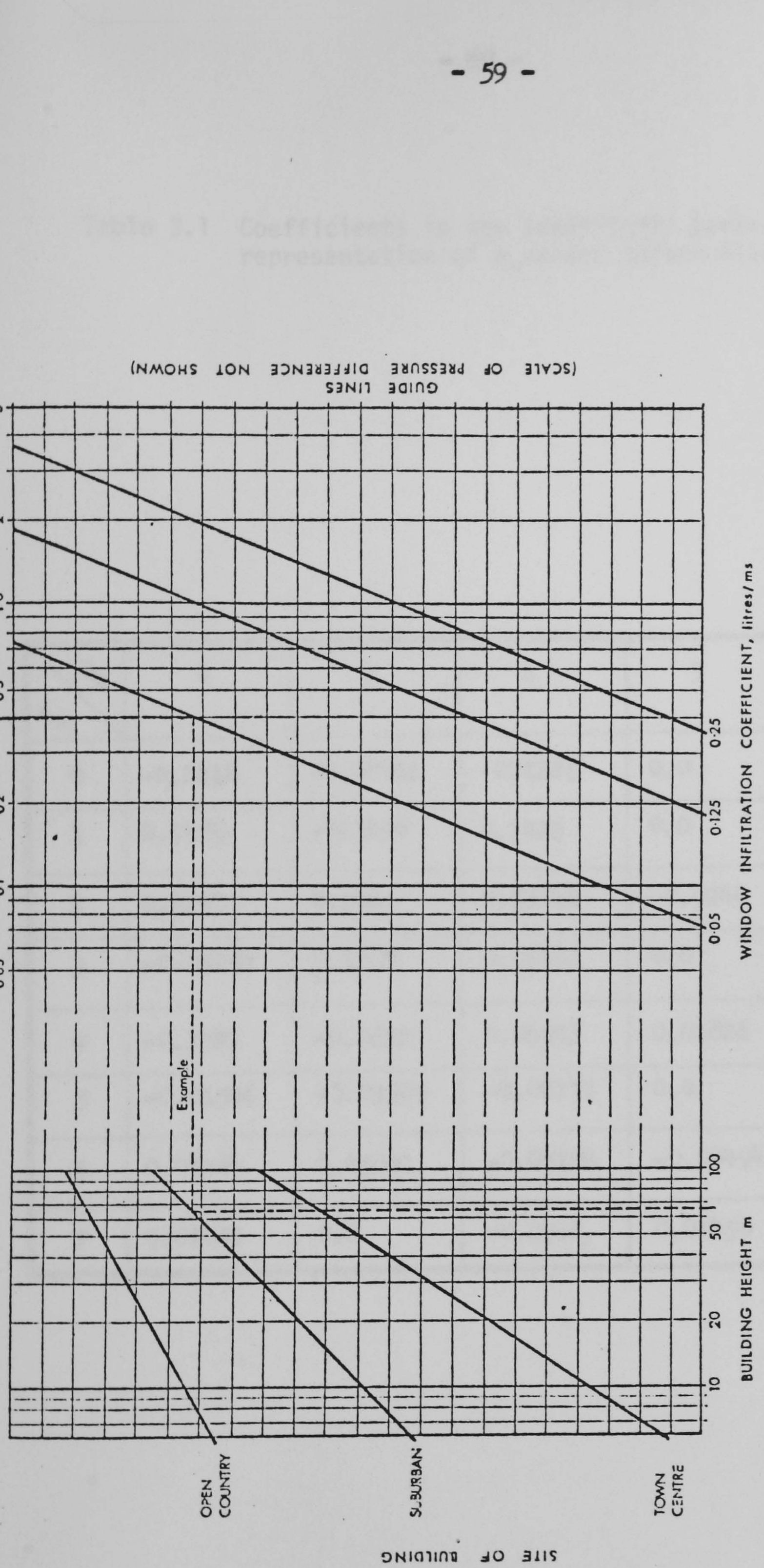

Fig. 3.1 Nomogram for calculating air infiltration rates into buildings {Extracted from CIBSE Guide (Ref. 56)}

Table 3.1 Coefficients in the logarithmic series representation of a_m values {After Allen (Ref. 58)}

a_m \ b_m	0	1	2	3	4
0	-0.2418	-0.07016	-0.1225	0.0	0.0441
1	0.9185	-0.1496	0.1226	0.0	-0.0596
2	0.6293	0.2420	0.03818	-0.0244	-0.02684
3	-0.06432	0.1207	0.05121	0.0	0.0
4	-0.1371	-0.0622	0.06033	0.01826	0.0
5	-0.01546	-0.09586	-0.08173	0.0	0.02441
6	0.05484	0.05083	-0.05104	-0.03494	0.01203
7	0.01092	0.0	-0.0316	0.01450	0.01844

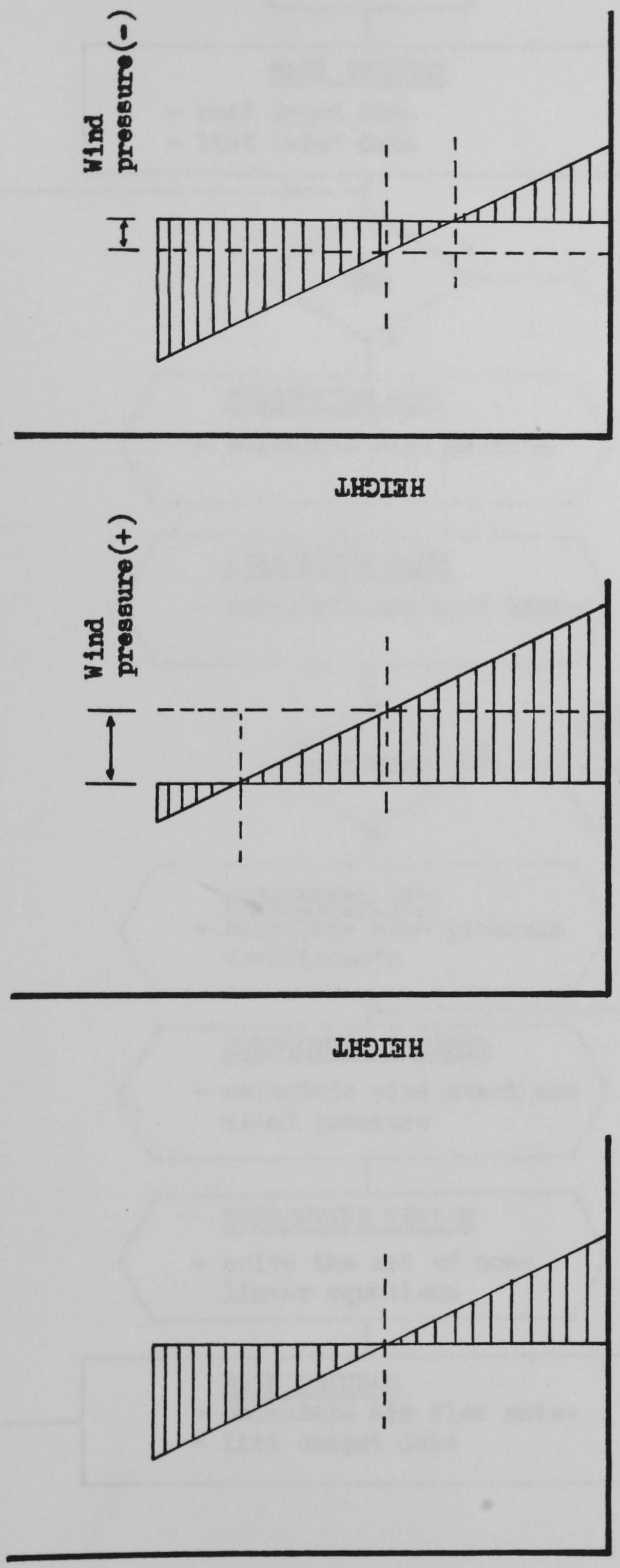

Fig. 3.2 Pressure differences on the exterior wall of a building: a) Stack effect only, b) Stack and wind effects (leeward) and c) Stack and wind effects (windward)

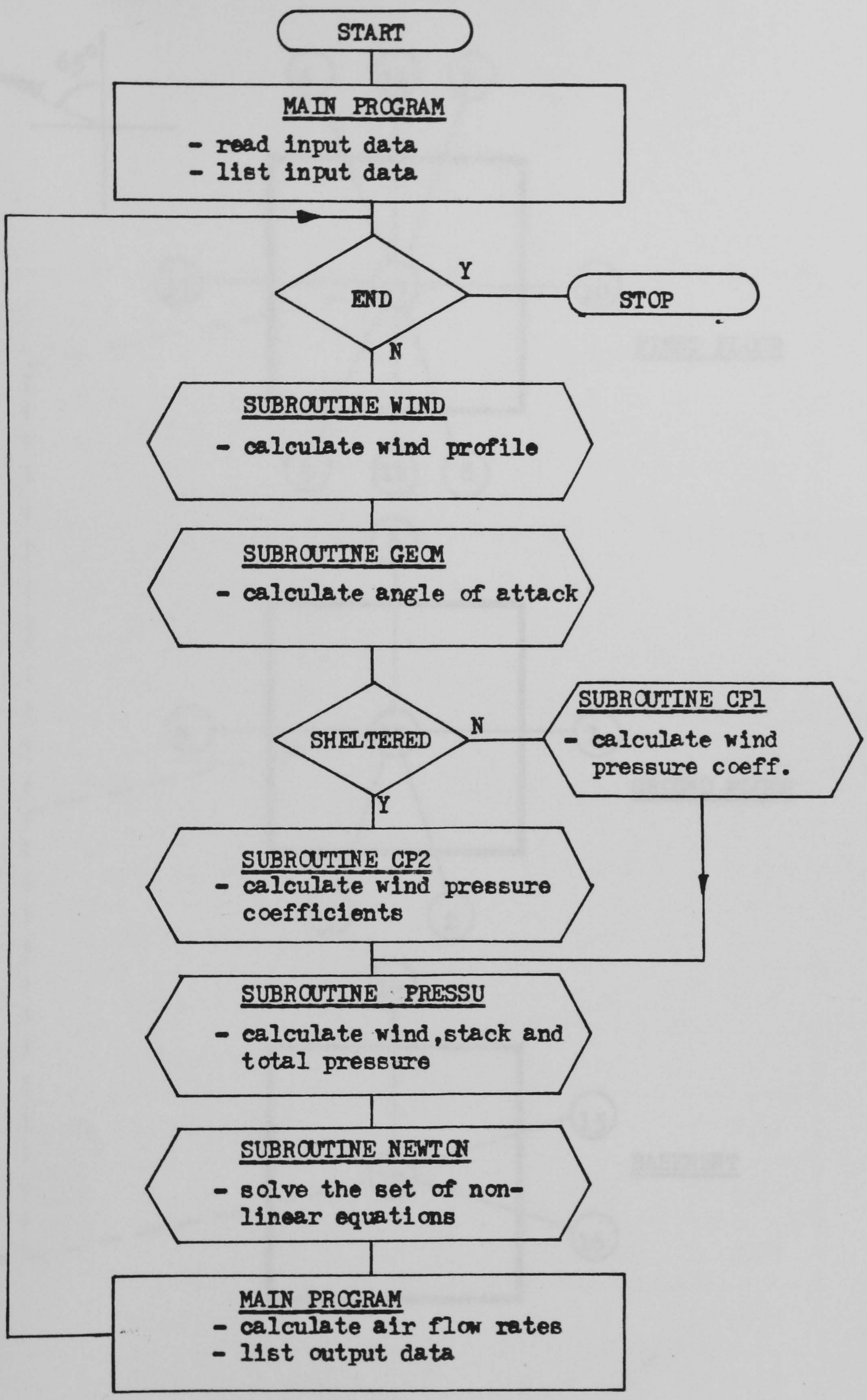

Fig. 3.3 Flow chart of the FLOW program

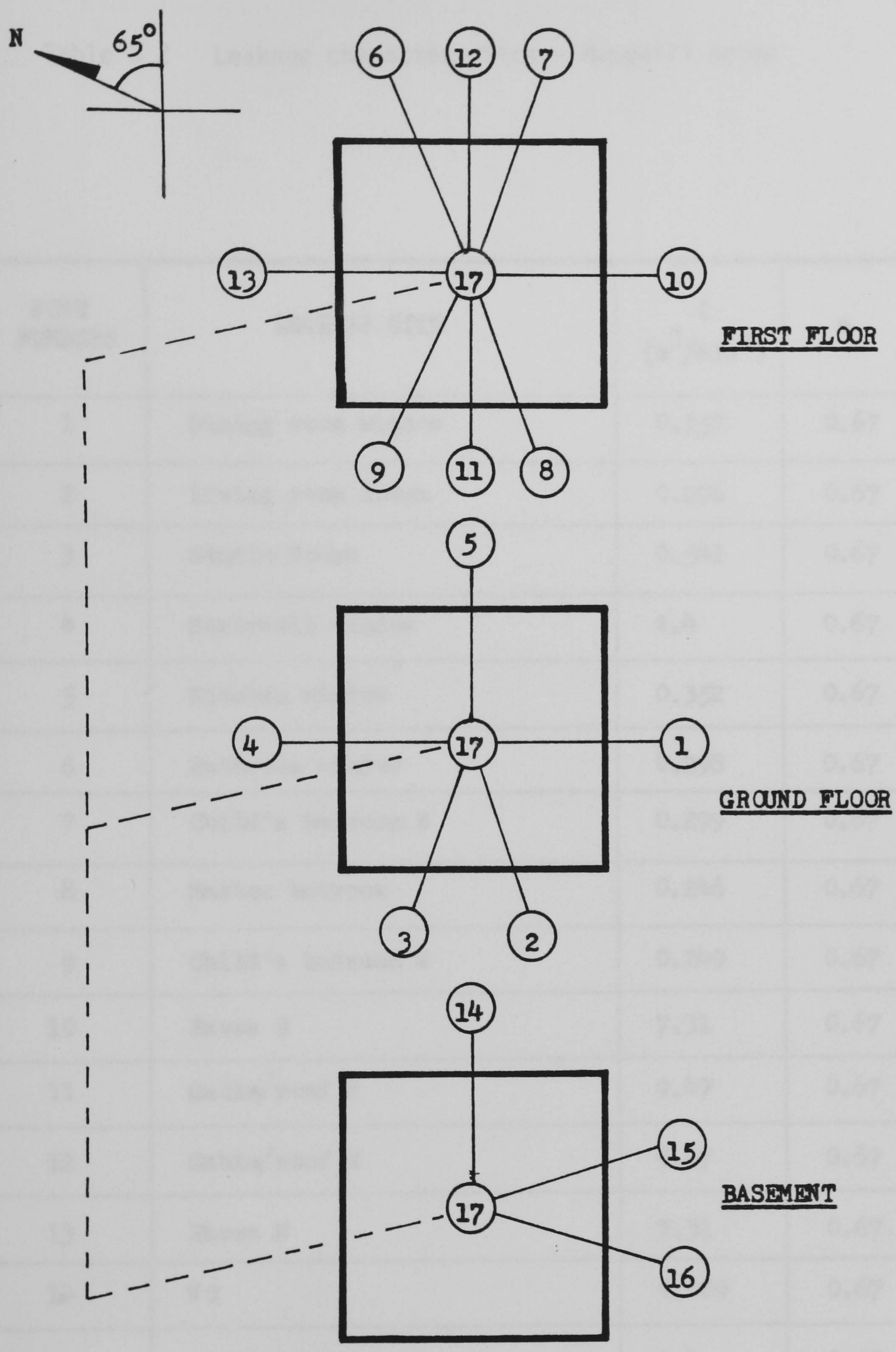

Fig. 3.4 Flow network - Maugwill house

Table 3.2 Leakage characteristics - Maugwill house

NODE NUMBERS	LEAKAGE SITE	C (m^3/hPa^n)	n
1	Dining room window	0.157	0.67
2	Living room doors	0.296	0.67
3	Studio doors	0.542	0.67
4	Stairwell window	2.4	0.67
5	Kitchen window	0.352	0.67
6	Bathroom window	0.298	0.67
7	Child's bedroom E	0.299	0.67
8	Master bedroom	0.246	0.67
9	Child's bedroom W	0.249	0.67
10	Eaves S	7.31	0.67
11	Gable/roof W	9.47	0.67
12	Gable/roof E	9.47	0.67
13	Eaves N	7.31	0.67
14	WC	0.089	0.67
15	Front door	5.4	0.50
16	Boiler room window	0.216	0.67
17	Internal node	-	-

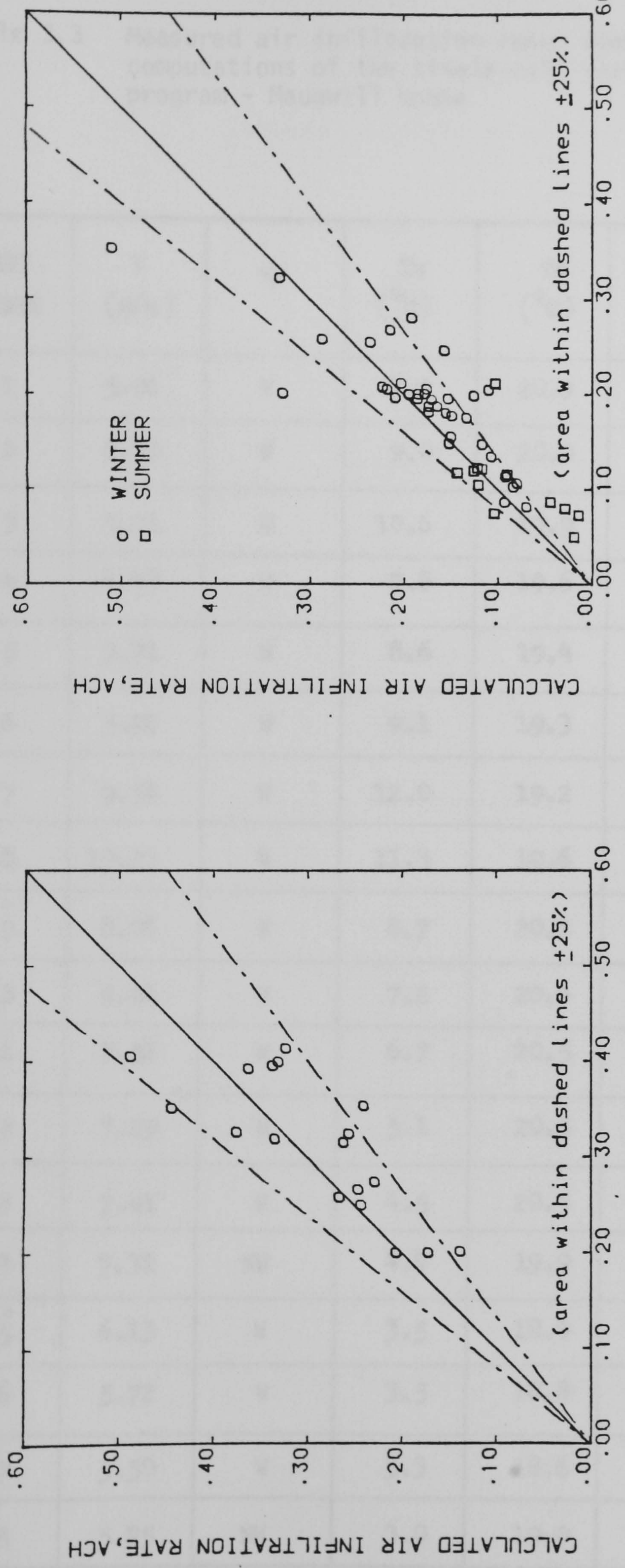

(b)

(a)

Fig. 3.5 Measured air infiltration rates compared with the computations of the single-cell version of the FLOW program: a) Maugwill house and b) HUDAC 'upgraded house'.

Table 3.3 Measured air infiltration rates compared with the computations of the single-cell version of the FLOW program - Maugwill house

TEST NUMBER	V (m/s)	Ψ	Te (°C)	Ta (°C)	Q(EXP) (ACH)	Q(CALC) (ACH)
1	5.96	W	8.9	20.9	0.266	0.247
2	6.33	W	9.0	20.9	0.258	0.267
3	5.21	W	10.6	19.9	0.200	0.206
4	4.48	W	9.8	19.6	0.200	0.172
5	3.71	W	8.6	19.4	0.201	0.138
6	5.92	W	9.1	19.3	0.250	0.244
7	9.54	W	12.0	19.2	0.351	0.445
8	10.23	W	11.3	19.6	0.405	0.489
9	8.06	W	8.7	20.2	0.392	0.363
10	8.24	W	7.2	20.4	0.326	0.376
11	7.52	W	6.7	20.5	0.319	0.335
12	7.29	W	5.1	20.5	0.413	0.324
13	7.41	W	4.5	20.5	0.399	0.332
14	7.32	NW	4.4	19.9	0.395	0.338
15	6.13	W	3.5	18.9	0.315	0.262
16	5.72	W	3.5	18.8	0.353	0.241
17	5.50	W	3.3	18.6	0.274	0.229
18	5.75	NW	3.0	19.0	0.324	0.257

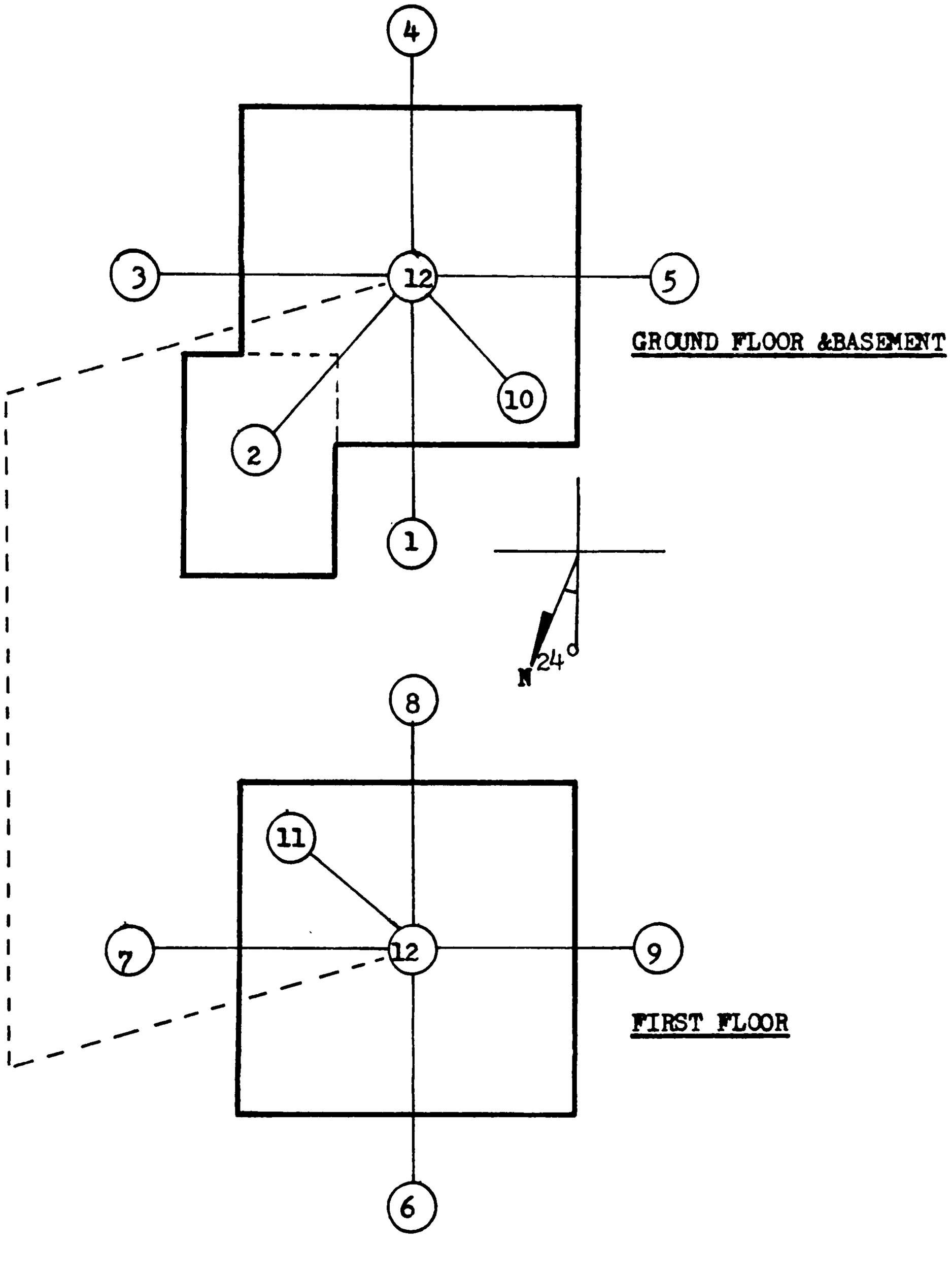

Fig. 3.6 Flow network - HUDAC 'upgraded' house

Table 3.4 Leakage characteristics - HUDAC 'upgraded' house

NODE NUMBERS	LEAKAGE SITE	C (m^3/hPa^n)	n
1	Front ground floor facade	4.03	0.71
2	Garage	4.04	0.71
3	NE Ground floor facade	4.03	0.71
4	Rear ground floor facade	5.87	0.71
5	SW ground floor facade	5.51	0.71
6	Front first floor facade	5.87	0.71
7	NE first floor facade	5.11	0.71
8	Rear first floor facade	5.87	0.71
9	SW first floor facade	5.11	0.71
10	Ground floor roof	1.48	0.71
11	First floor roof	14.65	0.71
12	Internal node	-	-

Table 3.5 Measured air infiltration rates compared with the computations of the single-cell version of the FLOW program - HUDAC 'upgraded house'

TEST NUMBER	V (m/s)	Ψ	Te (^{o}C)	Ta (^{o}C)	Q(EXP) (ACH)	Q(CALC) (ACH)
1	7.33	N	7.5	22.0	0.258	0.288
2	4.83	N	4.0	22.4	0.181	0.156
3	1.65	N	-12.7	20.4	0.176	0.134
4	0.98	N	-15.6	21.8	0.178	0.150
5	2.82	NW	16.2	22.5	0.082	0.070
6	5.27	NW	15.5	22.5	0.201	0.179
7	8.05	NW	15.0	22.5	0.322	0.333
8	5.99	NW	11.3	22.5	0.268	0.244
9	6.39	NW	9.3	22.2	0.255	0.237
10	3.93	NW	-2.6	20.7	0.205	0.110
11	10.55	NW	-10.6	22.0	0.352	0.510
12	4.11	NW	-16.1	22.1	0.199	0.126
13	3.84	W	15.0	22.5	0.114	0.092
14	3.35	W	9.5	22.5	0.087	0.093
15	6.12	W	-3.4	23.4	0.201	0.196
16	4.43	W	-4.4	21.8	0.156	0.150
17	9.61	W	-4.7	21.0	0.201	0.330
18	5.63	W	-5.5	22.6	0.196	0.186
19	4.69	W	-7.4	22.5	0.188	0.165
20	5.68	W	-9.3	19.8	0.181	0.192
21	5.23	W	-9.6	22.6	0.201	0.185
22	5.99	W	-10.8	23.1	0.197	0.210
23	6.30	W	-12.2	21.3	0.206	0.219
24	3.84	W	-15.4	22.1	0.188	0.174

Table 3.5 (continued)

25	5.23	W	-18.7	21.8	0.212	0.204
26	5.86	W	-19.9	20.7	0.208	0.224
27	1.07	W	3.9	21.4	0.103	0.084
28	1.61	NE	-2.0	22.8	0.135	0.108
29	7.38	S	-0.2	22.0	0.200	0.195
30	6.48	S	-3.7	22.4	0.206	0.176
31	5.01	E	12.5	21.1	0.107	0.080
32	9.34	E	4.6	22.5	0.182	0.175
33	8.05	E	3.8	22.2	0.149	0.152
34	7.64	E	-1.0	22.4	0.247	0.157
35	8.00	E	-4.7	22.0	0.195	0.171
36	1.43	E	-5.6	21.0	0.148	0.117
37	1.16	E	-15.9	22.0	0.196	0.154
38	3.13	N	25.4	22.2	0.166	0.090
39	3.49	N	25.1	22.2	0.075	0.104
40	3.93	N	25.1	22.2	0.123	0.122
41	3.84	N	24.6	22.2	0.122	0.117
42	5.14	W	29.0	21.1	0.105	0.121
43	2.28	W	26.5	22.2	0.087	0.044
44	4.60	W	19.0	21.7	0.212	0.103
45	1.12	NE	21.5	21.7	0.073	0.014
46	7.09	S	26.8	22.2	0.118	0.144
47	6.39	S	24.5	21.9	0.120	0.126
48	1.74	S	24.4	22.8	0.050	0.019
49	2.41	S	23.6	22.5	0.080	0.029

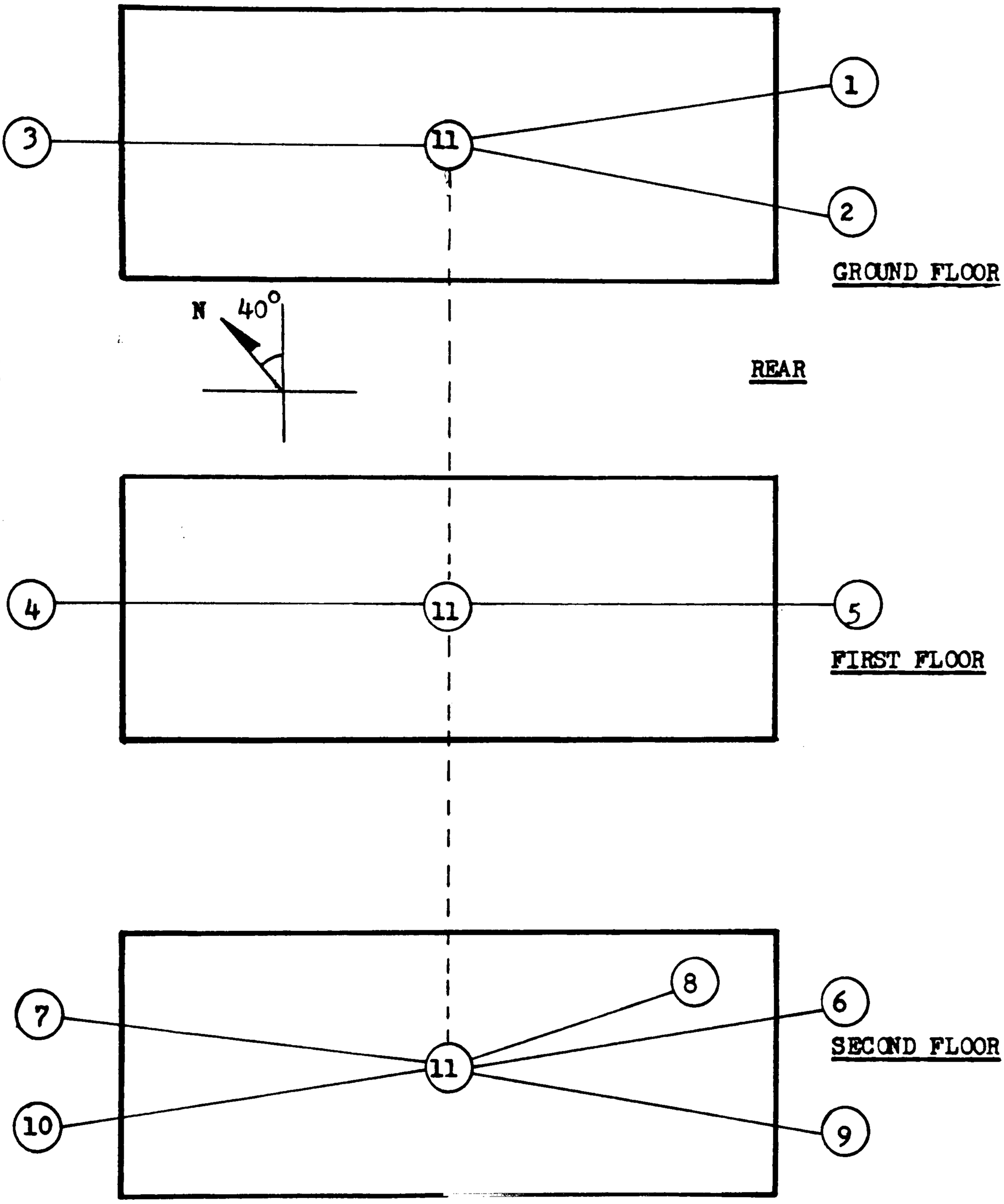

Fig. 3.7 Flow network - Runcorn house

Table 3.6 Leakage characteristics
- Runcorn house

NODE NUMBERS	LEAKAGE SITE	C (m^3/hPa^n)	n
1	Kitchen door	23.04	0.57
2	Kitchen window	7.63	0.64
3	Front door	22.61	0.56
4	Bedroom 1 window	13.36	0.60
5	Lounge window	17.60	0.58
6	Bedroom 3 window	10.08	0.63
7	Bedroom 2 window	10.19	0.60
8	Bathroom skylight and vents	16.60	0.73
9	Rear roof/wall junction	67.56	0.66
10	Front roof/wall junction	67.56	0.66
11	Internal node	-	-

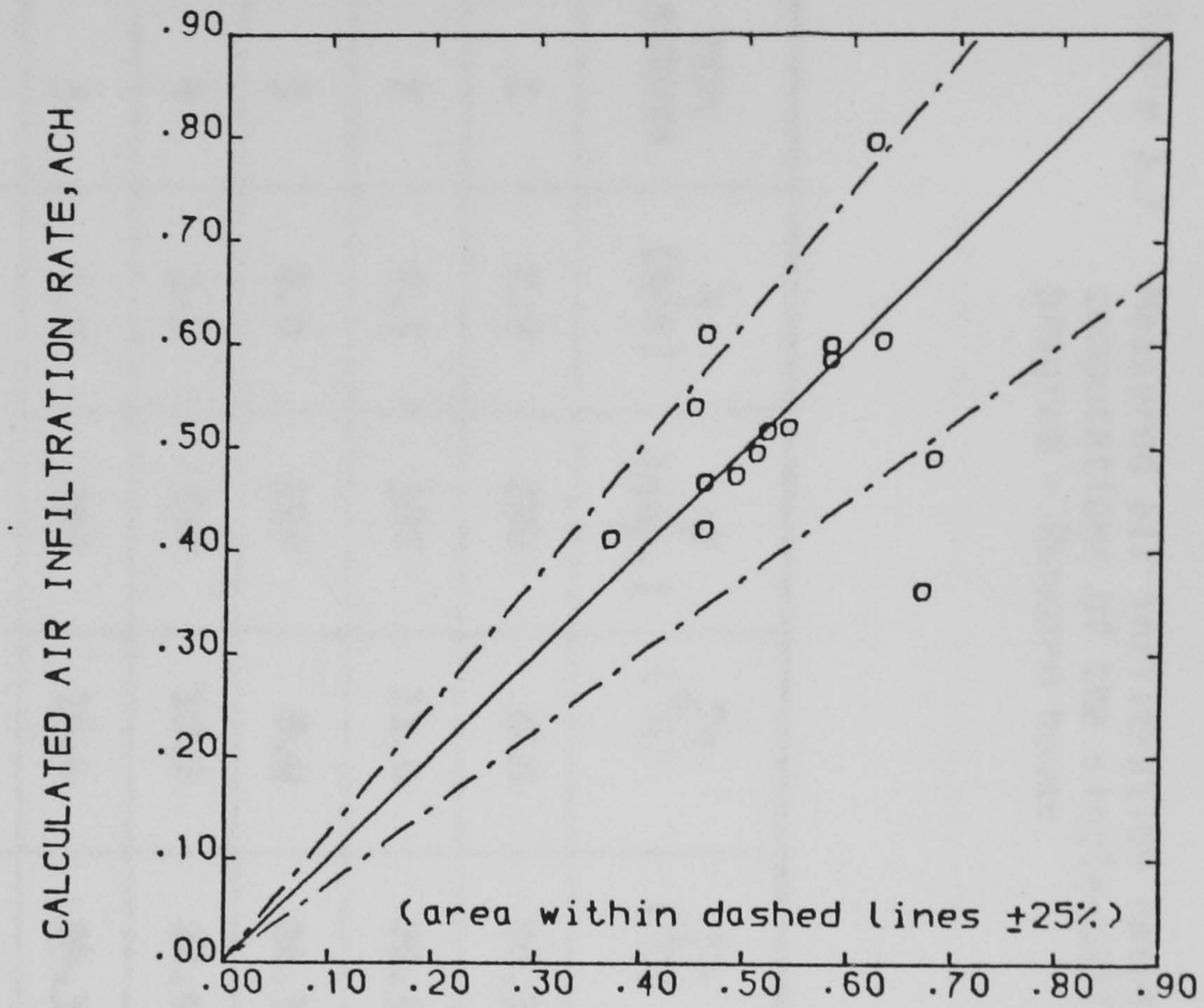

Fig. 3.8 Measured air infiltration rates compared with the computations of the single cell-version of the FLOW program - Runcorn house

Table 3.7 Measured air infiltration rates compared with the computations of the single-cell version of the FLOW program - Runcorn house

TEST NUMBER	V (m/s)	ψ (deg.)	Te (^{o}C)	Ta (^{o}C)	Q(EXP) (ACH)	Q(CALC) (ACH)
1	2.0	270	6.6	20.3	0.58	0.60
2	2.5	300	11.0	22.5	0.45	0.54
3	2.0	210	8.9	22.3	0.58	0.58
4	3.5	330	12.2	22.9	0.51	0.50
5	1.7	320	16.4	24.3	0.46	0.42
6	6.5	270	13.6	22.7	0.62	0.80
7	3.7	250	11.5	22.7	0.52	0.52
8	1.5	290	11.5	20.7	0.46	0.47
9	3.7	270	16.1	21.9	0.37	0.41
10	4.5	310	14.0	22.7	0.46	0.61
11	3.5	300	11.0	22.3	0.54	0.52
12	3.7	10	15.0	21.7	0.67	0.36
13	3.2	10	12.5	22.2	0.49	0.47
14	1.2	20	7.0	21.4	0.63	0.61
15	3.0	30	13.3	23.2	0.68	0.49

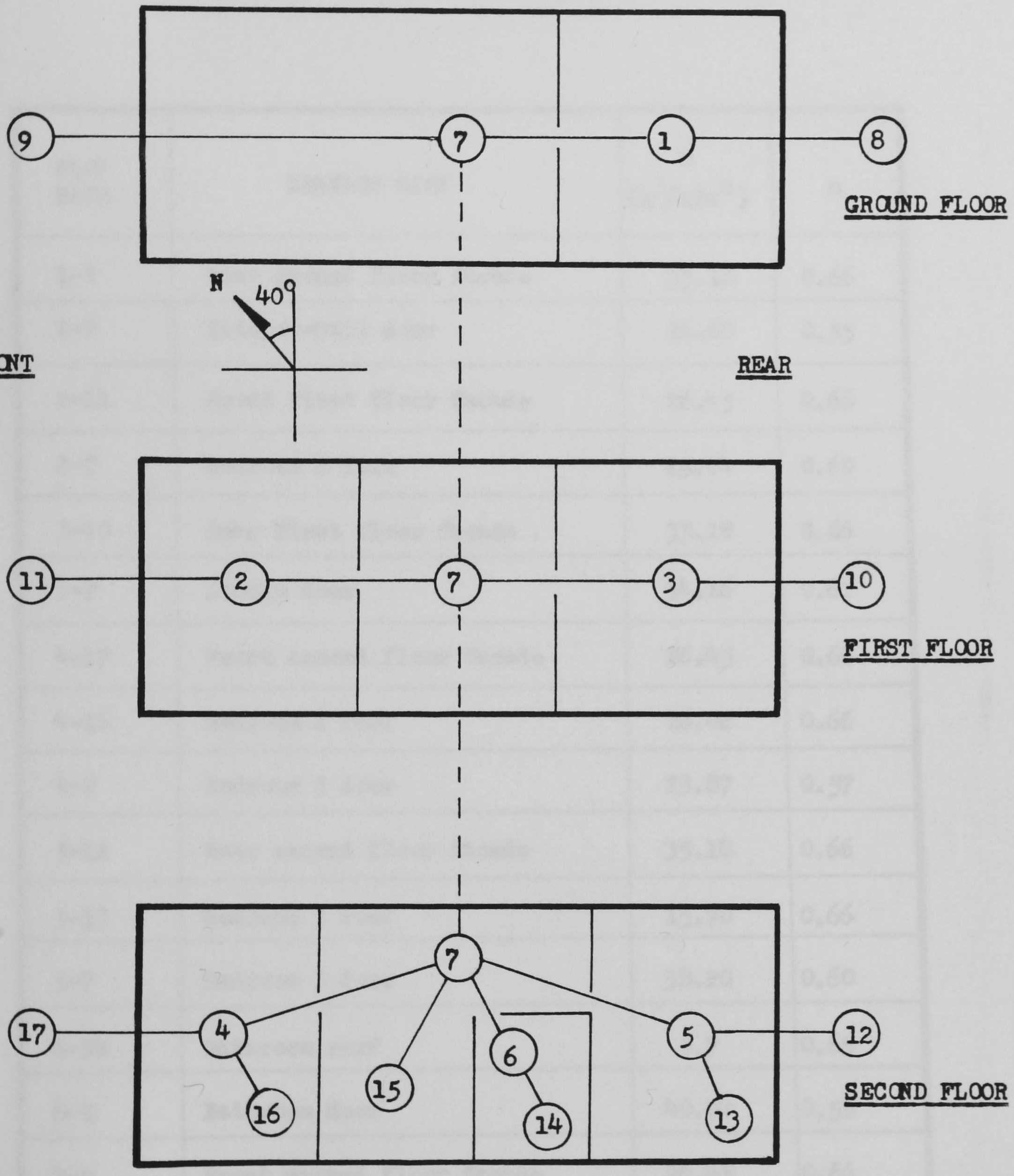

Fig. 3.9 Flow network - Runcorn house (multi-cell)

Table 3.8 Leakage characteristics - Runcorn house (multi-cell)

FLOW PATH	LEAKAGE SITE	C (m^3/hPa^n)	n
1-8	Rear ground floor facade	35.18	0.66
1-7	Kitchen-hall door	26.60	0.55
2-11	Front first floor facade	26.45	0.66
2-7	Bedroom 1 door	19.04	0.60
3-10	Rear first floor facade	35.18	0.66
3-7	Lounge door	34.16	0.61
4-17	Front second floor facade	26.45	0.66
4-16	Bedroom 2 roof	16.02	0.66
4-7	Bedroom 2 door	23.87	0.57
5-12	Rear second floor facade	35.18	0.66
5-13	Bedroom 3 roof	15.70	0.66
5-7	Bedroom 3 door	38.20	0.60
6-14	Bathroom roof	5.7	0.66
6-7	Bathroom door	40.64	0.56
7-9	Front ground floor facade	26.45	0.66
7-15	Stairwell roof	13.67	0.66

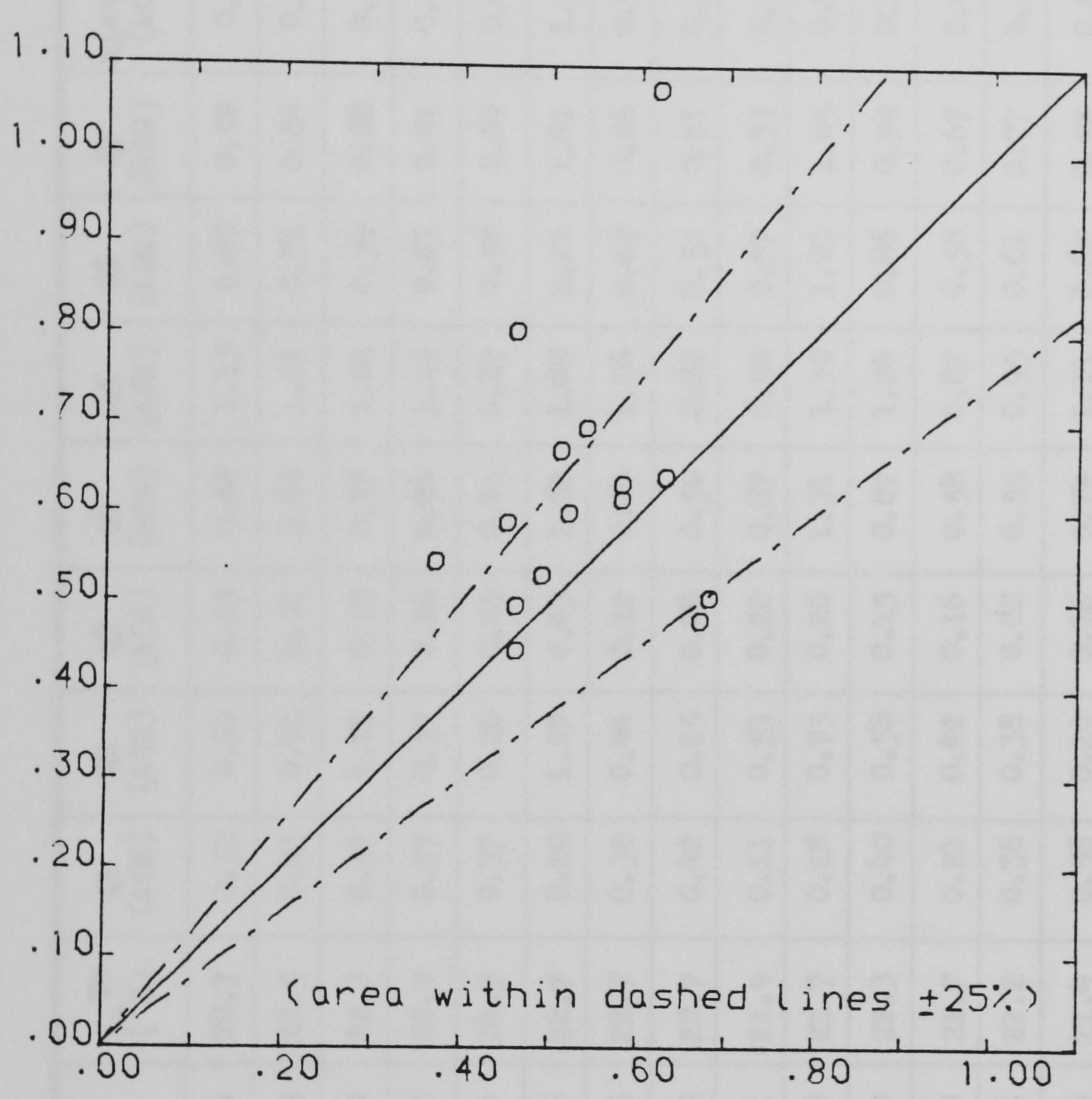

Fig. 3.10 Measured air infiltration rates compared with the computations of the multi-cell version of the FLOW program - Runcorn house

Table 3.9 Measured air infiltration rates compared with the computations of the multi-cell version of the FLOW program - Runcorn house

TEST NUMBER	V (m/s)	Ψ (deg.)	Te (°C)	Ta (°C)	Q1 (ACH)	Q2 (ACH)	Q3 (ACH)	Q4 (ACH)	Q5 (ACH)	Q6 (ACH)	Q7 (ACH)	Q(av.) (ACH)	Q(EXP) (ACH)
1	2.0	270	6.6	20.3	0.52	0.32	0.09	0.64	1.15	0.68	0.92	0.63	0.58
2	2.5	300	11.0	22.5	0.45	0.41	0.01	0.64	1.11	0.71	0.84	0.59	0.45
3	2.0	210	8.9	22.3	0.57	0.13	0.18	0.73	1.03	0.59	0.88	0.62	0.58
4	3.5	330	12.2	22.9	0.37	0.57	0.16	0.84	1.19	0.83	0.91	0.67	0.51
5	1.7	320	16.4	24.3	0.37	0.26	0.05	0.41	0.83	0.50	0.64	0.44	0.46
6	6.5	270	13.6	22.7	0.29	1.09	0.43	2.02	1.40	1.21	1.41	1.07	0.62
7	3.7	250	11.5	22.7	0.38	0.44	0.12	0.64	1.06	0.69	0.86	0.60	0.52
8	1.5	290	11.5	20.7	0.42	0.25	0.08	0.50	0.89	0.52	0.71	0.49	0.46
9	3.7	270	16.1	21.9	0.11	0.53	0.22	0.87	0.90	0.67	0.73	0.55	0.37
10	4.5	310	14.0	22.7	0.28	0.75	0.26	1.31	1.30	1.03	1.05	0.80	0.46
11	3.5	300	11.0	22.3	0.40	0.58	0.15	0.87	1.24	0.86	0.94	0.70	0.54
12	3.7	10	15.0	21.7	0.21	0.42	0.16	0.58	0.82	0.58	0.67	0.48	0.67
13	3.2	10	12.5	22.2	0.36	0.38	0.08	0.55	0.95	0.61	0.77	0.53	0.49
14	1.2	20	7.0	21.4	0.56	0.20	0.16	0.74	1.11	0.62	0.92	0.64	0.63
15	3.0	30	13.3	23.2	0.46	0.19	0.04	0.57	0.91	0.50	0.74	0.50	0.68

Table 3.10 Comparison between various infiltration models - % number of calculations within 25% of measurement

MODEL \ DATA SET	MAUGWILL HOUSE	HUDAC 'UPGRADED' HOUSE (1)	RUNCORN HOUSE
FLOW	83	84	73
BSRIA	94	44	-
NRC (2)	100	40	-
NRC (3)	44	72	80
IMG-TNO	82	-	-
BRITISH GAS (4)	-	84	67
BRITISH GAS (5)	-	71	80
NBRI	88	63 (6)	-
IGT	100	76	67
LBL	100	81	80
BRE	89	70	87
Reeves et al	100	57	14

(1) Winter data only
(2) Codes of practice pressure coefficients
(3) NRC pressure coefficients
(4) Without turbulent correction
(5) With turbulent correction
(6) Winter and summer data

CHAPTER 4

CHAPTER 4 - SENSITIVITY ANALYSIS ON THE NBSLD PROGRAM

4.1 - INTRODUCTION

In the context of the present work, it was felt desirable to quantify the influence of input values for air infiltration rates and internal/external convective heat transfer coefficients on the predicted heating/cooling load and/or on the internal air temperature within a typical domestic dwelling. The NBSLD program (Ref.20), which is one of the most sophisticated dynamic building thermal model, was chosen for this purpose for two main reasons: firstly because of the present author´s previous experience in its use (Ref.72) and secondly because it was well documented. An updated listing of the whole program was obtained with a full description of all subroutines involved and an user manual describing the various input/output data options.

The intention of this work was to incorporate all three sub-models (WIND-CHT,FLOW and ROOM-CHT) into the NBSLD program, and it was therefore felt necessary to understand this code in detail. In doing so , all its units were internally changed to the S.I. system necessitating a complete review of all the algorithm´s equations, rather than simply using a set of conversion factors for the input/output data. It was also necessary to make some adjustments to the program in order to enable it to simulating buildings in the United Kingdom. The SUN routine (solar energy predictions) was adjusted, since it did not work at longitudes below 1.3°W (Kew - 0.42°W), and a new HOLIDAY(British holidays) and DST(British summer/winter time) subroutines were developed. Some alterations were also necessary in order to calculate the solar radiation attenuation from clouds, since the CCF(cloud cover factor) parameter, as originally used by the NBSLD program, is not available for the United Kingdom. Finally, changes were made to make the program compatible with the format of the British meteorological data base system (Ref.73).

This revised version of the NBSLD program was then run using a input/output set of data, kindly provided by Dr. T. Kusuda of the U.S. National Bureau of Standards, for their Houston test house. The results obtained compared favourably with those from the original version of the NBSLD program. The program was also run with many different input options, such as thermal confort, daylighting, etc, in order to understand its potential and limitations. Approximately 40 tests were undertaken. During this last stage some inaccuracies were detected in the program, but as the aim of the present work was to assess the influence of the sub-models for internal/external convection and air infiltration rates on the predicted results, instead of refining the program, no corrections were made. An example of such inaccuracies is the fact that, in the program, the shape factors of windows and doors are only a function of their area, thereby disregarding any influence of the element´s location on the wall. However a ´strong depencence of the final results on one

variable,TIM, was found. This variable is subtracted from all the temperatures in order to minimize the digital errors which occur when a large number of numerical data are multiplied and added. Since the net effect of this subtraction is zero, no variations in the program results were expected when different values of TIM are specified at the begining of the program. Suprisingly, the program results changed in accordance to the specified TIM value. This was because the ground temperature below slab is calculated, in the first hourly iteration, by assuming the internal air temperature(not yet known) as equal to TIM . This value was not originally updated in the subsequent hourly iterations. Dr. T. Kusuda, in private correspondence, agreed that the program modifications made to eliminate this effect were both correct and desirable.

4.2 - FUNDAMENTALS OF THE NBSLD PROGRAM

In the NBSLD program the transient heat conduction through exterior walls of a room or space are handled by using the response factor technique. This technique makes extensive use of the 'convolution principle' to account for the thermal storage effect of the building structure. According to this principle any time-dependent variable,A, which may be expressed as a time series, and is influenced by another time series,B, can be written in linear form:

$$A_t = \sum_{j=0}^{m} X_j B_{t-j} \qquad (4.1)$$

In equation (4.1), the value of A at time t is expressed as a linear function of all the time values of B at t=t,t-1,t-2...t-m with $X_0, X_1, \ldots X_m$ being the time-dependent coefficients. The above equation is called the convolution and $X_0, X_1, \ldots X_m$ are called the response factors when refering to wall or roof heat conduction. The value of m in the convolution equation depends upon the degree to which the time parameter B_{t-m} (or B at m hours previous to time t) would influence the value of A . If the response of B_{t-m} upon A_t is insignificant, X_m is nearly zero and the values of B beyond the (t-m)th hour are of no importance.If no time lag effect exists between the two time series, A and B, then the value of m will be zero or the response factor X_j will be zero except for the first term X_0. Thus, by simulating the transient boundary temperatures by a sequence of pulses, and by summing up the heat flux caused by each pulse during preceding significant times, the total heat flux at a given time can be derived.

Stephenson and Mitalas (Ref.74) are responsible for the present day form of the response factor method. They introduced a triangular pulse representation technique as shown in Figure 4.1. Each term in

the time-series is considered as the magnitude of a triangular pulse centred at the particular time in question, with a base equal to twice the time step. The pattern of the straight lines connecting all peak points of the triangles is a good approximation of the original function as shown dotted in Figure 4.1. The way the response factors are calculated will not be described here, since it involves lengthy mathematical solutions to the standard transient heat conduction differential equation. Kusuda (Ref.75) provide an excellent background to these calculations.

The NBSLD program can be used for estimating the internal air temperature distribution in unconditioned buildings, or the heating/cooling load distribution for constant or varying internal conditions. Alternatively, it can determine the prevailing internal air temperature when the plant input or extract does not match the heating or cooling load required to maintain constant temperature conditions. The program can therefore be run in two different modes:room temperature calculation mode or the room load calculation mode. The room temperature mode requires the simultaneous solution of all the heat balance equations in order to determine the surface temperatures together with the internal air temperature. On the other hand, the room load calculation mode requires the room air temperature to be prescribed and only the room surface temperatures are computed. The convective heat exchange between the room air and the heat emitting surfaces is then the cooling load (or the heating load if the heat is lost from the surfaces).

4.2.1 - The room temperature calculation mode

This principle of calculation can be demonstrated by considering a fictitious space that is enclosed by 4 walls, a ceiling and floor and having infiltration and/or ventilation air as well as normal internal energy sources. The equation that governs the energy exchange at each of the six internal surfaces at a given time t is:

$$(q_c)_{i,t} + (q_r)_{i,t} + (q_{cd})_{i,t} + (q_{es})_{i,t} = 0 \qquad (4.2)$$

where q_c ,q_r ,q_{cd} and q_{es} are the heat fluxes due to convection, long-wave radiation, conduction and radiation from various other sources(solar radiation, lights, occupants and equipment), all for the i-th surface at a given time t respectively.

The convection heat flux at any enclosure surface is given by,

$$(q_c)_{i,t} = (h_c)_i \quad (Ta_t - Ti_{i,t}) \qquad (4.3)$$

where h_c is the inside surface convection heat transfer coefficient for the i-th surface, Ta_t is the internal air temperature at time t

and $Ti_{i,t}$ is the inside surface temperature for the i-th surface at time t.

The long-wave radiation heat flux to any surface from surrounding surfaces is given by,

$$(q_r)_{i,t} = \sum_{k=1}^{NS} (h_r)_{i,k} (Ti_{k,t} - Ti_{i,t}) \qquad (4.4)$$

where NS is the number of enclosure surfaces and $(h_r)_{i,k}$ is the radiation heat transfer coefficient between surfaces i and k, which is given by,

$$(h_r)_{i,k} = 4\sigma F_{i,k} Tav^3 \qquad (4.5)$$

where σ is the Stefan-Boltzman constant, $F_{i,k}$ is the grey body shape factor between surfaces i and k, and Tav is an assumed time-averaged value of all the inside surface (absolute) temperatures.

The radiation heat flux impinging upon the i-th surface at time t from various sources is given by,

$$(q_{es})_{i,t} = Rs_{i,t} + (Req_{i,t} + Roc_{i,t} + Rli_{i,t}) / \sum_{i=1}^{NS} A_i \qquad (4.6)$$

where $Rs_{i,t}$ is the solar energy coming through the windows and absorbed by the i-th surface at time t; $Req_{i,t}$, $Roc_{i,t}$, and $Rli_{i,t}$ are the rate of heat radiated from equipment, occupants and lights respectively and then absorbed by the i-th surface at time t; and A_i is the area of the i-th heat transfer surface.

The conduction heat flux can be expressed as the sum of the products of the surface temperature time-series and the appropriate response factors:

$$(q_{cd})_{i,t} = -\sum_{j=0}^{NR_i} X_{i,j} Ti_{i,t-j} + \sum_{j=0}^{NR_i} Y_{i,j} To_{i,t-j} - CR_i (q_{cd})_{i,t-1} \qquad (4.7)$$

where NR_i is the number of response factors of the i-th surface, $X_{i,j}$ and $Y_{i,j}$ are the response factors of the i-th surface at time t, CR_i is the common ratio for the response factors of the i-th surface and $To_{i,t}$ is the outside surface temperature for the i-th surface at time t. The common ratio, CR_i, is a common value for all response factors, obtained by dividing the response factors at time t+1 by the corresponding values at time t, for large value of t. In typical wall heat transfer calculations, the summation terms in equation (4.7) may be truncated at j=48. In other words, if the value of heat flux at time t is needed, it is necessary to have the hourly temperature history covering the previous 48 hours period as well as values of $X_{i,j}$ and $Y_{i,j}$. By making use of the heat flux at time t-1 and of the common

ratio, together with the temperature history, the maximum number of $j(NR_i)$ can be decreased considerably. This aspect is discussed in detail in the ASHRAE handbook (Ref.4).

The heat balance at the enclosure air point is formulated on the basis that the heat storage capacity of the enclosed air is small when compared to the total storage capacity of the surrounding fabric. Such a heat balance yields:

$$\sum_{i=1}^{NS} (h_c)_i \; A_i \, (Ti_{i,t} - Ta_t) + Mi_t \; Cpr \; (Te_t - Ta_t) +$$

$$+ Ms_t \; Cpr \; (Ts_t - Ta_t) + Ceq_t + Coc_t + Cli_t = 0 \qquad (4.8)$$

where Cpr is the specific heat of air; Mi_t is the mass air flow rate of outdoor air infiltrating into the room at time t; Ms_t and Ts_t are the mass air flow rate and temperature of the supply air from the central system at time t; Te_t is the outdoor dry-bulb air temperature at time t; and Ceq_t, Coc_t, and Cli_t are the rate of heat from equipment, occupants and lights respectively convected into the room air at time t.

In this calculation mode, the internal air temperature is not initially known and it is necessary to solve the six internal surface heat balance equations simultaneously with the enclosure air heat balance equation. This complete set of heat transfer equations is solved, within the program, by solving the following matrix:

$$\begin{bmatrix} A_{1,1} \; \cdots \; A_{1,NS+1} \\ A_{2,1} \; \cdots \; A_{2,NS+1} \\ \cdots\cdots\cdots \\ \cdots\cdots\cdots \\ A_{NS,1} \; \cdots \; A_{NS,NS+1} \\ A_{NS+1,1} \; \cdots \; A_{NS+1,NS+1} \end{bmatrix} \begin{bmatrix} Ti_{1,t} \\ Ti_{2,t} \\ \cdots \\ \cdots \\ Ti_{NS,t} \\ Ta_t \end{bmatrix} \begin{bmatrix} B_1 \\ B_2 \\ \cdots \\ \cdots \\ B_{NS} \\ B_{NS+1} \end{bmatrix} \qquad (4.9)$$

where:

$$A_{i,i} = X_{i,1} + (h_c)_i + \sum_{k=1}^{NS} (h_r)_{i,k} \qquad (4.10)$$

$$A_{i,K} = -(h_r)_{i,k} \tag{4.11}$$

$$A_{i,NS+1} = -(h_c)_i \tag{4.12}$$

$$B_i = -\sum_{j=1}^{NR_i} X_{i,j}\ Ti_{i,t-j} + \sum_{j=0}^{NR_i} Y_{i,j}\, To_{i,t-j} - CR_i (q_{cd})_{i,t-1} + (q_{es})_{i,t} \tag{4.13}$$

$$A_{NS+1,k} = A_k\ (h_c)_k \tag{4.14}$$

$$A_{NS+1,NS+1} = -(Mi_t + Ms_t)\ Cpr - \sum_{k=1}^{NS} (h_c)_k\ A_k \tag{4.15}$$

$$B_{NS+1} = -Ceq_t - Coc_t - Cli_t - Mi_t\ Cpr\ Te_t - Ms_t Cpr\ Ts_t \tag{4.16}$$

4.2.2 - The room load calculation mode

In this mode of calculation the heating/cooling load is determined relative to some prescribed internal air temperature. Consequently, only the room surface temperatures are computed and, therefore, the matrix presented in the previous section, reduces to:

$$\begin{bmatrix} A_{1,1} & \cdots & A_{1,NS} \\ A_{2,1} & \cdots & A_{2,NS} \\ \cdots\cdots\cdots & & \\ \cdots\cdots\cdots & & \\ A_{NS,1} & & A_{NS,NS} \end{bmatrix} \begin{bmatrix} Ti_{1,t} \\ Ti_{2,t} \\ \cdots \\ \cdots \\ Ti_{NS,t} \end{bmatrix} = \begin{bmatrix} B'_1 \\ B'_2 \\ \cdot \\ \cdot \\ B'_{NS} \end{bmatrix} \tag{4.17}$$

where

$$B'_i = B_i - A_{i,NS+1}\ Ta_t \tag{4.18}$$

once the internal surface temperature profile is known, the sensible load, QLS_t, at a given time t, can be determined via equation (4.8) to give:

$$QLS = \sum_{i=1}^{NS} (h_c)_i \; A_i (Ti_{i,t} - Ta_t) + Mi_t \; Cpr \; (Te_t - Ta_t) +$$

$$+Ceq_t + Coc_t + Cli_t \qquad (4.19)$$

It should be pointed out that for ordinary load calculations, Ms_t and Ts_t are not used as long as the following condition is satisfied:

$$|QLS_t| < |Ms_t \; Cpr \; (Ta_t - Ts_t)| \qquad (4.20)$$

In other words, the desired or prescribed room temperature can be maintained as long as the calculated load is less than the maximum capacity of the central system. When the above condition is not satisfied due to inadequate values for either the air supply rate or the supply air temperature, the room temperature used for the load calculation must be corrected, by first calculating it as outlined in the sub-section 4.2.1.

4.3 - THE TEST HOUSE

The WIND-CHT, FLOW and ROOM-CHT programs had all been individually verified prior to incorporation into the NBSLD program. Nevertheless it was felt desirable to validate the revised version of the NBSLD program (standard version + sub-models). Theoreticaly ,this can only be performed by comparing the program results with the corresponding field measurement data. In practice, however, such a task is faced with many difficulties. Problems commonly encountered in this area include (i)changes experienced in the thermal properties of the building fabric due to fluctuations in moisture content, (ii)actions of occupants with regard to window opening and blind operation, (iii)the quality of the building workmanship, (iv)the availability of a comprehensive set of simultaneously recorded climatic data and structural design information, and (v)the expense associated with extensive building instrumentation. These comments are in line with one of the conclusions from the IEA Annex I (Ref.76), which stated that: ´in order to define a building and/or a system in sufficient detail such that analysts need make no assumptions about the input data, an incredible amount of detail has to be provided, which is not realistic in the design situation. Consequently, differences arising from interpretations of the specification are liable to produce significant differences in predicted energy consumption, irrespective of the computer program quality´. Nevertheless, an attempt was made to validate the standard version of the NBSLD program in 1974 by Burch, Peavy and Powell (Ref.77). They used an experimental masonary building placed in an environmental chamber ,thereby avoiding many of the uncontrolled variations indicate above. The results were very good , with a maximum difference between

the computed and measured heating load of only 8%, and the average difference of 4.3% for all tests.

According to Bloomfield (Ref.78), when a validation study is performed by a program's author and/or associates there is a 'strong' possibility of good agreement between computed and measured values being achieved. This happens because the modellers very often have many degrees of freedom for specifying the values of the input data. The validation study is thereby reduced to a model/compare/refine loop which works until a 'reasonable' agreement is obtained. In the previously mentioned validation study by Burch et al (Ref.77), for instance, the internal and external convective heat transfer coefficients and the air infiltration rate, among other variables, were assumed to be constants. By changing the values of these constants the computed results can be adjusted until a good 'agreement' is achieved, due to a combination of errors giving false matches with real data.

Unfortunatelly, no field measurements appear to be available to facilitate a proper validation study (this is one of the aims of the recently formed BRE/SERC validation group). It was therefore decided to perform only a sensitivity analysis on the NBSLD program by adopting a 'hypothetical' detached house broadly based on the multi-layered construction of the 3-bedroomed, terraced houses in Livingston, Scotland that were studied by Clarke and Forrest (Ref.79). In addition, a ground floor insulation slab was included to reflect a 'heavy' (or thermally 'massive') structure, while the height of each room in the two-storey dwelling were assumed to be 2.8 metres. The cavity air gaps and the floor slab were subsequently removed in order to loosely simulate the effect of a 'light' structure. Figure 4.2 shows the constituent elements of each multilayered construction, while Table 4.1 lists the thermal properties of each element and Figure 4.3 illustrates the test house itself in section and plan views. All external surfaces have an emissivity of 0.9 with a solar absortivity of 0.6. Installed window glazing was specified as 4 mm single clear sheet with a normal incidence solar transmittance of 0.84 and a thermal transmittance value of 5.7 $W\ m^{-2}\ ^{\circ}K^{-1}$. Table 4.2 gives the representative infiltration rates selected for each space by Clarke and Forrest (Ref.79).

4.4 - THE METEOROLOGICAL SET OF DATA

In order to simulate the heating load and internal air temperature for a typical winter and summer days within the Livingston 'test house' , meteorological data for Kew, London (51° 28'N,0° 19'W) on the 21 st December 1964/21st June 1965 was employed. This constitutes part of the data base for the CIBSE 'Example Weather Year' (Ref.80). Tables 4.3 and 4.4 show the relevant meteorological parameters necessary for winter and summer simulations. Where the calculations were performed for the 'whole' heating season, meteorological data from 15/10/64 until 15/3/65 were employed.

4.5 - THE EFFECT OF THE EXTERNAL CONVECTIVE HEAT TRANSFER COEFFICIENTS

In the NBSLD program the outside surface temperatures, at a given time t, are calculated by solving a heat balance equation at each external surface of a building. Two components of such heat balance equation are of special interest to this study; the convective heat transfer from the surface to the ambient air and the radiative heat transfer emitted by the surface. In the original version of the NBSLD program, these two components are reduced to only one by employing the combined radiative and convective film coefficient obtained by Rowley et al (Ref.16). In the new version, which will be hereafter generally be referred to as NBSWIND, the convective coefficients are calculated by employing the WIND-CHT program which was incorporated as an additional subroutine into the NBSLD code. In order to replace Rowley's coefficients it was necessary to combine the convective heat transfer coefficients, h_c, with the radiative heat transfer coefficient, h_r. In this case, h_r is defined as the radiative heat transfer coefficient between a point on the outside surface and the hypothetical black hemispherical surface surrounding the point,

$$(h_r)_{i,t} \, (To_{i,t} - Te_t) = E \, To_{i,t}^4 - \sigma \, Te_t^4 \qquad (4.21)$$

Equation (4.21) can easily be reduced to,

$$(h_r)_{i,t} = 0.9 \, \sigma \, [(To_{i,t} + Te_t) \; (To_{i,t}^2 + Te_t^2)] \qquad (4.22)$$

where To and Te are the absolute values of the external surface and dry-bulb temperatures, and the surface emissivity, E, is assigned a value of 0.9.

The procedure originally adopted for estimating the external surface coefficients in the NBSLD program yields inappropriate values for those parameters, as discussed in chapter 2. Figure 4.4 shows a comparison between the convective heat transfer coefficients computed using the standard version of the NBSLD program and those for the WIND-CHT program. These apply to the Livingston 'test house' with three different kinds of terrain. The NBSLD program values were calculated in accordance to equation (2.33) and subsequently decreased by a factor of 4.0 in order to eliminate the radiative component. The WIND-CHT program values represent an area-weighted average for all surfaces and for all wind directions.

In order to simulate the heating load, an intermittent heating cycle typical of United Kingdom practice was assumed (see Figure 4.5). The house was treated as a five-zone system, with identical conditions in the zones adjacent to that being simulated. The heating load profiles computed by the standard version of the NBSLD program, together with those using the NBSWIND program, for a heavyweight and

for a lightweight structure are shown in Figures 4.5(a) and 4.5(b) respectively. The daily energy consumption computed by the standard program for the heavyweight(lightweight) structure was 61(69) KWh, and this decreased by 10(11) per cent when the NBSWIND code was used. These are corrected values compared with those originally presented by Alamdari, Hammond and Melo (Ref.19) when employing an earlier version of the NBSWIND program. It was later found that, although the WIND-CHT code had been adequately incorporated into the NBSLD program , there were some undetected instructions, employing values calculated by the original surface heat transfer coefficients routine. The program therefore adopted a constant value for the heat transfer coefficient, which was always higher than the values given by the original routine. Consequently, the resultant daily energy consumption was found to be higher than that computed by the original version of the NBSLD program. The latest computations required central processor time on a DEC VAX 11/782 computer of 58(56) and 60(59) seconds for the standard and modified(NBSLD+WIND-CHT) versions respectively. Figure 4.6 and Table 4.5 show the monthly total energy consumption also calculated using the two different versions of the NBSLD program. Finally, Figures 4.6-4.12 show the resultant internal air temperature for a typical summer day, calculated by using both versions of the NBSLD program.

The standard version of the NBSLD program employs values for the combined external heat transfer coefficients always higher than the values computed via the WIND-CHT program under comparable environmental conditions. This accounts for the difference in the computed heating loads and summer internal air temperatures. When the combined external heat transfer coefficients are decreased the heat balances at the exterior surfaces of a building are modified in such a way that the heat released by the combined action of radiation and convection to the surrounding air becomes smaller and, consequently, the external surfaces temperatures become higher. This increases the summer internal air temperature, and decreases the heating load.

4.6 - THE EFFECT OF THE AIR INFILTRATION RATES

The NBSLD program, although otherwise sophisticated, estimates the air infiltration rates into a building by employing the empirical Achenbach-Coblentz correlation (Ref.81) derived by regression analysis of data obtained by Bahnfleth et at (Ref.82) from two test houses at the University of Illinois-USA, with the constants arbitrarily multiplied by a correction factor, δ, to "more closely correspond to a typical house" (Ref.83). The air infiltration rate, in air changes per hour,I, is calculated using the expression:

$$I = (0.15 + 0.0291\ V + 0.009\ \Delta T)\ \delta \qquad (4.23)$$

where:

$$\delta = Iw / 0.695 \qquad (4.24)$$

where Iw is an assumed typical hourly air change rate during the winter months and ΔT is the indoor-outdoor temperature difference. Care must be taken in using this general regression equation as a predictive model for an arbitrary house because the constants will vary from site to site. Furthermore, this analysis takes no account of the complex interactions between wind-speed, indoor-outdoor temperature difference and fan operation.

Comparisons between the measured air infiltration rates and the estimates made by the FLOW and NBSLD programs for the Maugwill, HUDAC 'upgraded' and Runcorn houses (Ref.59) are shown in Figures 4.12,4.13 and 4.14. Following the NBSLD normal procedure, the Iw value was taken as unity, increasing in this way, the original Achenbach-Coblentz relationship by 44%. The FLOW program ,as expected, gives good agreement for all three of the key data sets. The NBSLD relationship, on the other hand, yields large discrepancies between measured and calculated values for the Maugwill and HUDAC 'upgraded' houses. The apparent agreement between the NBSLD results and measurements for the Runcorn house was simply a matter of coincidence since they do not account for the leakage characteristics of the structure.

In order to calculate the heating load and internal air temperature it was necessary to estimate the leakage distribution of the Livingston 'test house'. The leakage characteristics of windows and doors were determined from published values given by ASHRAE (Ref.4). In addition the total building leakage was estimated ,again following ASHRAE recommendations, by considering that the leakage from windows and doors represent 15% of its value. The leakage characteristics of windows and doors were used directly, while the deficit between component and total building leakage was evenly distributed along the roof/wall junction and the gable/roof junction for the single-cell version and in accordance with the exposed area for the multi-cell version. The assumed flow networks are illustrated in Figures 4.15 and 4.16, and the corresponding leakage characteristics of each flow path are given in Tables 4.6 and 4.7 for the single and multi-cell versions respectively. Tables 4.8,4.9 and 4.10 show the air infiltration rates for the Livingston 'test house' on a typical winter day, computed by the single and multi-cell versions of the FLOW program and by the original version of the NBSLD program, respectively. The necessary values of Iw in equation (4.23) were taken from Table 4.2.

The upper part of Figures 4.17-4.22 and Figures 4.23-4.28 show the air infiltration rates computed by the NBSLD program and by both versions(single and multi-cell) of the FLOW program, on a typical winter day, for a heavyweight and lightweight structure respectively. The lower part of these figures show the resultant heating load profiles when the NBSLD program is 'fed' with these air infiltration rate profiles. Table 4.11 shows a comparison between the daily energy consumption computed by the NBSLD and by both versions of the NBSFLOW (NBSLD+FLOW) program, on a typical winter day, for each room and for the 'whole house'; again for both heavyweight and lightweight structures. It can be seen in this table that the 'whole house' energy consumption for a heavyweight(lightweight) structure was

approximately 61(69) Kwh and this increased by 7(6) or 2(2) percent as either the single or multi-cell version of the FLOW program were added. Although the 'whole house' results obtained by using the multi-cell version of the FLOW program were little different from those of the NBSLD program, the room individual results were significantly altered. In the case of bedroom 3, the difference was as great as 17(15) percent. Figure 4.29 shows the monthly total energy consumption computed by the original version of the NBSLD program and by both versions of the NBSFLOW program. The small difference between the results of the original NBSLD code and by both versions of the NBSFLOW program gives a false impression of the accuracy of the NBSLD relationship employed for estimating the air infiltration rates. In reality, a combination of errors in estimating the individual room air infiltration rates leads to a false match with the 'whole house' data. Another important factor which contributes to this apparent match was the present author's decision to employ the 'selected' air infiltration rates for the individual rooms, presented by Clarke and Forrest (Ref.79;see Table 4.2), as the Iw values. When the 'selected' air infiltration rates are employed for estimating the amount of air infiltrating into the 'whole house', the values arising from the original Achenbach-Coblentz relationship are multiplied by a volume-weighted δ value of 0.70. This is instead of being multiplied by 1.44 when the common value of Iw is employed for all rooms. This procedure reduces the air infiltration rates typically employed in the NBSLD program by approximately 50%. It therefore contributes to the apparent (superficial) match with the values arising from the FLOW program.

In order to investigate the effect of the air infiltration rates on the computed internal air temperatures, during a typical summer day, a 'hypothetical' internal air temperature profile was adopted, since the FLOW program depends on these values. The latter program was fed with the average internal air temperature profile, obtained by running the standard version of the NBSLD program. This approximation is quite acceptable, since the indoor-outdoor temperature differences are small and the simulations are not being, performed for a tall building, for which stack effect would be significant. The air infiltration rates were then computed by using the single and multi-cell versions of the FLOW program. These are depicted in Figures 4.30-4.32 where they are compared with the air infiltration rates computed by the NBSLD program. The values adopted for Iw, required by the NBSLD program for estimating the air infiltration rates, were again those of Table 4.2. Tables 4.12-4.14 show the numerical values of the air infiltration rates plotted in Figures 4.30-4.32. Finally, the NBSLD program was 'fed' with the air infiltration rates obtained using the NBSLD relationship (eq. 4.23) and those given by both versions of the FLOW program, and the corresponding internal air temperature profiles were computed. The air infiltration rate predictions show only a small variation between themselves. This was mainly because of the present author's decision of use the 'selected' infiltration rates as the Iw values. It should be noted that in the kitchen, where Iw is approximately 1.0 (common value adopted by the NBSLD program), a slight difference was observed. However, even with this difference in the air infiltration rates, the corresponding internal air temperatures are very similar (Figure

4.33). This is because the indoor-outdoor temperature difference is small and, consequently, the amount of energy carried into the building by the infiltration air is also small, thereby producing only a small effect on the room heat balance.

4.7 - THE EFFECT OF THE INTERNAL CONVECTIVE HEAT TRANSFER COEFFICIENTS

The original version of the NBSLD program employs a set of constants for specifying the convective heat transfer coefficients on the internal surfaces of a building. A value of 3.08, 0.92 and 4.04 $W\ m^{-2}\ °K^{-1}$ is adopted, respectively for the vertical walls, floor and ceiling when the internal surfaces temperatures are smaller than the internal air temperature. When this condition does not prevail, the ceiling and floor values are switched. This procedure is obviously inadequate for modern requirements, since it seems to ignore the possibility of variation in surface coefficients due to different air supply conditions and room configurations.

In the new version, which will be hereafter generally be referred to as NBSROOM, the convective coefficients are calculated by employing the ROOM-CHT program (Ref.14) which was incorporated as an additional subroutine into the NBSLD code. This routine prescribes the flow and thermal field using the known characteristics of two and three-dimensional wall jets. Such jets are the normal means of air distribution in buildings with forced convective heating systems. They are assumed to spread out from their supply aperture and sequentially flow over the room surfaces. The mean-flow properties for the two-dimensional version of the code are calculated from the empirical data for plane wall-jets rewieved by Hammond (Ref.10), while that for its three-dimensional counterpart are taken from Rajaratnam (Ref.84). The local heat transfer ditribution across the room surfaces is then calculated via an 'optimum log-law' obtained by Hammond (Ref.11) using wall-jet profile analysis. This formula yields the local wall-jet Stanton number ($St=(h_c)_m / \rho\ Cpr\ Vs_m$) in the form:

$$St = St\ (Re_m, Pr) \qquad (4.25)$$

where Vs_m is the wall-jet maximum velocity at any downstream location and Re_m is the corresponding local Reynolds number. The heat transfer coefficient itself is defined by:

$$(h_c)_m = q_i / (Ts_m - Ti) \qquad (4.26)$$

where q_i is the surface (or wall) heat flux, Ts_m is the wall-jet maximum temperature at the downstream location and Ti is the surface temperature. However , building thermal modellers conventionally use heat transfer coefficients based on the notional room air temperature,

Ta,

$$h_c = q_c / (Ta - Ti) \qquad (4.27)$$

This coefficient is related to that of the wall-jet, from equations (4.26) and (4.27) by

$$h_c = (h_c)_m \; [(Ts_m - Ti)/(Ta - Ti)] \qquad (4.28)$$

This coefficient may locally fall below the value corresponding to the buoyancy-driven convection at the same room temperature difference. In these situations the calculation method adopts the appropriate heat transfer coefficient for buoyancy-driven convection calculated from the correlating equations of Alamdari and Hammond (Ref.12).

The equations that form the 'kernel' of the ROOM-CHT program are generally explicit, algebraic ones, except for the wall-jet heat transfer log-law which is implicit and is solved using the Newton-Raphson iterative method. The computational grid normally employed has around 10 uniformly-spaced calculation points per metre length of surface. Once the local heat transfer at the mesh nodes is computed, the program performs multiple (space and time) averaging by successive numerical integrations depending on the requirements of the heating system control.

In order to incorporate the ROOM-CHT program into the NBSLD code some adaptations were necessary. Firstly, it was necessary to develop a set of instructions in order to correctly transfer the output convection coefficients from the ROOM-CHT program to the NBSLD program. This problem arises from the use of different indexation techniques by those programs. The surfaces are numbered, in the ROOM-CHT program, in accordance to the surface position relative to the supply air aperture, while in the NBSLD program they are referred to the South axis. Secondly, it was felt desirable to develop a set of instructions in order to reduce the number of times that the ROOM-CHT code is 'called' within the NBSLD program and, consequently, to reduce the computer time requirements. This problem has special interest for heavyweight walls, such as slab on grade floor, where the temperature difference between wall and internal air is usually very small. Under this condition the ROOM-CHT code prescribes very high heat transfer coefficients, and consequently, in the next iteration, the temperature difference will be even smaller, and so on. The procedure adopted was to stop calling the ROOM-CHT code whenever the room mean radiant temperature, between iterations, is smaller than 0.5°C. This procedure dramatically reduced the computer time and the final results were practically unaffected.

The heating load profiles computed by the standard version of the NBSLD program, together with those using the NBSROOM program, for a heavyweight and for a lightweight structure are shown in Figures 4.34(a) and 4.34(b), respectively. The daily energy consumption

computed by the standard program for the heavyeight(lightweight) structure was 61(69) KWh, and this increased by 4.3(7.5) percent when the NBSROOM code was used. These computations required corresponding central processor time of 58(56) and 131(126) seconds, on a VAX 11/782 computer, for the standard and modified versions respectively. The central processor time now required by the NBSROOM program represents only 25% of the computer time originally required by this program when no attempt was made to optimise it (Ref.19). Figure 4.35 and Table 4.5 show the computations of the NBSLD and NBSROOM programs for the 'whole' heating season. The NBSROOM program results, as expected, are higher than those arising from the standard version of the NBSLD program. This is because the convective heat transfer coefficients, generated by the NBSROOM program, are dependent on the supply air conditions and, therefore, normally higher than the constant values adopted by the standard version of the program.

Summer comparisons will not be presented, since there was no appreciable difference between the internal air temperature profile computed by the standard and modified versions of the NBSLD program. In this situation, the air movement inside the dwelling is caused only by buoyancy, due to the absence of any mechanically-ventilatted supply air. The difference between the adopted and computed heat transfer coefficients is therefore very small.

4.8 - THE COMBINED EFFECT OF THE EXTERNAL AND INTERNAL HEAT TRANSFER COEFFICIENTS AND THE AIR INFILTRATION RATES

In this section, the influence of all three sub-models on the NBSLD program are compared simultaneously.Figures 4.36 and 4.37 show the heating load profiles computed by the NBSLD program when it is sequentially modified by adding the WIND-CHT, ROOM-CHT, and FLOW programs for a single-cell and a multi-cell system, respectively. The daily energy consumption computed by the combined version, which will be hereafter be referred to as NBSALL, for the single-cell system is 1.4(3.2) percent higher than the values computed by the standard version for a heavyweight(lightweight) structure. When the 'hypothetical' Livingston test house is treated as a multi-zone system, the NBSALL results are 3.3 percent lower and approximatelly 1.0 percent higher, than the standard version for a heavyweight and lightweight structure respectively. Figure 4.38 and Table 4.16 show the monthly total energy consumption computed by the NBSLD and by the single and multi-cell versions of the NBSALL program for both structures. Finally, Figures 4.39(a),4.40(a) and 4.39(b), 4.40(b) show the total energy consumption during the 'whole' heating season prescribed by the NBSLD, NBSWIND, NBSROOM and by the single and multi-cell versions of the NBSFLOW and NBSALL programs, for a heavyweight and lightweight structure respectively. The total energy consumption computed by the NBSALL program is about 4-9 percent lower than the computations of the NBSLD program, depending on the type of structure and version of the FLOW program being employed. Once again this 'false' agreement does not reflect the accuracy of the standard version of the NBSLD program. It is simply due to a combination of

errors in estimating the internal and external heat transfer coefficients and the air infiltration rates (as shown in Figures 4.39 and 4.40). These errors will not, in general, cancel each other out, and the original version of the NBSLD program cannot be regarded as universally reliable in this regard.

4.9 - CONCLUSIONS

The algorithms employed by the original version of the NBSLD program for estimating the external and internal convective heat tranfer coefficients and air infiltration rates appear inadequate. The NBSLD program places a 'strong' emphasis in the calculation of the heat fluxes through walls and roofs due to its use of the response factor technique. The internal and external surfaces resistances need not be specified when calculating the walls and roof response factors. Consequently, the heat fluxes are evaluated by using the outside and inside surfaces temperatures, which are computed by solving a set of heat balance equations. Inadequate values for the convective heat transfer coefficients and air infiltration rates are employed in these heat balance equations, and therefore incorrect values for the internal and external surfaces temperatures are obtained. A very sophisticated response factor technique is therefore employed using unreliable values of the boundary surfaces temperatures.

The NBSLD air infiltration rates are calculated disregarding any influence of the leakage characteristics of the building being simulated. This kind of approach is no longer acceptable for modern purposes since the amount of air infiltrating into a building has a instantaneous effect on the resulting heating/cooling load. It therefore needs to be accurately determined.

The NBSLD program, in common with other dynamic building thermal models, can only provide comparative results between various design options, because it cannot, at the moment, accurately compute the heating/cooling capacity of any air conditioning system. The program performance was considerably improved by incorporating the WIND-CHT, FLOW and ROOM-CHT programs. However, a lot of research effort has still to be undertaken before this program can be accepted as a general 'tool' for calculating the cooling/heating requirements of a building.

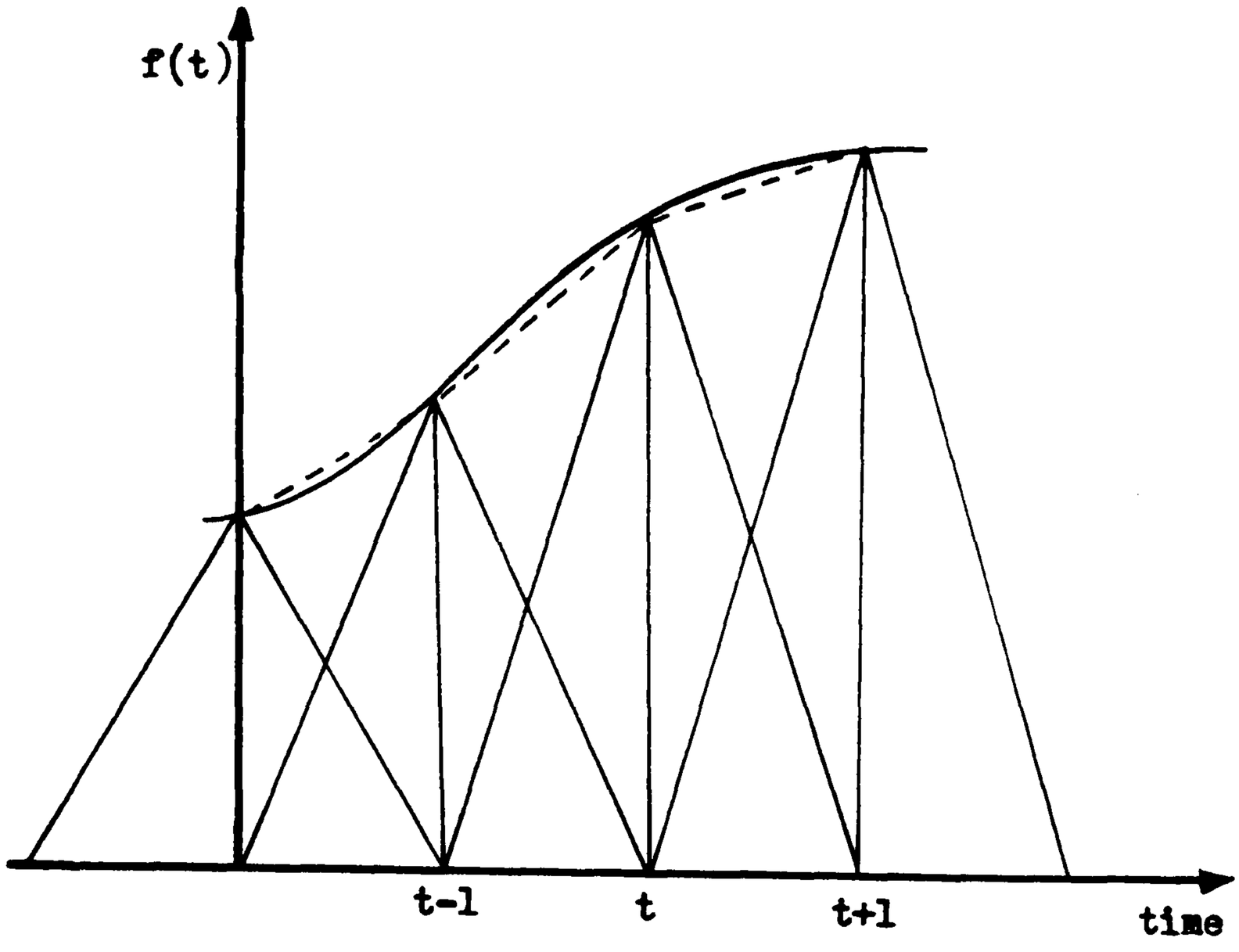

Fig. 4.1 Triangular pulse representation of a continuous function

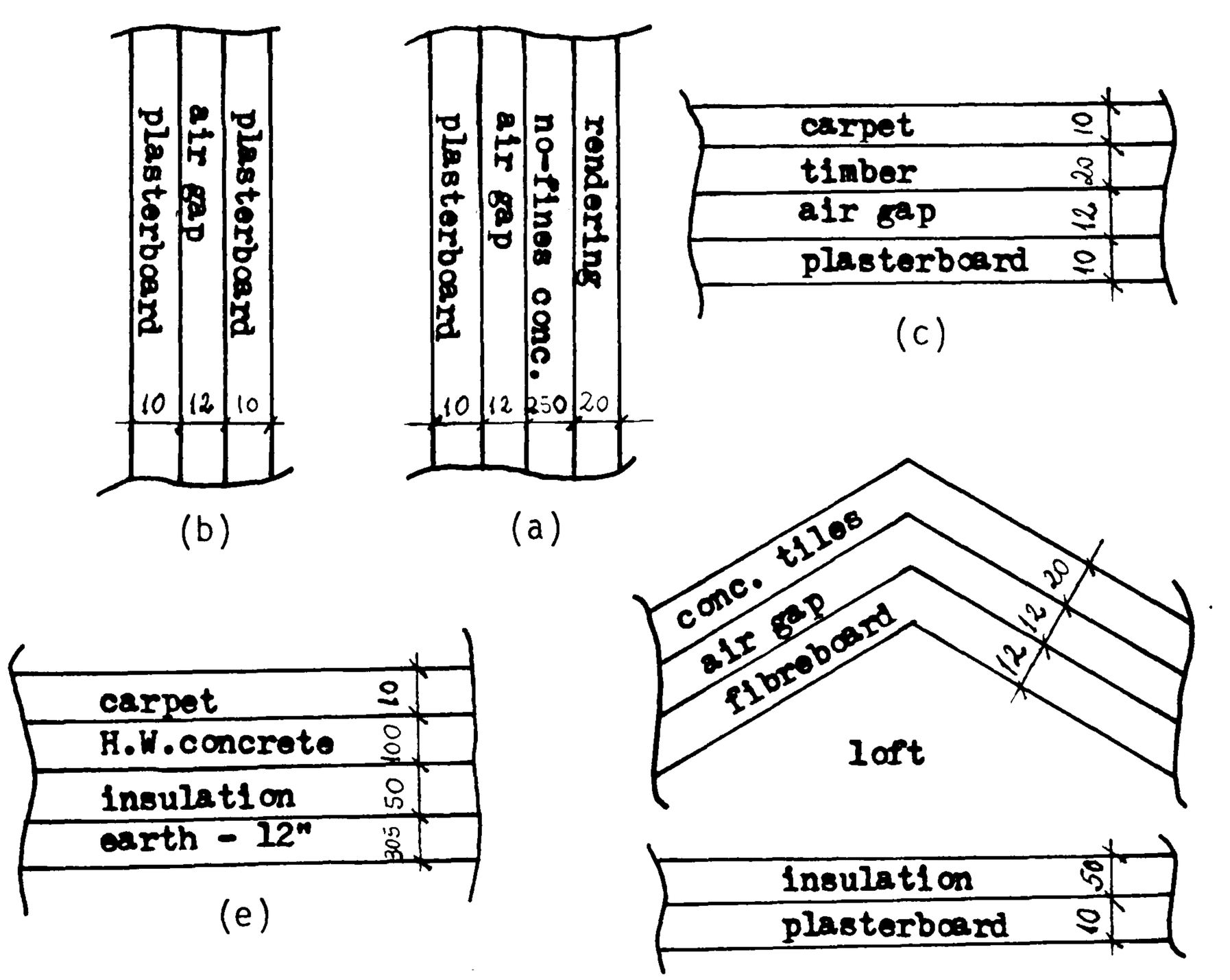

Fig. 4.2 Multi-layered construction - Livingston 'test house':
a) External wall, b) Partition wall, c) Ceiling,
d) Roof and e) Floor

Table 4.1 Thermal properties - Livingston 'test house'

Element	k ($W/m^{\circ}C$)	ρ (Kg/m^3)	Cpr ($J/Kg^{\circ}C$)	R ($m^2{}^{\circ}C/W$)
Rendering	0.50	1300	1000	-
No-fines conc.	0.70	1700	840	-
Air Gap	-	-	-	0.18
Plasterboard	0.16	950	840	-
Plaster	0.50	1300	1000	-
Timber	0.14	640	1210	-
Concrete tiles	0.52	1600	1000	-
Fibreboard	0.06	400	1000	-
Insulation	0.033	25	1380	-
Carpet	0.064	112	752	-
H.W.concrete	1.73	2243	838	-
Earth - 12 in	0.63	2002	1798	-

Table 4.2 'Recommended' infiltration rates of the Livingston 'test house'. {After Clarke and Forrest (Ref. 79)}

SPACE	AIR INFILTRATION RATE (ACH)
Living room	0.5
Kitchen	1.1
Bedroom 1	0.6
Bedroom 2	0.5
Bedroom 3	0.4
Hall	1.4

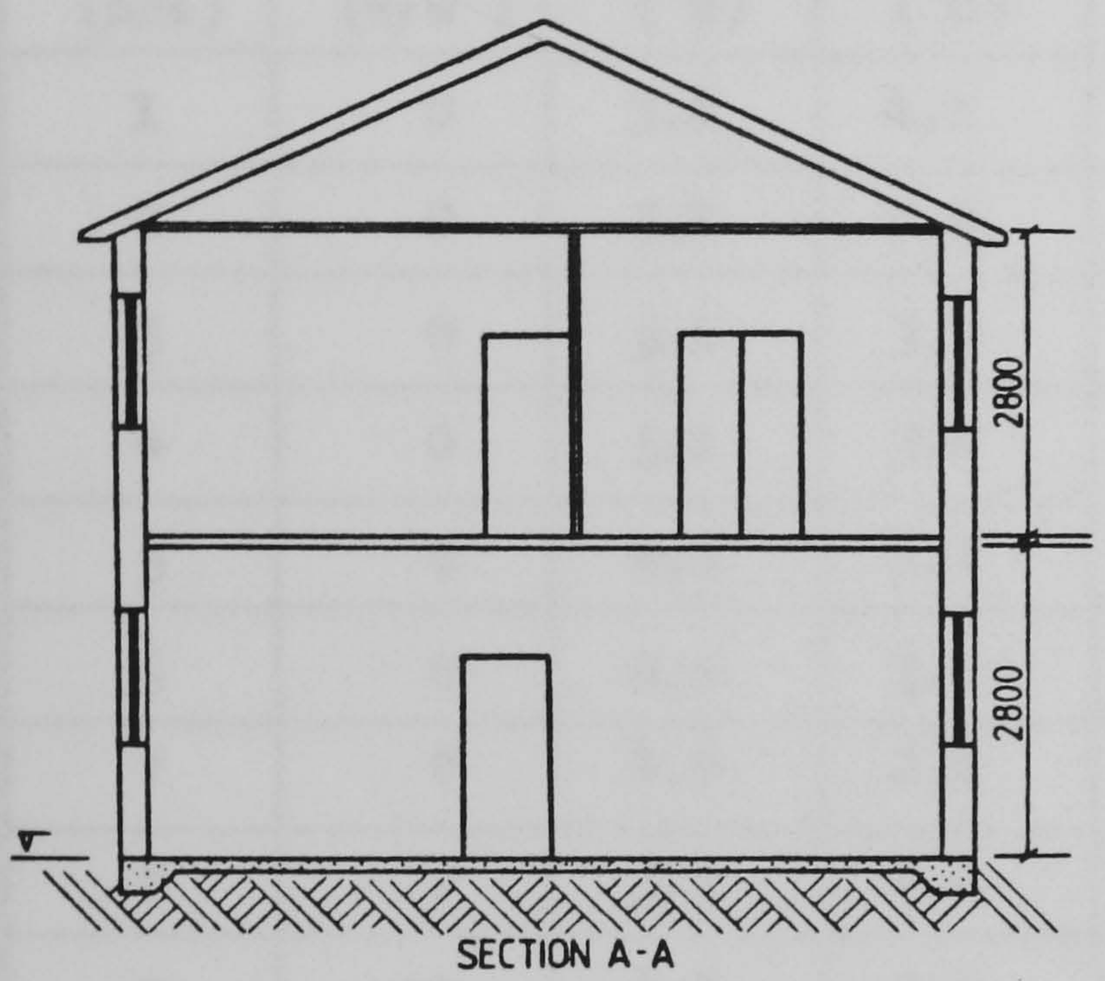

LIVINGSTON 'TEST HOUSE'
(DIMENSIONS IN mm)

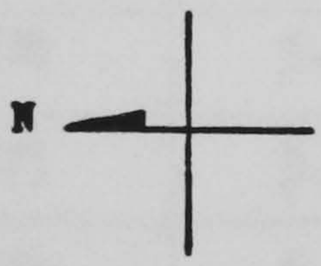

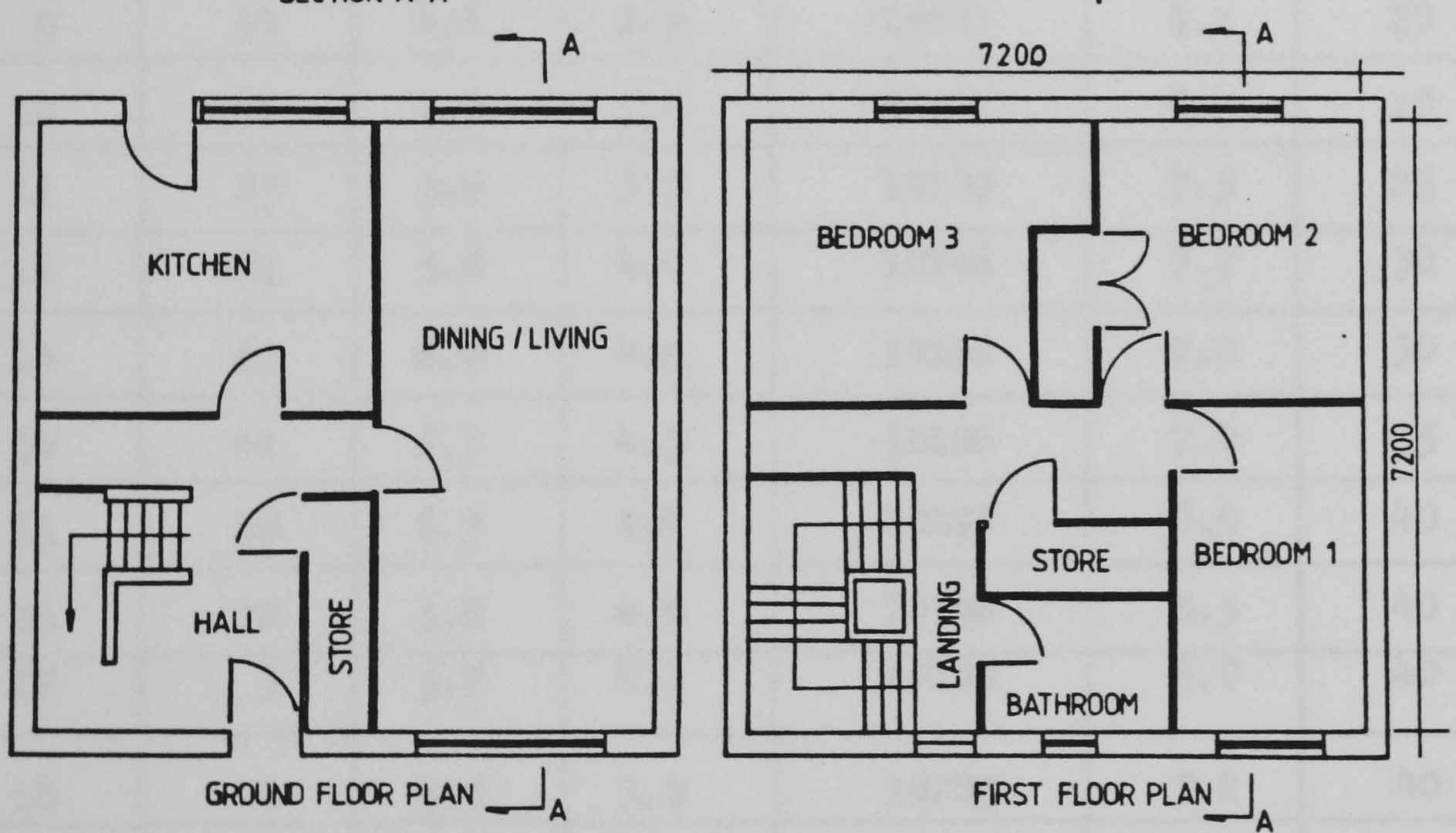

Fig. 4.3 Livingston 'test house'

Table 4.3 Meteorological parameters (Kew - 21st December)

time (hrs)	Qsun (W/m^2)	Te (^oC)	Wb (^oC)	Pb (Pa $x10^{-1}$)	V (m/s)	Ψ (deg.)
1	0	5.6	4.1	10215	5.7	20
2	0	5.2	3.9	10213	6.2	20
3	0	5.1	3.7	10212	6.2	20
4	0	5.1	3.4	10210	6.2	20
5	0	4.9	3.1	10207	5.9	20
6	0	4.9	3.0	10206	5.4	20
7	0	4.9	2.8	10202	5.4	20
8	0	5.3	2.9	10203	5.9	20
9	10	4.8	2.9	10203	6.2	20
10	41	4.9	3.0	10206	6.7	20
11	65	5.4	3.5	10209	7.5	25
12	71	5.8	4.0	10208	7.7	30
13	63	6.0	4.2	10199	7.0	30
14	41	6.3	4.5	10196	7.0	35
15	28	6.3	4.4	10196	8.0	40
16	16	5.8	4.2	10198	8.5	40
17	3	5.7	4.1	10200	8.0	40
18	0	5.5	3.9	10205	7.2	40
19	0	5.2	3.7	10207	7.2	40
20	0	5.2	3.7	10212	7.2	40
21	0	4.6	3.3	10214	7.0	40
22	0	4.5	3.3	10218	6.7	45
23	0	4.6	3.2	10222	6.7	45
24	0	4.6	3.2	10224	7.2	45

Table 4.4 Meteorological parameters (Kew - 21st June)

time (hrs)	Qsun (W/m^2)	Te (^oC)	Wb (^oC)	Pb (Pa $x10^{-1}$)	V (m/s)	ψ (deg.)
1	0	14.3	12.0	10172	0.8	185
2	0	13.3	11.3	10161	1.3	185
3	0	13.8	11.4	10157	2.3	200
4	5	13.6	11.3	10152	2.3	205
5	35	12.8	10.7	10147	1.3	175
6	136	13.7	11.0	10140	0.8	160
7	210	15.1	12.4	10138	1.5	180
8	248	15.9	12.8	10134	2.1	180
9	313	17.5	14.1	10124	1.0	190
10	239	18.6	14.9	10114	1.3	240
11	201	16.6	14.0	10108	1.8	265
12	180	17.3	15.3	10104	1.0	240
13	165	17.2	15.9	10099	0.8	205
14	325	18.6	16.7	10089	1.8	165
15	406	20.1	17.3	10082	2.6	165
16	286	20.3	16.9	10072	2.3	215
17	199	20.4	16.1	10072	3.1	240
18	150	19.8	15.4	10070	4.1	235
19	76	18.9	15.7	10069	4.6	215
20	52	17.1	15.5	10064	5.1	210
21	27	16.5	15.1	10060	5.1	220
22	5	16.1	14.7	10058	5.1	215
23	0	16.1	14.7	10058	4.6	205
24	0	15.5	14.3	10050	3.9	190

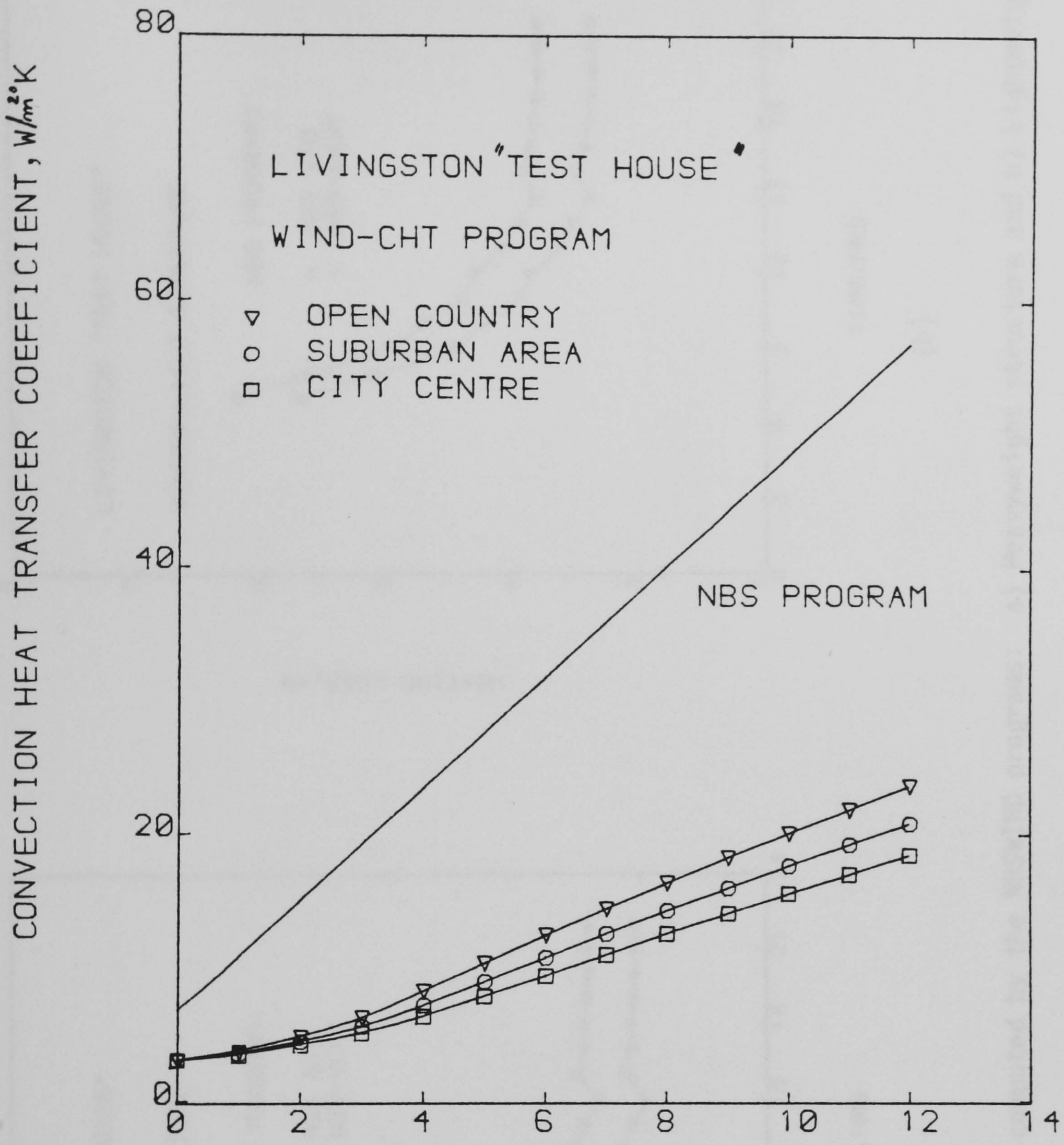

Fig. 4.4 Convective heat transfer coefficients computed by the NBSLD and WIND-CHT programs

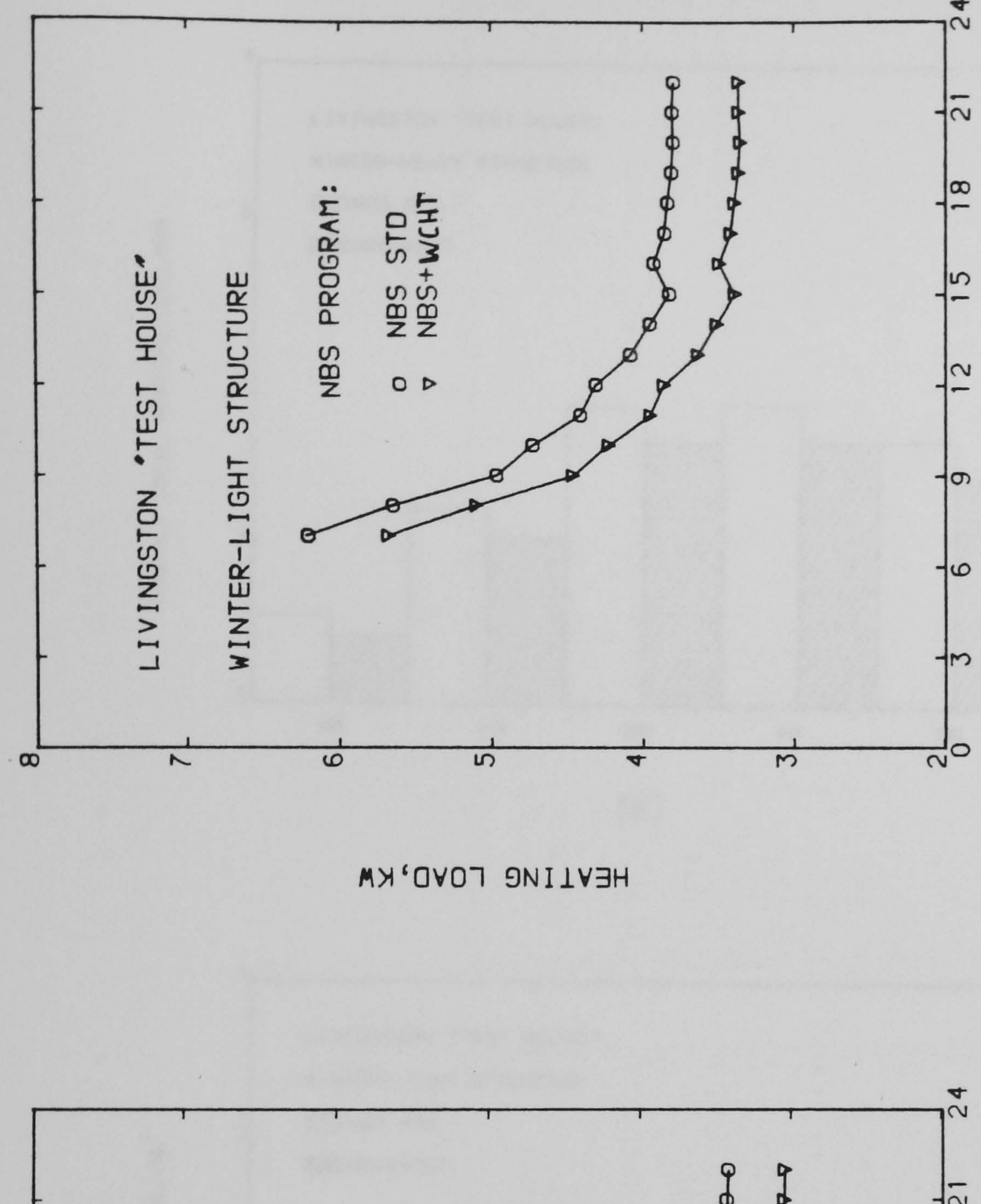

Fig. 4.5 Daily heating load computed by the NBSWIND programs: a) Heavyweight structure and b) Lightweight structure

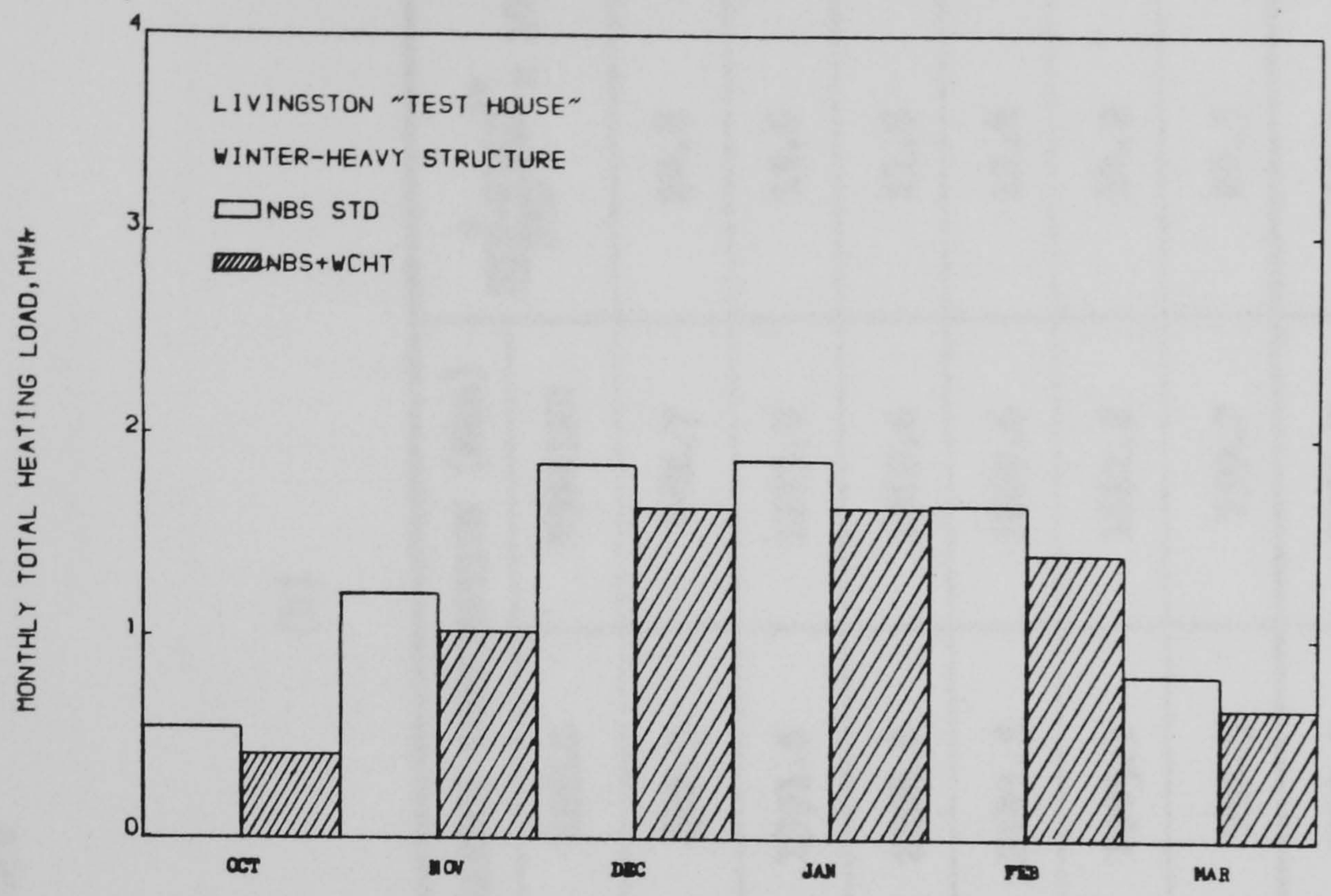

(a)

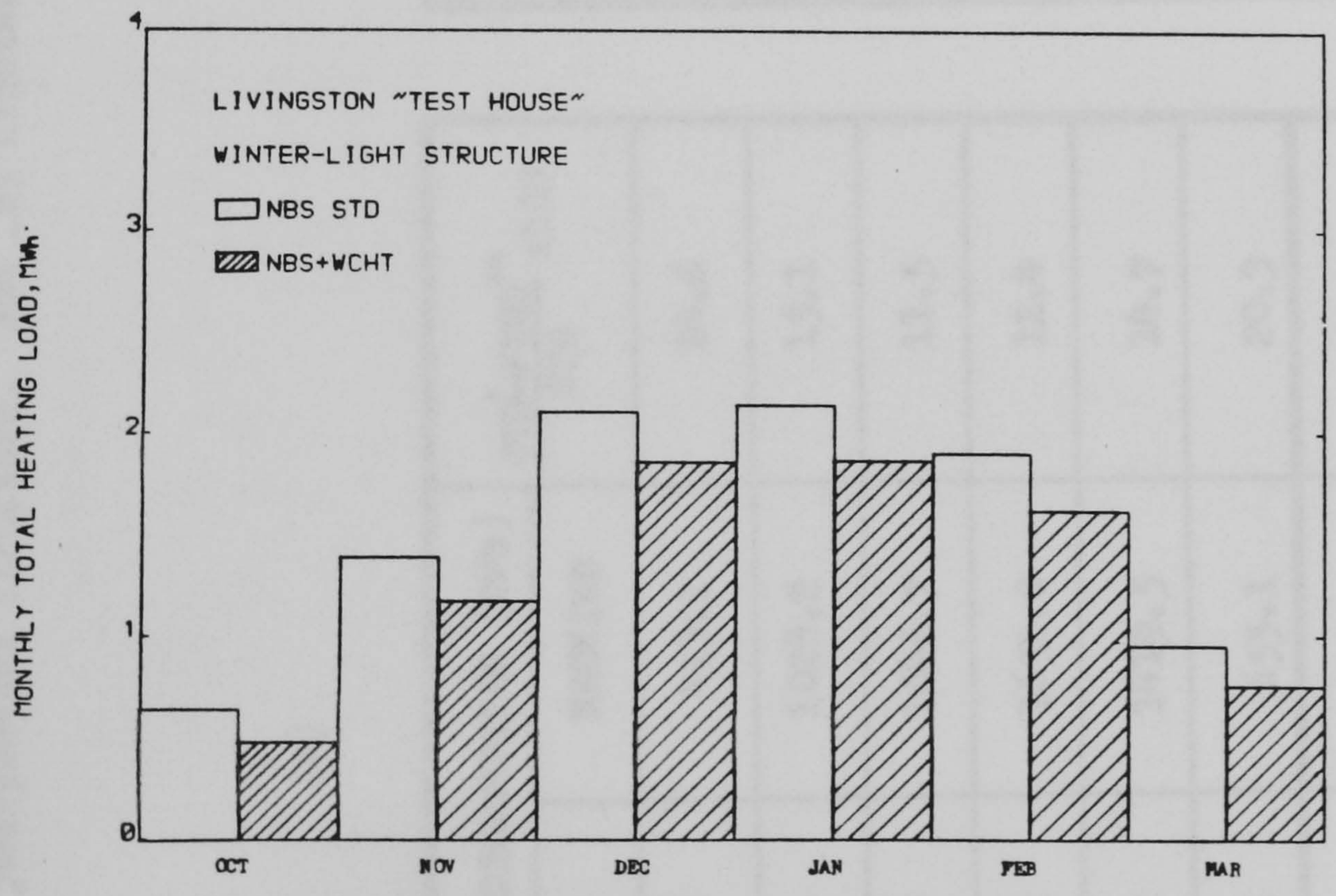

(b)

Fig. 4.6 Monthly total energy consumption computed by the NBSLD and NBSWIND programs: a) Heavyweight structure, and b) Lightweight structure

Table 4.5 Monthly total energy consumption computed by the NBSLD and NBSWIND programs: a) Heavyweight structure, and b) Lightweight structure

(a)

MONTH	ENERGY CONSUMPTION (MWh)		$\frac{STD^{*}-WIND^{**}}{STD} \times 100$
	NBSLD	NBSWIND	
OCT	547.8	413.1	24.6
NOV	1211.6	1028.2	15.1
DEC	1860.9	1646.7	11.5
JAN	1884.7	1651.0	12.4
FEB	1663.7	1419.5	14.7
MAR	821.6	655.1	20.3
TOTAL	7990.2	6813.6	14.7

(b)

MONTH	ENERGY CONSUMPTION (MWh)		$\frac{STD^{*}-WIND^{**}}{STD} \times 100$
	NBSLD	NBSWIND	
OCT	642.3	482.7	24.8
NOV	1391.6	1173.9	15.6
DEC	2108.8	1860.6	11.8
JAN	2143.5	1869.6	12.8
FEB	1905.3	1622.2	14.9
MAR	955.5	759.7	20.5
TOTAL	9147.0	7768.7	15.1

(*) NBSLD standard
(**)NBSWIND

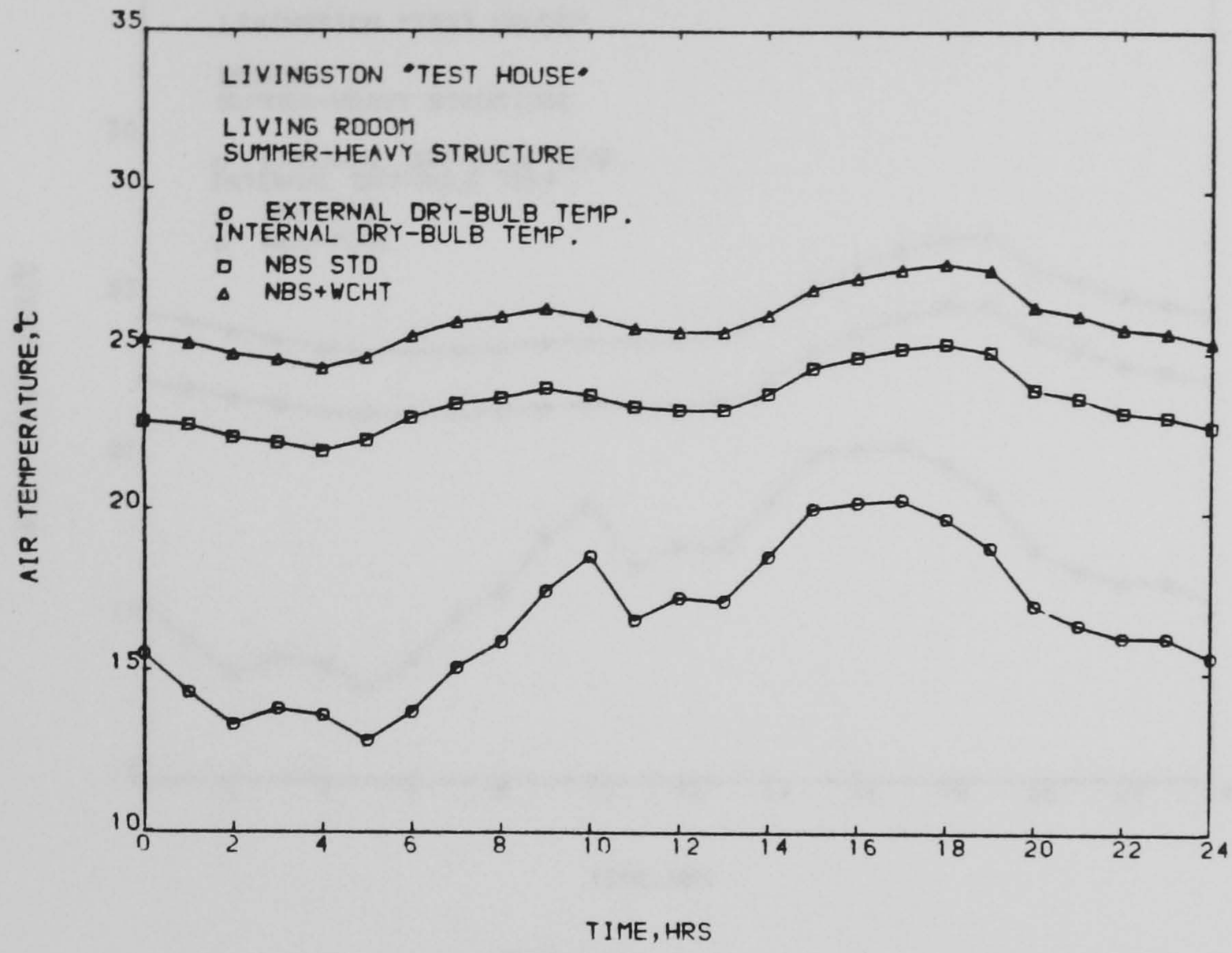

(a)

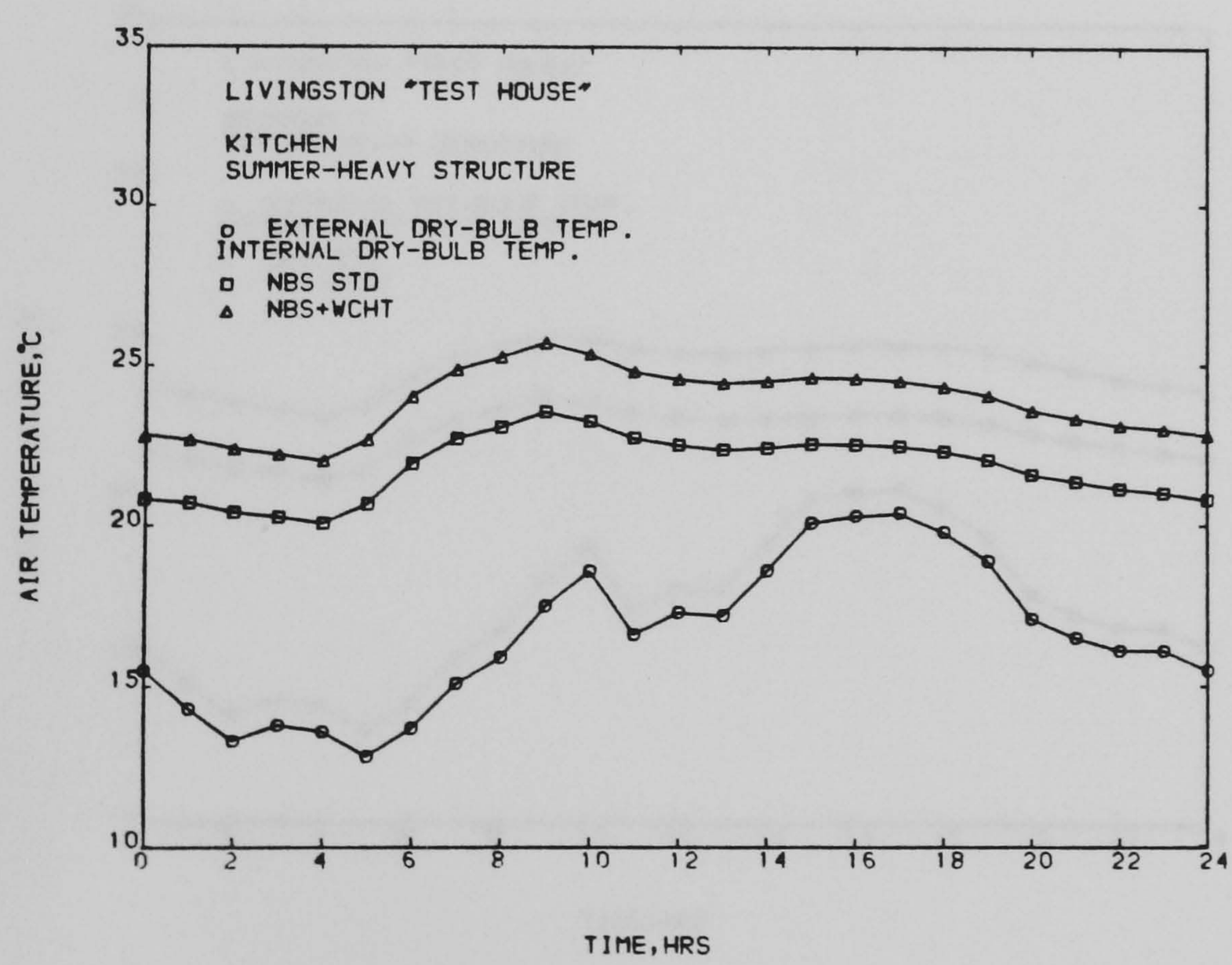

(b)

Fig. 4.7 Summer internal air temperature profile computed by the NBSLD and NDSWIND programs for a heavyweight structure: a) Living room, and b) Kitchen

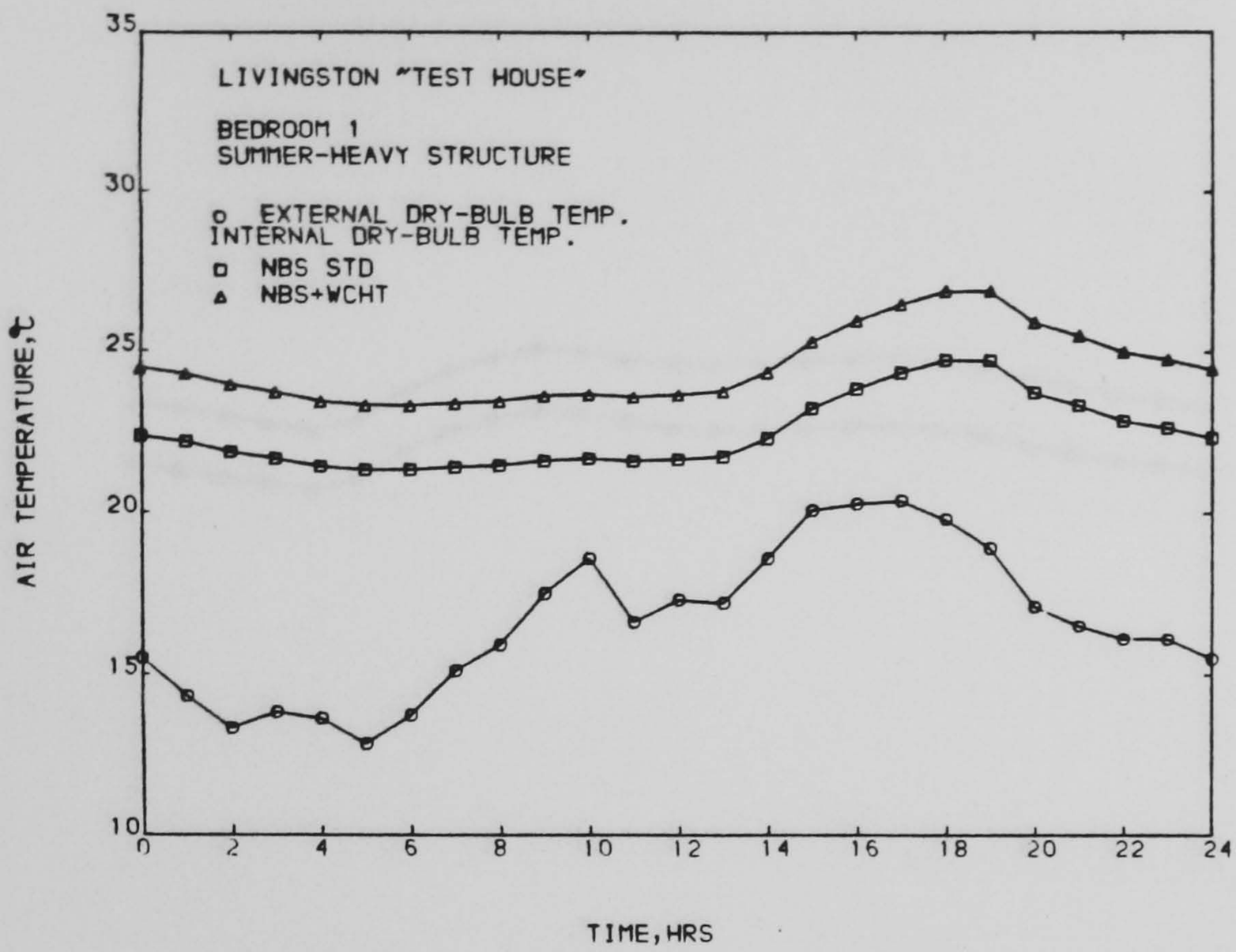

(a)

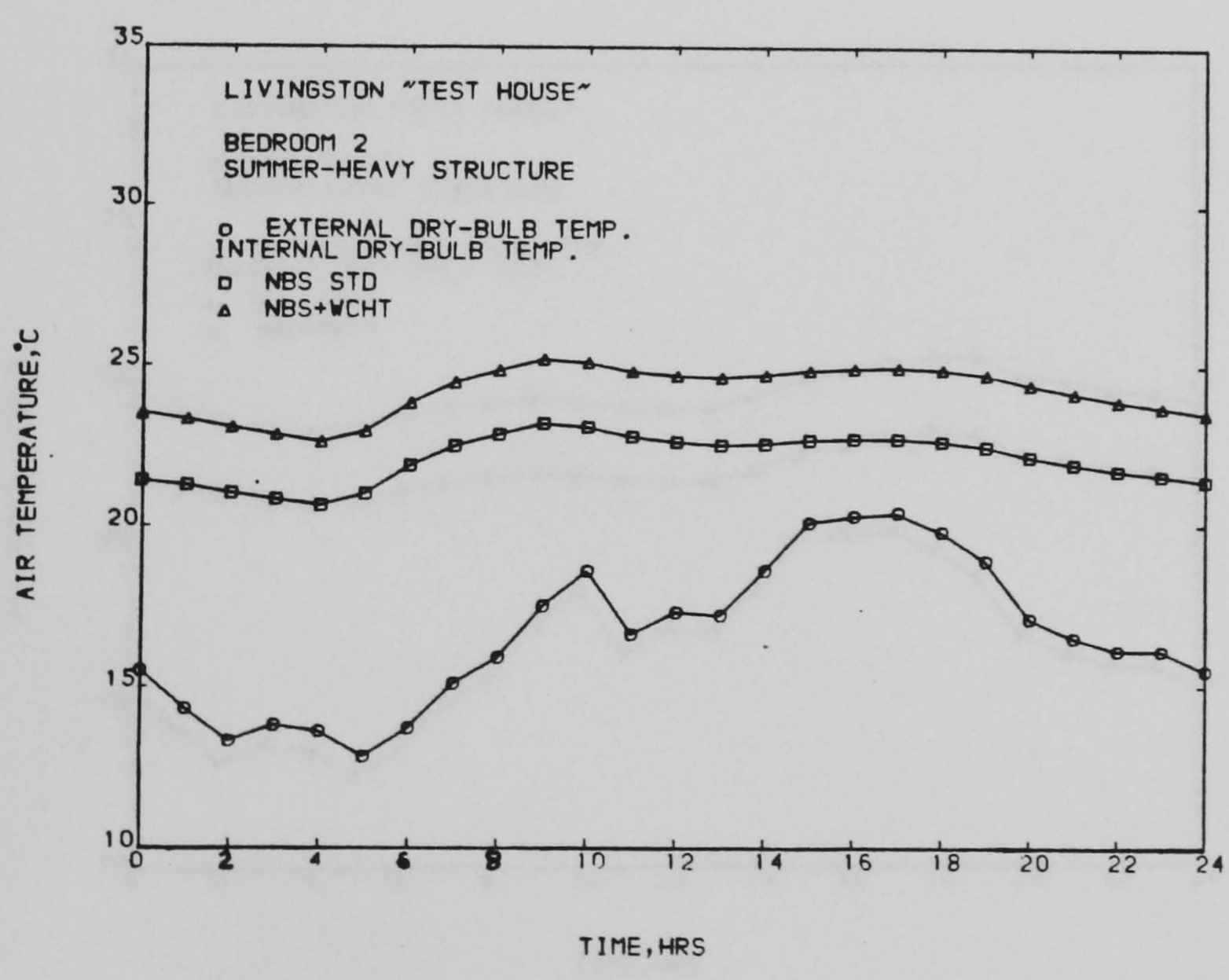

(b)

Fig. 4.8 Summer internal air temperature profile computed by the NBSWIND programs for a heavyweight structure. a) Bedroom 1, and b) Bedroom 2

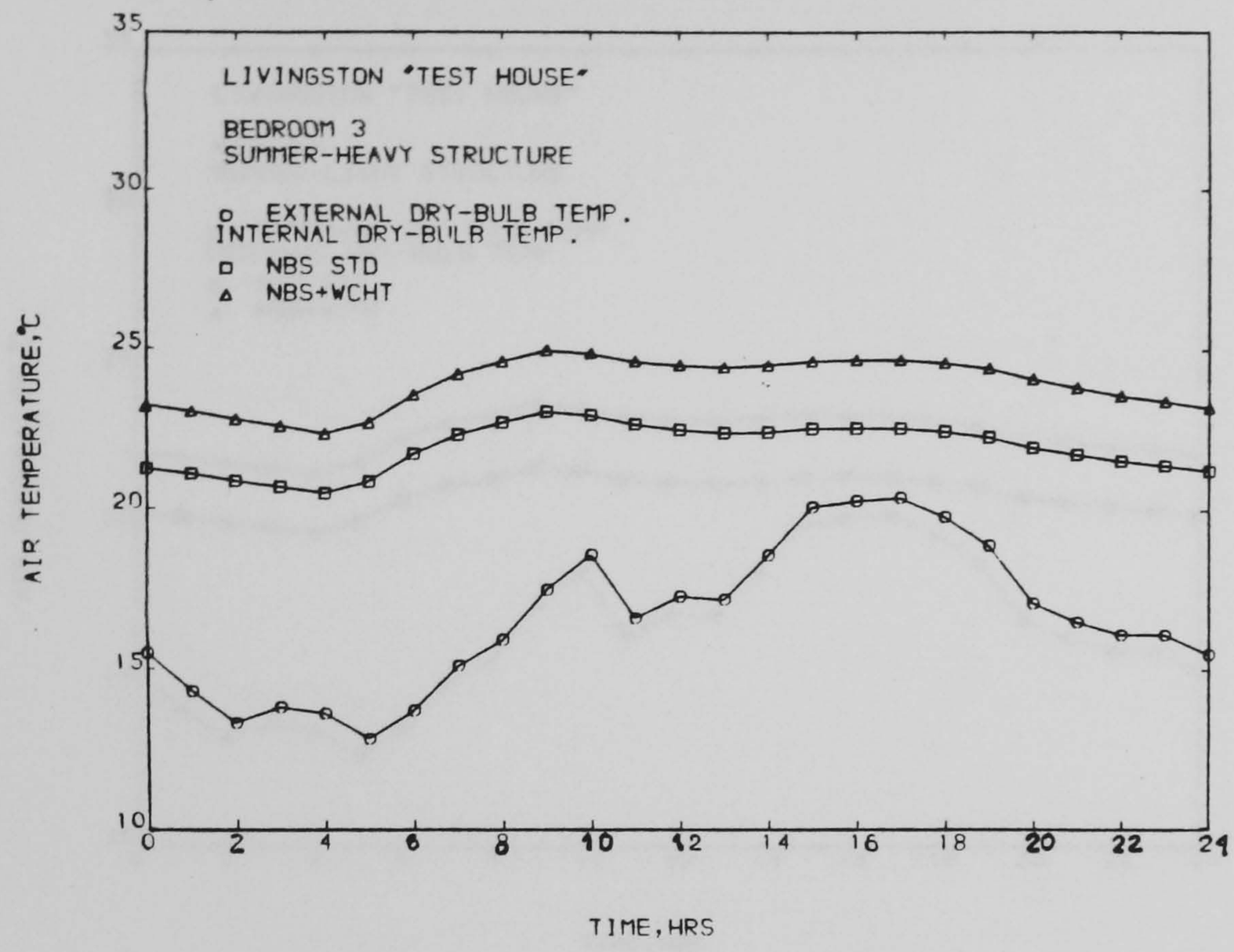

(a)

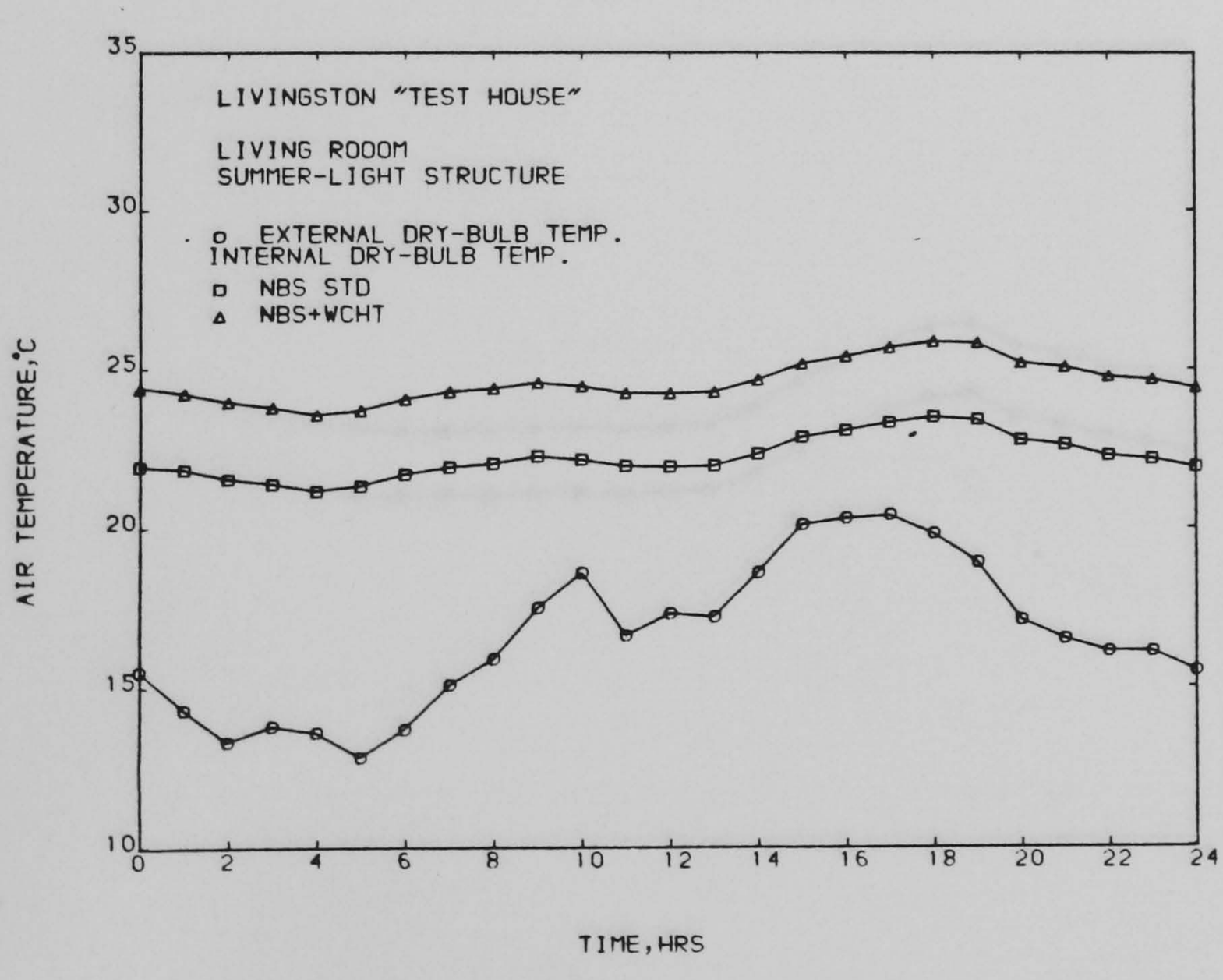

(b)

Fig. 4.9 Summer internal air temperature profile computed by the NBSLD and NBSWIND programs: a) Heavyweight structure - Bedroom 3, and b) Lightweight structure - Living room

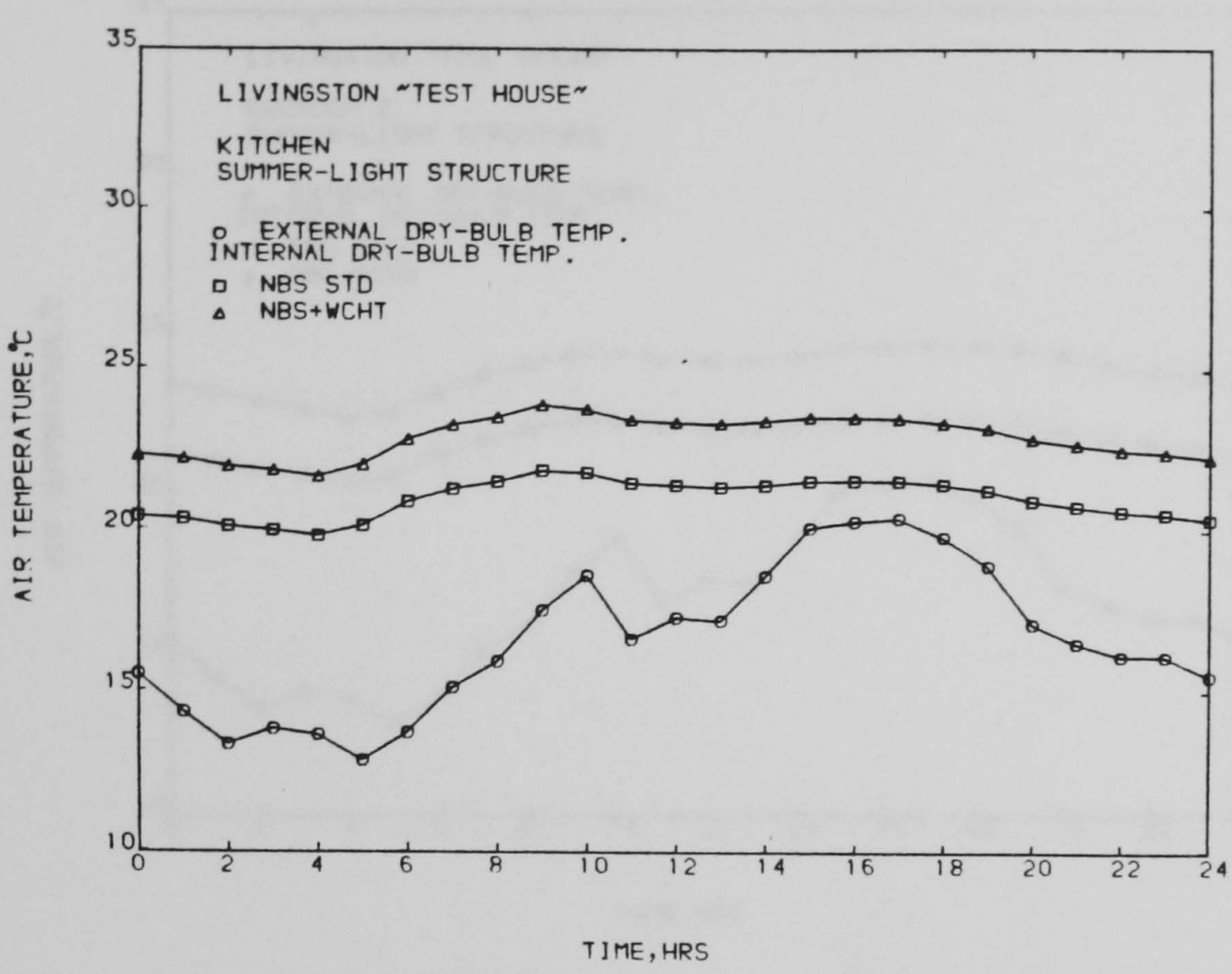

(a)

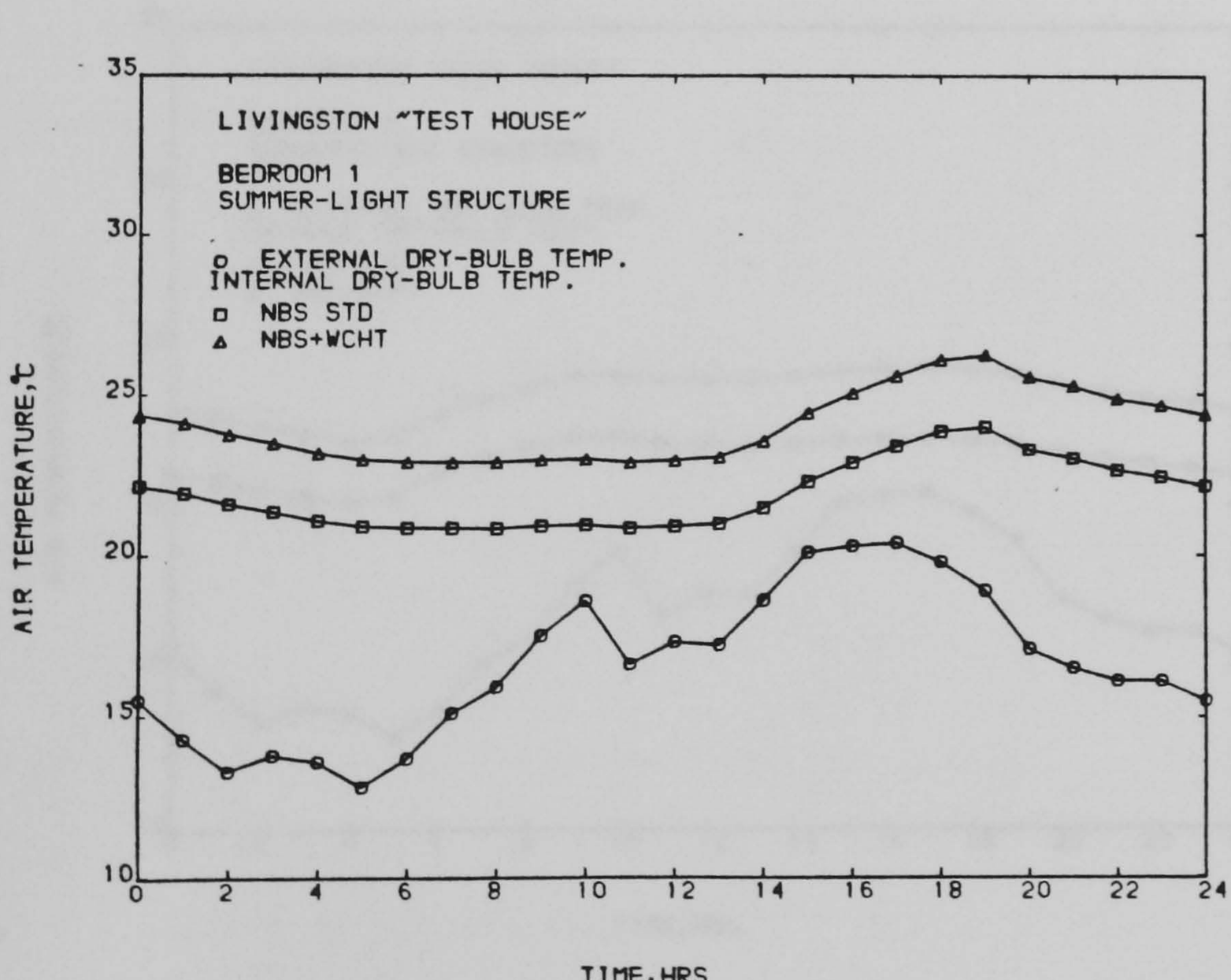

(b)

Fig. 4.10 Summer internal air temperature profile computed by the NBSWIND programs for a lightweight structure: a) Kitchen, and b) Bedroom 1

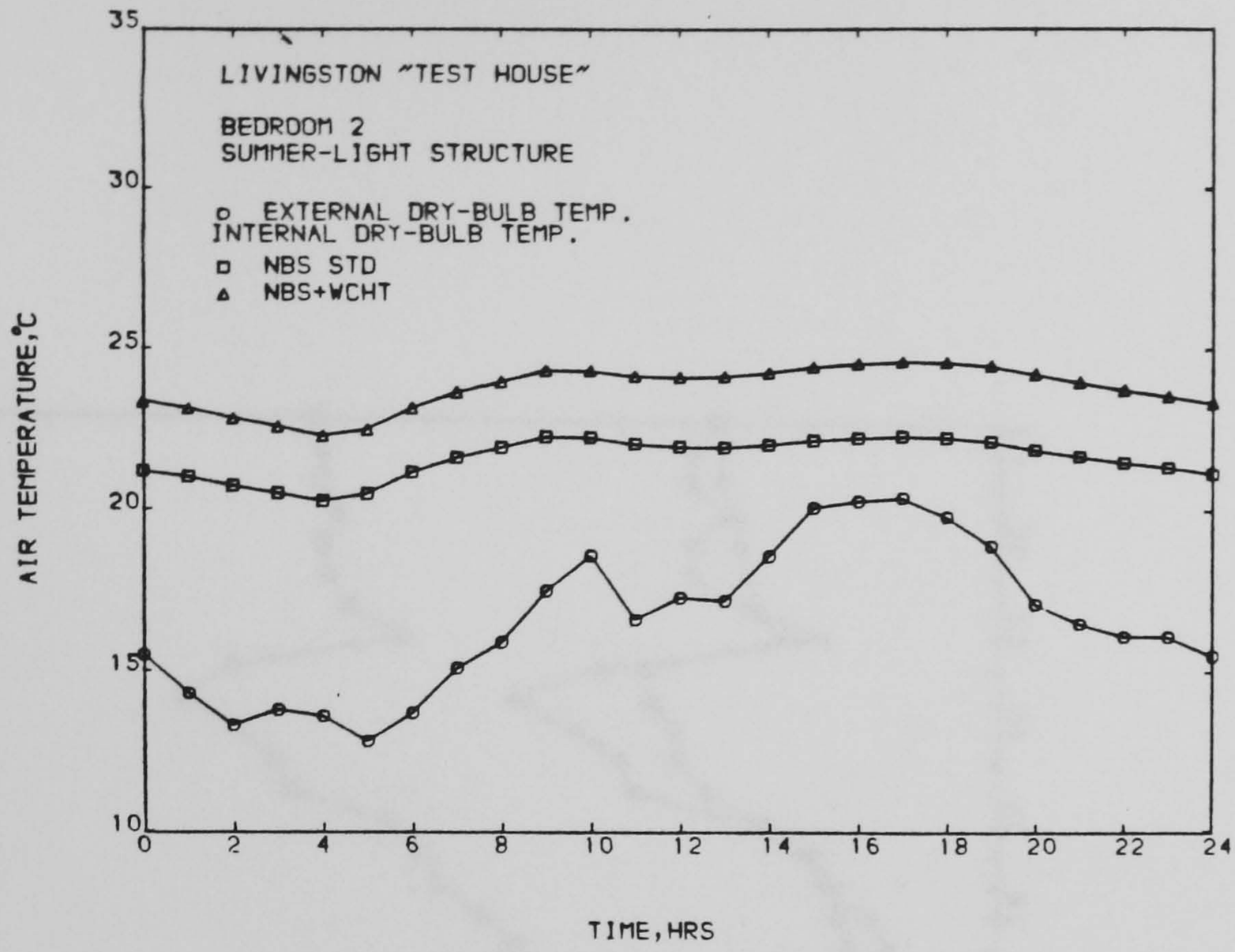

(a)

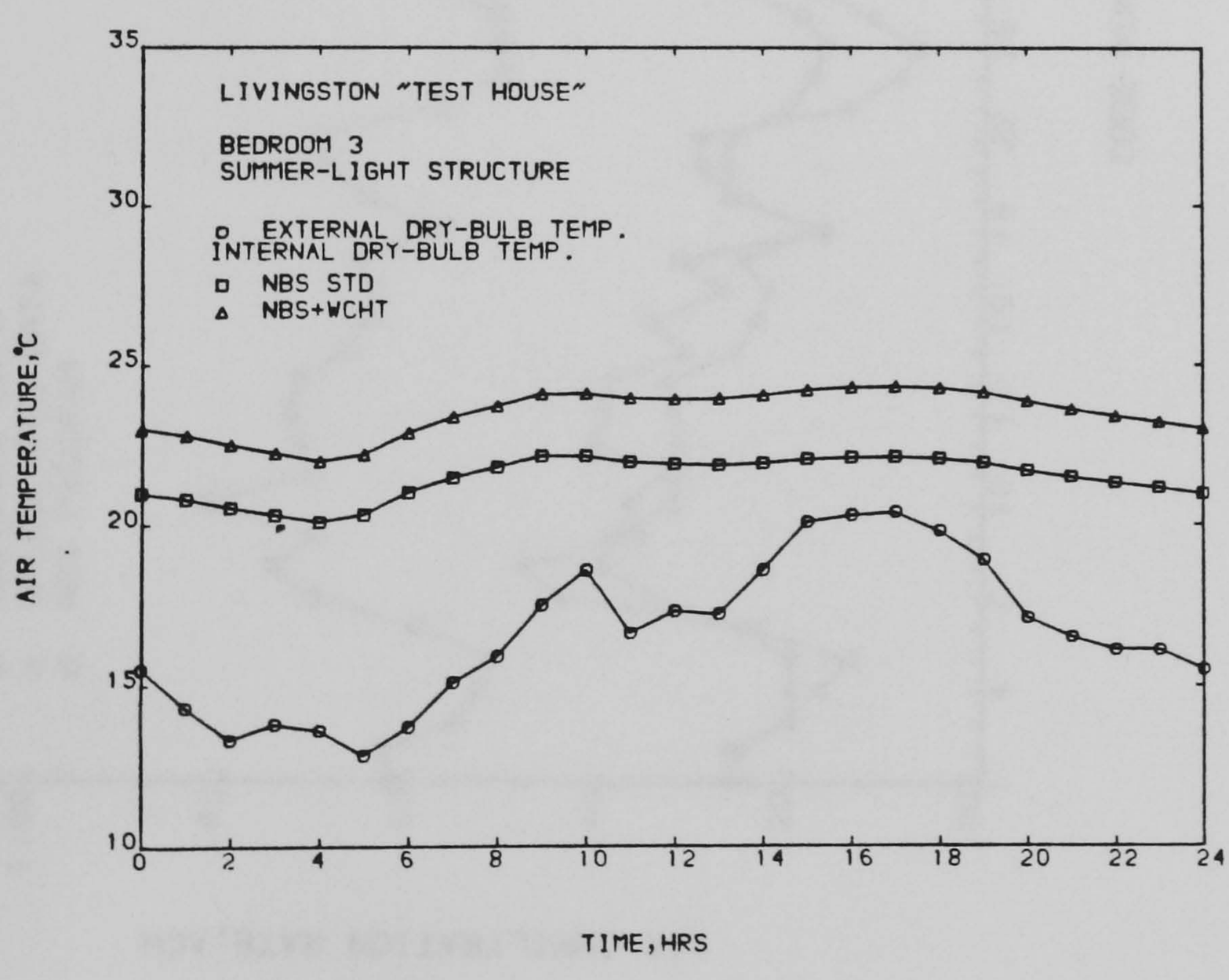

(b)

Fig. 4.11 Summer internal air temperature profile computed by the NBSLD and NESWIND programs for a heavyweight structure: a) Bedroom 2, and b) Bedroom 3

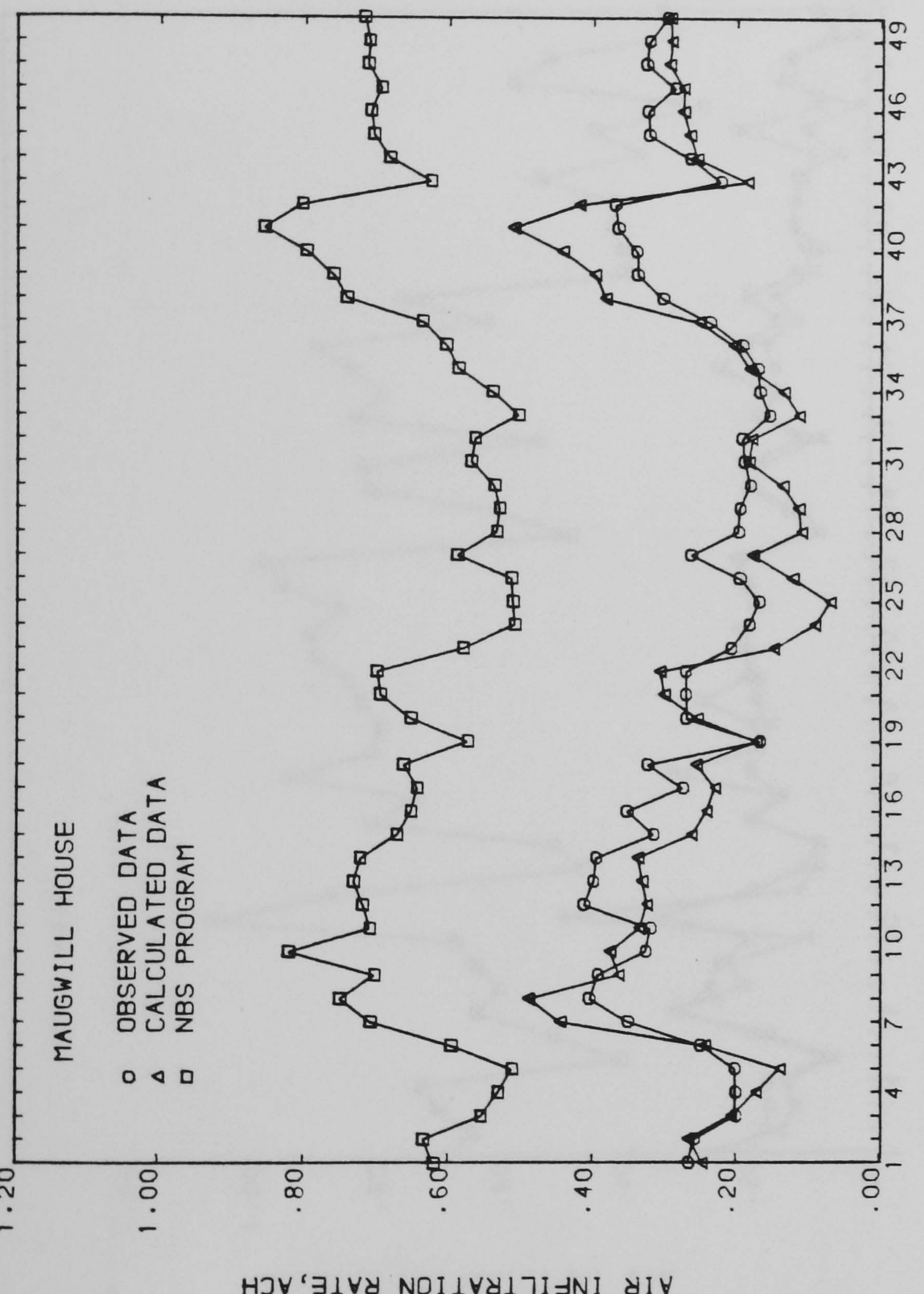

Fig. 4.12 Measured air infiltration rates compared with the computations of the FLOW and NBSLD programs - Maugwill house

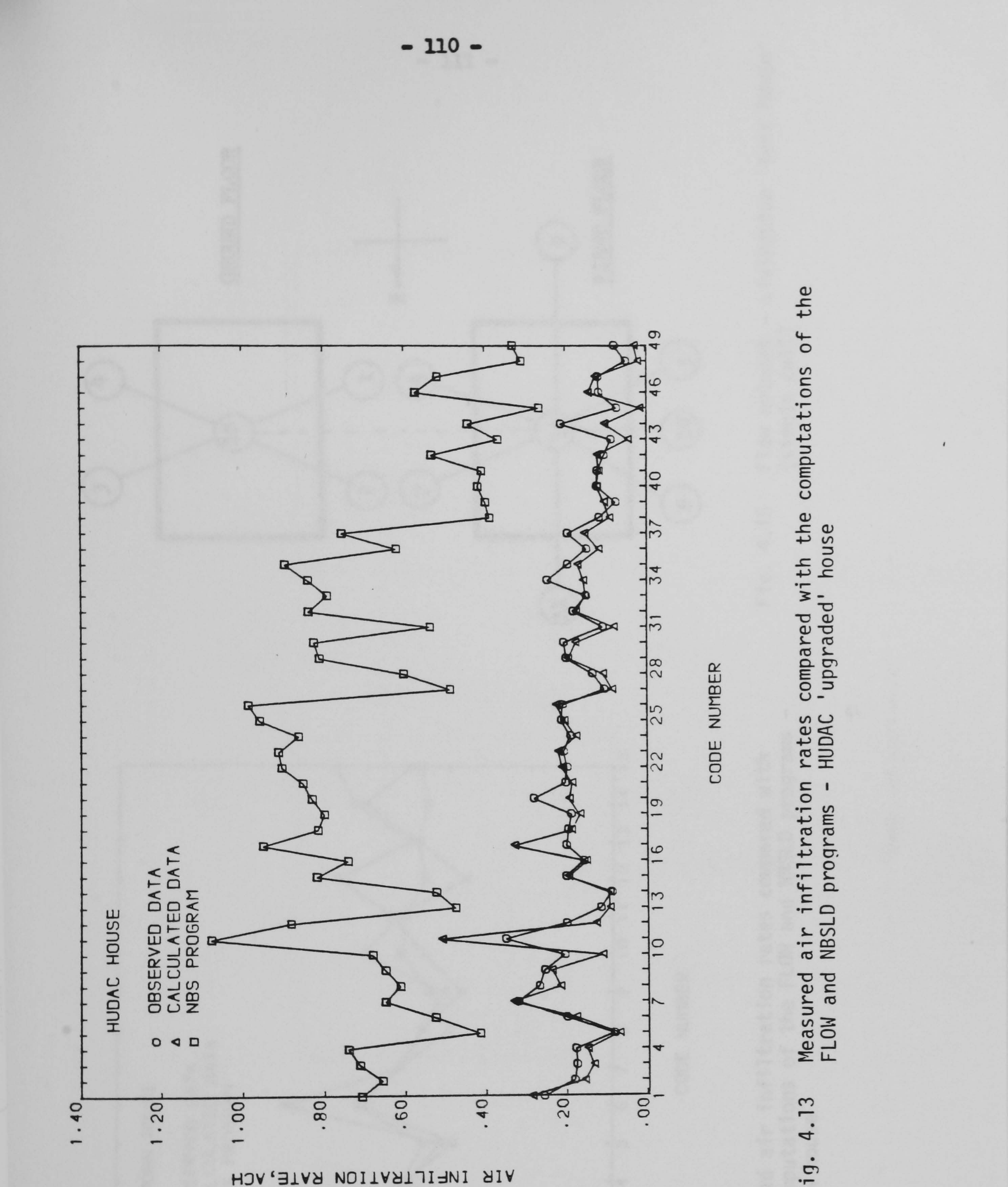

Fig. 4.13 Measured air infiltration rates compared with the computations of the FLOW and NBSLD programs - HUDAC 'upgraded' house

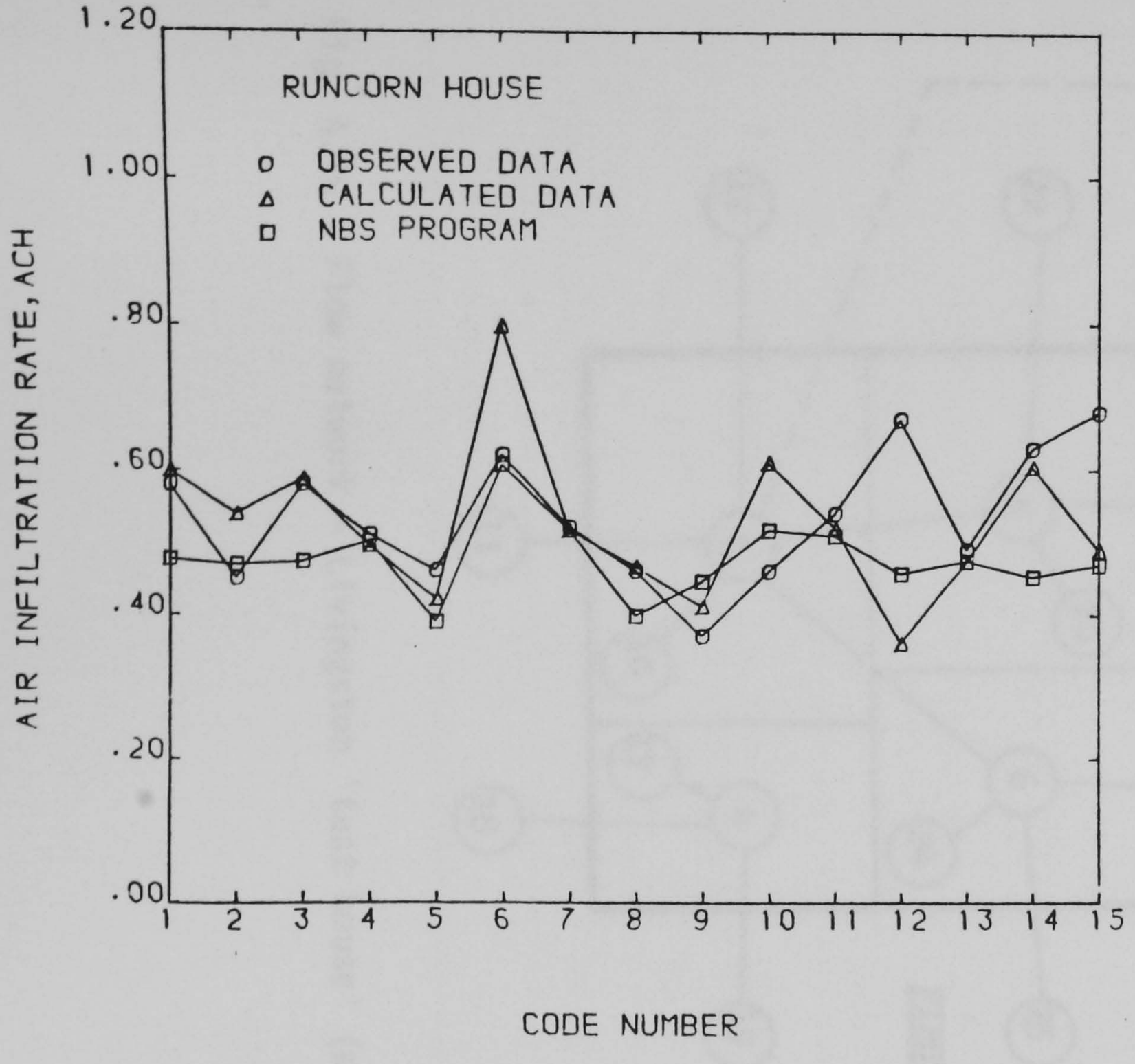

Fig. 4.14 Measured air infiltration rates compared with the computations of the FLOW and NBSLD programs - Runcorn house

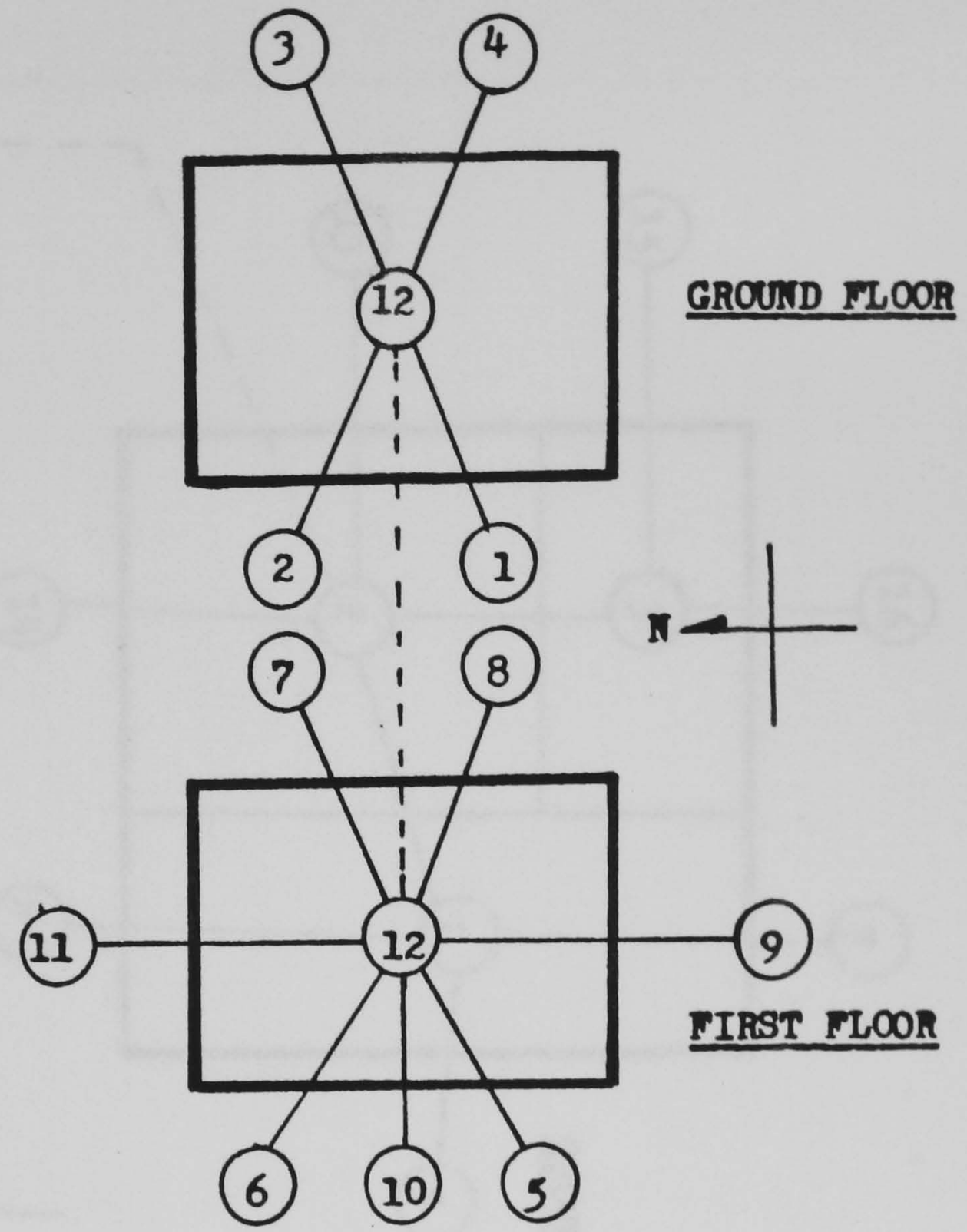

Fig. 4.15 Flow network - Livingston 'test house' (single cell)

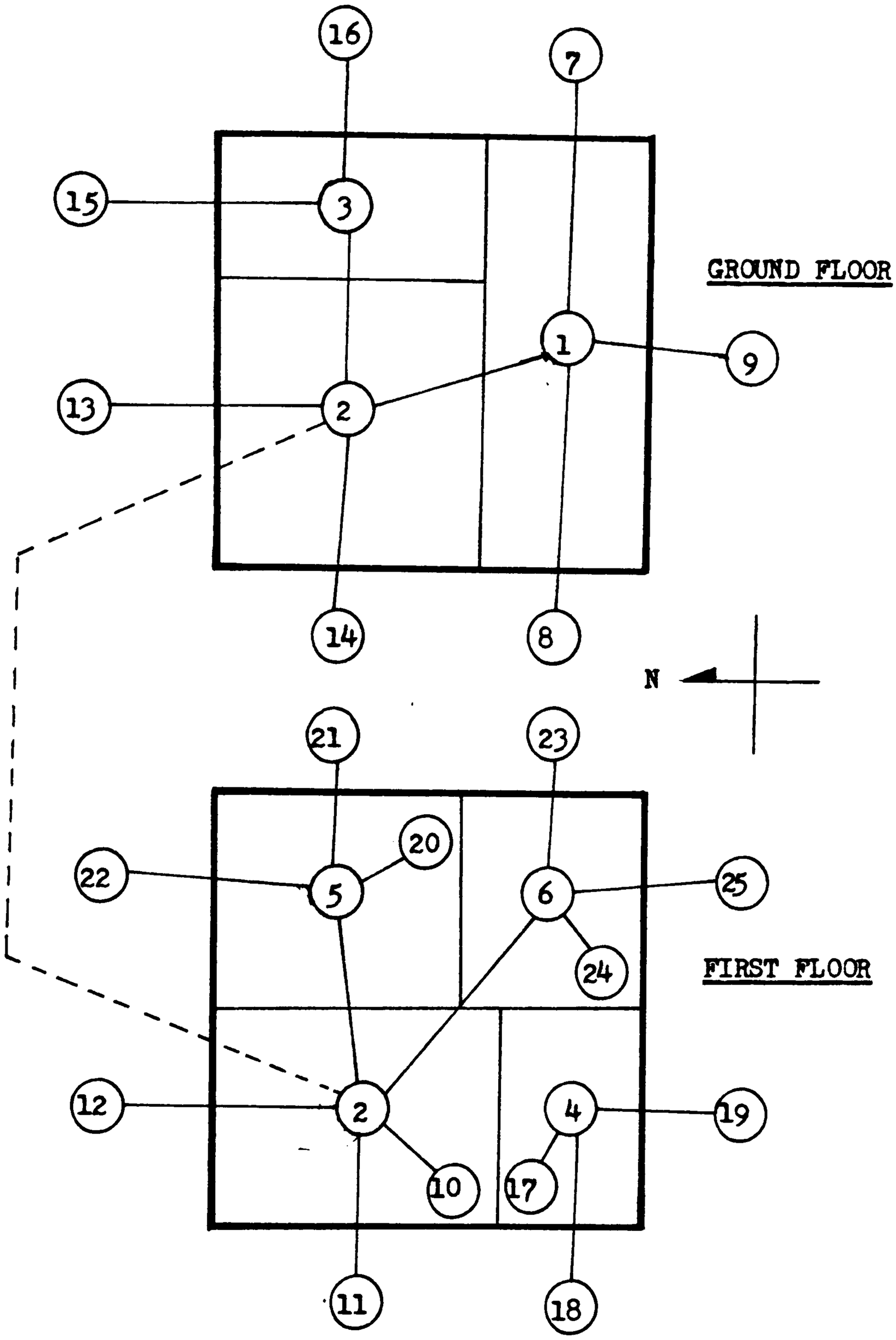

Fig. 4.16 Flow network - Livingston 'test house' (multi-cell)

Table 4.6 Leakage characteristics - Livingston 'test house' (single-cell)

NODE NUMBERS	LEAKAGE SITE	C (m^3/hPa^n)	n
1	Dining room window (W)	2.11	0.66
2	Front door	4.37	0.66
3	Rear door	4.37	0.66
4	Kitchen + Dining room window (E)	3.54	0.66
5	Bedroom 1 window	1.52	0.66
6	Bathroom + Landing window	1.55	0.66
7	Bedroom 2 + Bedroom 3 window	3.04	0.66
8	Eaves (E)	29.04	0.66
9	Gable/roof (S)	29.04	0.66
10	Eaves (W)	29.04	0.66
11	Gable/roof (N)	29.04	0.66
12	Internal node	-	-

Table 4.7 Leakage characteristics - Livingston 'test house' (multi-cell)

NODE NUMBERS	LEAKAGE SITE	C (m^3/hPa^n)	n
1	Internal node - Dining room	-	-
2	Internal node - Hall	-	-
3	Internal node - Kitchen	-	-
4	Internal node - Bedroom 1	-	-
5	Internal node - Bedroom 2	-	-
6	Internal node - Bedroom 3	-	-
7	Dining room facade (E)	5.90	0.66
8	Dining room facade (W)	5.83	0.66
9	Dining room facade (S)	11.90	0.66
10	Hall - roof	11.51	0.66
11	Hall 2nd floor facade (W)	9.35	0.66
12	Hall 2nd floor facade (N)	6.45	0.66
13	Hall 1st floor facade (N)	6.11	0.66
14	Hall 1st floor facade (W)	9.54	0.66
15	Kitchen facade (N)	5.62	0.66
16	Kitchen facade (E)	10.13	0.66
17	Bedroom 1 roof	5.06	0.66
18	Bedroom 1 facade (W)	4.27	0.66
19	Bedroom 1 facade (S)	6.45	0.66
20	Bedroom 3 roof	7.98	0.66
21	Bedroom 3 facade (E)	7.41	0.66
22	Bedroom 3 facade (N)	5.45	0.66
23	Bedroom 2 facade (E)	5.75	0.66
24	Bedroom 2 roof	6.04	0.66
25	Bedroom 2 facade (S)	5.45	0.66

Table 4.8 Air infiltration rates computed by the single-cell version of the FLOW program for the Livingston 'test house' - (Kew 21st December)

TIME	V (m/s)	Ψ (deg.)	Te (°C)	Ta (°C)	Q (ACH)
1	5.7	20	5.6	14.0	0.470
2	6.2	20	5.2	14.0	0.524
3	6.2	20	5.1	14.0	0.524
4	6.2	20	5.1	14.0	0.524
5	5.9	20	4.9	14.0	0.493
6	5.4	20	4.9	14.0	0.441
7	5.4	20	4.9	20.0	0.449
8	5.9	20	5.3	20.0	0.501
9	6.2	20	4.8	20.0	0.534
10	6.7	20	4.9	20.0	0.588
11	7.5	25	5.4	20.0	0.671
12	7.7	30	5.8	20.0	0.749
13	7.0	30	6.0	20.0	0.660
14	7.0	35	6.3	20.0	0.693
15	8.0	40	6.3	20.0	0.855
16	8.5	40	5.8	20.0	0.928
17	8.0	40	5.7	20.0	0.857
18	7.2	40	5.5	20.0	0.747
19	7.2	40	5.2	20.0	0.748
20	7.2	40	5.2	20.0	0.748
21	7.0	40	4.6	20.0	0.722
22	6.7	45	4.5	20.0	0.700
23	6.7	45	4.6	14.0	0.699
24	7.2	45	4.6	14.0	0.769

Table 4.9 Air infiltration rates computed by the multi-cell version of the FLOW program for the Livingston 'test house' - (Kew 21st December)

TIME	Q(LIV) (ACH)	Q(KIT) (ACH)	Q(BED 1) (ACH)	Q(BED 2) (ACH)	Q(BED 3) (ACH)	Q(AV.) (ACH)
1	0.168	0.429	0.433	0.362	0.585	0.362
2	0.185	0.479	0.482	0.402	0.655	0.403
3	0.184	0.479	0.482	0.401	0.655	0.402
4	0.185	0.479	0.482	0.402	0.655	0.403
5	0.177	0.450	0.454	0.381	0.613	0.380
6	0.162	0.401	0.407	0.344	0.544	0.340
7	0.178	0.405	0.419	0.361	0.541	0.350
8	0.192	0.453	0.464	0.397	0.609	0.387
9	0.203	0.483	0.494	0.421	0.652	0.413
10	0.218	0.534	0.543	0.459	0.724	0.452
11	0.232	0.559	0.585	0.648	0.902	0.532
12	0.288	0.512	0.556	0.771	1.024	0.580
13	0.255	0.452	0.495	0.685	0.898	0.513
14	0.286	0.378	0.400	0.770	0.947	0.519
15	0.386	0.471	0.561	1.000	1.185	0.660
16	0.423	0.508	0.605	1.082	1.287	0.729
17	0.384	0.473	0.565	1.003	1.186	0.673
18	0.328	0.418	0.500	0.882	1.028	0.586
19	0.329	0.420	0.501	0.883	1.028	0.587
20	0.329	0.420	0.501	0.883	1.028	0.587
21	0.318	0.409	0.488	0.857	0.990	0.567
22	0.327	0.405	0.538	0.881	0.966	0.576
23	0.336	0.391	0.521	0.824	0.975	0.568
24	0.374	0.426	0.569	0.946	1.074	0.624

Table 4.10 Air infiltration rates computed by the NBSLD program for the Livingston 'test house' - (Kew 21st December)

TIME	Q(LIV) (ACH)	Q(KIT) (ACH)	Q(BED 1) (ACH)	Q(BED 2) (ACH)	Q(BED 3) (ACH)	Q(AV.) (ACH)
1	0.281	0.619	0.337	0.281	0.225	0.341
2	0.288	0.635	0.346	0.288	0.231	0.350
3	0.295	0.649	0.354	0.295	0.236	0.358
4	0.295	0.649	0.354	0.295	0.236	0.358
5	0.290	0.638	0.348	0.290	0.232	0.352
6	0.389	0.280	0.616	0.336	0.389	0.340
7	0.319	0.701	0.382	0.319	0.255	0.486
8	0.326	0.719	0.392	0.326	0.262	0.397
9	0.336	0.739	0.403	0.336	0.269	0.409
10	0.346	0.761	0.415	0.346	0.277	0.419
11	0.360	0.792	0.432	0.360	0.288	0.438
12	0.361	0.795	0.433	0.361	0.289	0.439
13	0.345	0.760	0.414	0.345	0.276	0.420
14	0.343	0.755	0.412	0.343	0.275	0.416
15	0.364	0.801	0.437	0.364	0.291	0.442
16	0.377	0.831	0.453	0.377	0.302	0.458
17	0.368	0.810	0.442	0.368	0.295	0.447
18	0.352	0.776	0.423	0.352	0.282	0.424
19	0.354	0.780	0.425	0.354	0.284	0.430
20	0.354	0.780	0.425	0.354	0.284	0.430
21	0.354	0.779	0.425	0.354	0.283	0.429
22	0.348	0.766	0.418	0.348	0.279	0.422
23	0.309	0.681	0.371	0.309	0.248	0.375
24	0.319	0.703	0.383	0.319	0.256	0.387

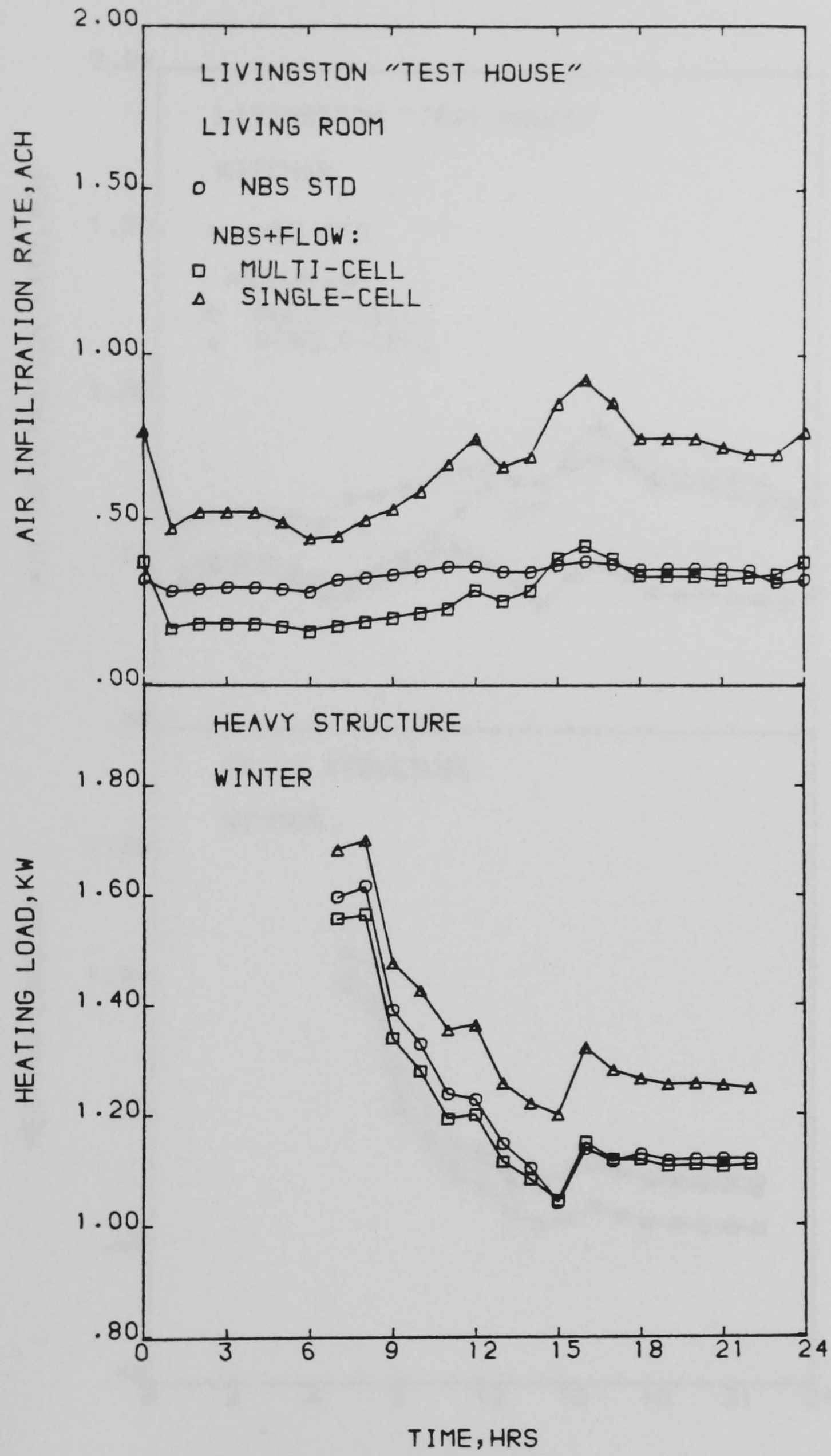

Fig. 4.17 Air infiltration rates and heating loads computed by the NBSLD and NBSFLOW programs for a heavyweight structure on a typical winter day - Living room

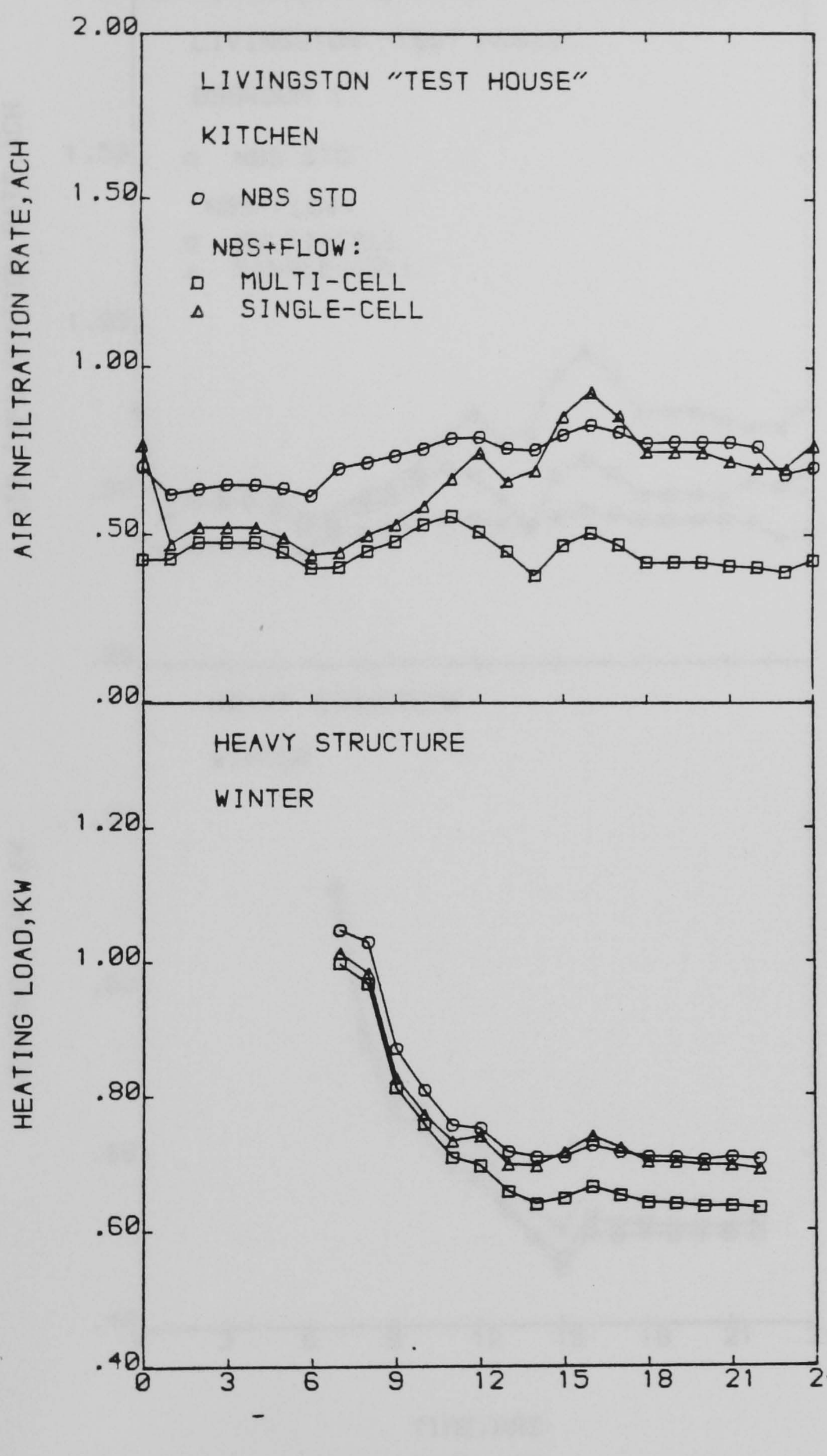

Fig. 4.18 Air infiltration rates and heating loads computed by the NBSLD and NBSFLOW programs for a heavyweight structure on a typical winter day - Kitchen

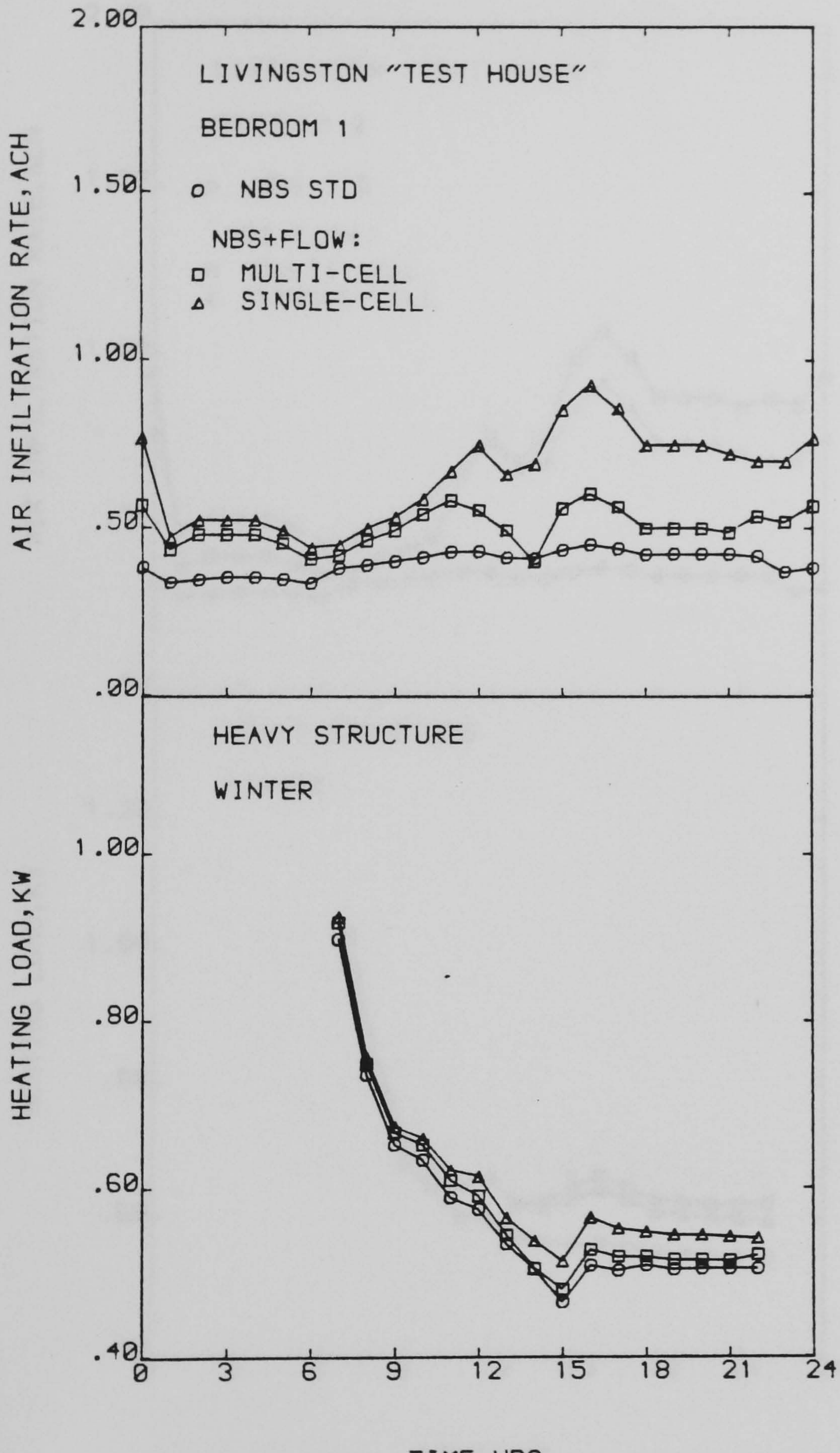

Fig. 4.19 Air infiltration rates and heating loads computed by the NBSFLOW programs for a heavyweight structure on a typical winter day - Bedroom 1.

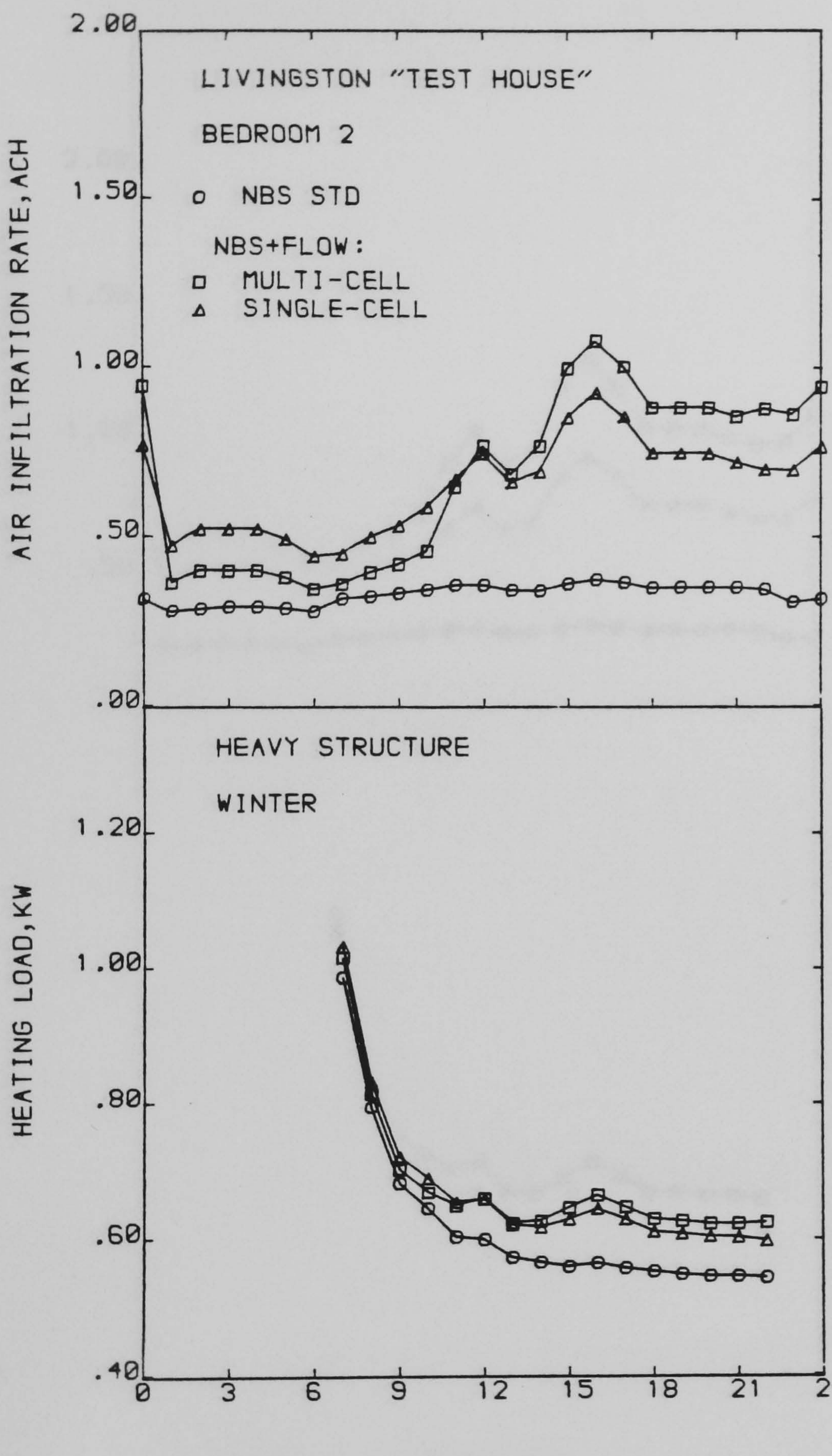

Fig. 4.20 Air infiltration rates and heating loads computed by the NBSLD and NBSFLOW programs for a heavyweight structure on a typical winter day - Bedroom 2

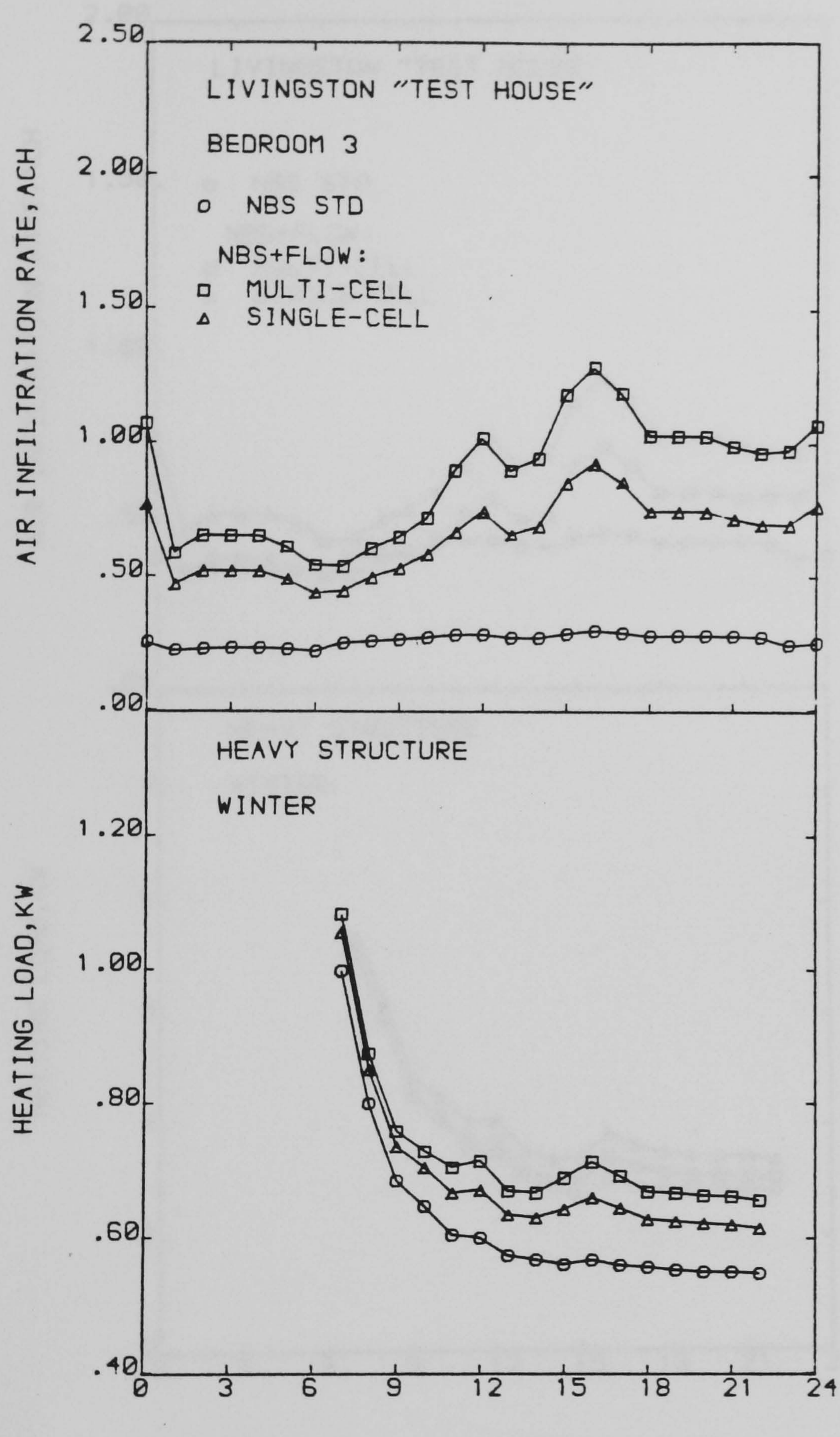

Fig. 4.21 Air infiltration rates and heating loads computed by the NBSLD and NBSFLOW programs for a heavyweight structure on a typical winter day - Bedroom 3

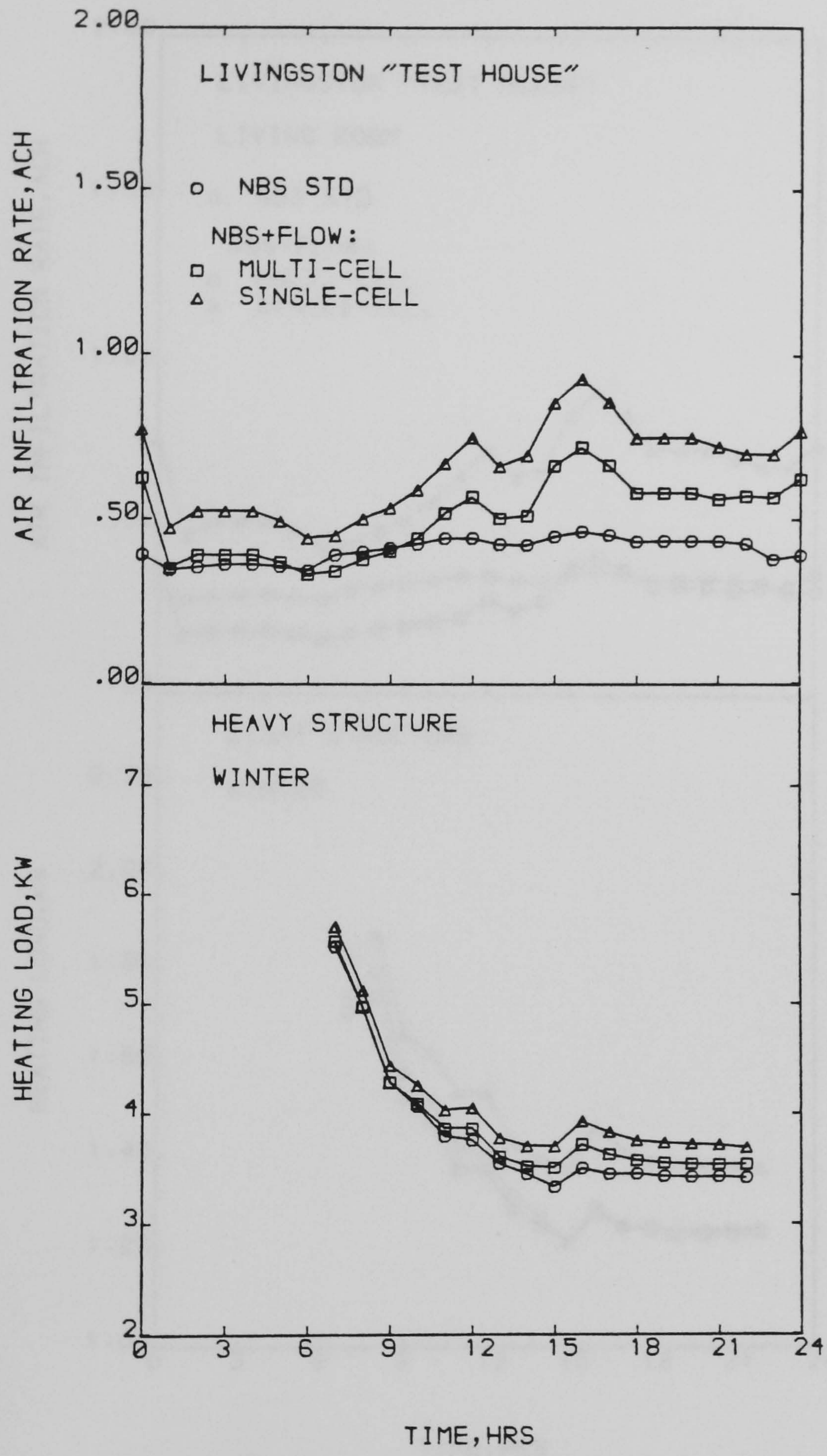

Fig. 4.22 Air infiltration rates and heating loads computed by the NBSLD and NBSFLOW programs for a heavyweight structure on a typical winter day - 'Whole' house

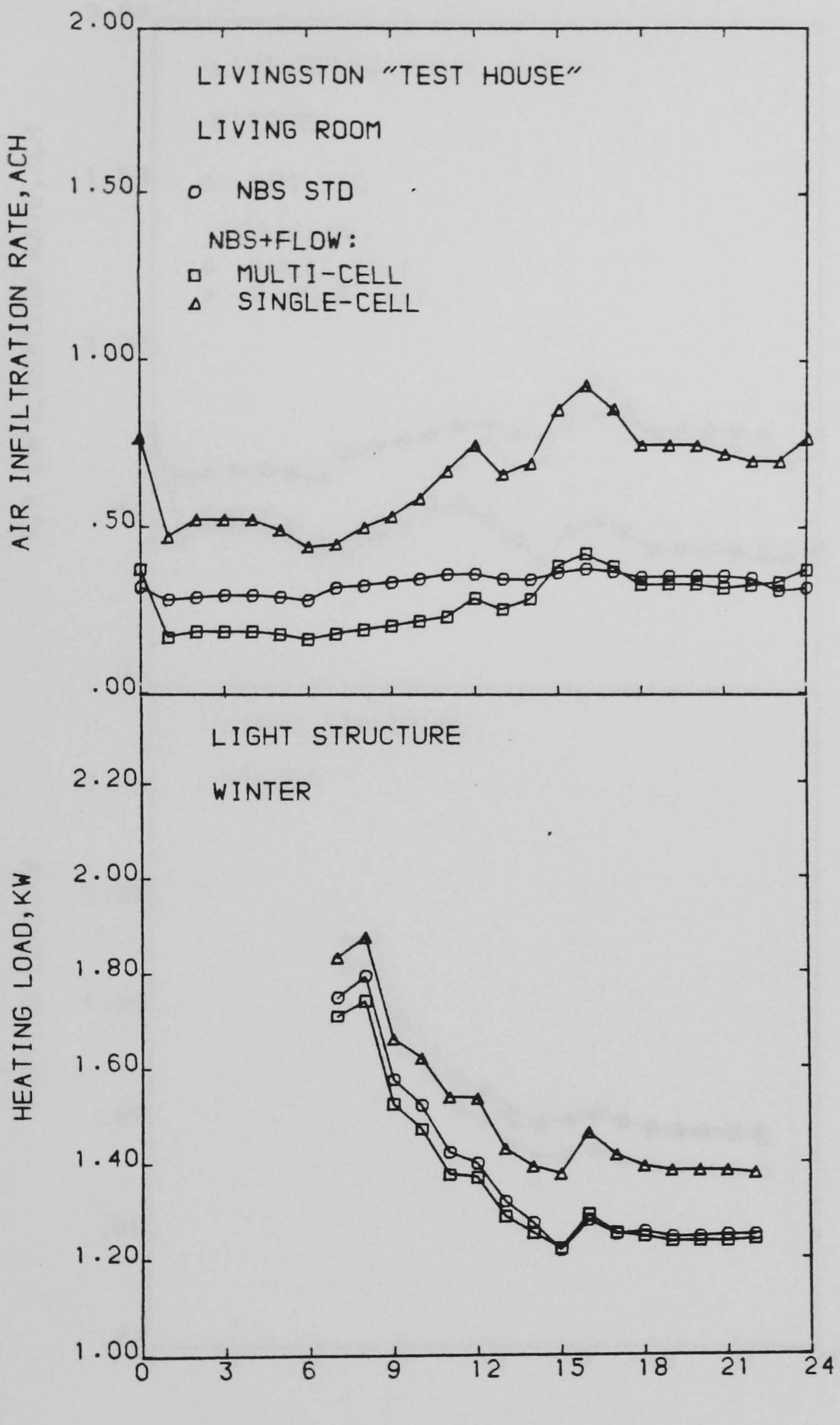

Fig. 4.23 Air infiltration rates and heating loads computed by the NBSLD and NBSFLOW programs for a lightweight structure on a typical winter day - Living room

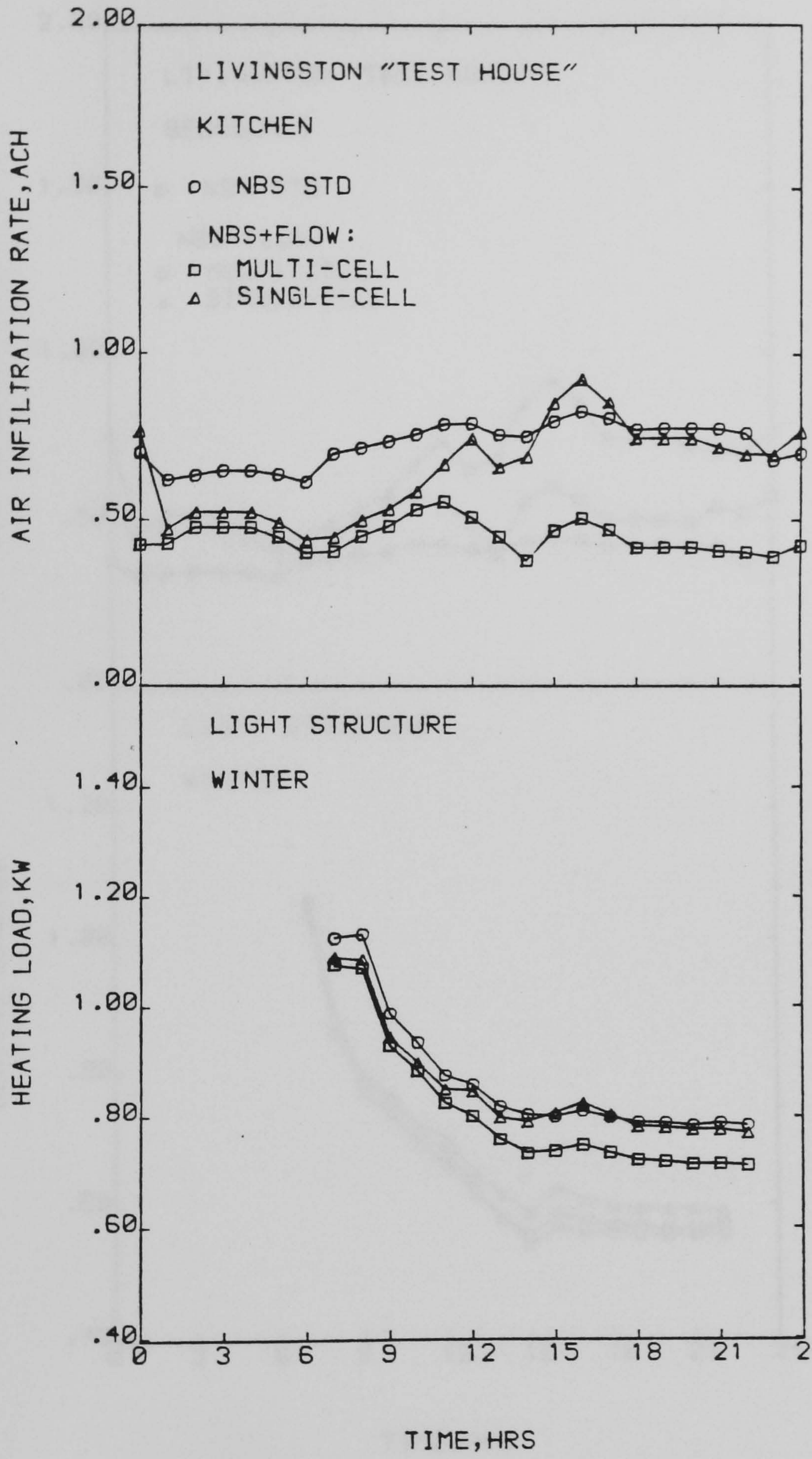

Fig. 4.24 Air infiltration rates and heating loads computed by the NBSLD and NBSFLOW programs for a lightweight structure on a typical winter day - Kitchen

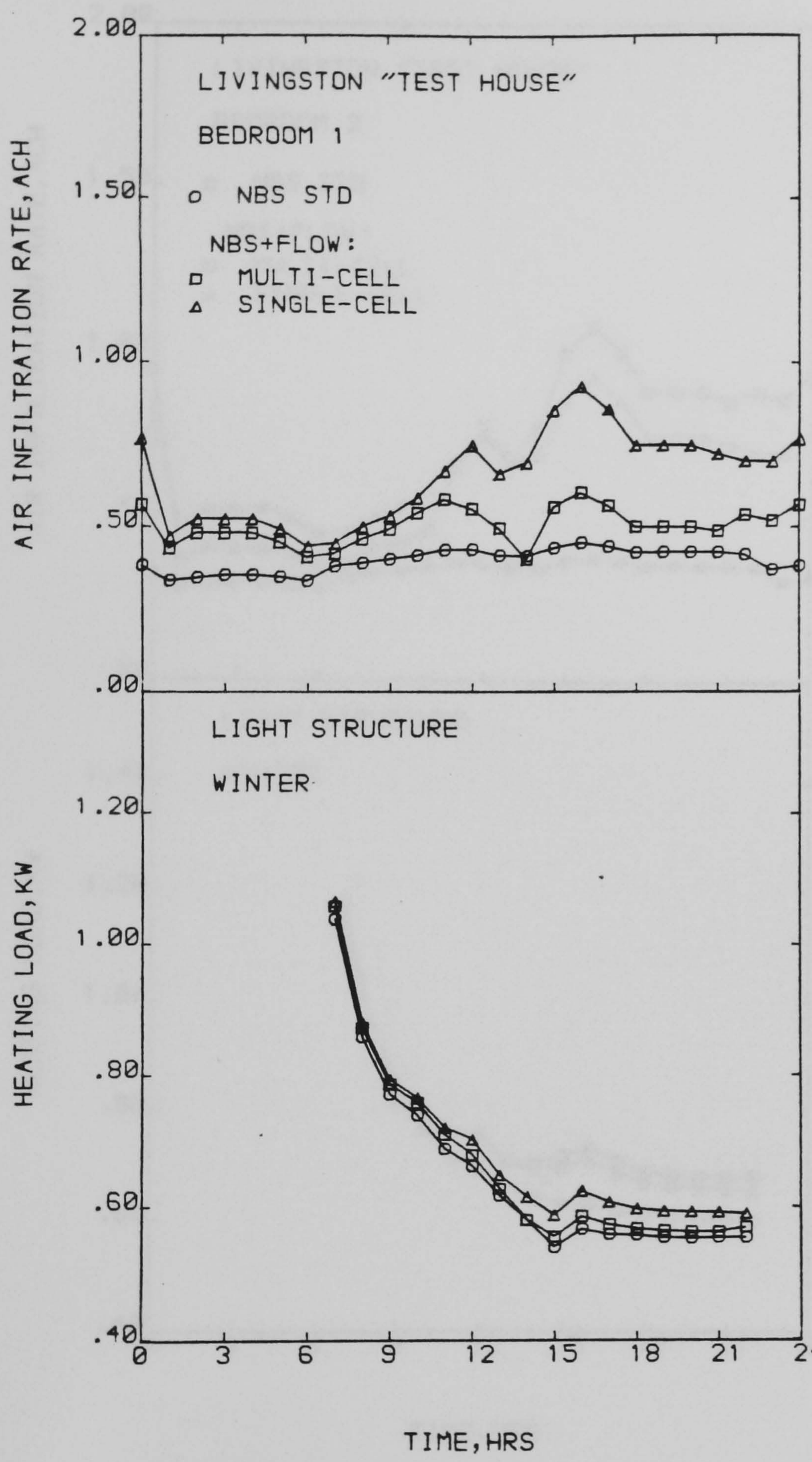

Fig. 4.25 Air infiltration rates and heating loads computed by the NBSLD and NBSFLOW programs for a lightweight structure on a typical winter day - Bedroom 1

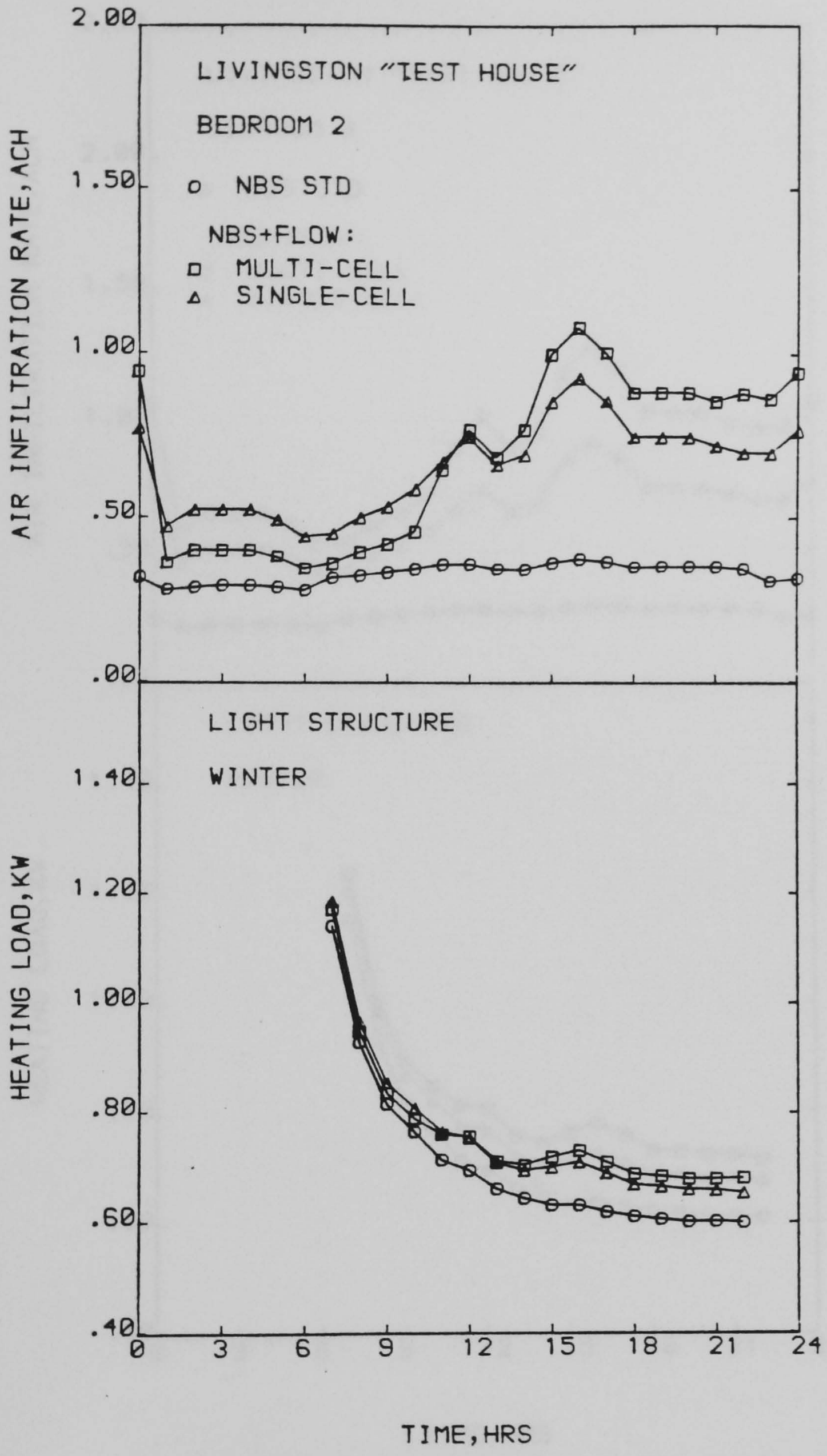

Fig. 4.26 Air infiltration rates and heating loads computed by the NBSLD and NBSFLOW programs for a lightweight structure on a typical winter day - Bedroom 2

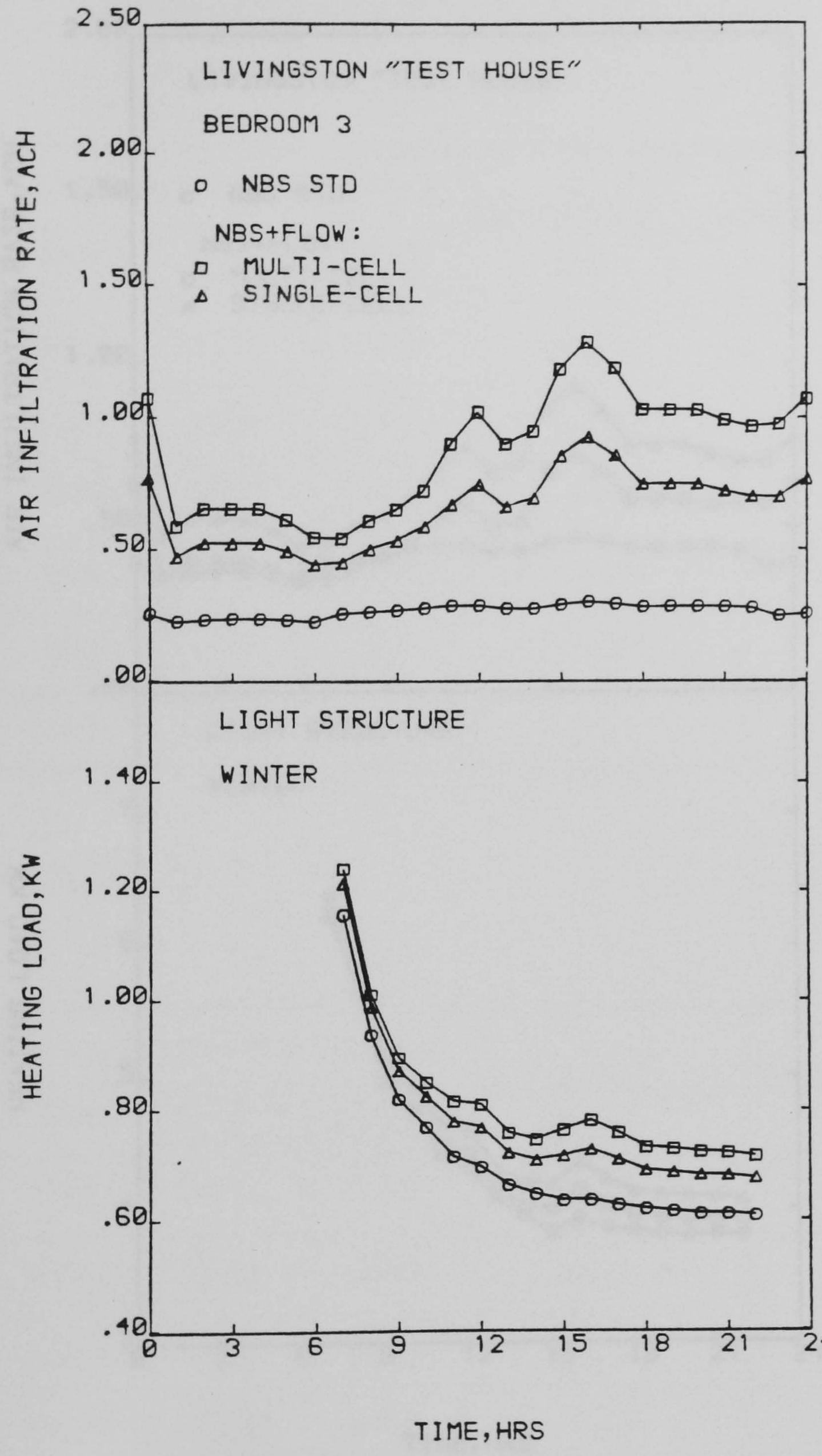

Fig. 4.27 Air infiltration rates and heating loads computed by the NBSLD and NBSFLOW programs for a lightweight structure on a typical winter day - Bedroom 3

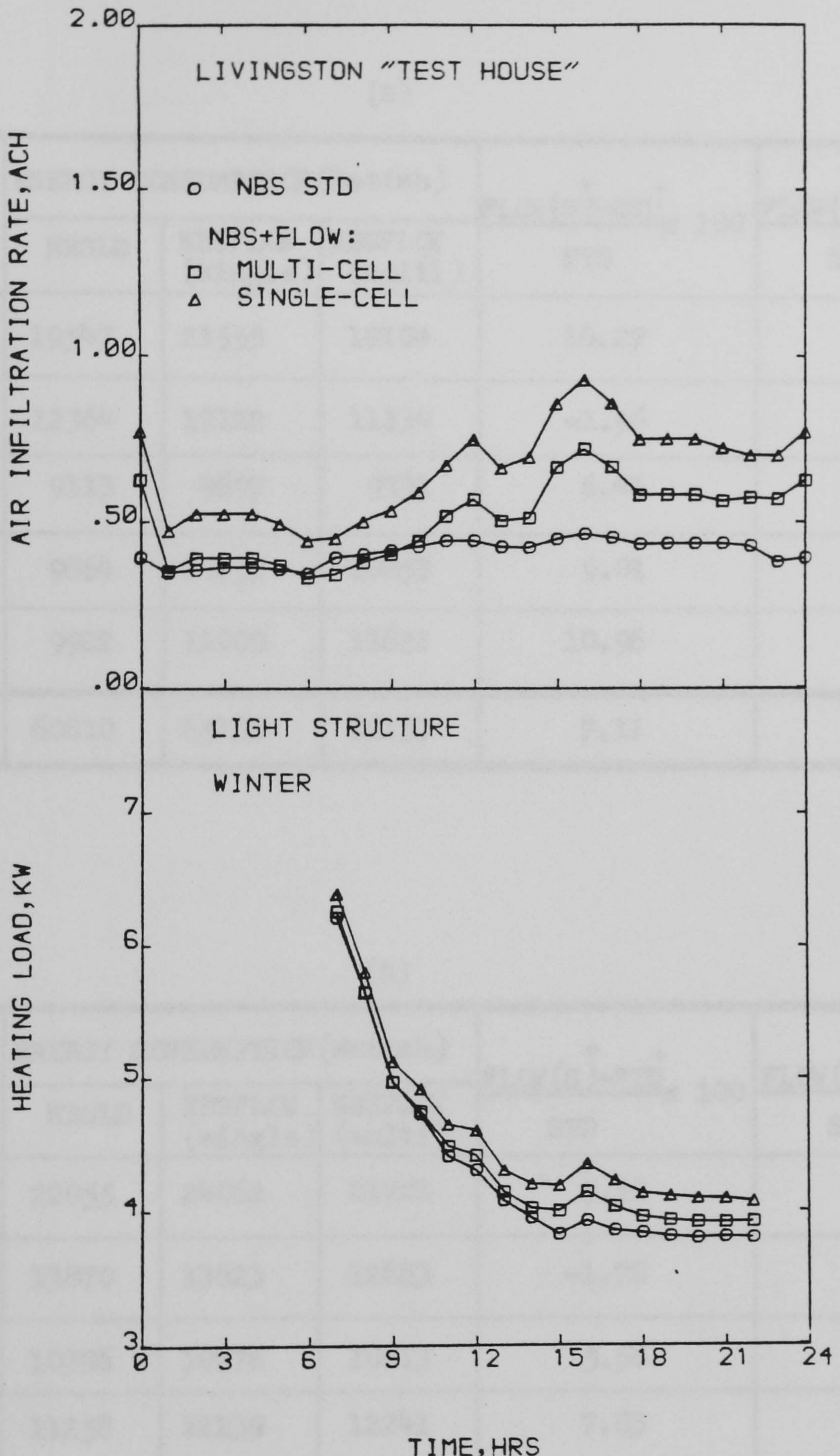

Fig. 4.28 Air infiltration rates and heating loads computed by the NBSLD and NBSFLOW programs for a lightweight structure on a typical winter day - 'Whole' house

Table 4.11 Daily energy consumption computed by the NBSLD and NBSFLOW programs on a typical winter day:
a) Heavyweight structure, and b) Lightweight structure

(a)

ROOM	ENERGY CONSUMPTION(Wattsh)			$\frac{FLOW(S^{*})-STD^{+}}{STD} \times 100$	$\frac{FLOW(M^{**})-STD}{STD} \times 100$
	NBSLD	NBSFLOW (single)	NBSFLOW (multi)		
Living	19547	21555	19194	10.27	-1.81
Kitchen	12364	12122	11134	-1.96	-9.95
Bedrooml	9113	9697	9331	6.41	2.39
Bedroom2	9864	10753	10853	9.01	10.03
Bedroom3	9922	11009	11621	10.96	17.12
TOTAL	60810	65136	62133	7.11	2.18

(b)

ROOM	ENERGY CONSUMPTION(Wattsh)			$\frac{FLOW(S^{*})-STD^{+}}{STD} \times 100$	$\frac{FLOW(M^{**})-STD}{STD} \times 100$
	NBSLD	NBSFLOW (single)	NBSFLOW (multi)		
Living	22055	24062	21701	9.10	-1.61
Kitchen	13870	13623	12883	-1.78	-7.12
Bedrooml	10396	10976	10613	5.58	2.09
Bedroom2	11258	12139	12241	7.83	8.73
Bedroom3	11373	12450	13057	9.47	14.81
TOTAL	68952	73250	70495	6.23	2.24

(+) NBSLD program (*) single-cell version of the NBSFLOW program
(**) multi-cell version of the NBSFLOW program

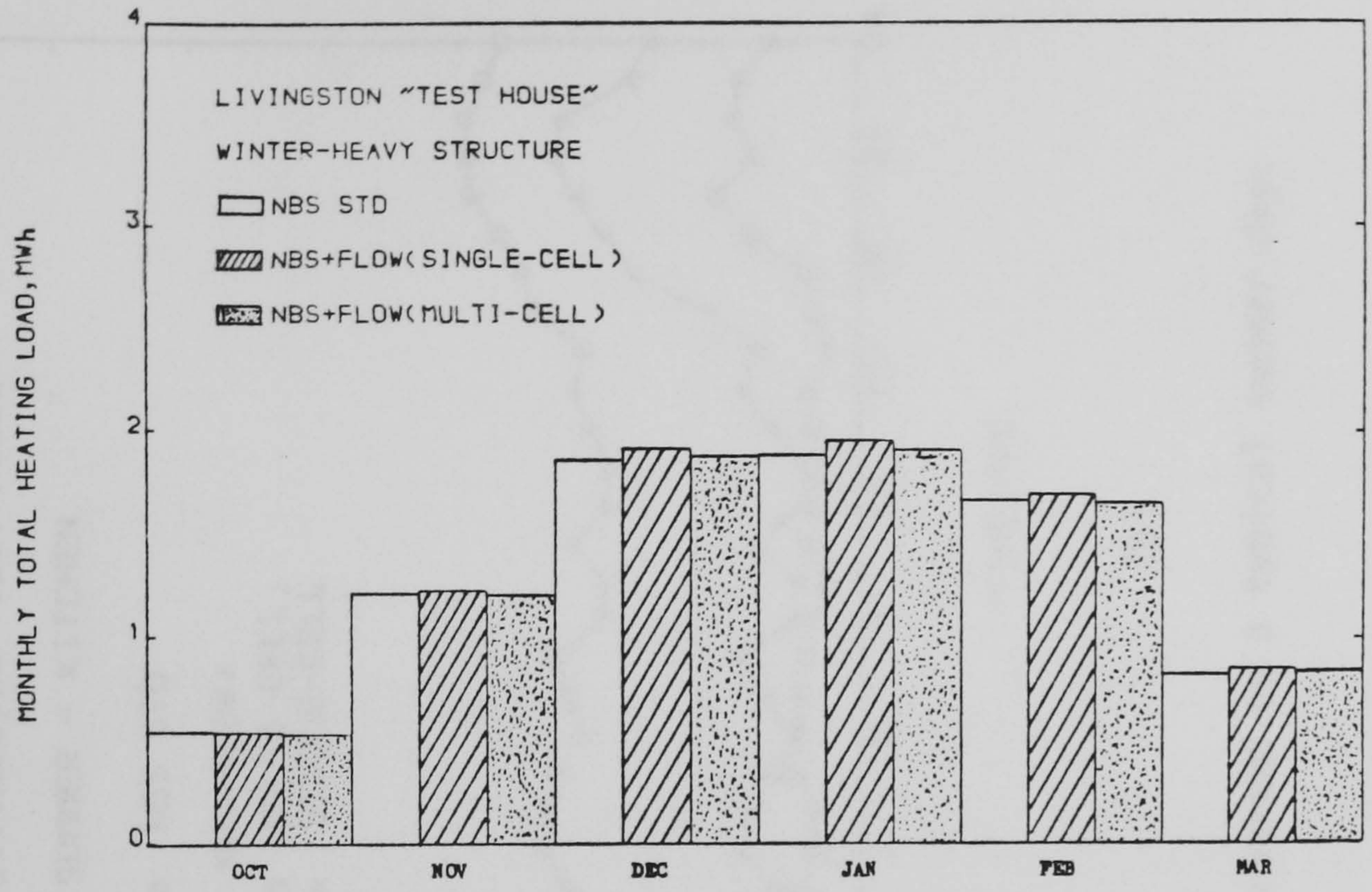

(a)

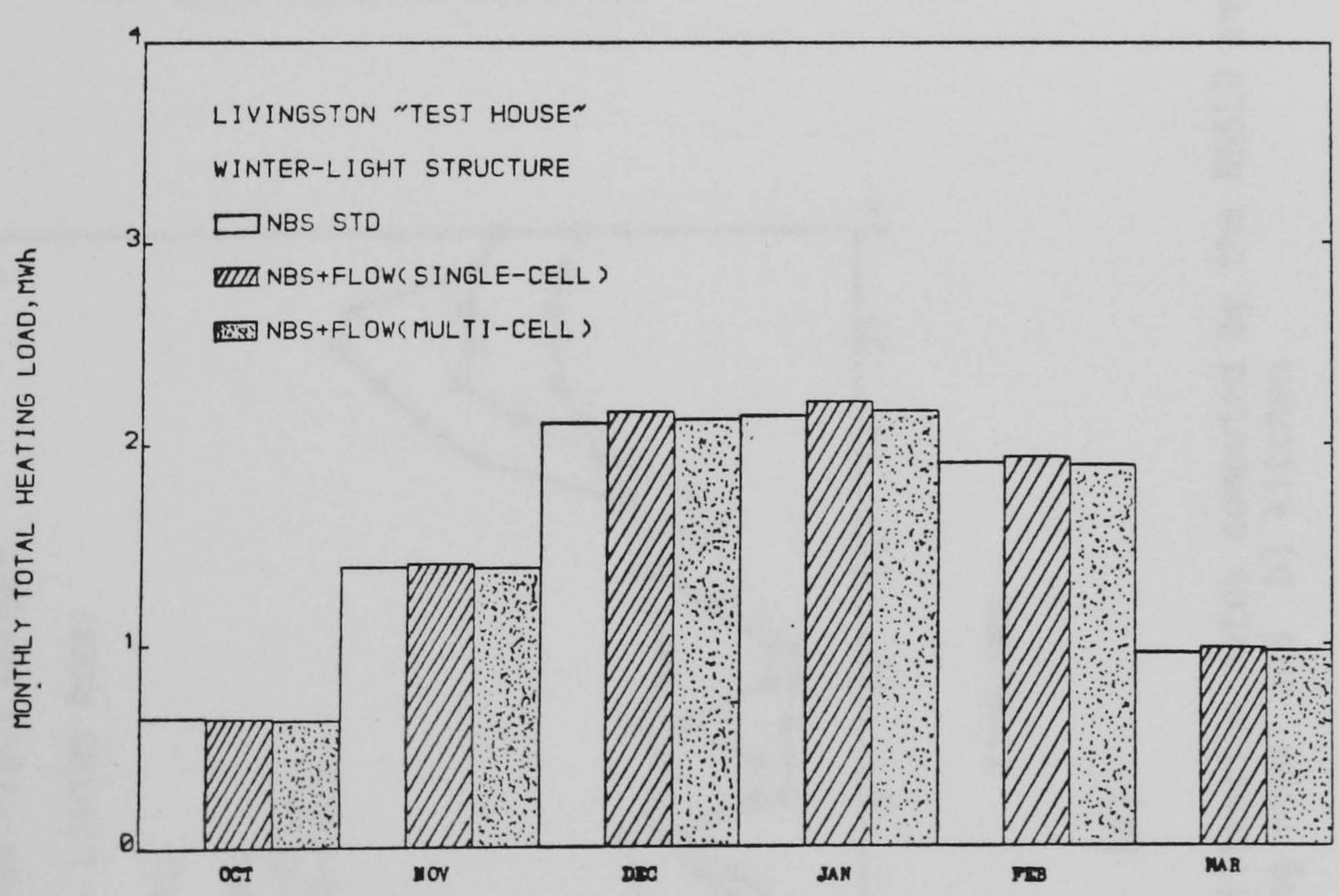

(b)

Fig. 4.29 Monthly total energy consumption computed by the NBSLD and NBSFLOW programs: a) Heavyweight structure and b) Lightweight structure

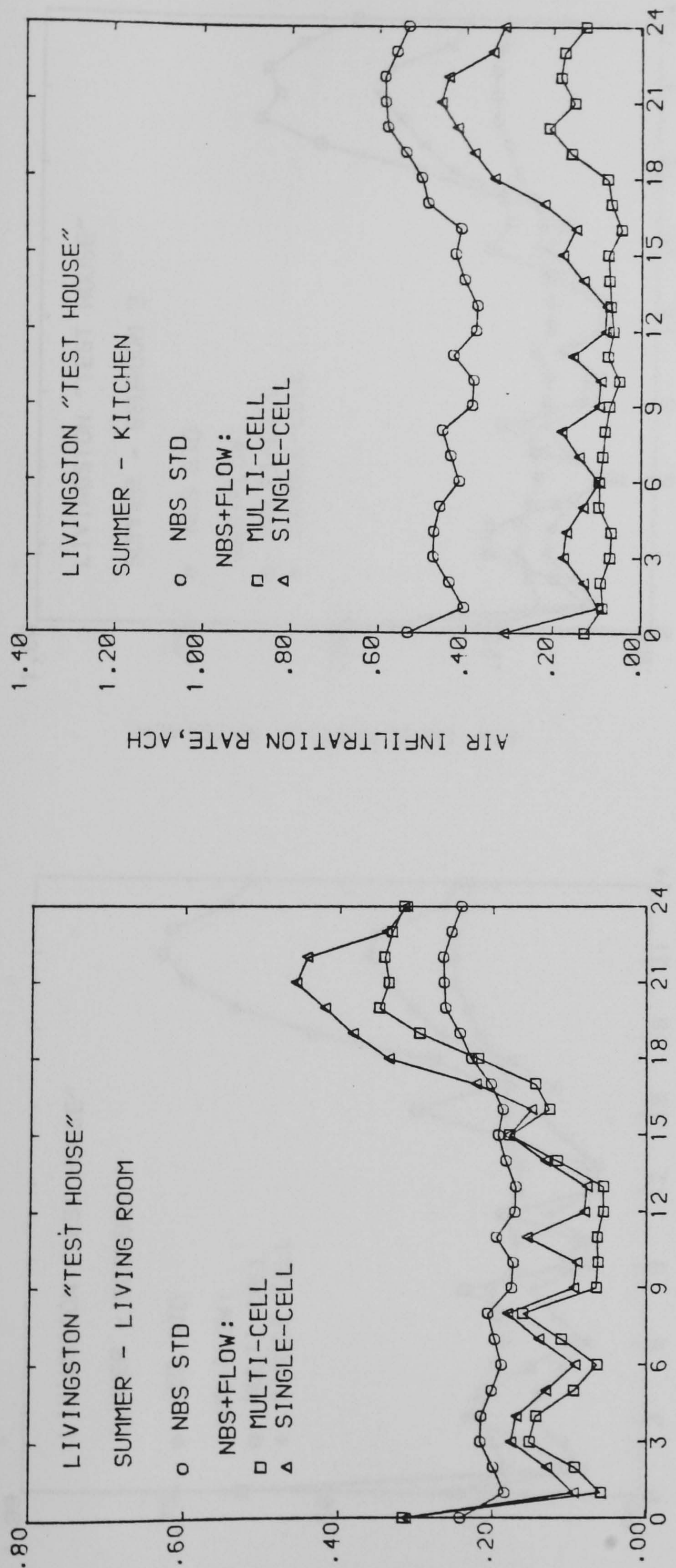

Fig. 4.30 Air infiltration rates computed by the NBSLD and NBSFLOW programs on a typical summer day:
a) Living room and b) Kitchen

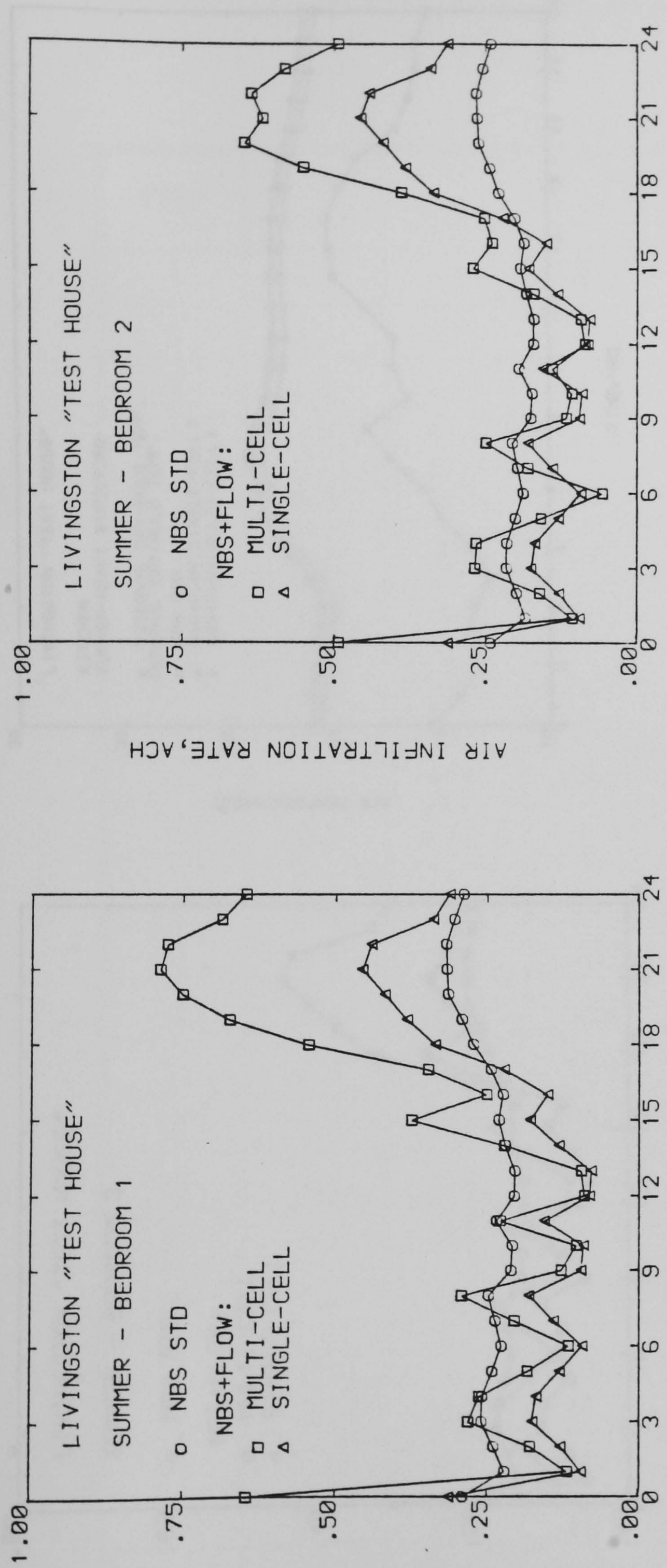

Fig. 4.31 Air infiltration rates computed by the NBSLD and NBSFLOW programs on a typical summer day:
a) Bedroom 1 and b) Bedroom 2

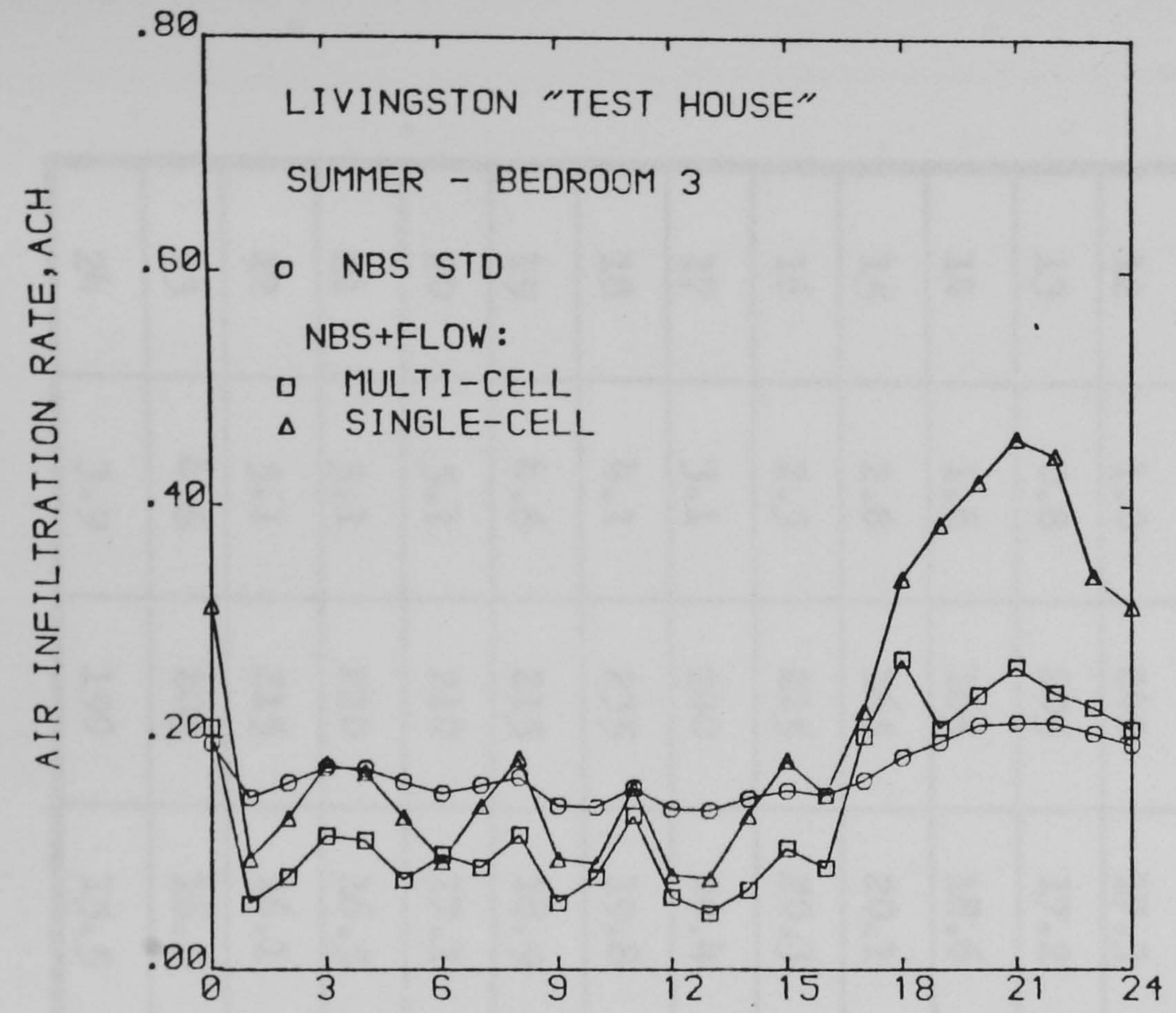

Fig. 4.32 Air infiltration rates computed by the NBSLD and NBSFLOW programs on a typical summer day - Bedroom 3

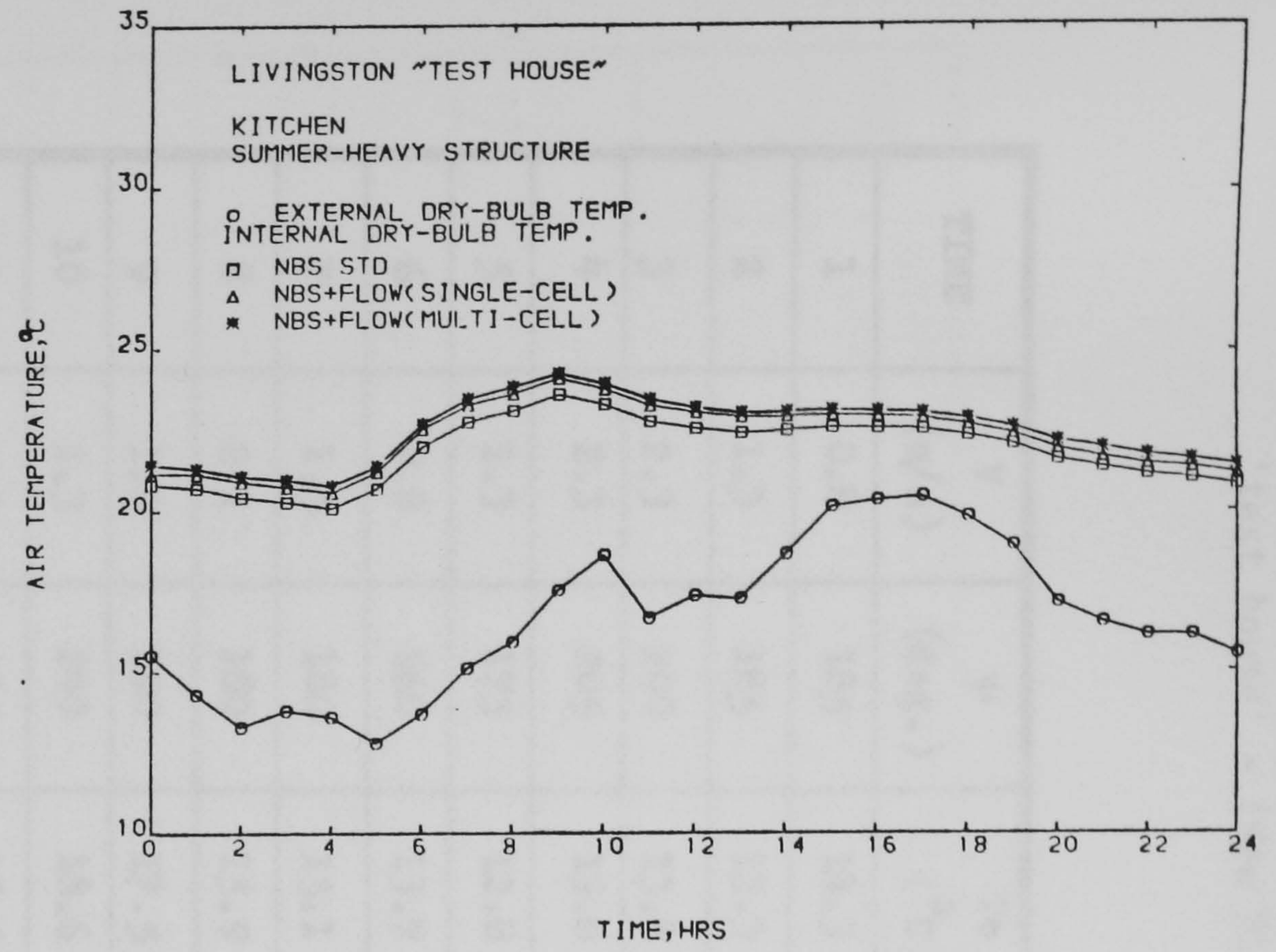

Fig. 4.33 Internal air temperature profile computed by the NBSLD and NBSFLOW programs for a heavyweight structure on a typical summer day - Kitchen

Table 4.12 Air infiltration rates computed by the single-cell version of the FLOW program for the Livingston 'test house' - (Kew 21st June)

TIME	V (m/s)	ψ (deg.)	Te (°C)	Ta (°C)	Q (ACH)
1	0.8	185	14.3	21.36	0.085
2	1.3	185	13.3	21.08	0.119
3	2.3	200	13.8	20.89	0.167
4	2.3	205	13.6	20.67	0.160
5	1.3	175	12.8	20.90	0.121
6	0.8	160	13.7	21.53	0.084
7	1.5	180	15.1	21.93	0.130
8	2.1	180	15.9	22.16	0.173
9	1.0	190	17.5	22.46	0.083
10	1.3	240	18.6	22.37	0.079
11	1.8	265	16.6	22.12	0.146
12	1.0	240	17.3	22.04	0.072
13	0.8	205	17.2	22.02	0.067
14	1.8	165	18.6	22.25	0.120
15	2.6	165	20.1	22.63	0.169
16	2.3	215	20.3	22.82	0.153
17	3.1	240	20.4	22.98	0.226
18	4.1	235	19.8	23.05	0.339
19	4.6	215	18.9	22.93	0.384
20	5.1	210	17.1	22.38	0.422
21	5.1	220	16.5	22.16	0.458
22	5.1	215	16.1	21.87	0.443
23	4.6	205	16.1	21.73	0.342
24	3.9	190	15.5	21.51	0.302

Table 4.13 Air infiltration rates computed by the multi-cell version of the FLOW program for the Livingston 'test house' - (Kew 21st June)

TIME	Q(LIV) (ACH)	Q(KIT) (ACH)	Q(BED 1) (ACH)	Q(BED 2) (ACH)	Q(BED 3) (ACH)	Q(AV.) (ACH)
1	0.053	0.072	0.109	0.099	0.051	0.070
2	0.090	0.076	0.172	0.153	0.074	0.104
3	0.151	0.067	0.288	0.261	0.109	0.160
4	0.142	0.063	0.269	0.259	0.105	0.153
5	0.091	0.082	0.175	0.151	0.071	0.105
6	0.058	0.080	0.108	0.091	0.048	0.071
7	0.107	0.070	0.196	0.173	0.082	0.116
8	0.158	0.067	0.298	0.241	0.109	0.160
9	0.061	0.055	0.118	0.107	0.051	0.072
10	0.056	0.038	0.099	0.099	0.074	0.068
11	0.059	0.067	0.219	0.134	0.127	0.103
12	0.049	0.048	0.079	0.080	0.058	0.059
13	0.049	0.053	0.086	0.084	0.039	0.058
14	0.113	0.057	0.228	0.166	0.066	0.155
15	0.177	0.066	0.381	0.275	0.100	0.180
16	0.121	0.059	0.265	0.277	0.084	0.143
17	0.140	0.072	0.358	0.243	0.196	0.180
18	0.216	0.083	0.553	0.382	0.264	0.266
19	0.293	0.166	0.682	0.544	0.207	0.337
20	0.349	0.216	0.759	0.640	0.232	0.394
21	0.334	0.158	0.794	0.612	0.257	0.383
22	0.339	0.190	0.783	0.630	0.239	0.388
23	0.331	0.183	0.690	0.570	0.223	0.361
24	0.315	0.122	0.650	0.497	0.203	0.324

Table 4.14 Air infiltration rates computed by the NBSLD program for the Livingston 'test house' - (Kew 21st June)

TIME	Q(LIV) (ACH)	Q(KIT) (ACH)	Q(BED 1) (ACH)	Q(BED 2) (ACH)	Q(BED 3) (ACH)	Q(AV.) (ACH)
1	0.184	0.405	0.221	0.184	0.147	0.213
2	0.199	0.438	0.239	0.199	0.160	0.242
3	0.216	0.475	0.259	0.216	0.173	0.263
4	0.215	0.473	0.258	0.215	0.172	0.262
5	0.201	0.459	0.241	0.201	0.161	0.248
6	0.188	0.415	0.226	0.188	0.151	0.229
7	0.197	0.434	0.236	0.197	0.158	0.240
8	0.206	0.453	0.247	0.206	0.165	0.251
9	0.175	0.385	0.210	0.175	0.140	0.213
10	0.173	0.382	0.208	0.173	0.139	0.211
11	0.195	0.429	0.234	0.195	0.156	0.237
12	0.171	0.377	0.205	0.171	0.137	0.208
13	0.170	0.374	0.204	0.170	0.207	0.207
14	0.183	0.404	0.220	0.183	0.147	0.223
15	0.193	0.424	0.231	0.193	0.154	0.234
16	0.187	0.412	0.224	0.187	0.150	0.228
17	0.203	0.448	0.244	0.203	0.163	0.247
18	0.229	0.503	0.274	0.229	0.183	0.278
19	0.244	0.538	0.293	0.244	0.196	0.297
20	0.263	0.579	0.316	0.263	0.211	0.320
21	0.265	0.584	0.318	0.265	0.213	0.323
22	0.266	0.586	0.319	0.266	0.213	0.324
23	0.255	0.560	0.306	0.255	0.204	0.311
24	0.242	0.533	0.291	0.242	0.194	0.295

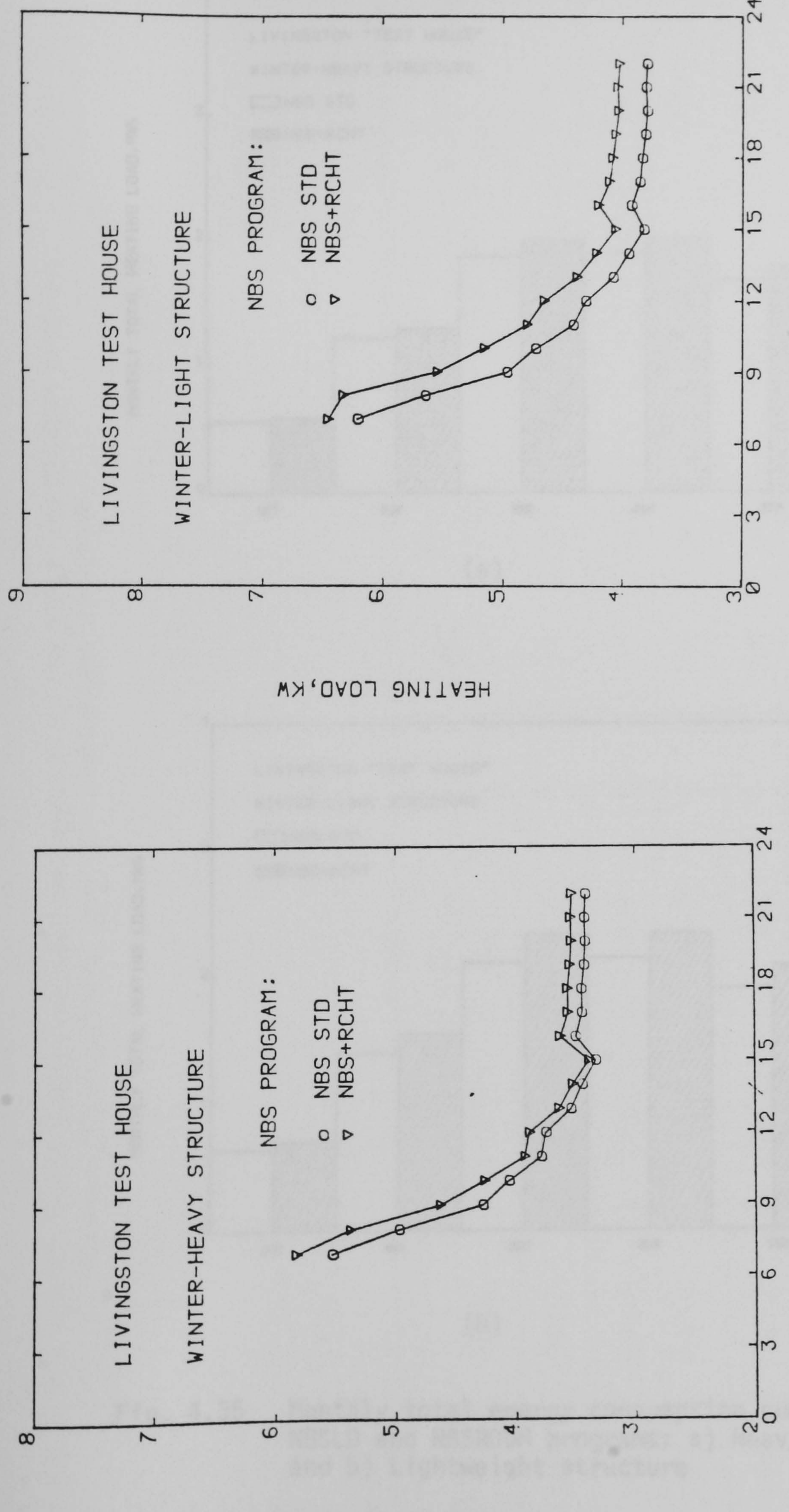

Fig. 4.34 Daily heating load computed by the NBSLD and NBSROOM programs: a) Heavyweight structure and b) Lightweight structure

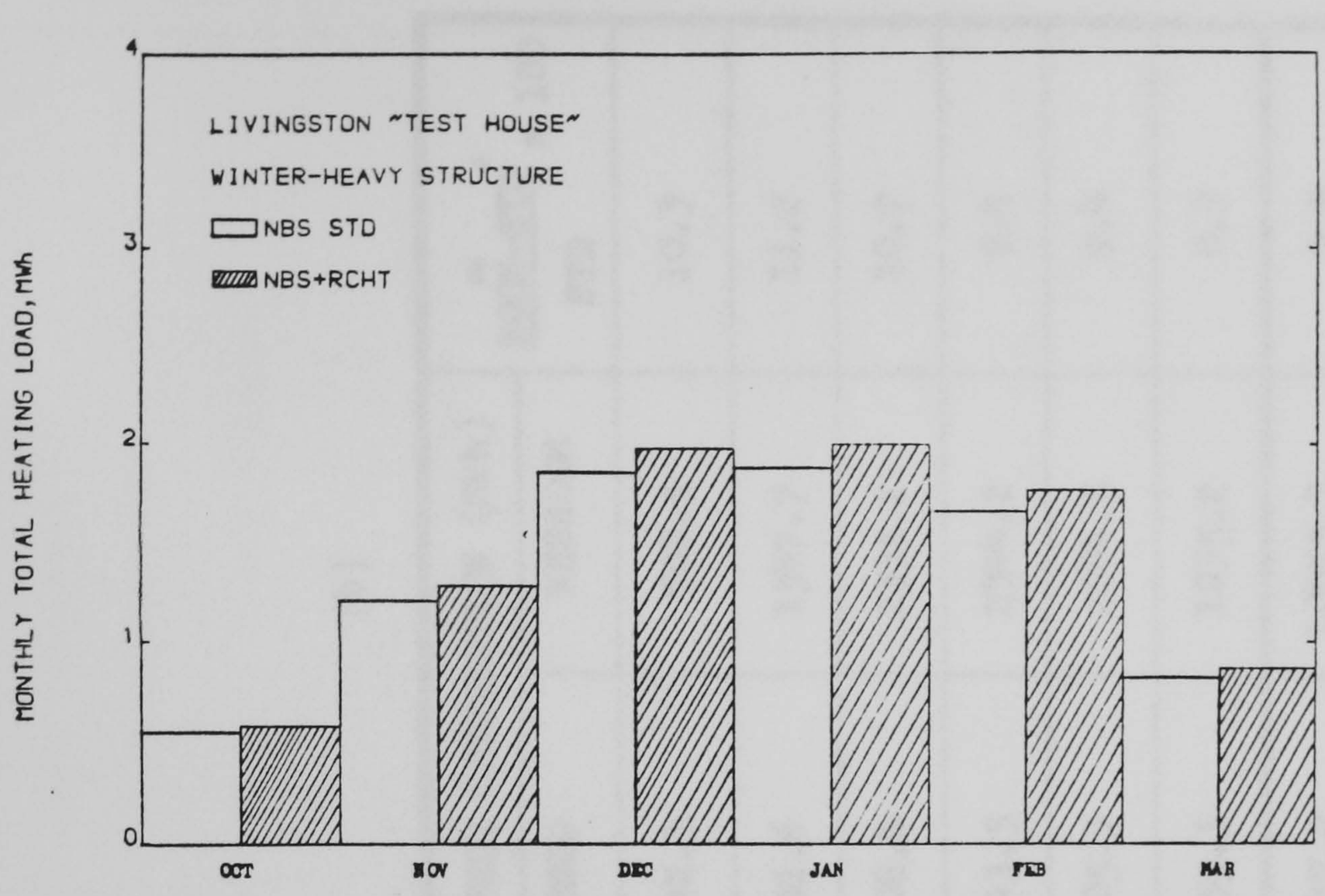

(a)

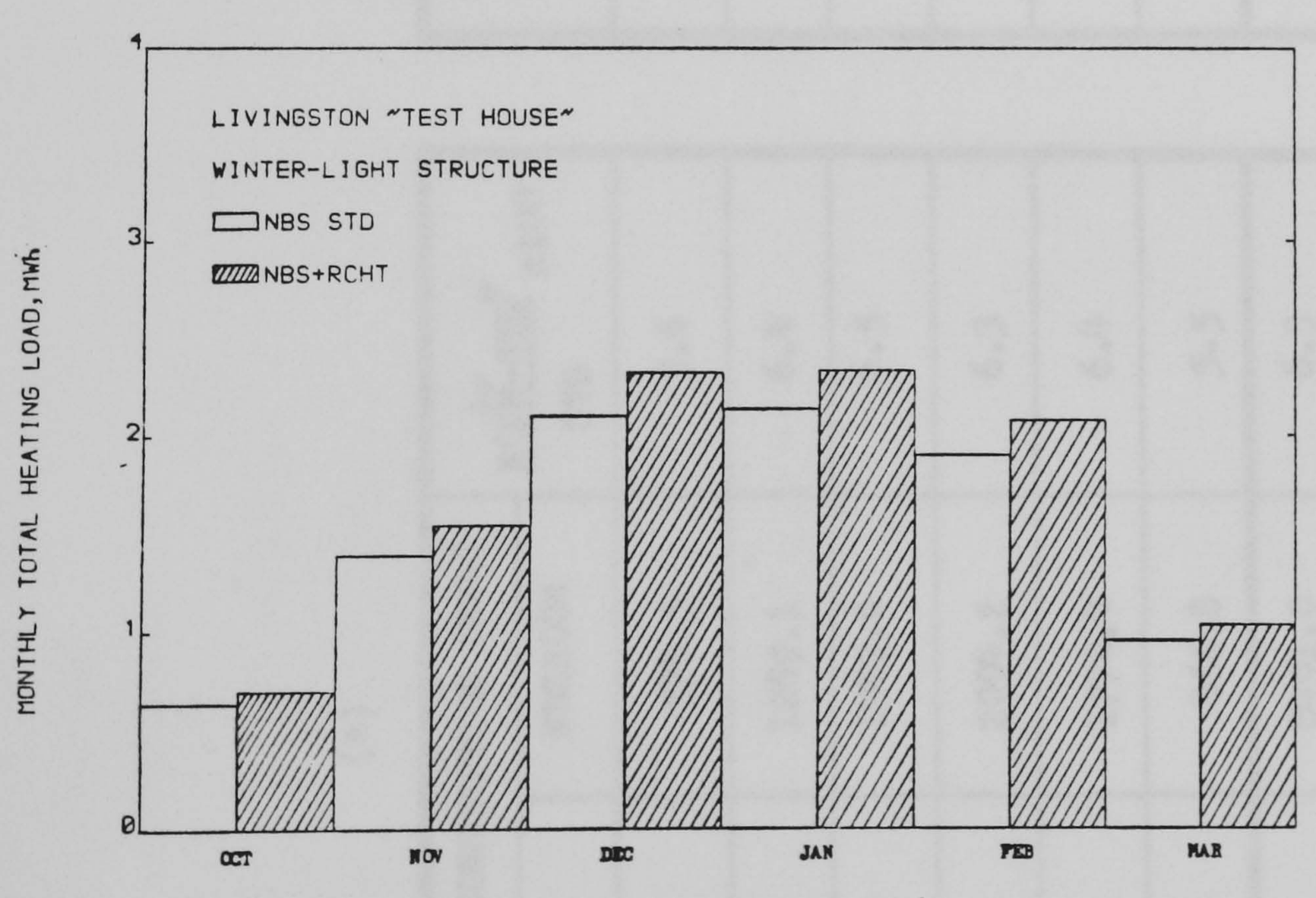

(b)

Fig. 4.35 Monthly total energy consumption cumputed by the NBSLD and NBSROOM programs: a) Heavyweight structure, and b) Lightweight structure

Table 4.15 Monthly total energy consumption computed by the NBSLD and NBSROOM programs: a) Heavyweight structure, and b) Lightweight structure

(a)

MONTH	ENERGY CONSUMPTION (MWh)		$\frac{(**)-(*)}{(*)} \times 100$
	NBSLD	NBSROOM	
OCT	547.8	578.5	5.6
NOV	1211.6	1289.1	6.4
DEC	1860.9	1982.0	6.5
JAN	1884.7	2004.2	6.3
FEB	1663.7	1770.4	6.4
MAR	821.6	866.8	5.5
TOTAL	7990.2	8491.0	6.3

(*) NBSLD standard

(**) NBSLD + ROOM-CHT

(b)

MONTH	ENERGY CONSUMPTION (MWh)		$\frac{(**)-(*)}{(*)} \times 100$
	NBSLD	NBSROOM	
OCT	642.3	708.5	10.3
NOV	1391.6	1547.7	11.2
DEC	2108.8	2335.2	10.7
JAN	2143.5	2344.2	9.4
FEB	1905.3	2084.5	9.4
MAR	955.5	1035.2	8.3
TOTAL	9147.0	10055.3	9.9

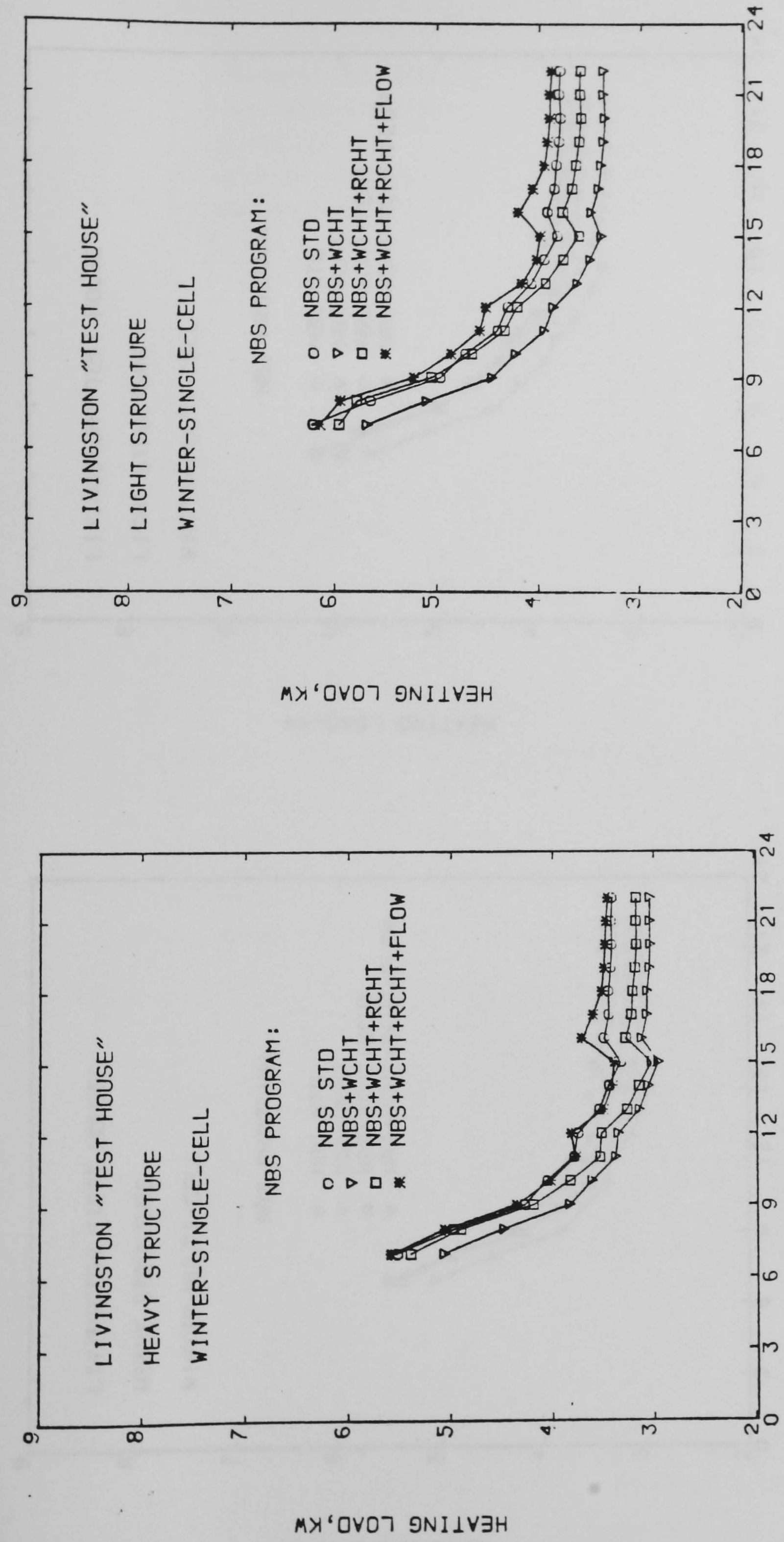

Fig. 4.36 Influence of all three sub-system models on the NBSLD heating load computations for a single-cell system: a) Heavyweight structure, and b) Lightweight structure

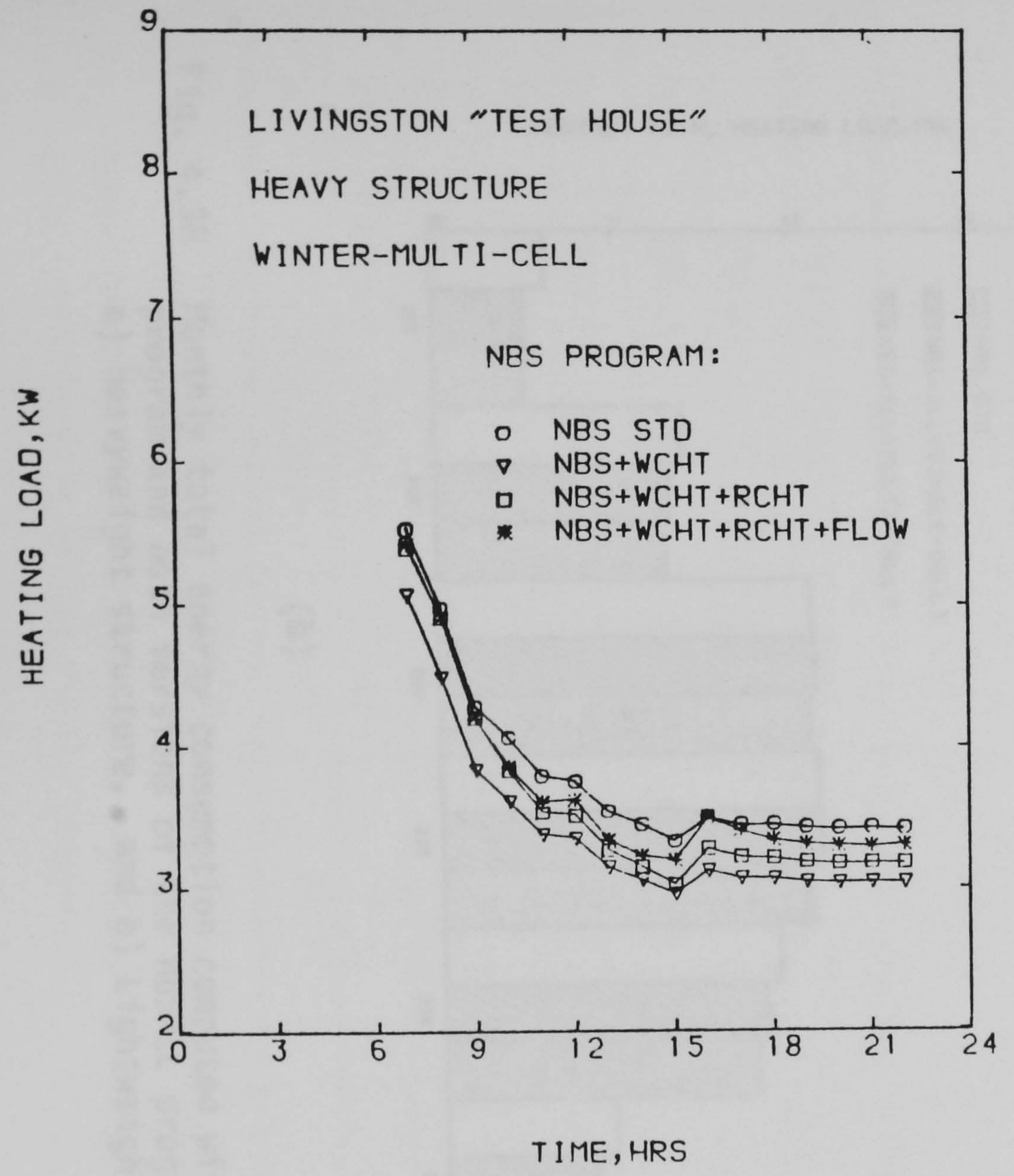

Fig. 4.37 Influence of all three sub-system models on the NBSLD heating load computations for a multi-cell system: a) Heavyweight structure, and b) Lightweight structure.

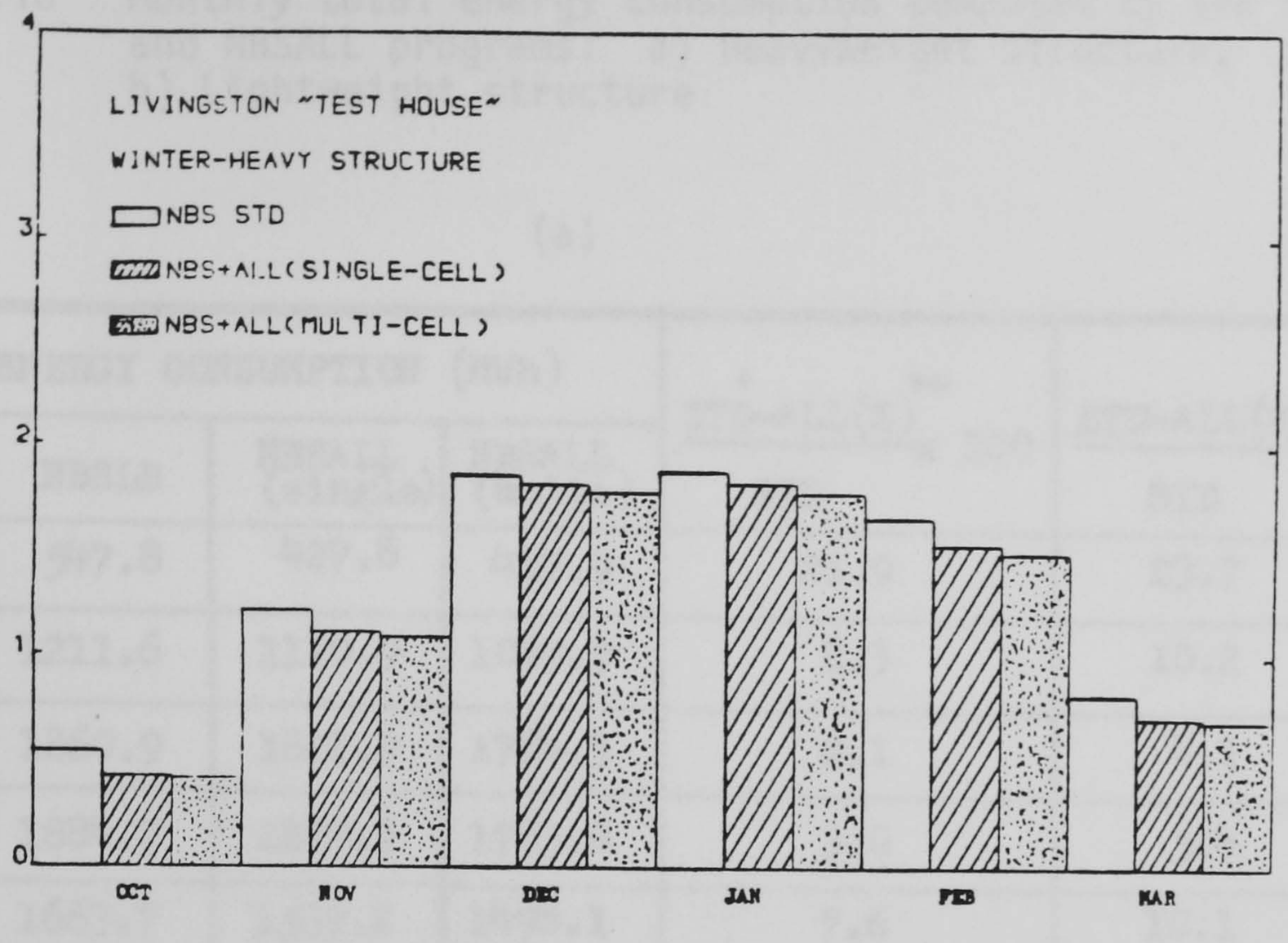

(a)

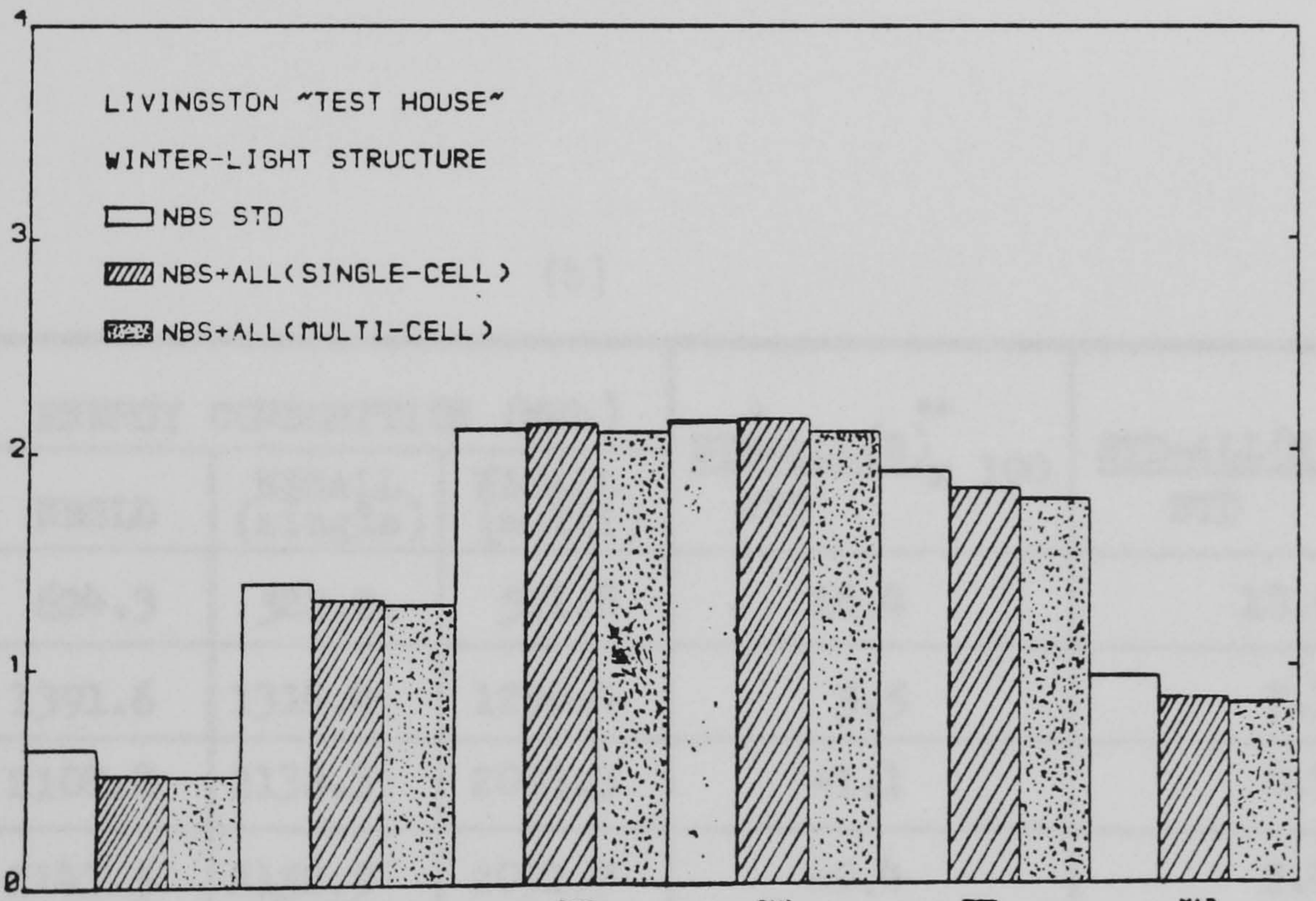

(b)

Fig. 4.38 Monthly total energy consumption computed with the NBSLD program and both versions of the NBSALL program: a) Heavyweight structure, and b) Lightweight structure

Table 4.16 Monthly total energy consumption computed by the NBSLD and NBSALL programs: a) Heavyweight structure, and b) Lightweight structure

(a)

MONTH	ENERGY CONSUMPTION (MWh)			$\frac{\text{STD-ALL(S)}^{+}}{\text{STD}}{}^{**} \times 100$	$\frac{\text{STD-ALL(M)}^{*}}{\text{STD}} \times 100$
	NBSLD	NBSALL (single)	NBSALL (multi)		
OCT	547.8	427.8	417.9	21.9	23.7
NOV	1211.6	1110.9	1087.9	8.3	10.2
DEC	1860.9	1821.9	1784.3	2.1	4.1
JAN	1884.7	1828.9	1783.0	3.0	5.4
FEB	1663.7	1537.2	1496.1	7.6	10.1
MAR	821.6	714.6	700.4	13.0	14.8
TOTAL	7990.2	7441.3	7269.6	6.9	9.0

(b)

MONTH	ENERGY CONSUMPTION (MWh)			$\frac{\text{STD-ALL(S)}^{+}}{\text{STD}}{}^{**} \times 100$	$\frac{\text{STD-ALL(M)}^{*}}{\text{STD}} \times 100$
	NBSLD	NBSALL (single)	NBSALL (multi)		
OCT	624.3	522.2	511.8	16.4	18.0
NOV	1391.6	1314.4	1290.4	5.5	7.3
DEC	2108.8	2132.3	2093.3	-1.1	0.7
JAN	2143.5	2152.9	2091.7	-0.4	2.4
FEB	1905.3	1826.5	1774.5	4.1	6.9
MAR	955.5	857.0	837.7	10.3	12.3
TOTAL	9147.0	8805.5	8599.4	3.7	6.0

(+) NBSLD program (**) single-cell version of the NBSALL program
(*) multi-cell version of the NBSALL program

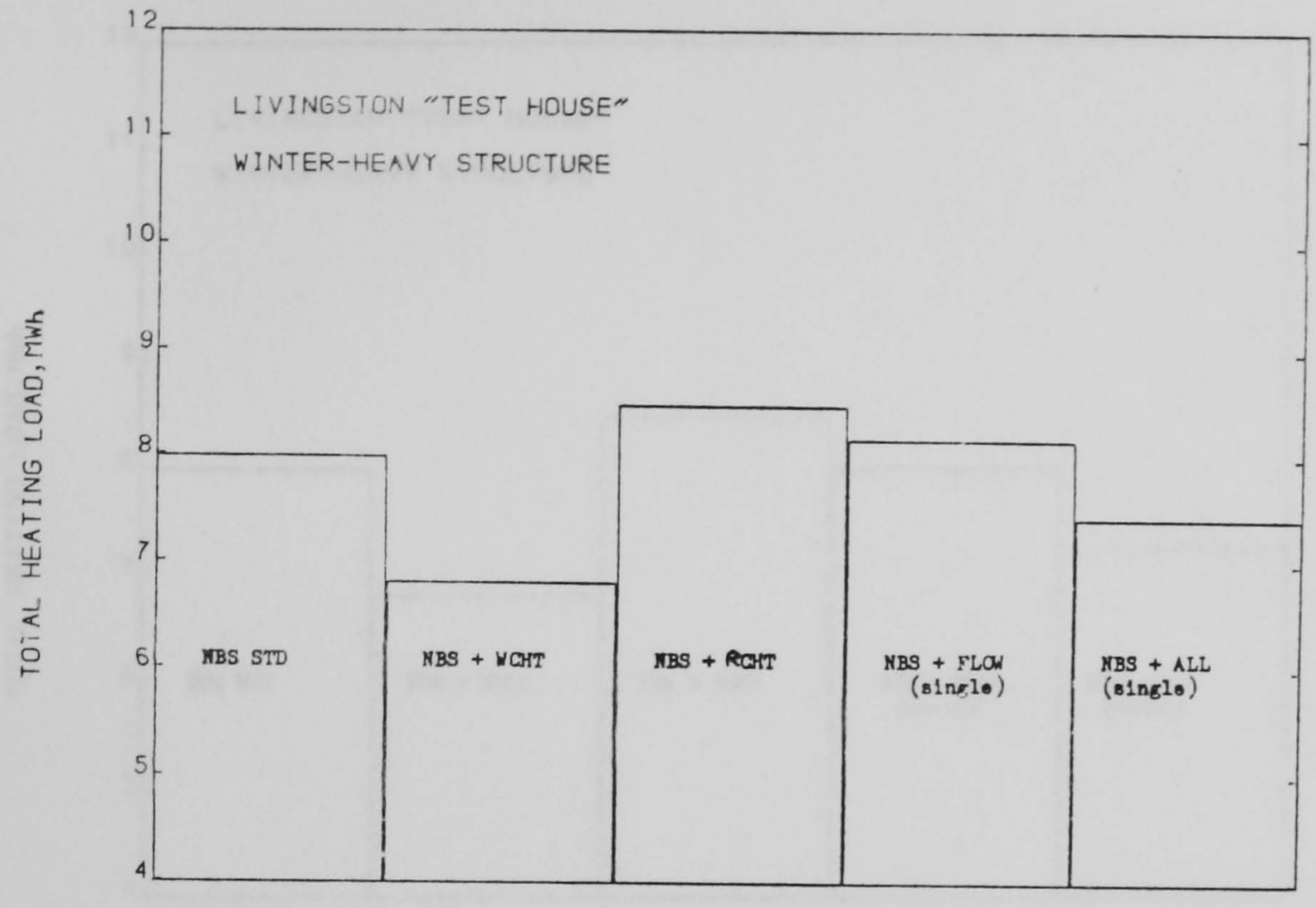

(a)

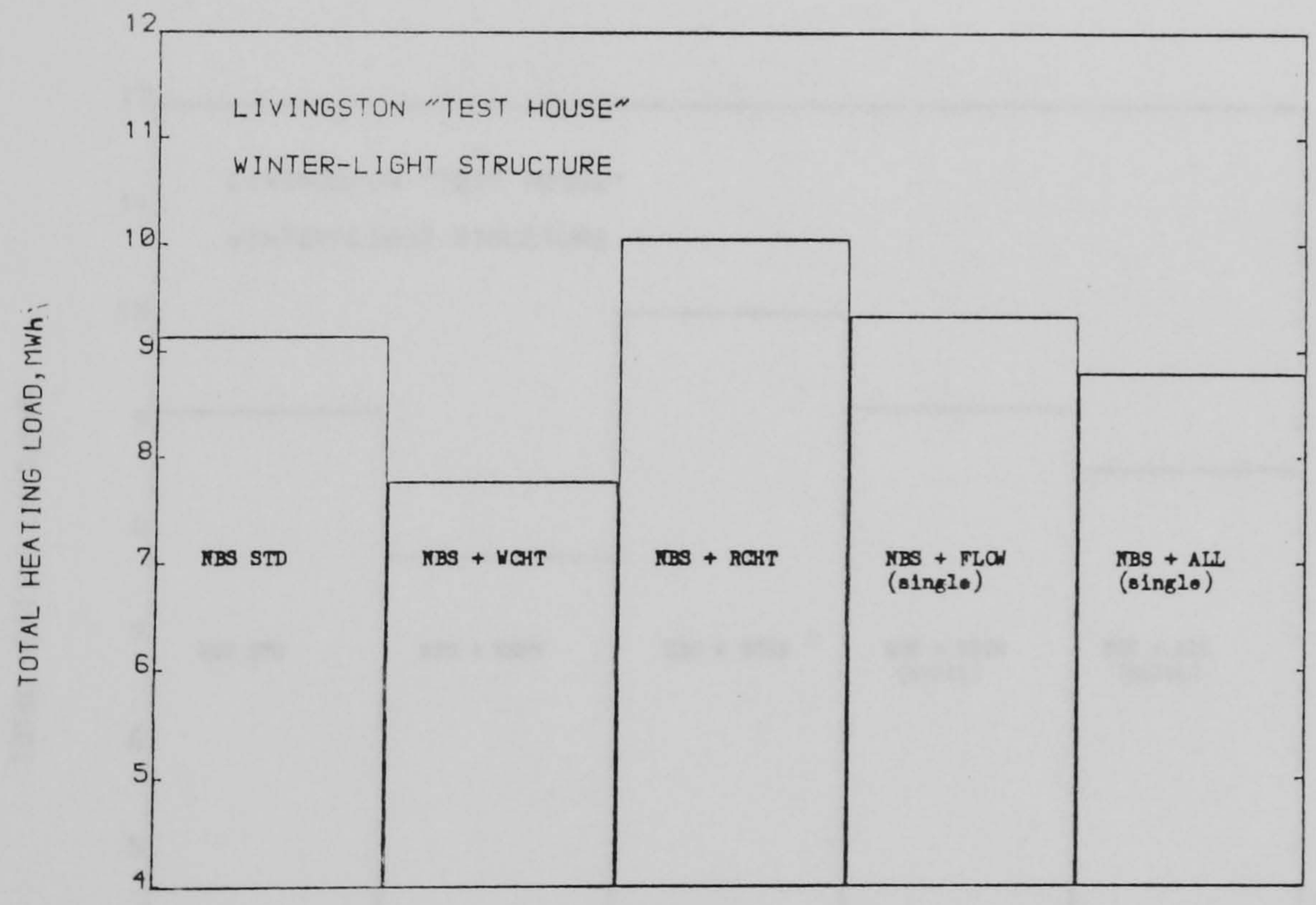

(b)

Fig. 4.39 Total energy consumption during the 'whole' heating season computed by the various versions of the NBSLD program: a) Heavyweight structure, and b) Lightweight structure

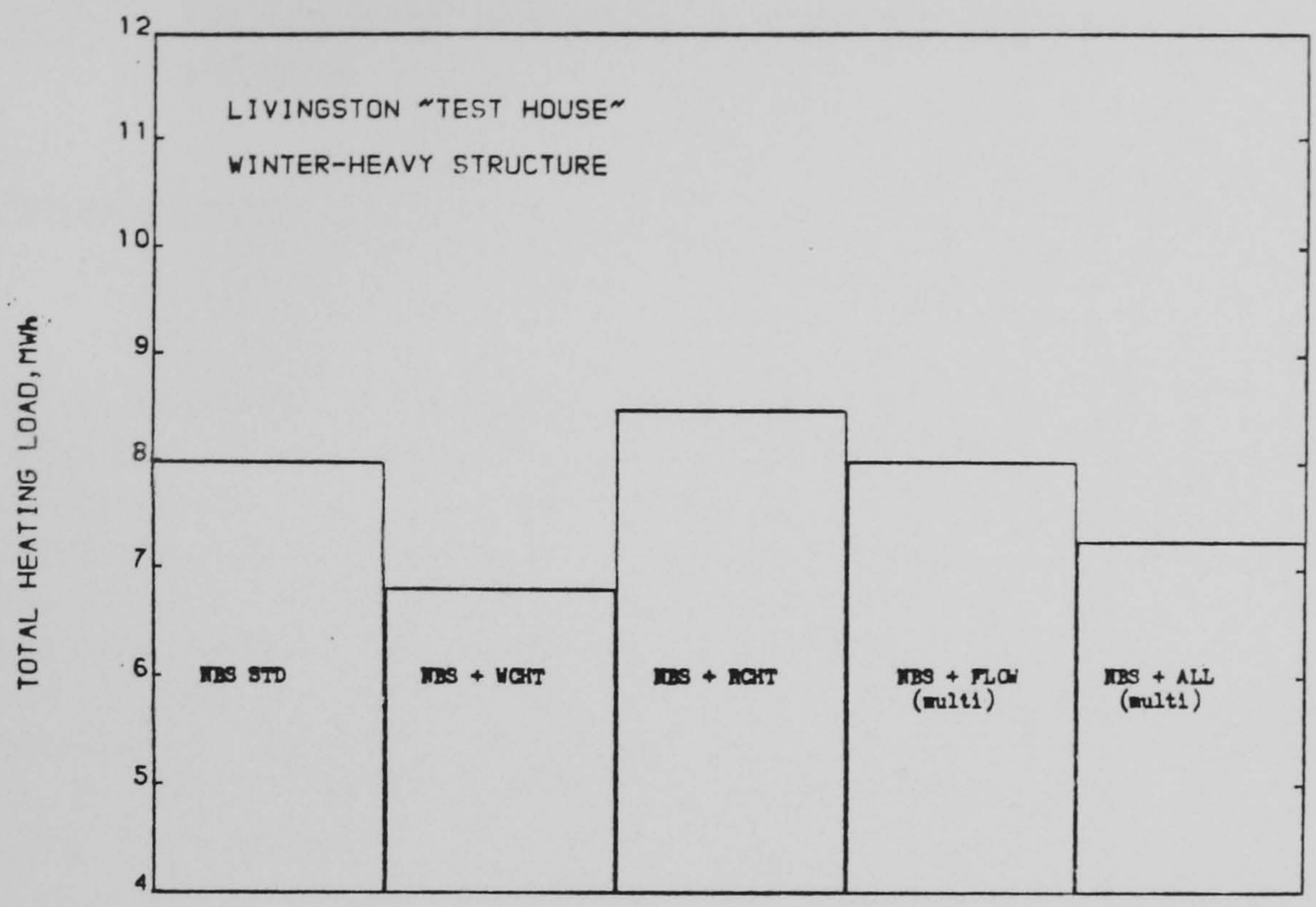

(a)

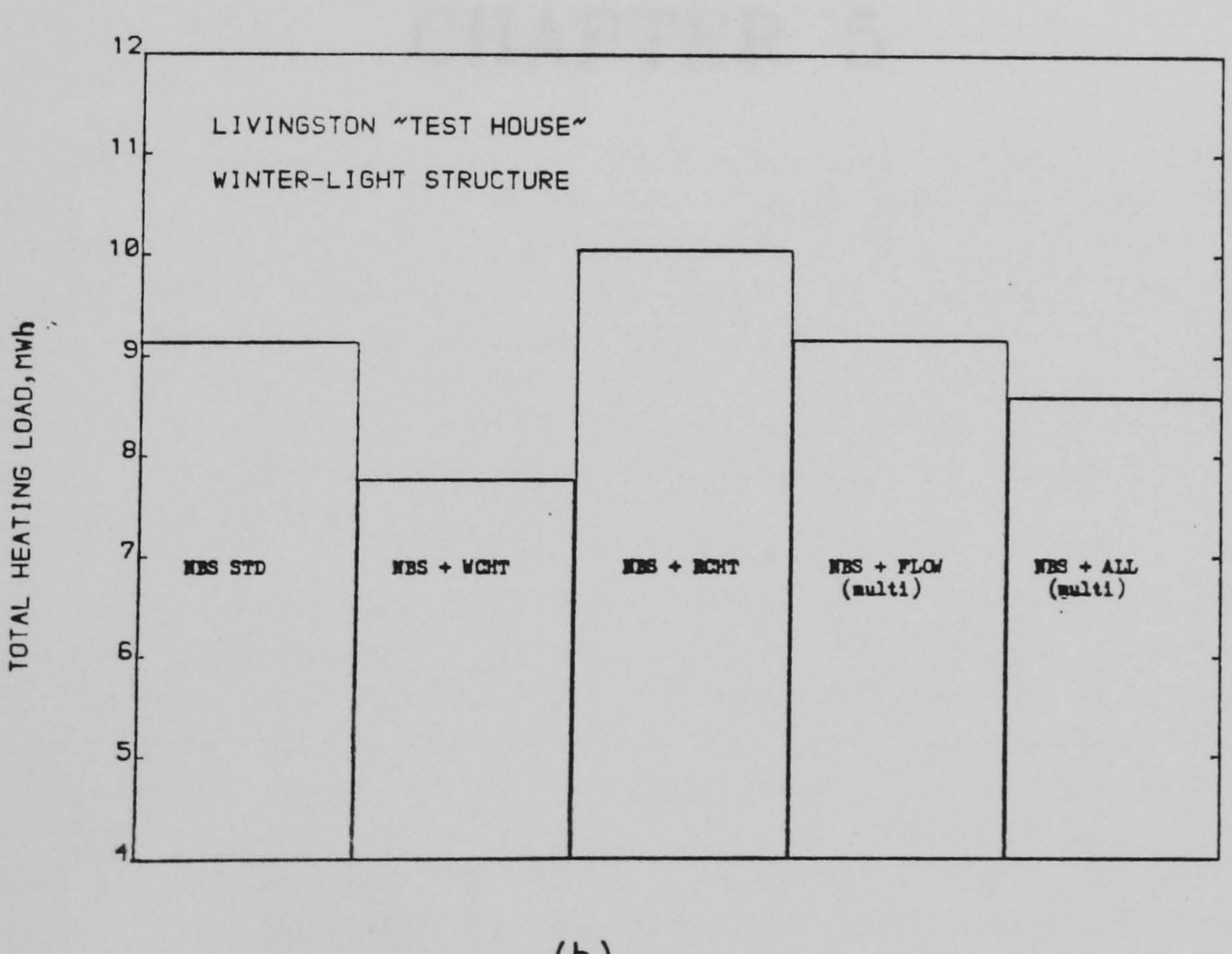

(b)

Fig. 4.40 Total energy consumption during the 'whole' heating season computed by various versions of the NBSLD program: a) Heavyweight structure, and b) Lightweight structure.

CHAPTER 5

CHAPTER 5 - SENSITIVITY ANALYSIS ON THE BRE 'ADMITTANCE PROCEDURE' PROGRAM

5.1 - INTRODUCTION

In the context of the present work it was desirable to quantify the influence of the convection and infiltration sub-system models on the results given by the Building Research Establishment's (BRE) 'admittance procedure' program. The admittance procedure itself forms the basis of the CIBSE guide recommendations (Ref.85) for calculating the transient thermal performance of building structures. It has been developed at BRE by Danter (Ref.86,87), Loudon(Ref.88), Milbank and Harrington-Lynn (Ref.89), Harrington-Lynn (Ref.90,91) and others over a number of years and is arguably the most widely used method by UK consulting engineers.

The fundamental assumption made in this program is that the time variations of temperature and energy are steady-cyclic, i.e., repeatable over a number of days. In this way, the energy balance may be considered in two stages corresponding to the 24 hours mean condition (steady-state term) and the cyclic variations about the mean. By considering the actual excitation in the form of a Fourier-sine series, the transient heat conduction differential equation can be then solved.

The sensitivity tests were performed by using a floppy disk containing a suite of programs, developed by BRE for a PET microcomputer, together with documentation describing their use and theoretical basis (Ref.21). The suite of programs consists of two main codes, which are denoted as THERMALFACTORS and HEATCOOL. The THERMALFACTORS code allows the calculation of the thermal characteristics of a wall, floor or ceiling while the HEATCOOL code calculates the hourly values of internal air temperature with or without heating or cooling plant.

The next sections are concerned with the individual and simultaneous influences, of all three sub-system models on the computed heating load or internal air temperature for the hypothetical Livingston test house(described in the previous chapter) for typical winter and summer conditions. A comparison with the standard results of the BRE program will always be made, and therefore it was felt necessary to describe, in this section, the convection and infiltration data employed by the standard input data set. A value of 0.12 $m^2 °K\ W^{-1}$ was adopted for the internal resistance of all surfaces, while a value of 0.06(0.04) $m^2 °K\ W^{-1}$ was adopted for the outside wall(roof) surface resistances. These values were taken from tables A.35 and A.36 of CIBSE guide respectively (Ref.23). Both cases presume a surface emissivity factor of 0.9, and the external surface resistance also presumes normal wind exposure. Due to the absence of any recommendation related to the choice of an appropriate value for the air infiltration rates, a volume-weighted average between the 'selected' infiltration rates for the Livingston 'test house', from

Table 4.2, was adopted. This average air infiltration rate took the value of 0.87 ACH, and was assumed to be constant throughout the day.

Finally, it should be pointed out that the BRE program was always treated as a 'black box', with all the simulations performed by altering the input data set only.

5.2 - THE EFFECT OF THE EXTERNAL CONVECTIVE HEAT TRANSFER COEFFICIENTS

The WIND-CHT program was run for the Livingston 'test house' together with the meteorological data base(presented in chapter 4), in order to determine the appropriate heat transfer coefficients. For a typical winter day, 24-hour averaged surface resistance values of 0.11 and 0.08 $m^2 °K W^{-1}$ were obtained for the external walls and roof respectively, while for summer conditions these same parameters were estimated to be 0.22 and 0.18 $m^2 °K W^{-1}$. These values were then incorporated into the BRE input data set, and the simulations were performed. Figure 5.1 and 5.2 show respectively the heating load and internal air temperature profiles, computed by the BRE program, when employing the standard and revised external heat transfer coefficients. The winter daily energy consumption and the summer mean internal air temperature computed using the standard version for a heavyweight(lightweight) structure were approximately 122(144) KWh and 18(17) °C. These changes to 118(138) KWh and 23(22) °C respectively when the convection coefficients from the WIND-CHT program were employed. The convection coefficients given in the CIBSE guide (Ref.23) and employed by the standard BRE input data set, are calculated in accordance with Jurges' relationship (eq.2.30). This equation does not take account of the most important variables affecting the convective heat exchange at the exterior surfaces of a building and usually overestimates the convection coefficients (see Figure 2.12). The daily averaged wind velocity used by the WIND-CHT program for calculating the summer heat transfer coefficients is 2.6 m s^{-1}. This value is close to the value of 3 m s^{-1} adopted by the CIBSE guide for normal wind exposures. However, the computed heat transfer coefficients for the external walls(roof) are some 260(330) percent lower than the corresponding guide values. On the typical winter day, the daily averaged wind velocity increases to 6.8 m s^{-1} and this reduces the discrepancies between the computed and guide values to 83(100) percent. The CIBSE guide convection coefficients, as indicated by Bloomfield (Ref.21), are therefore inadequate. This is because the guide disregards any influence of wind direction, surface area and type of terrain. The revised values, given by the WIND-CHT program, appear to be more adequated for building thermal simulation applications (Ref.17).

5.3 - THE EFFECT OF THE AIR INFILTRATION RATES

The revised winter air infiltration rates are those presented in Table 4.8. The summer values were calculated using the single-cell version fo the FLOW program together with the internal air temperature profile given by the standard version of the BRE program (see section 4.6). The leakage distribution and meteorological conditions were those given in Tables 4.6 and 4.4, respectively. Table 5.1 shows the revised summer air infiltration rates for the Livingston 'test house'. The air infiltration rates so obtained were then averaged over two 12 hour periods, starting at 7.0 a.m. and 22.0 p.m. respectively , and values of 0.68 and 0.56 ACH and 0.20 and 0.15 ACH were respectively obtained for the typical winter and summer days. These values were incorporated into the BRE input data set, replacing the constant value of 0.87 ACH employed by the standard version. Figures 5.3 and 5.4 show the results of these alterations for typical winter and summer conditions respectively. The winter daily energy consumption and the summer mean internal air temperature given by the BRE program, when using the standard input data set, for a heavyweight(lightweight) structure were approximately 122(144) Kwh and 18(17) °C respectively. These values changed to 115(137) KWh and 19(18) °C when the results of the FLOW program were employed. The air infiltration rates adopted in the standard BRE program input data set for simulating the 7.0 a.m.-22.0 p.m.(22.0 p.m.-7.0 a.m.) period are 28(55) percent and 335(480) percent higher than the values computed by the FLOW program for winter and summer conditions respectively. This accounts for the differences in the computed heating load and internal air temperature profiles.

The BRE program manual (Ref.21) makes no recommendation as to the method for calculating or selecting the appropriate air infiltration rates. Due to this lack of information, the BRE program users are led to employ either the air change or the crack method, outlined in section 3.2.2. These methods give very crude estimates of the actual air infiltration rates. It was therefore decided to adopt a volume-weighted averaged value between the 'selected' air infiltration rates for the Livingston 'test house', presented by Clarke and Forrest (Ref.79) ,instead of employing the 'traditional' methods. It is argued that this procedure yields values that are closer to the actual values than those arising from the air change or crack methods. However, large discrepancies between the averaged values based on the 'selected' and computed air infiltration rates were found for the summer condition. This is probably due to the difference between the wind velocity pattern on the simulated day and on the day when the tracer gas studies were undertaken (Ref.79). However the air infiltration rates have only a minor effect on the internal air temperature profile on the typical summer day (see section 4.6).

5.4 - THE EFFECT OF THE INTERNAL CONVECTIVE HEAT TRANSFER COEFFICIENTS

In order to calculate the internal surface resistances needed to replace those assumed by the standard BRE input data set, it was felt necessary to use average values for the internal convection coefficients over walls, roof and floor obtained by running the NBSROOM (NBSLD+ROOM-CHT) program. This was because the ROOM-CHT program, by itself, can only determine the appropriate surface coefficients if the temperature of the walls and internal air are previously known. These are not usually available, and therefore the program needs to be used in conjunction with some building thermal model, which 'feeds' the ROOM-CHT program with the required temperatures. Consequently, reliable predictions of the internal convective heat transfer coefficients can be made. Such an inter connection was made when assessing the sensitivity of the NBSLD program (in section 4.7), for which the ROOM-CHT program was incorporated as an additional routine into the NBSLD code. However, this procedure was felt inappropriate for the BRE program, due to the size and complexity of the ROOM-CHT code in relation to this particular building thermal model. The internal convective heat transfer coefficients computed by the NBSROOM program, although not entirely appropriate for the BRE program (due to the differences in the internal air and surface temperature profiles given by these programs) were nevertheless adopted for convenience. This procedure was found to be satisfactory and was certainly much more reliable than using the ROOM-CHT program together with some assumed temperature distribution.

The internal heat transfer coefficients obtained using the NBSROOM program were averaged over 24 hour, and then the corresponding internal surface resistances were calculated. Table 5.2 gives the surface resistances for each internal surface on a typical winter day, while a constant value of 0.16 $m^2\,°K\,W^{-1}$ was obtained for both kinds of structure under summer condition. The standard values were then replaced by these revised values, and the resulting changes are illustrated in Figures 5.5 and 5.6 for typical winter and summer conditions respectively. The winter daily energy consumption for the heavyweight(lightweight) structure computed using the BRE program, with the standard input data set, was approximately 122(144) Kwh. This decreased by 1.2(0.9) percent when the revised internal convective heat transfer coefficients were employed. This small variation was expected because the values given in Table 5.2 are not very different from the standard value of 0.12 $m^2\,°K\,W^{-1}$. The floor internal surface resistance is 58 percent lower than the standard value, but this has little effect on the heating load profile. This is because the heat flux through the floor is very small when compared with those through external walls and roof, due to its heavyweight construction. For summer conditions no appreciable variations in the internal air temperature profile was detected due to the small difference between the standard and revised internal surface resistances. This arises, as stressed in section 4.7, from the absence of any mechanically-ventilated supply air.

5.5 - THE COMBINED EFFECT OF THE EXTERNAL AND INTERNAL CONVECTIVE HEAT TRANSFER COEFFICIENTS AND THE AIR INFILTRATION RATES

In this section, the simultaneous influence of all three sub-system models (WIND-CHT, FLOW and ROOM-CHT) on the results computed using the BRE program are assessed. The standard input data set, described in section 5.1, was therefore replaced by the revised values described in section 5.2,5.3 and 5.4. The results of these alterations are shown in Figures 5.7 and 5.8 for a typical winter and summer day respectively. The winter daily energy consumption and the mean internal air temperature computed by the BRE program, when using the standard input data set, for a heavyweight(lightweight) structure were approximately 122(144) KWh and 18(17) °C. These decreased to 109(130) KWh and increased to 26(24) °C respectively when the revised convection and infiltration data were employed.

5.6 - CONCLUSIONS

The common practice in building thermal models of adopting constant values for the convective heat transfer coefficients and air infiltration rates, is inadequate since these parameters are very much dependent on the meteorological conditions and, in the particular case of the internal coefficients, on the supply air condition. The BRE program does not permit 24 hour input data profiles to be specified, although this would be more realistic. It was therefore necessary to employ averaged values in order to assess the sensitivity of this program to the specification of external and internal convective heat transfer coefficients and air infiltration rates. This procedure yielded only small variations in the BRE program results when the individual effect of each of the sub-system models was assessed. However large variations were detected when assessing simultaneously the effect of all three sub-system models (see Figure 5.9). This is because the individual effects of replacing the standard external and internal surface resistances and air infiltration rates by 'improved' values, are to decrease the heating load on a typical winter day or, conversely to increase the internal air temperature on a typical summer day.

The BRE program is more sensitive to the combined action of all three sub-system models than is the NBSLD program. In the NBSLD program, the effect of the revised external convective heat transfer coefficients is nearly equal ,but opposite, to the effect resulting from the combined action of the revised internal convective heat transfer coefficients and air infiltration rates (see Figures 4.36 and 4.37). Consequently, the combined impact of all three sub-system models leads to an apparent ,although spurious, match between the computations of the standard and revised versions of the NBSLD program.

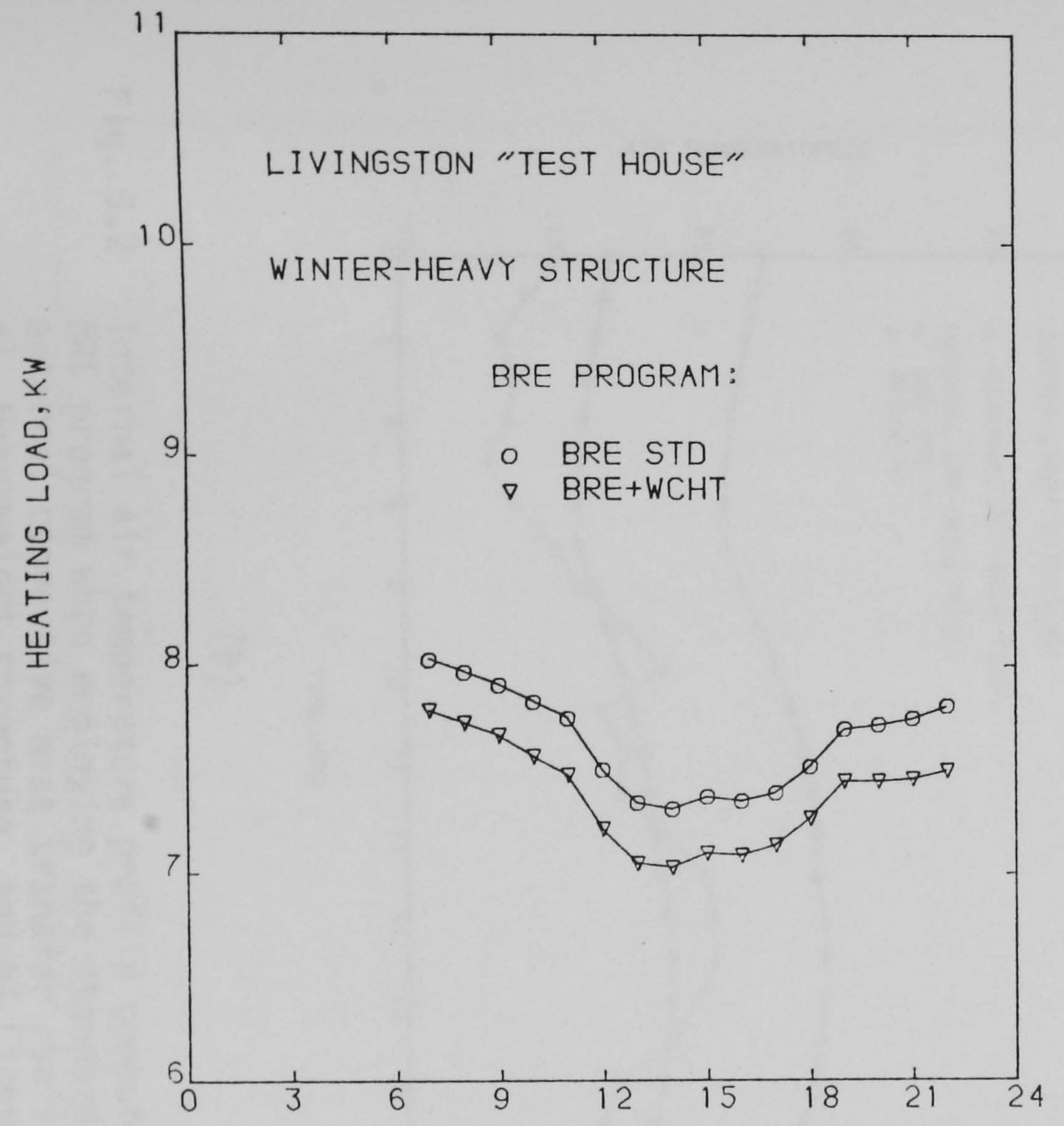

(a)

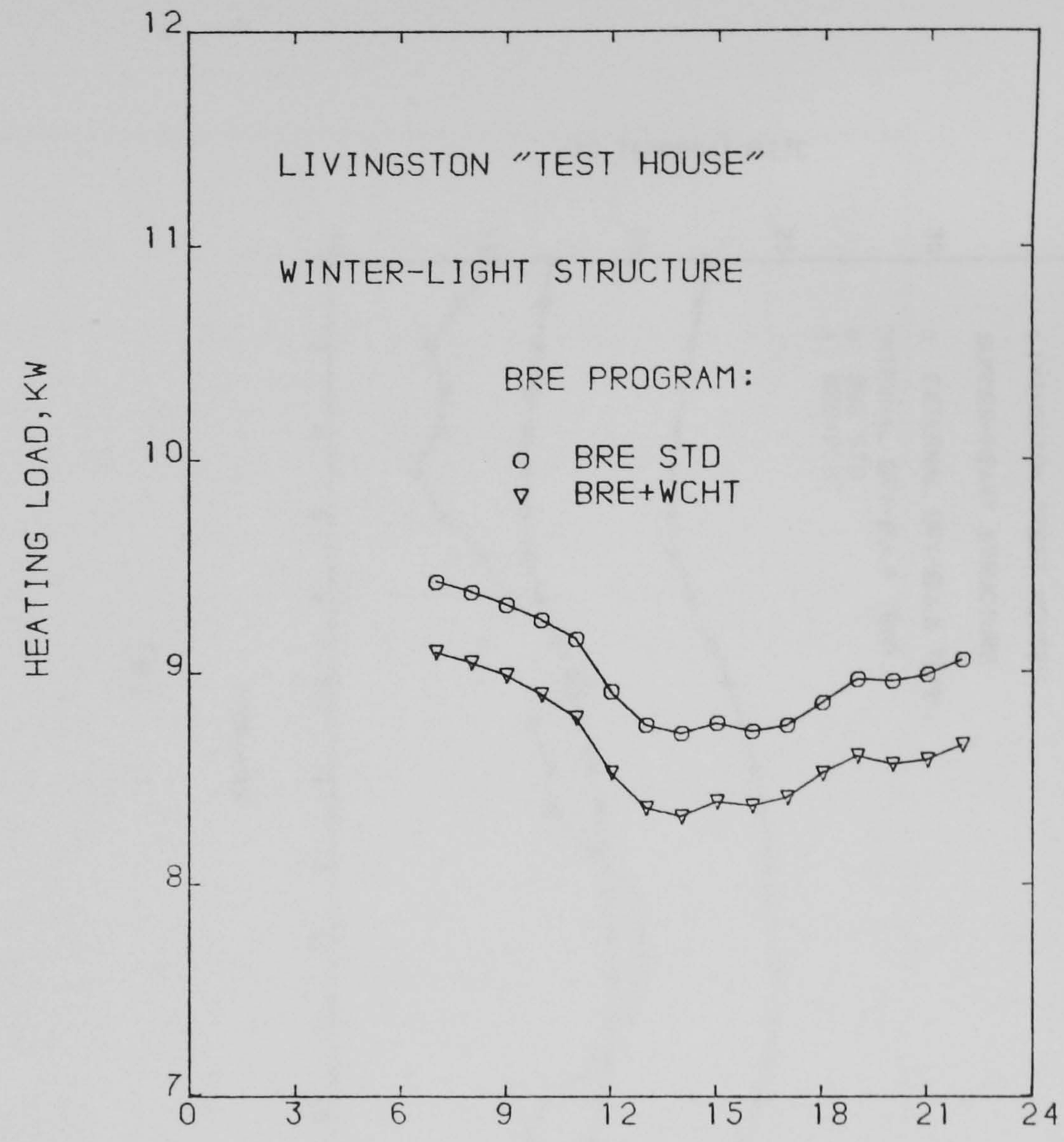

(b)

Fig. 5.1 Heating load profile computed by the BRE program when employing the standard and revised external convective heat transfer coefficients: a) Heavyweight structure, and b) Lightweight structure.

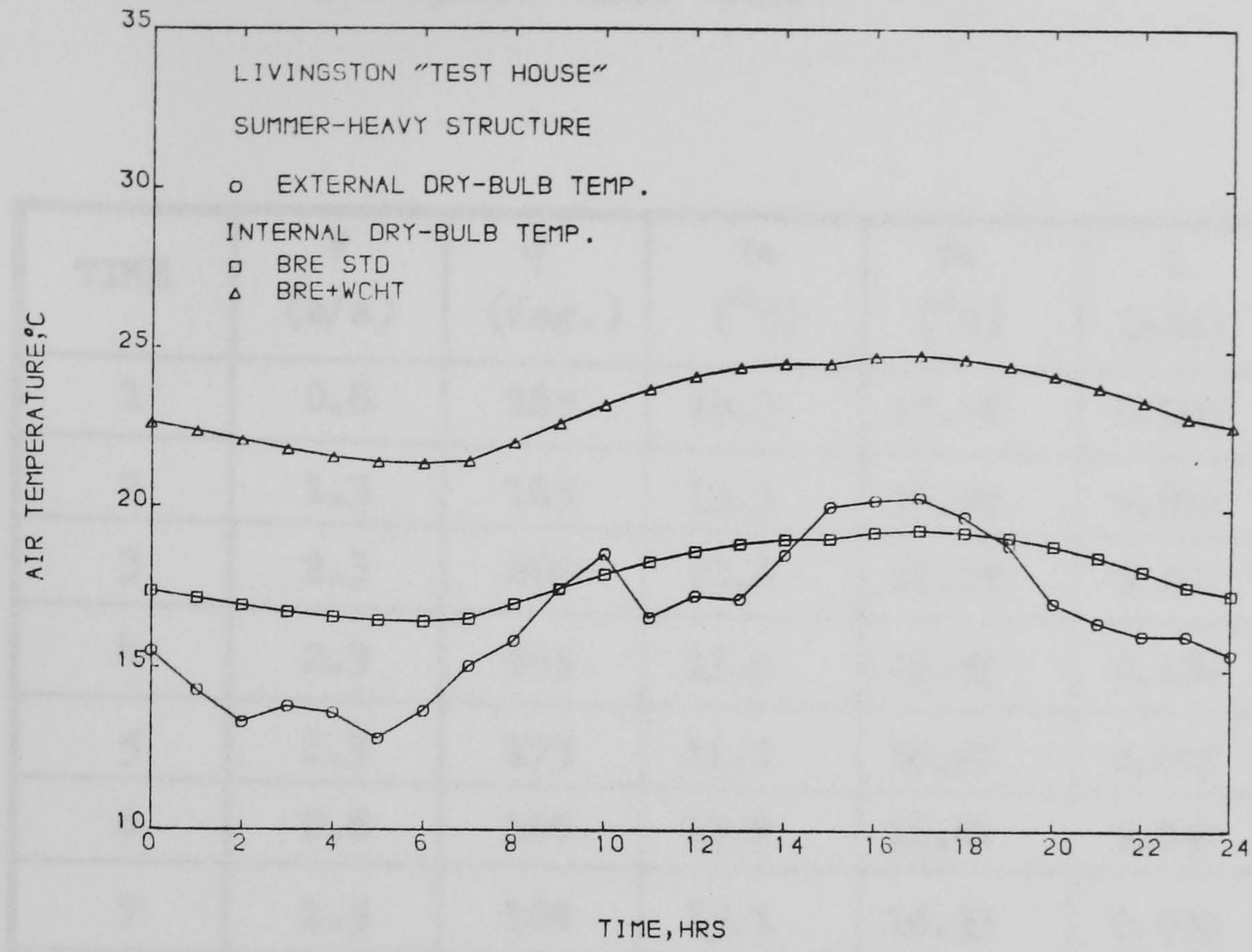

(a)

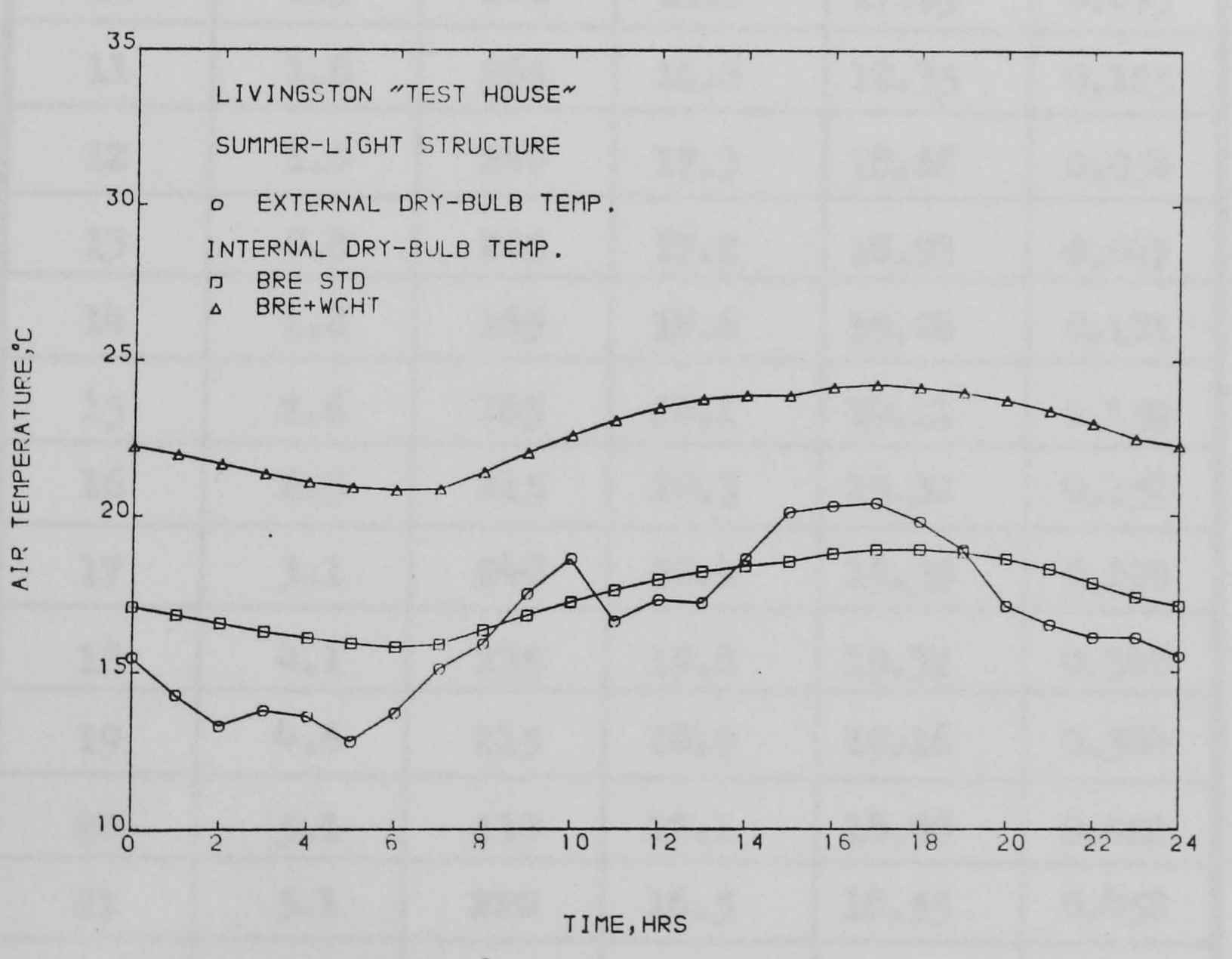

(b)

Fig. 5.2 Internal air temperature profile computed by the BRE program when employing the standard and revised external convective heat transfer coefficients: a) Heavyweight $tructure and b) Lightweight structure

Table 5.1 Revised summer air infiltration rates for the Livingston 'test house'

TIME	V (m/s)	ψ (deg.)	Te (°C)	Ta (°C)	Q (ACH)
1	0.8	185	14.3	17.14	0.062
2	1.3	185	13.3	16.92	0.097
3	2.3	200	13.8	16.72	0.141
4	2.3	205	13.6	16.57	0.134
5	1.3	175	12.8	16.47	0.097
6	0.8	160	13.7	16.44	0.057
7	1.5	180	15.1	16.53	0.099
8	2.1	180	15.9	17.00	0.140
9	1.0	190	17.5	17.49	0.047
10	1.3	240	18.6	17.95	0.073
11	1.8	265	16.6	18.35	0.125
12	1.0	240	17.3	18.68	0.054
13	0.8	205	17.2	18.93	0.047
14	1.8	165	18.6	19.08	0.101
15	2.6	165	20.1	19.11	0.159
16	2.3	215	20.3	19.32	0.152
17	3.1	240	20.4	19.39	0.228
18	4.1	235	19.8	19.32	0.340
19	4.6	215	18.9	19.16	0.384
20	5.1	210	17.1	18.90	0.422
21	5.1	220	16.5	18.55	0.458
22	5.1	215	16.1	18.12	0.443
23	4.6	205	16.1	17.63	0.343
24	3.9	190	15.5	17.37	0.291

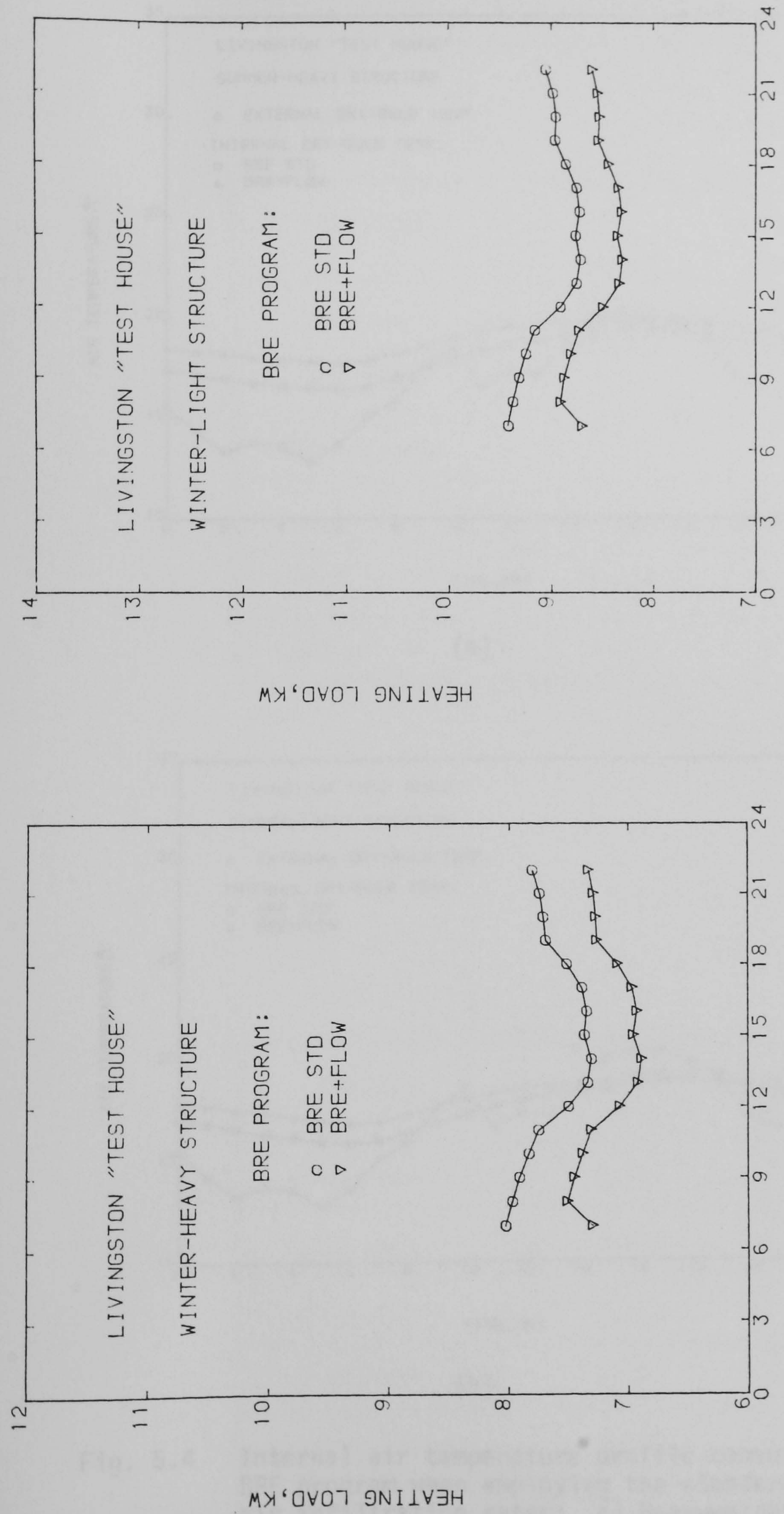

Fig. 5.3 Heating load profile computed by the BRE program when employing the standard and revised air infiltration rates: a) Heavyweight structure, and b) Lightweight structure.

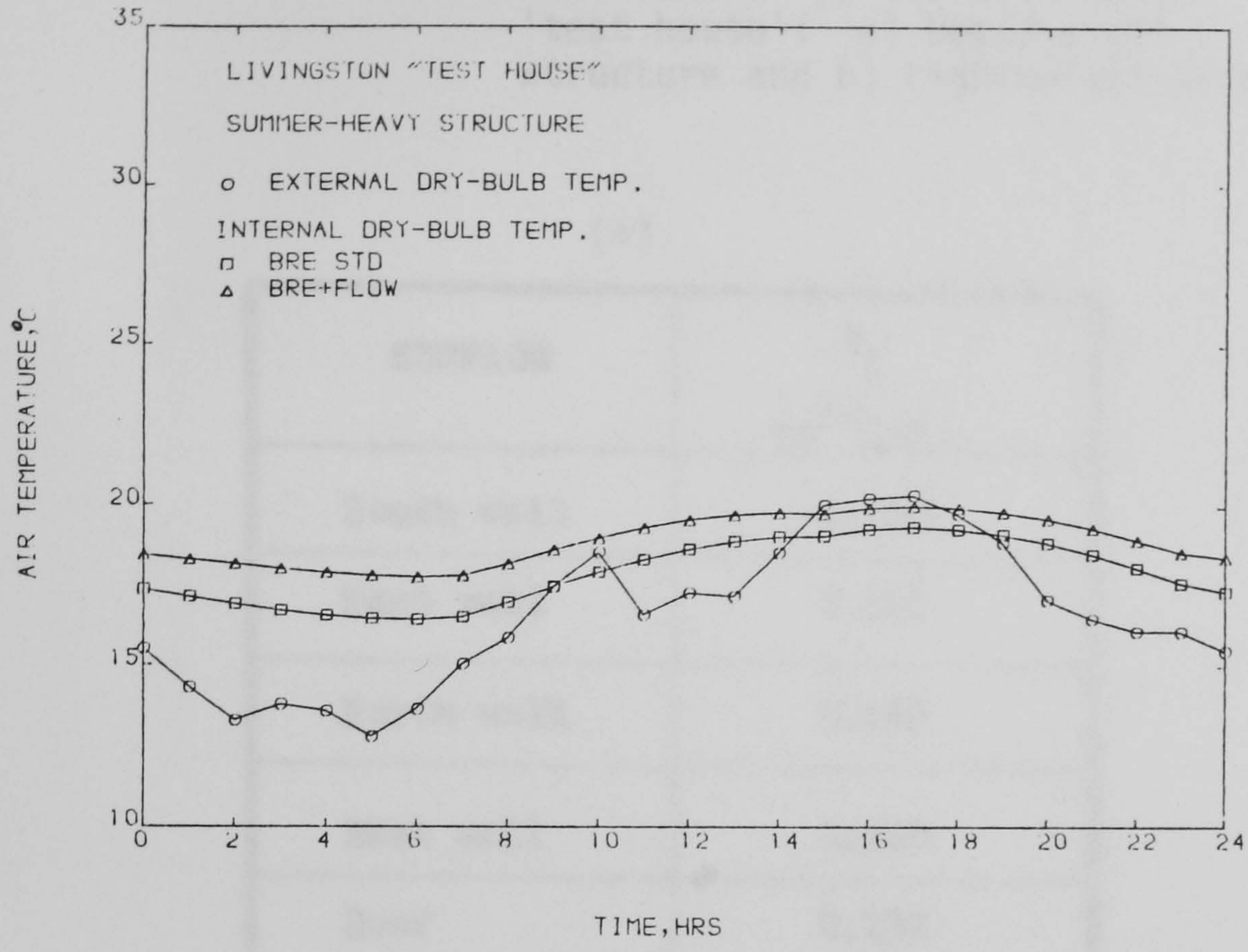

(a)

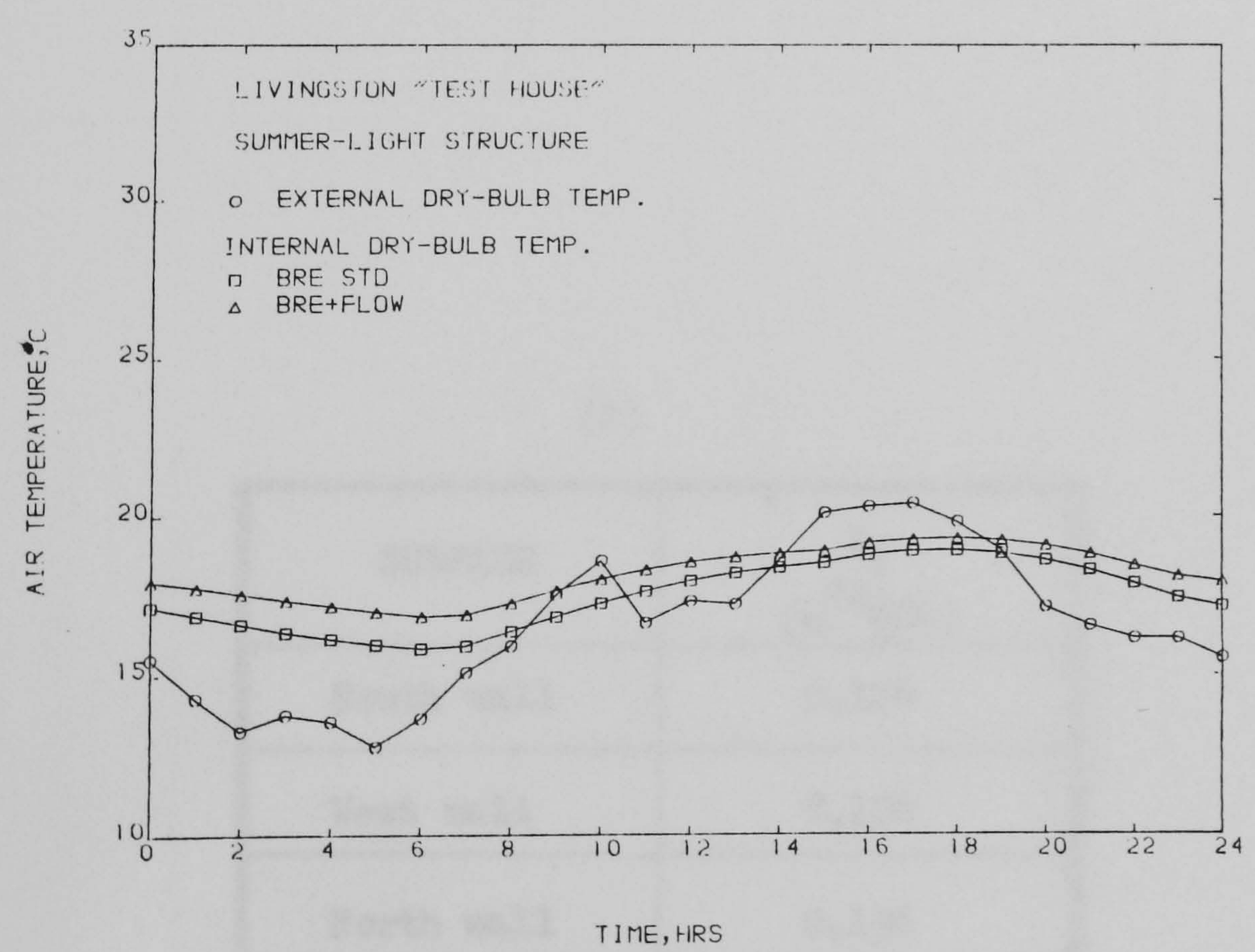

(b)

Fig. 5.4 Internal air temperature profile computed by the BRE program when employing the standard and revised air infiltration rates: a) Heavyweight structure, and b) Lightweight structure.

Table 5.2 Revised winter internal surface resistances for the Livingston 'test house': a) Heavyweight structure and b) Lightweight structure

(a)

SURFACE	R_i ($m^2{}^oC/W$)
South wall	0.120
West wall	0.163
North wall	0.163
East wall	0.120
Roof	0.132
Floor	0.073

(b)

SURFACE	R_i ($m^2{}^oC/W$)
South wall	0.120
West wall	0.156
North wall	0.156
East wall	0.120
Roof	0.136
Floor	0.077

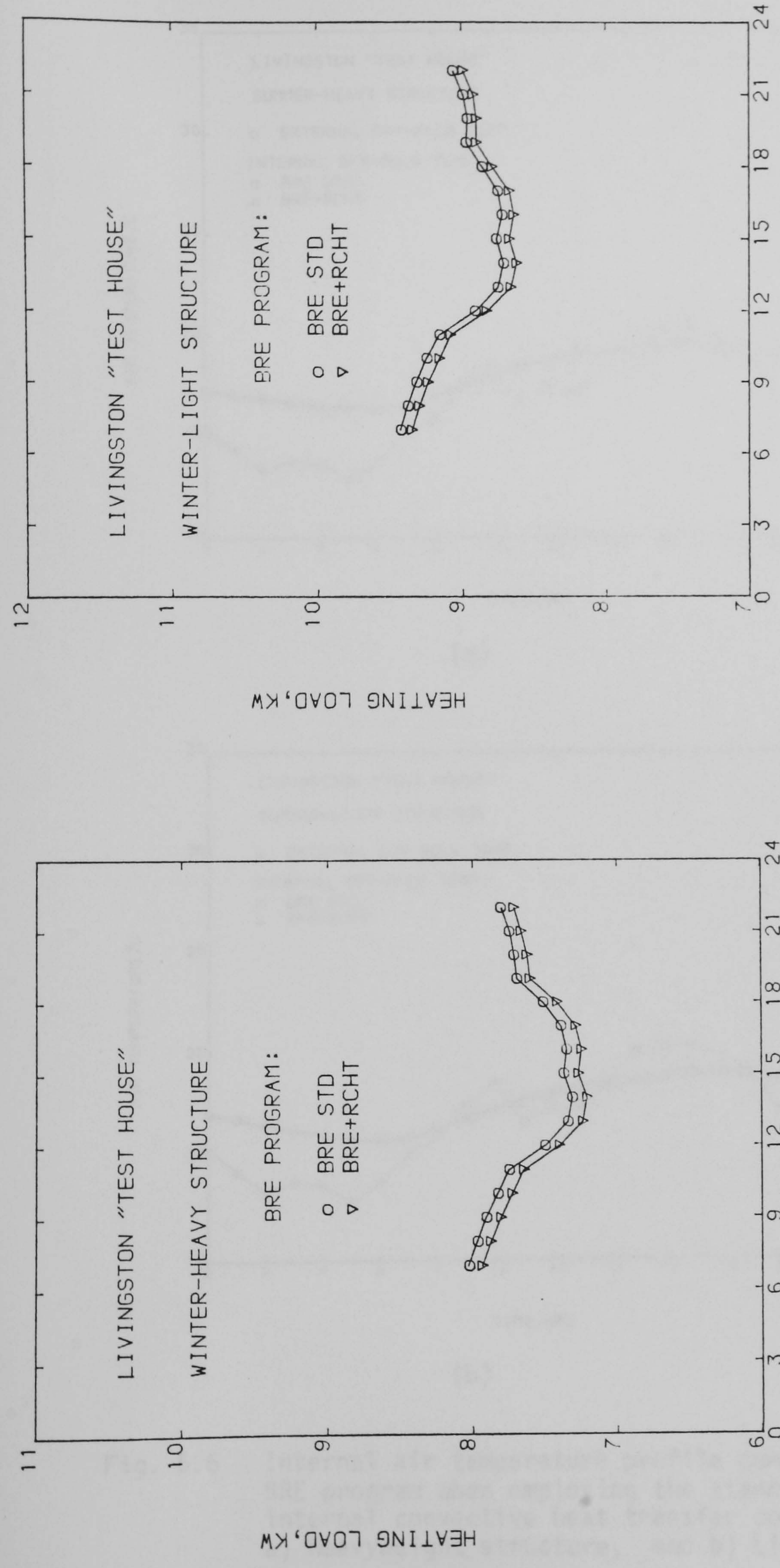

Fig. 5.5 Heating load profile computed by the BRE program when employing the standard and revised internal convective heat transfer coefficients: a) Heavyweight structure, and b) Lightweight structure.

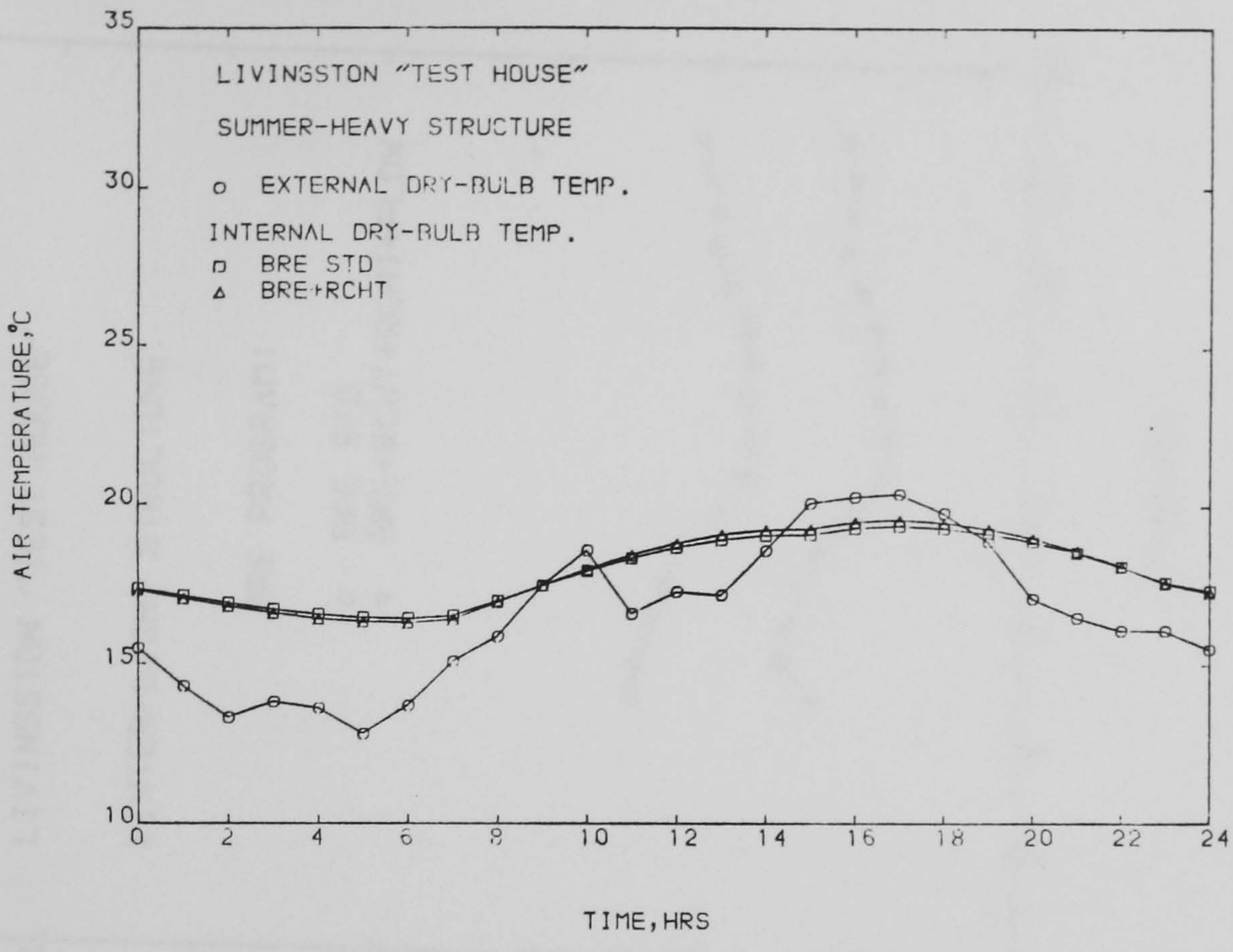

(a)

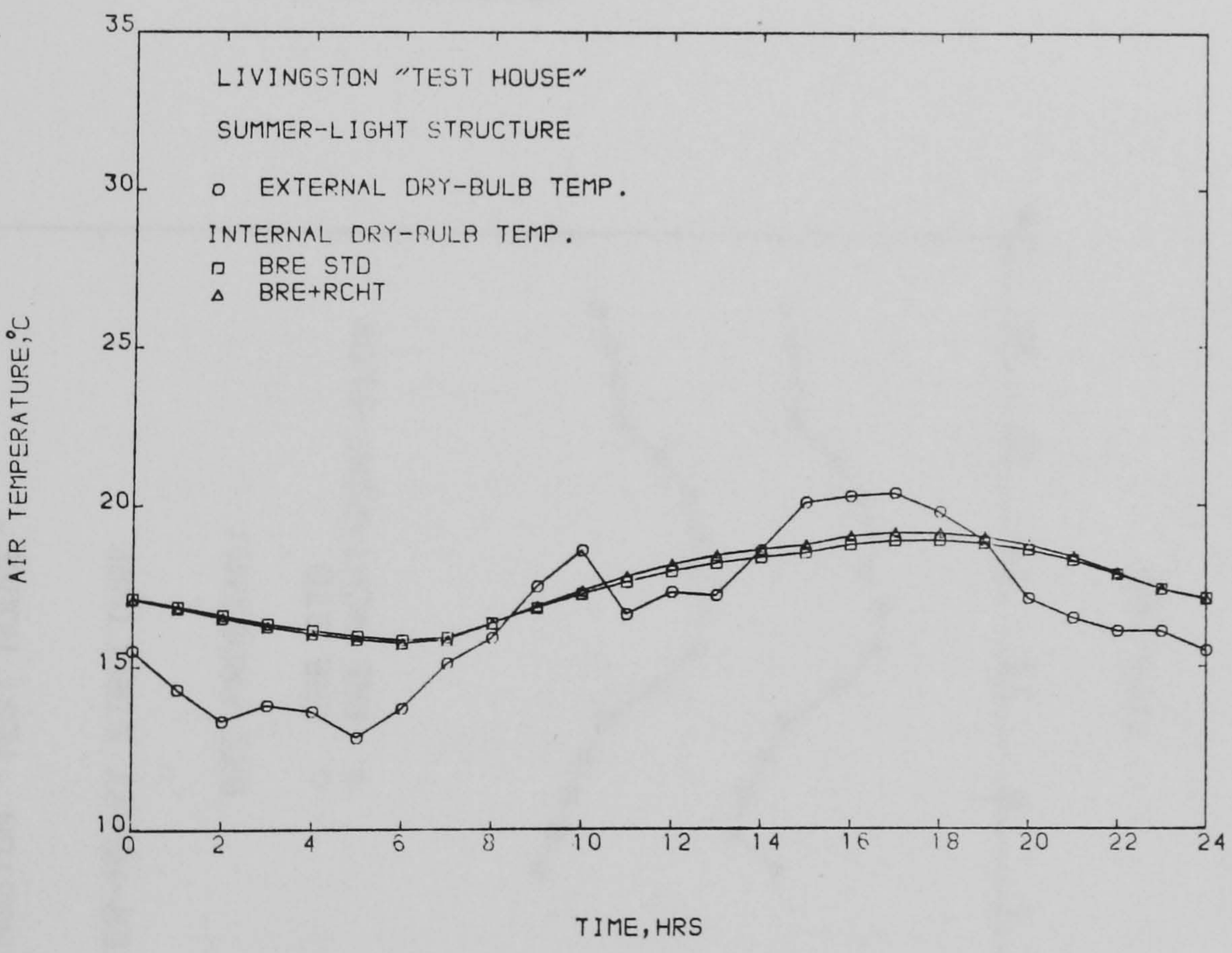

(b)

Fig. 5.6 Internal air temperature profile computed by the BRE program when employing the standard and revised internal convective heat transfer coefficients: a) Heavyweight structure, and b) Lightweight structure

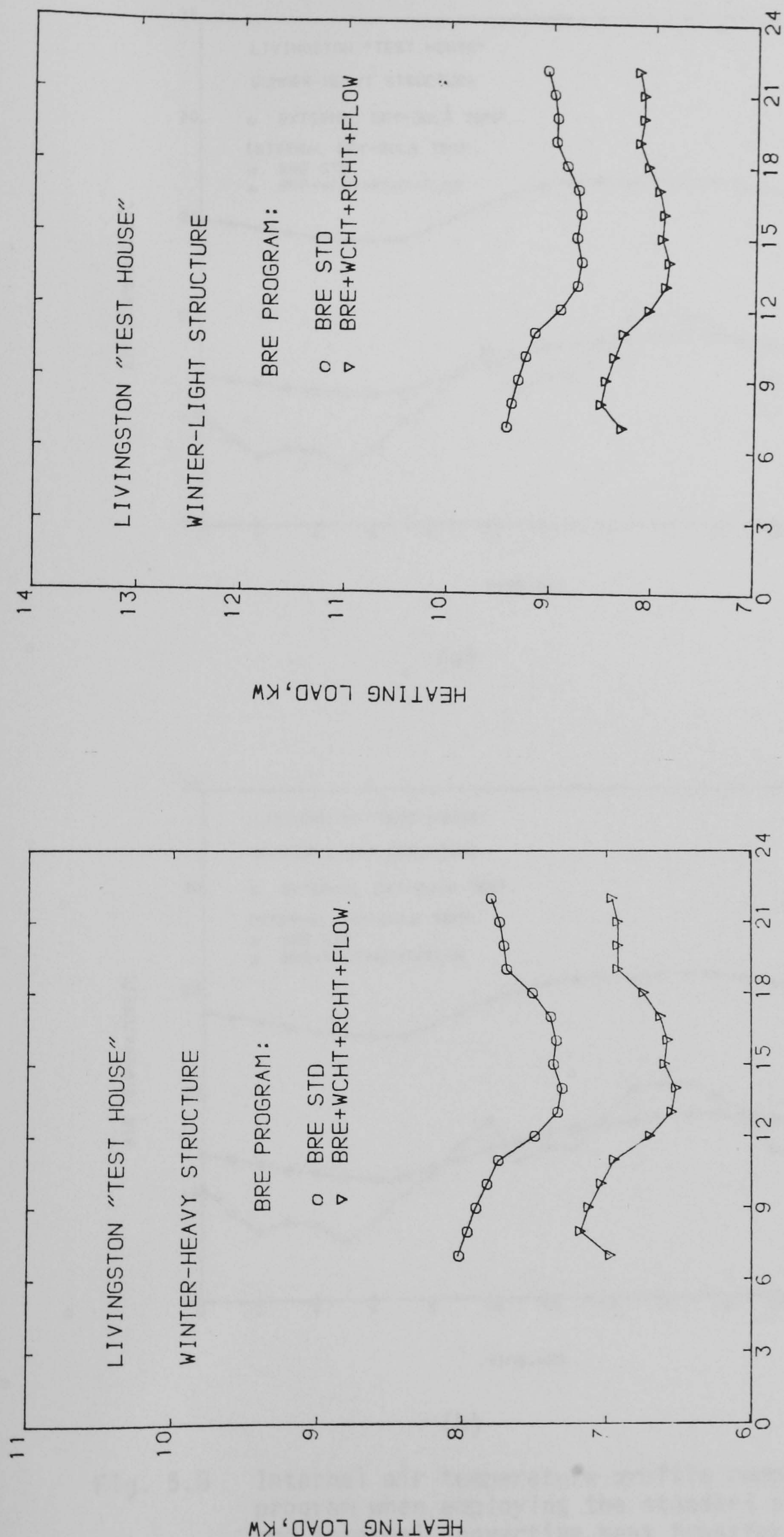

Fig. 5.7 Heating load profile computed by the BRE program when employing the standard and revised external and internal convective heat transfer coefficients and air infiltration rates: a) Heavyweight structure, and b) Lightweight structure.

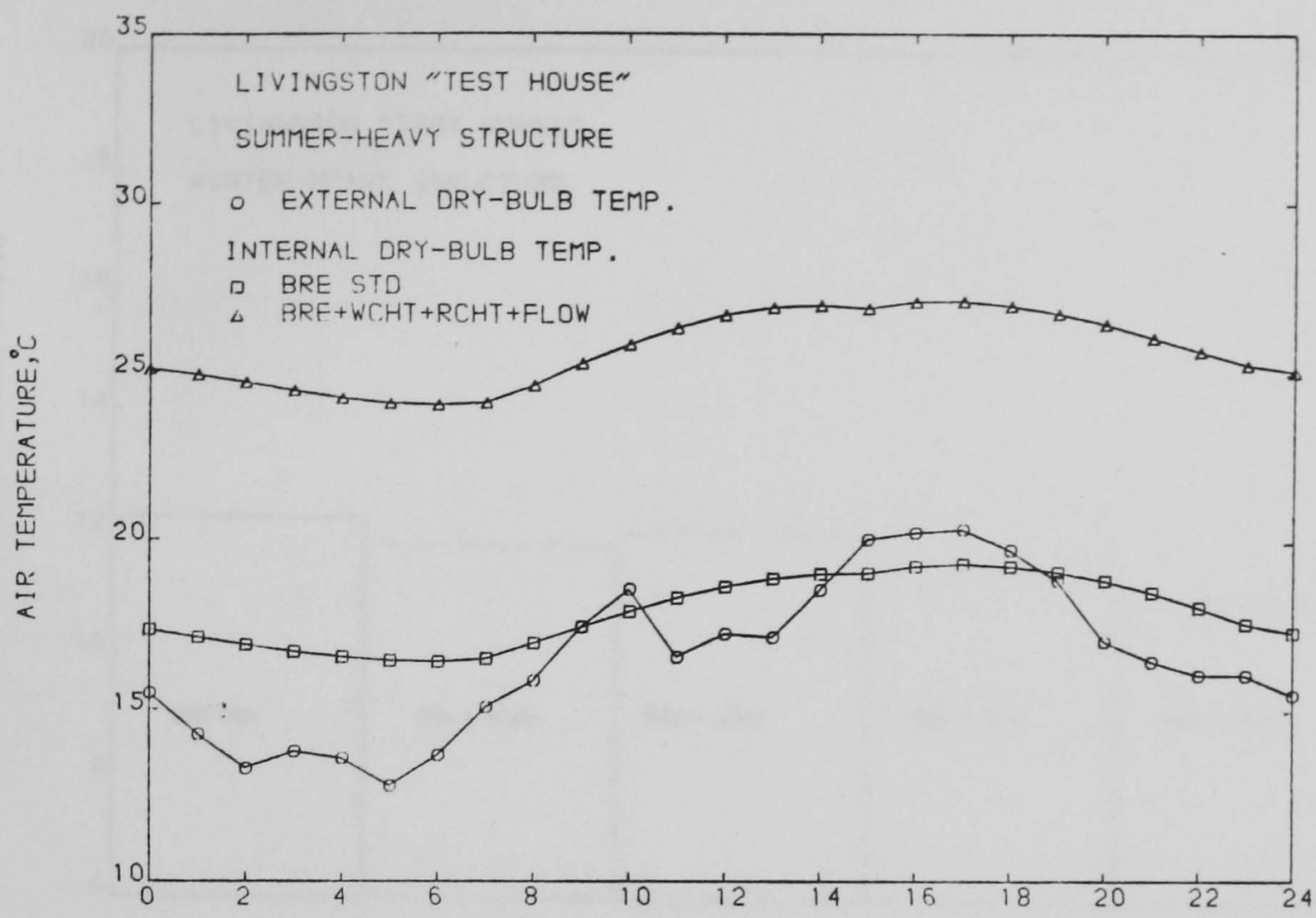

(a)

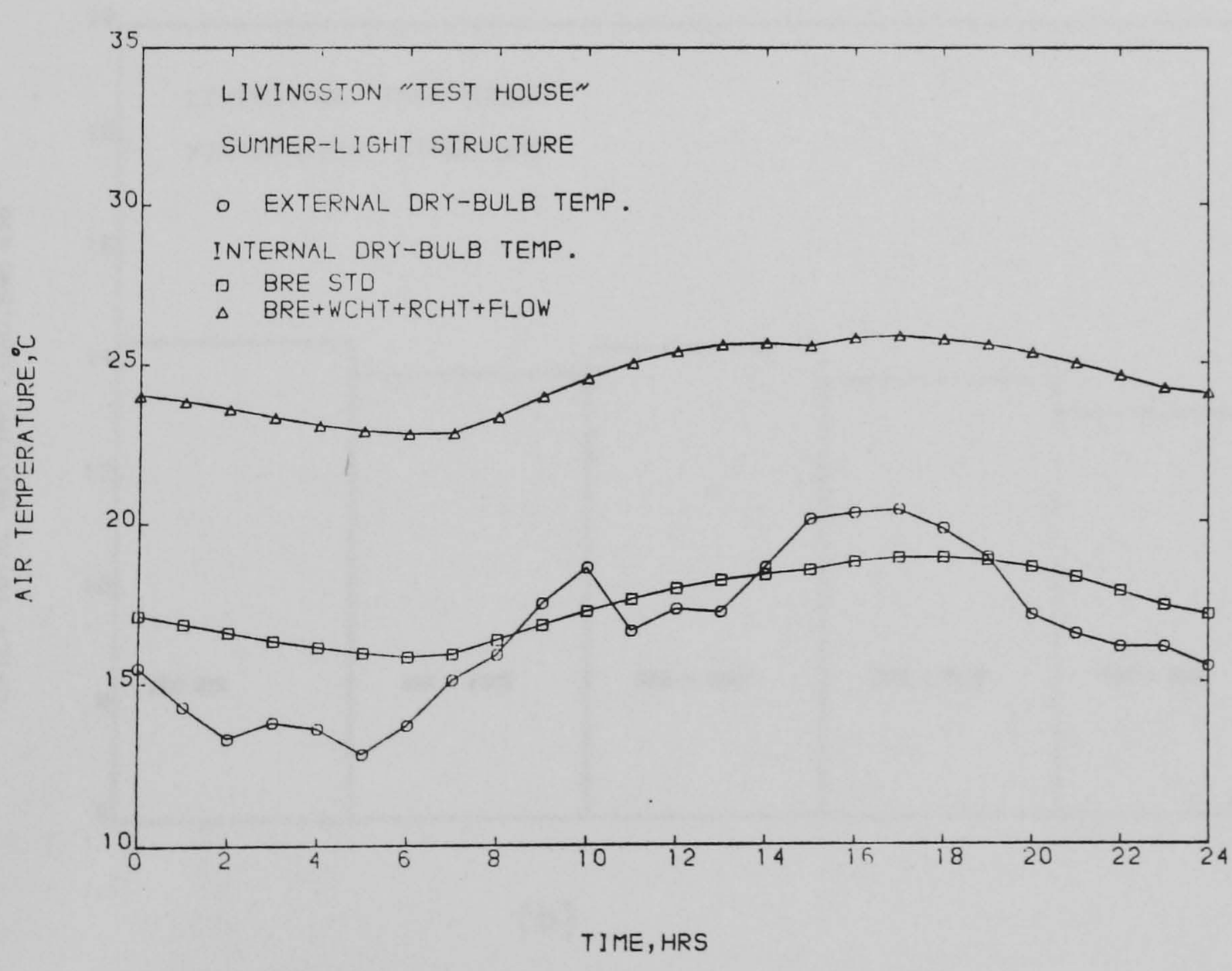

(b)

Fig. 5.8 Internal air temperature profile computed by the BRE program when employing the standard and revised external and internal convective heat transfer coefficients and air infiltration rates: a) Heavyweight structure, and b) Lightweight structure.

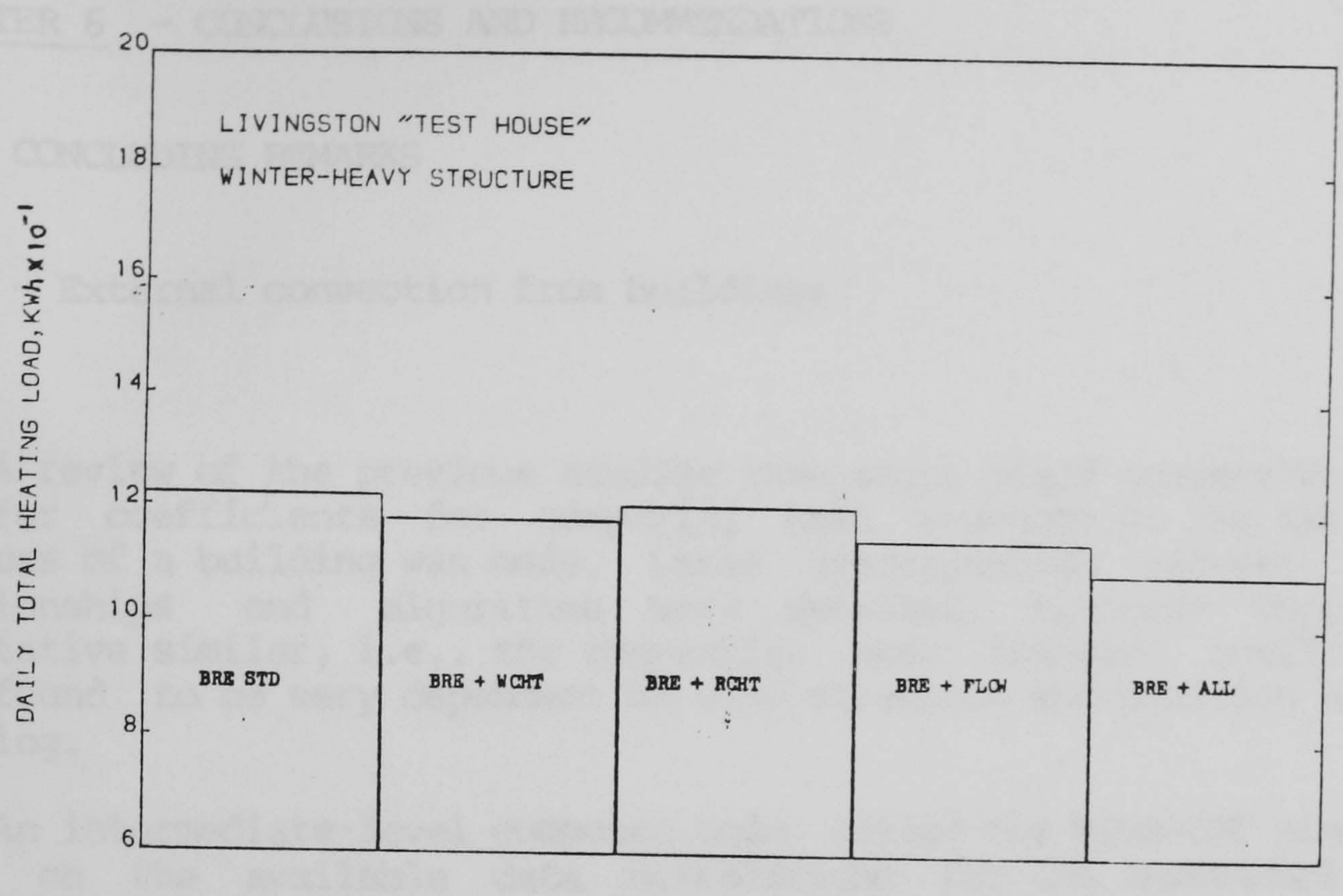

(a)

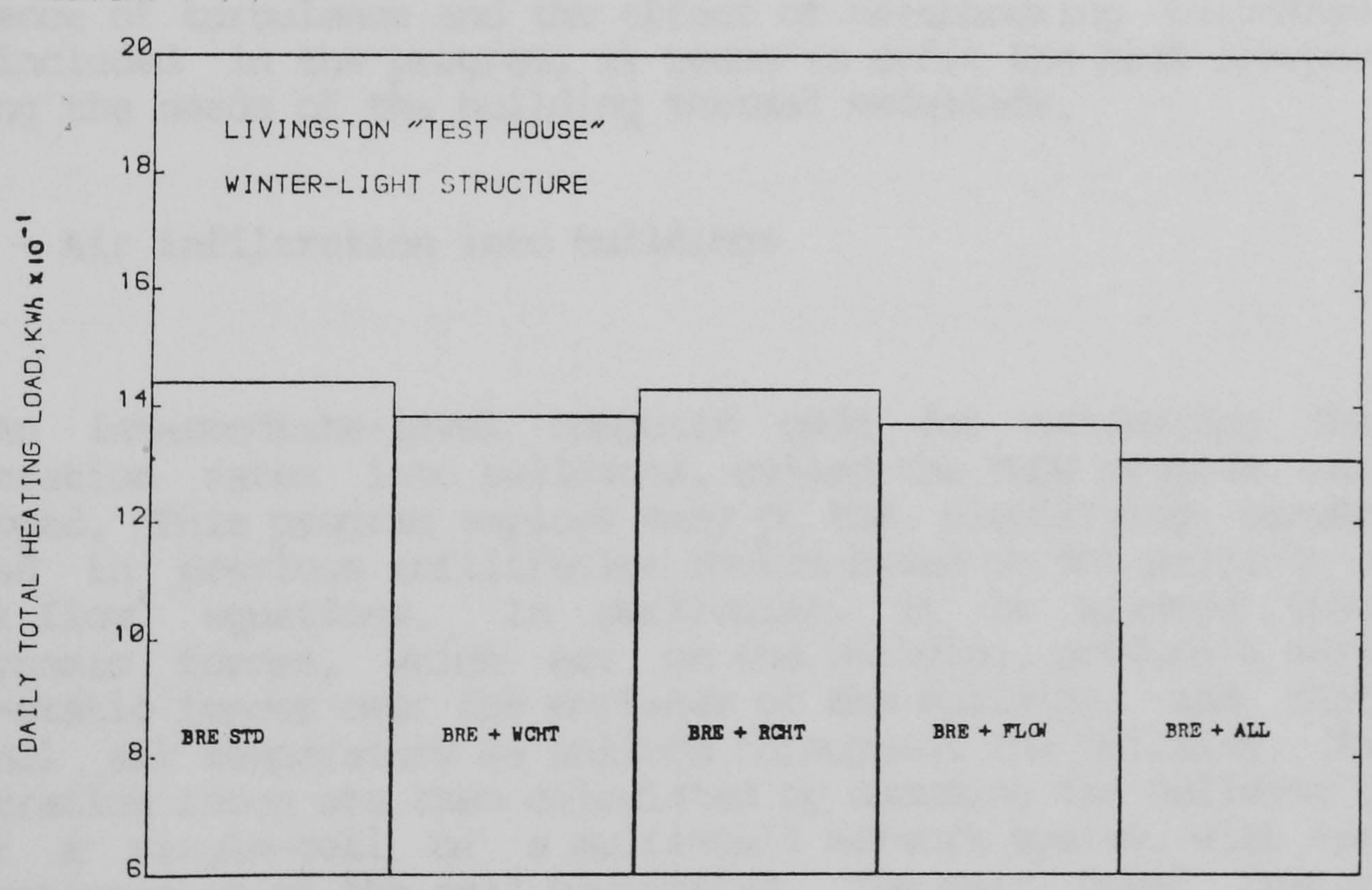

(b)

Fig. 5.9 Separate and combined effects of all three sub-system models on the BRE program computed daily energy consumption: a) Heavyweight structure, and b) Lightweight structure

CHAPTER 6 - CONCLUSIONS AND RECOMMENDATIONS

6.1 - CONCLUDING REMARKS

6.1.1 - External convection from buildings

A review of the previous studies that might yield convective heat transfer coefficients for computing heat exchange at the external surfaces of a building was made. Large discrepancies between these relationships and algorithms were detected, although they are qualitative similar, i.e., the convective heat transfer coefficient was found to be very dependent on wind direction and position on the building.

An intermediate-level computer code, called the WIND-CHT program, based on the available data correlations for the individual flow regimes that prevail around buildings was then developed. This program estimates the convective heat transfer coefficients on the external facades of a building taking into account most of the relevant variables such as wind speed and direction, the change in shape and height of the atmospheric boundary-layer over different terrains and the relative dimensions of the building. Although the influence of turbulence and the effect of neighbouring buildings are not included in the program, it seems to offer the best prospect for meeting the needs of the building thermal modellers.

6.1.2 - Air infiltration into buildings

An intermediate-level computer code for estimating the air infiltration rates into buildings, called the FLOW program, was also developed. This program employs many of the simplifying assumptions adopted in previous infiltration models based on the solution of the 'crack flow' equations. In particular, it is assumed that the aerodynamic forces, which act on the building, produce a series of quasi-static forces over the surfaces of the building, and that the internal air temperature is uniform throughout the building. The air infiltration rates are then calculated by assuming the building to be either a single-cell or a multi-cell network system, with specific flow resistances at the cell boundaries. The main novel feature of this program is that the wind pressure coefficients are internally calculated, thereby avoiding the common and inadequate practice of selecting these parameters from wind load tables. As insufficient information on pressure fluctuations and its effect on the air infiltration rates is available, at the present time, no corrections to allow for this effect is made in the program. Nevertheless, the FLOW program appears to be one of the best models currently available to compute the air infiltration rates required for building thermal models (see section 3.4).

6.1.3 - Sensitivity of building thermal models to input convection and infiltration data

The WIND-CHT and FLOW intermediate-level computer codes, together with the ROOM-CHT program developed by Alamdari and Hammond (Ref.14) for estimating the convective heat transfer coefficients on the internal surfaces of mechanically-ventilated buildings, were employed to assess the sensitivity of two modern building thermal models to the infiltration and convection input data. The BRE admittance procedure program and the NBSLD response factor program were chosen for this purpose. Significant variations were detected in the computed results of the NBSLD program when assessing the individual effect of each of the intermediate-level sub-system models. However, the simultaneous effect of all of these subroutines yielded only a small difference between the standard and modified versions of the NBSLD program in the case of the 'test house' considered in the present study. This anomalous match arises from a fortuitous combination of inaccuracies in estimating the external and internal convective heat transfer coefficients and air infiltration rates. Conversely, the BRE program showed only a small sensitivity to the individual effect of each of the intermediate-level computer codes, but a significant variation in its results when all the sub-system models were replaced simultaneously (see section 5.6).

Both building thermal simulation models displayed a considerable sensitivity to the intermediate-level computer codes,although the extent of the impact of these codes is likely to depend on the conditions prevailing in and around the simulated building.

6.1.4 - Appropriateness of intermediate-level sub-system models

Intermediate-level sub-system models for convective heat transfer and air infiltration, of the type described in this thesis, appear to offer the best prospect for meeting the requirements of the new generation of dynamic building thermal models in terms of accuracy, economy and user friendliness. The lower-level methods, such as analytical solutions and empirical data correlations, are simple to use, but apply to only a very narrow class of flows or range of conditions. In contrast, higher-level computer codes, although potentially capable of handling complex flows, require computational resources that are of the same order as building thermal models themselves. It would not therefore be a realistic approach to couple these codes together ,as any benefits that might be gained in terms of accuracy (over the intermediate-level methods) would be far out-weighed by the extra resources consumed. The main limitation of intermediate-level calculation methods is that ,although more general than lower-level ones, they have a restricted range of application, and need to be used in conjunction with a flow classification scheme. However, this is not a serious weakness as building thermal modellers are well used to working with problem-specific input data. In any

case, around five variants of the present intermediate-level models should be quite able to handle all the normal flow situations that are found in the built environment. Nevertheless, it needs to be stressed that intermediate-level computer codes rely for their success on both lower and higher-level calculation methods. These latter methods, together with experimental data, provide the basis for interactively developing and verifying the intermediate-level ones. Thus, all these methods should be viewed as complementary rather than competitive. Indeed, intermediate-level computer codes may simply be regarded as a way of transferring information provided by the other models in a form appropriate to the needs of building thermal modellers and energy-conscious designers.

6.2 - RECOMMENDATIONS FOR FURTHER WORK

The following suggestions for further research should lead to improvements in the accuracy with which the intermediate-level computer codes are able to compute the convective heat transfer coefficients and air infiltration rates.

i) Further series of full-scale convection measurements on the exterior facades of buildings of different shapes and placed in different kinds of terrain should be made. Special attention should be given to houses with pitched roofs, since this kind of building have not yet been systematically assessed by field measurements. The experiments must always offer the possibility of correlating the measured heat transfer coefficients with the meteorological wind speed and direction. The turbulence level should be recorded in all observations and tentative attempts at correlating the heat transfer coefficients with the turbulence intensity should be made.

ii) Further wind-tunnel tests should be carried out in order to investigate the effect of other building shapes,e.g. buildings with pitched roofs, on the wind pressure coefficients. The sheltering effect of neighbouring buildings on the pressure distributions also needs further investigation.

iii) An experimental full-scale study aimed to determining the air infiltration rates in all rooms of a building simultaneously also needs to be carried out. This will facilitate the proper validation of multi-cell programs for computing the air infiltration rates into buildings.

iv) The ROOM-CHT program range of application should be extended to other forms of supply air apertures, e.g. ceiling diffusers, and to room of other shape, e.g. those composed of a combination of simple rectangular blocks.

REFERENCES

1. CLARKE,J.A.; Computer applications in the design of energy-conscious buildings, Computer-aided Design, Vol 14, 1, January 1982, pp 3-9.

2. DAY,B.; Computation of the dynamic thermal performance of buildings, Computer-aided Design, Vol 14, 1, January 1982, pp 49-54.

3. IRVING, S.J.; Energy program validation: Conclusions of IEA Annex I, Computer-aided Design, Vol 14, 1, January 1982, pp 33-38.

4. ASHRAE; Handbook of Fundamentals, New York, 1981.

5. CIBSE GUIDE; C3-Heat transfer, London, 1976.

6. YANESKE,P.P. and FORREST,I.D.; The thermal response of rooms with intermittent, forced convective heating, Building Services Engineer, Vol 46, 4, 1978, pp 13-17.

7. ALAMDARI,F.;CHAN,J.K.C. and HAMMOND,G.P.; An intermediate-level model of heat transfer for mechanically-ventilated enclosures with 'linear' supply apertures, Paper in preparation.

8. KOOI,J.VAN DER and BEDEKE,K.; Improvement of cooling load programs by measurements in a climate room with mass, Proc. 16th Int. Congress of Refrigeration, Paris, paper E1-359, 1983, pp 54-60.

9. WATERS,J.R.; The experimental verification of a computerised thermal model for buildings, BSERT,Vol 1, 2, 1980, pp 76-82.

10. HAMMOND,G.P.; Complete velocity profile and 'optimum' skin friction formulas for the plane wall-jet, ASME Journal of Fluids Engineering, Vol 104, 1982, pp 59-66.

11. HAMMOND,G.P.; Profile analysis of heat/mass across the plane wall-jet, Heat Transfer 1982:Proc. 7th Int. Heat Transfer Conference, Munich, Vol 3, 1982, pp 349-355.

12. ALAMDARI,F. and HAMMOND,G.P.; Improved data correlations for buoyancy-driven convection in rooms, BSERT, Vol 4, 1983, pp 106-112.

13. ALAMDARI,F.; Convective heat transfer within mechanically-ventilated building spaces, Ph.D. Thesis, Cranfield Institute of Technology, April 1984.

14. ALAMDARI,F. and HAMMOND,G.P.; Time-dependent convective heat transfer in warm-air heated rooms, Proc. 3rd Int. Symp. Energy Conservation in the Built Environment, Dublin, Vol 14, 1982, pp 209-220.

15. Mc ADAMS,W.C.; Heat transmission, Mc Graw-Hill, New York, 3rd edition, 1954, p.249.

16. ROWLEY,F.B.; ALGREEN,A.B. and BLACKSHAW,J.L.; Surface conductances as affected by air velocity, temperature and character of surface, ASHVE Transactions, Vol 36, 1930, pp 429-446.

17. GRANDRILLE,T.; HAMMOND,G.P. and MELO,C.; An intermediate-level model for external convection from buildings, Paper in preparation.

18. HAMMOND,G.P. and MELO,C.; Flow - An algorithm for calculating air flow into buildings, Paper in preparation.

19. ALAMDARI,F.; HAMMOND.G.P. and MELO,C.; Appropriate calculation methods for convective heat transfer from buildings surfaces, Proc. 1st UK National Heat Transfer Conference, Leeds, Vol 2, 3-5 July 1984, pp 1201-1211.

20. KUSUDA,T.; NBSLD:The computer program for heating and cooling loads in buildings, US National Bureau of Standards, Building Science Series 69, Washington, D.C., 1981.

21. BLOOMFIELD,D.P.; BRE microcomputer package for prediction of building temperatures and heating/cooling loads using the admittance method, BRE, 1984.

22. INCROPERA,F.P. and De WITT,D.P.; Fundamentals of heat transfer, John Wiley and Sons, New York, 1982, pp 322-330.

23. CIBSE GUIDE; A3-Thermal Properties of building structures, London ,1980.

24. DUFFIE,J.A and BECKMAN,W.A.; Solar energy thermal process, John Wiley and Sons, New York, 1974.

25. ROWLEY,F.B. and ECKLEY,W.A.; Surface coefficients as affected by direction of wind, ASHVE Transactions, Vol 38, 1932, pp 33-46.

26. PARMELEE,G.V. and HUEBSCHER,R.G.; Forced convection heat transfer from flat surfaces, ASHRAE Transactions, Vol 58, 1947, pp 85-106.

27. SOGIN,H.H.; Heat transfer from the rear of bluff objects to a low speed air stream, Aeronautical Research Laboratory Report 62-361, Ohio, June 1962.

28. SOGIN,H.H.; A summary of experiments on local heat tranfer from the rear of bluff obstacles to a low speed airstream, ASME Journal of Heat Transfer, Vol 86, 1964, pp 202-202.

29. RICHARDSON,P.D.; Heat and mass transfer in turbulent separated flows, Chemical Engineering Science, Vol 18, 1963, pp 149-155.

30. OLIPHANT,M.V.; Measurement of wind speed distributions across a solar collector, Solar Energy, Vol 24, 1980, pp 402-405.

31. SPARROW,E.M. and TIEN,K.K.; Forced convection heat transfer at an inclined and yawed square plate-application to solar collectors, ASME Journal of Heat Transfer, Vol 99, November 1977 , pp 507-512.

32. SPARROW,E.M.; RAMSEY,J.M. and MASS,E.A.; Effect of finite width on heat transfer and fluid flow about an inclined rectangular plate, ASME Journal of Heat Transfer, Vol 101, May 1979, pp 199-204.

33. TIEN,K.K. and SPARROW,E.M.; Local heat transfer and fluid flow characteristics for airflow oblique or normal to a square plate, International Journal of Heat and Mass Transfer, Vol 22, 1979, pp 349-360.

34. SPARROW,E.M.; NELSON,J.S. and TAO,W.Q.; Effect of leeward orientation, adiabatic framing surfaces, and eaves on solar-collector-related heat transfer coefficients, Solar Energy, Vol 29, No.1, 1982, pp 33-41.

35. TEST,F.L.; LESSMANN,R.C. and JOHARY,A.; Heat transfer during wind flow over rectangular bodies in the natural environment, ASME Journal of Heat Transfer, Vol 102, February 1980, pp 146-151.

36. TEST,F.L. and LESSMANN,R.C.; An experimental study of heat transfer during forced convection over a rectangular body, ASME Journal of Heat Transfer, Vol 102, February 1980, pp 146-151.

37. JUNKHAN,G.H. and SEROVY,G.K.; Effects of free-stream turbulence and pressure gradient on flat-plate boundary-layer velocity profiles and on heat transfer, ASME Journal of Heat Transfer, May 1967, pp 169-176.

38. STURROCK,N.S.; Localised boundary layer heat transfer from external building surfaces, Ph.D. Thesis, University of Liverpool, 1971.

39. COLE,R.J. and STURROCK,N.S.; The convective heat exchange at the external surface of buildings, Building and Environment, Vol 12, 1977, pp 207-214.

40. ITO,N.; KIMURA.K. and OKA,J.; A field experiment study on the exterior surface of a building, ASHRAE Semmiannual Meeting, New Orleans, LA, January 23-27, 1972.

41. BURNS,A.P.; Wind-induced heat loss from buildings, Proc. 5th Int. Conference on Wind Engineering, Fort Collins, USA, July 8-14, 1979.

42. BURNS,A.P.; An experimental study of heat transfer from a bluff body to a turbulent free-stream as applied to building heat loss, Ph.D. Thesis, University of Glasgow, 1976.

43. KELNHOFER,W.J. and THOMAS,C.J.; External convection heat transfer coefficients on a building model, ASME paper 76-WA/FE-30, 1976.

44. SHARPLES,S.; Forced convective heat transfer from buildings facades, Ph.D. Thesis, University of Sheffield, 1981.

45. SHARPLES,S.; Full-scale measurements of convective energy losses from exterior building surfaces, Building and Environment, Vol 19, No.1, 1984, pp 31-39.

46. CERMAK,J.E.; Applications of fluid mechanics to wind engineering -A freeman scholar lecture, ASME Jounal of Fluids Engineering, March 1975,pp 9-38.

47. ASHRAE TASK GROUP; Procedure for determining heating and cooling load for computerising energy calculations, Algorithms for building heat transfer subroutines, ASHRAE, New York, 1975.

48. PENWARDEN,A.D. and WISE,A.F.E.; Wind environment around buildings, BRE Report, HMSO, london, 1975.

49. HANSON,T.; SMITH,F.; SUMMERS,D. and WILSON,C.B.; Computer simulation of wind flow around buildings, Computer-aided Design, Vol 14, 1, January 1982, pp 27-31.

50. COUNIHAN,J.; Adiabatic atmospheric boundary layers: A review and analysis of data from the period 1880-1972, Atmospheric Environment, Vol 9, No.10, October 1975, pp 871-905.

51. DAVENPORT,A.G.; The relationship of wind structure to wind loading, Proc. National Physical Laboratory Symposium No.16: Wind effects on buildings and structures, 26-28 June 1963, pp 54-111.

52. TAYLOR,R.J.; Small-scale advection and the neutral wind profile, Journal of Fluid Mechanics, Vol 13, 1962, pp 529-539.

53. SIEBERS,D.L.; SCHWIND,R.G. and MOFFAT,R.J.; Experimental mixed convection from a large, vertical plate in a horizontal flow, Heat Transfer 1982:Proc. of the 7th Int. Heat Transfer Conference, Munich, 1982, pp 477-482.

54. SHERMAN,M.T. and GRIMSRUD,D.T.; Infiltration-pressurization correlation: simplified physical modelling, ASHRAE Transactions, Vol 86, part II, 1980, pp 778-807.

55. SHERMAN,M.T. and GRIMSRUD,D.T.; Measurement of infiltration using fan pressurization and weather data, AIC Conference - Instrumentation and measuring techniques, Windsor, UK, 1980, pp 279-322.

56. CIBSE GUIDE; A4-Air infiltration, London, 1976.

57. JACKMAN,P.J.; A study of the natural ventilation of tall office buildings, Journal Inst. Heat Vent. Eng., Vol 38, August 1970, pp 103-118.

58. ALLEN,C.; Wind pressure data requirements for air infiltration calculation, Air Infiltration Centre Techincal Note AIC-13, Bracknell, UK, 1984.

59. LIDDAMENT,M. and ALLEN,C.; The validation and comparison of mathematical models of air infiltration, Air Infiltration Centre Technical Note AIC-11, Bracknell, UK, 1983.

60. SHAW,C.Y.; Wind and temperature induced pressure differentials and an equivalent pressure difference model for predicting air infiltration in schools, ASHRAE Transactions, Vol 86, part II, 1980, pp 268-269.

61. BOWEN,A.J.; A wind tunnel investigation using simple building models to obtain mean surface wind pressure coefficients for air infiltration estimates, National Aeronautical Establishment Report LTR LA209, NRCC, Canada, 1976.

62. AKINS,R.E.; PETERKA,J.A.; and CERMAK,J.E.; Average pressure coefficients for rectangular buildings, Proc. 5th International Conference on Wind Engineering, Vol 1, Fort Collins, Colorado-USA, 8-14 July 1979, pp 369-380.

63. SHAW,C.Y.; A method for predicting air infiltration rates for a tall building surrounded by lower structures of uniform height, ASHRAE Transactions, Vol 85, part I, 1979, pp 72-84.

64. HILL,J.E. and KUSUDA,T.; Dynamic characteristcs of air infiltration ,ASHRAE Transactions, Vol 81, part I, 1975, pp 168-185.

65. POTTER,N.; Effect of fluctuating wind pressures on natural ventilation rates, ASHRAE Transactions, Vol 85, part II, 1979, pp 445-457.

66. GRIMSRUD,D.T.; SHERMAN,M.H.; DIAMOND,R.C.; CONDON,P.E. and ROSENFELD,A.H.; Infiltration-pressurization correlations:Detailed measurements on a California house, ASHRAE Transactions,Vol 85, part I, 1979, pp 851-865.

67. ETHERIDGE,D.W. and NOLAN,J.A.; Ventilation measurements at model scale in a turbulent flow, Building and Environment, Vol 14, 1979, pp 53-64.

68. ETHERIDGE,D.W. and ALEXANDER.D.K.; The british gas multi-cell model for calculating ventilation, ASHRAE Transactions, Vol 86, part II, 1980, pp 808-821.

69. TAMURA,G.T. and SHAW,C.Y.; Studies on exterior wall tightness and air infiltration of tall buildings, ASHRAE Transactions, Vol 82, part I, 1976, pp 122-134.

70. TAMURA,G.T. and WILSON,A.G.; Pressure differences caused by chimney effect in three high buildings, ASHRAE Transactions, Vol 73, part II, 1967, pp II.1.1-II.1.10.

71. SHAW,C.Y. and TAMURA,G.T.; The calculation of air infiltration rates caused by wind and stack action for tall buildings, ASHRAE Transactions, Vol 83, part II, pp 145-158.

72. MELO,C.; The influence of geometrical and physical parameters on air conditioning calculations, M.Sc. Thesis, Federal University of Santa Catarina-Brazil, September 1980. (in portuguese)

73. SMITH,W.A. and PAGE,J.K.; A meteorological data base system for architectural and building engineering designers, SERC grant No.GR/B/40219, November 1982.

74. STEPHENSON,D.G. and MITALAS,G.P.; Room thermal response factors, ASHRAE Transactions, Vol 73, part I, 1967, pp III2.1-2.10.

75. KUSUDA,T.; Thermal response factors for multi-layer structures of various heat conduction systems, ASHRAE Transactions, Part I, 1969, pp 250-269.

76. OSCAR FABER AND PARTNERS; IEA Annex I - Computer modelling of buildings energy performance: results and analysis of Avonbank building simulation, 1980.

77. BURCH,D.M.; PEAVY,B.A. and POWELL,F.J.; Experimental validation of the NBS load and indoor temperature prediction model, ASHRAE Transactions, Vol 80, part II, 1974, pp 291-313.

78. BLOOMFIELD,D.; Appraisal techniques for methods of calculating the thermal performance of buildings, BRE/SERC Validation group open meeting, Leicester Polytechnic, 31st october 1984.

79. CLARKE,J.A. and FORREST,I.; Validation of the ESP thermal simulation program, ABACUS, paper No.61, Dept. of Architecture, University of Strathclyde, August 1978.

80. HOLMES,M.J. and HITCHIN,E.R.; An "example year" for the calculation of energy demand in buildings, BSE, Vol 45, January 1978, pp 186-189.

81. COBLENTZ,C.W. and ACHENBACH,P.R.; Field measurements of air infiltration in ten electrically-heated houses, ASHRAE Transactions, Vol 69, 1963, pp 358-365.

82. BAHNFLETH,D.R.; MOSELEY,T.D. and HARRIS,W.S.; Measurements of infiltration in two residences - Part I: Technique and measured infiltration, ASHRAE Transactions, Vol 63, 1957, pp 439-452.

83. MACRISS,R.A.; COLE,J.T.; and ZAWACKI,T.S.; An air infiltration model for modern single family dwellings, 72nd Annual Meeting of the Air Pollution Control Association, Cincinati-Ohio, June 24-29, 1979.

84. RAJARATNAM,N.; Turbulent jets, Elsevier scientific publishing company, 1976, pp.277-290.

85. CIBSE GUIDE; A5-Thermal response of buildings, London, 1969.

86. DANTER,E.; Periodic heat flow characteristics of simple walls and roofs, Journal Inst. Heat Vent. Eng.,Vol 28, 1960, pp 136-146.

87. DANTER,E.; Heat exchanges in a room and the definition of room temperature, BRE current paper 18/75, 1975.

88. LOUDON,A.G.; Summertime temperatures in buildings without air-conditioning, JIHVE, Vol 37, 1970, pp 280-292.

89. MILBANK,N.O. and HARRINGTON-LYNN,J.; Thermal response and the admittance procedure, BRE current paper 61/74, 1974.

90. HARRINGTON-LYNN,J.; The admittance procedure:Intermittent plant operation, Building Services Engineer, Vol 42, December 1974, pp 219-221.

91. HARRINGTON-LYNN,J.; The admittance procedure:Variable ventilation, Building Services Engineer, Vol 42, November 1974, pp 199-200.